An experimental study of ethanol-diesel dual-fuel combustion for high efficiency and clean heavy-duty engines

A thesis submitted for the degree of
Doctor of Philosophy

by

Vinícius Bernardes Pedrozo

Department of Mechanical, Aerospace and Civil Engineering
College of Engineering, Design and Physical Sciences
Brunel University London

November 2017

Abstract

Higher atmospheric concentration of greenhouse gases (GHG) such as carbon dioxide and methane has contributed to an increase in Earth's mean surface air temperature and caused climate changes. This largely reflects the increase in global energy consumption, which is heavily dependent on oil, natural gas, and coal. If not controlled, the combustion of these fossil fuels can also produce high levels of nitrogen oxides (NOx) and soot emissions, which adversely affect the air quality. New and extremely challenging fuel efficiency and exhaust emissions regulations are driving the development and optimisation of powertrain technologies as well as the use of low carbon fuels to cost-effectively meet stringent requirements and minimise the transport sector's GHG emissions. In this framework, the dual-fuel combustion has been shown as an effective means to maximise the utilisation of renewable liquid fuels such as ethanol in conventional diesel engines while reducing the levels of NOx and soot emissions.

This research has developed strategies to optimise the use of ethanol as a substitute for diesel fuel and improve the effectiveness of dual-fuel combustion in terms of emissions, efficiency, and engine operational cost. Experimental investigations were performed on a single cylinder heavy-duty diesel engine equipped with a high pressure common rail injection system, cooled external exhaust gas recirculation, and a variable valve actuation system. A port fuel injection system was designed and installed, enabling dual-fuel operation with ethanol energy fractions up to 0.83. At low engine loads, in-cylinder control strategies such as the use of a higher residual gas fraction via an intake valve re-opening increased the combustion efficiency (from 87.7% to 95.9%) and the exhaust gas temperature (from 468 K to 531 K). A trade-off between operational cost and NOx reduction capability was assessed at medium loads, where the dual-fuel engine performance was less likely to be affected by combustion inefficiencies and in-cylinder pressure limitations. At high load conditions, a Miller cycle strategy via late intake valve closing decreased the in-cylinder gas temperature during the compression stroke, delaying the autoignition of the ethanol fuel and reducing the levels of in-cylinder pressure rise rate. This allowed for the use of high ethanol energy fractions of up to 0.79. Finally, the overall benefits and limitations of optimised ethanol-diesel dual-fuel combustion were compared against those of conventional diesel combustion. Higher net indicated efficiency (by up to 4.4%) combined with reductions in NOx (by up to 90%) and GHG (by up to 57%) emissions can help generate a viable business case of dual-fuel combustion as a technology for future high efficiency and clean heavy-duty engines.

List of contents

Nomenclature

1D: one-dimensional
2EVO: exhaust valve re-opening
2IVO: intake valve re-opening
$\%C_{fuel}$: carbon mass content
$\%H_{fuel}$: hydrogen mass content
$\%O_{fuel}$: oxygen mass content
a: crank radius
ASC: ammonia slip catalyst
ATDC: after firing top dead centre
B: bore
BMEP: brake mean effective pressure
BTU: British thermal unit
C: carbon
$c_{p,v}$: vapour specific heat capacity
CA_P_{max}: crank angle of maximum in-cylinder gas pressure
CA10: crank angle of 10% cumulative heat release
CA10-CA50: 10-50% cumulative heat release
CA10-CA90: combustion duration or 10-90% cumulative heat release
CA50: combustion phasing or crank angle of 50% cumulative heat release
CA90: crank angle of 90% cumulative heat release
CAD: crank angle degree
CDC: conventional diesel combustion
CF: port and valve flow coefficients
CH_4: methane
CI: compression ignition
CO: carbon monoxide
CO_2: carbon dioxide
CO_{2eq}: carbon dioxide equivalent
$CO(NH_2)_2$: urea
$Conv.Eff$: NOx conversion efficiency of the SCR aftertreatment system
COV_IMEP: coefficient of variation of IMEP
COV_P_{max}: coefficient of variation of maximum in-cylinder gas pressure
$C_xH_yO_z$: normalised molecular composition of the actual in-cylinder fuel mixture
D: valve reference diameter
DAQ: data acquisition
DDFS: direct dual fuel stratification
DEF: diesel exhaust fluid
DI: direct injection
DOC: diesel oxidation catalyst
DPF: diesel particulate filter
E10: gasoline with 10% ethanol in a volume basis
E100: anhydrous ethanol
E50W50: wet ethanol containing 50% of water on a volume basis
E65W35: wet ethanol containing 35% of water on a volume basis
E80W20: wet ethanol containing 20% of water on a volume basis
E85: gasoline with 85% ethanol in a volume basis
ED95: mixture of ethanol and 5% of ignition improver
EC: European Commission
ECR: effective compression ratio
ECU: engine control unit
EEVC: early exhaust valve closing
EEVO: early exhaust valve opening
EF: ethanol energy fraction
EGR: exhaust gas recirculation
EIVC: early intake valve closing

EGT: exhaust gas temperature
EPA: Environmental Protection Agency
$EOCR$: engine operational cost ratio
ET: energising time delay
EU: European Union
EUCAR: European Council for Automotive R&D
EVC: exhaust valve closing
EVO: exhaust valve opening
FAME: fatty acid methyl ester
FID: flame ionisation detector
FS: full scale
FTP: Federal Test Procedure
GCR: geometric compression ratio
GDCI: gasoline direct injection compression ignition
GHG: greenhouse gas
GWP: global warming potential
H_2O: water
H_2O_2: hydrogen peroxide
H: hydrogen
H_a: intake air humidity
H_f: humidity introduced by the water-in-fuel content
HC: hydrocarbons
HCCI: homogeneous charge compression ignition
HCLD: heated chemiluminescence detector
HD: heavy-duty
HHD: heavy heavy-duty
HHR: heat release rate
HVO: hydrotreated vegetable oil
IAT: intake manifold air temperature
IC: internal combustion
iEGR: internal exhaust gas recirculation
IFPRI: International Food Policy Research Institute
iLUC: indirect land-use change
IMEP: net indicated mean effective pressure
IPCC: intergovernmental panel on climate change
ISCO: net indicated specific emissions of carbon monoxide
$ISCO_2$: net indicated specific emissions of carbon dioxide
ISHC: net indicated specific emissions of unburnt hydrocarbons
ISNOx: net indicated specific emissions of nitrogen oxides
ISsoot: net indicated specific emissions of soot
IVC: intake valve closing
IVO: intake valve opening
JCR: Joint Research Centre
$k_{f,w}$: fuel specific factor of wet exhaust
$k_{h,D}$: ambient humidity correction factor for nitrogen oxides
$k_{w,r}$: dry/wet correction factor for the raw exhaust gas
k_{FID}: correction factor for the FID response to oxygenated fuels
l: connecting rod length
L: valve lift
LHV: lower heating value
LHV_{CO}: lower heating value of carbon monoxide
LHV_{mix}, actual lower heating value of the in-cylinder fuel mixture
LHV_{diesel}: lower heating value of diesel
$LHV_{ethanol}$: lower heating value of ethanol
LIVC: late intake valve closing

LIVO: late intake valve opening
LTC: low temperature combustion
m/m: mass basis
$\dot{m}_{air}$: mass flow rate of fresh air
$\dot{m}_{diesel}$: mass flow rate of diesel
$\dot{m}_{dry\ air}$: mass flow rate of dry air
$\dot{m}_{ethanol}$: mass flow rate of ethanol
$\dot{m}_{exh}$: mass flow rate of exhaust gas
$\dot{m}_{f}$: in-cylinder fuel mass flow rate
$\dot{m}_{CO}$: mass flow rate of carbon monoxide
$\dot{m}_{HC}$: mass flow rate of unburnt hydrocarbons
$\dot{m}_{H_2O}$: mass flow rate of water-in-fuel
$\dot{m}_{humidty}$: mass flow rate of humidity
$\dot{m}_{NOx}$: mass flow rate of nitrogen oxides
$\dot{m}_{soot}$: mass flow rate of soot
$\dot{m}_{urea}$: mass flow rate of aqueous urea solution
$m_{air/cycle}$: mass of fresh air inducted per cycle
$m_{ethanol/cycle}$: mass of ethanol injected per cycle
$m_{fuel/cycle}$: mass of fuel injected per cycle
$m_{rg/cycle}$: mass of residual gas trapped at exhaust valve closing
m_{RP}: mass of mixture (burnt or unburnt) per mole of O_2 in the mixture
$m_{total/cycle}$: total in-cylinder mass per cycle
M_b: molecular weight of the burned gas
M_{CO_2}: molar mass of CO_2
$M_{dry\ air}$: molar mass of dry air
M_{fuel}: molar mass of the fuel
M_{H_2O}: molar mass of water
M_{N_2}: molar mass of nitrogen
M_{O_2}: molar mass of oxygen
MF: ethanol mass fraction
MFB: mass fraction burnt
MK: modulated kinetics
MPA: magneto-pneumatic detector
n_b: number of moles of burnt gas
N: engine speed
N_2: nitrogen
N_2O: nitrous oxide
NG: natural gas
NH_3: ammonia
NHTSA: National Highway Traffic Safety Administration
NMHC: non-methane hydrocarbons
NO: nitrogen oxide
NO_2: nitrogen dioxide
NOx: nitrogen oxides
NVO: negative valve overlap
O_2: oxygen
OH: hydroxyl
p: pressure
p_{amb}: ambient air pressure
p_{EVC}: in-cylinder gas pressure at exhaust valve closing
p_{vapour}: partial pressure of water vapour in the air
p_{sat}: saturation pressure of water vapour
P_{ind}: net indicated power
PCCI: premixed charge compression ignition
PFI: port fuel injector
PI: positive ignition
PM: particle matter
P_{max}: maximum in-cylinder gas pressure
PMEP: pumping mean effective pressure
PN: particle number
PPC: partially premixed combustion

PPCI: partially premixed charge compression ignition
ppm: parts per million
PRR: pressure rise rate
$\tilde{R}$: universal gas constant
R: specific gas constant
R^2: coefficient of determination
RCCI: reactivity controlled compression ignition
REF: trigger signal
RGF: residual gas fraction
RH: relative humidity in ambient air
rpm: revolutions per minute
RON: research octane number
S: stroke
SCR: selective catalytic reduction
SET: Supplemental Emissions Test
SI: spark ignition
SOC: start of combustion
SOI: actual start of injection
SOI_1: actual start of first diesel injection (pre-injection)
SOI_2: actual start of second diesel injection (main injection)
T: temperature
T_{amb}: ambient air temperature
$T_{cyl,i}$: mean in-cylinder gas temperature
T_{IVC}: mean in-cylinder gas temperature at intake valve closing
TDC: firing top dead centre
TTW: tank-to-wheels
$TTW\ CO_2$: tank-to-wheels CO_2 emissions
$TTW\ CO_{2eq}$: tank-to-wheels CO_2 equivalent emissions
u_{CO}: carbon monoxide to exhaust gas density ratio
u_{gas}: component to exhaust gas density ratio
$u_{gas,\ mix}$: component to exhaust gas density ratio for the dual-fuel operation
u_{HC}: unburnt hydrocarbons to exhaust gas density ratio
u_{NOx}: nitrogen oxides to exhaust gas density ratio
u_{soot}: soot to exhaust gas density ratio
UNIBUS: uniform bulky combustion system
US: United States
v/v: volume basis
V: volume
V_c: clearance volume
V_d: displaced volume
V_{EVC}: in-cylinder volume at exhaust valve closing
VF: volumetric fraction of ethanol in the total fuel injected
VPR: actual volumetric price ratio
VPR_{max}: maximum volumetric price ratio
VVA: variable valve actuation
$W_{c,ind}$: net indicated work per cycle
WHTC: world harmonized transient driving cycle
WHSC: world harmonized steady state cycle
WTT: well-to-tank
$WTT\ CO_{2eq}$: well-to-tank CO_2 equivalent emissions
WTW: well-to-wheels
$WTW\ CO_{2eq}$: well-to-wheels CO_2 equivalent emissions
x: molar carbon to carbon ratio
y: molar hydrogen to carbon ratio

z: molar oxygen to carbon ratio

$(A/F)_{stoich}$: stoichiometric air/fuel ratio

[CO]: concentration of carbon monoxide in the exhaust gas

[CO_2]: concentration of carbon dioxide in the exhaust gas

[FSN]: filter smoke number

[HC]: concentration of unburnt hydrocarbons in the exhaust gas

$[HC]_{actual}$: actual concentration of unburnt hydrocarbons in the exhaust gas

[NOx]: concentration of nitrogen oxides in the exhaust gas

[soot]: concentration of soot in the exhaust gas

α: response factor for the ethanol constituent

γ: ratio of specific heats (c_p/c_v)

Φ: global fuel/air equivalence ratio

Φ’: premixed fuel/air equivalence ratios

θ: crank angle position

λ: lambda or relative air/fuel ratio

ρ: density

ρ_{diesel}: diesel density

$\rho_{ethanol}$: ethanol density

ρ_{exh}: exhaust gas density

List of figures

List of tables

List of publications related to this research

[1] Pedrozo VB, Zhao H. Improvement in high load ethanol-diesel dual-fuel combustion by Miller cycle and charge air cooling. Applied Energy 2018;210:138–51. doi:10.1016/j.apenergy.2017.10.092.

[2] Pedrozo VB, Lanzanova TDM, Zhao H. The effects of wet ethanol injection and Miller cycle on a heavy-duty diesel engine operating at full load. Internal Combustion Engines Conference 2017 - IMechE 2017.

[3] Pedrozo VB, May I, Zhao H. Exploring the mid-load potential of ethanol-diesel dual-fuel combustion with and without EGR. Applied Energy 2017;193:263–75. doi:10.1016/j.apenergy.2017.02.043.

[4] Pedrozo VB, May I, Guan W, Zhao H. Efficient ethanol-diesel dual-fuel combustion: A comparison with conventional diesel combustion. 13th International Congress on Engine Combustion Processes (ENCOM 2017) 2017.

[5] Pedrozo VB, May I, Lanzanova TDM, Zhao H. Potential of internal EGR and throttled operation for low load extension of ethanol–diesel dual-fuel reactivity controlled compression ignition combustion on a heavy-duty engine. Fuel 2016;179:391–405. doi:10.1016/j.fuel.2016.03.090.

[6] Pedrozo VB, May I, Zhao H. Characterization of Low Load Ethanol Dual-Fuel Combustion using Single and Split Diesel Injections on a Heavy-Duty Engine. SAE Technical Paper 2016. doi:10.4271/2016-01-0778.

[7] Pedrozo VB, May I, Dalla Nora M, Cairns A, Zhao H. Experimental analysis of ethanol dual-fuel combustion in a heavy-duty diesel engine: An optimisation at low load. Applied Energy 2016;165:166–82. doi:10.1016/j.apenergy.2015.12.052.

Acknowledgements

My time at Brunel University London has been a memorable, challenging, and extremely rewarding experience. I am especially indebted to my supervisor, Professor Hua Zhao, for providing support, guidance, and a stimulating environment to carry out engine research. Moreover, my PhD studies at Brunel would not have been possible without the support of CAPES Foundation (Coordenação de Aperfeiçoamento de Pessoal de Nível Superior), a government agency of the Brazilian Ministry of Education.

Many people at Brunel have made significant contributions to this project. Special thanks to Ian, Macklini, Thompson, and Wei. You were not only colleagues but awesome friends and have been instrumental in conducting this research as well as providing professional and personal advice. I will never forget all the great moments and experiences we have shared together. I also would like to thank the technicians Andy, Chris, Clive, Eamon, Greg, and William for their indispensable help in the lab and commitment to the completion of several tasks.

I also want to acknowledge several individuals that have helped me in various ways over the last few years. I am deeply grateful to Professor Mario Martins at the Federal University of Santa Maria (UFSM) for helping and encouraging me to pursue my degree here in the UK. I would like to thank former colleagues and friends at Fiat Chrysler LATAM, FPT Industrial, Iveco, CNH Industrial, Bosch, and Marelli, as well as Professor Paulo Romeu and Fernando Bayer at UFSM for providing valuable guidance on internal combustion engine testing and validation. Particular thanks to Professor Alasdair Cairns at the University of Nottingham for providing interesting conversation and the opportunity to work with alternative fuels. Thank you as well to my friends Akira, Alessandro, Apostolos, Hassan, Irene, Khalifa, Kobi, Mahmoud, Meghna, Mohsen, Pin, Ray, Reza, Thais, Thiago, Xinyan, Yan, Yuanping, Ward, and Wing Hei for all the help you gave me during my PhD.

I would like to extend my sincerest thanks to my parents, Jairo and Odete, and brother Vitor for their unwavering support, counsel, and encouragement in my personal and professional endeavours. Last and foremost, I am eternally thankful for the love and support of my wife, Jessika, whose daily encouragement and happiness have given me the strength to pursue my dreams.

Chapter 1

Introduction

1.1 Preface

Internal combustion (IC) engines date back to 19th century [8,9] and have evolved into one of the world's most capable and reliable forms of power generation. The knowledge of engine processes and fuels has increased significantly with the introduction of new technologies and environmental constraints on energy use. Global concern about air pollution, rising atmospheric carbon dioxide (CO_2) emissions, and their resulting effects on human health and climate has required the establishment of fuel efficiency targets and exhaust emissions limits for the transport sector. These measures have forced research and development efforts of the scientists, engineers, and entrepreneurs to obtain more advanced and cleaner IC engines and fuels.

Higher fuel conversion efficiency and lower levels of pollutants are generally achieved by innovations such as new combustion strategies and improved aftertreatment systems. The introduction of less carbon-intensive fuels to the transport sector also help cut the levels of CO_2 emissions. Therefore, the combination of low carbon fuels with high efficiency IC engines can minimise anthropogenic emissions of greenhouse gases which cause the Earth to warm in response.

In particular, heavy-duty vehicles are typically equipped with compression ignition diesel engines and represent one of the largest contributors of global transport-related CO_2 emissions [10]. The partial substitution of diesel in favour of a fuel produced from renewable feedstocks such as ethanol can reduce the greenhouse gas (GHG) intensity of these vehicles. In this context, the dual-fuel operation can represent an effective means to promote the use of biofuels in conventional diesel engines. This is a result of the potential superior fuel conversion efficiency and lower levels of exhaust emissions [11].

Figure 1.1 shows the working principle of most dual-fuel engines, which are designed to operate with direct injection of a high reactivity fuel such as diesel and port fuel injection of a low reactivity fuel like ethanol, gasoline, or natural gas (NG). The consumed energy fraction of each fuel may vary depending on the engine operating condition.

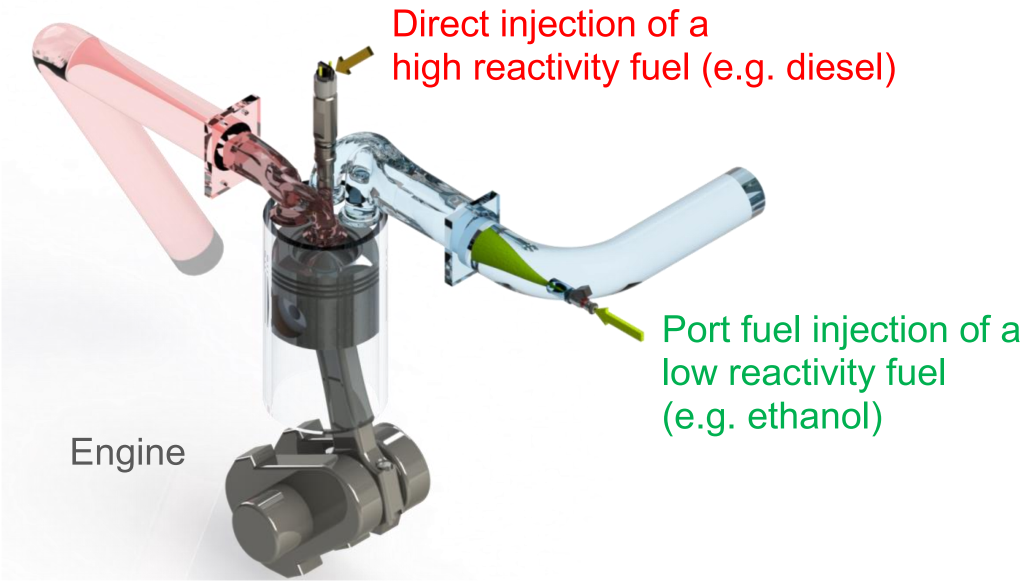

Figure 1.1 – Schematic diagram of a typical dual-fuel engine equipped with direct injection of a high reactivity fuel and port fuel injection of a low reactivity fuel.

The main challenges encountered by dual-fuel engines are poor fuel conversion efficiency at low load due to incomplete combustion and excessive combustion noise caused by rapid burn rates at high engine loads, which limit the premixed fuel energy fraction to low percentages. Alternative combustion control strategies have to be developed to minimise these undesirable effects. Therefore, an experimental investigation has been carried out to characterise the dual-fuel combustion and optimise the performance and emissions of a heavy-duty engine fuelled with diesel and ethanol.

1.2 Research objectives

The primary goal of this research is to achieve high efficiency and clean dual-fuel operation from low to high engine load using ethanol as a partial substitute for diesel. The specific objectives of this study comprise:

- To overcome the limitations of current dual-fuel engines through advanced combustion control strategies such as multiple diesel injections, variable valve timing, and exhaust gas recirculation.
- To explore the potential of ethanol-diesel dual-fuel combustion for improved fuel conversion efficiency, lower exhaust emissions, and minimum engine operational costs.
- To maximise the use of ethanol and minimise the carbon footprint of heavy-duty engines.

1.3 Thesis outline

The thesis is arranged in eight chapters. Chapter 1 provides an introduction, delimiting the thesis scope and objectives. Chapter 2 presents a review of the literature relevant to this research, which helped support the methodology employed and the discussion of results.

Topics such as GHG emissions, climate change, and regulatory standards are assessed. Technologies introduced to the transport sector, particularly to heavy-duty vehicles, have been described. Potential in-cylinder control strategies, aftertreatment systems, and alternative fuels are explored. The limitations faced by current dual-fuel engines are discussed. Chapter 3 presents the research engine and test cell facilities. The equations used and methodology followed for acquisition and analysis of engine data are also described.

Chapters 4, 5, and 6 investigate means of improving the efficiency and minimising exhaust emissions of ethanol-diesel dual-fuel combustion at low, medium, and high engine loads. Chapter 4 explores the effect of diesel injection characteristics, residual gas fraction, fuel/air equivalence ratio, external exhaust gas recirculation, and ethanol energy fraction on dual-fuel combustion. Chapter 5 assesses mid-load limitations and determines the effectiveness of the dual-fuel combustion in terms of efficiency, emissions, and operational cost. Chapter 6 characterises the effect of high engine load on dual-fuel operation and evaluates alternative in-cylinder strategies to overcome the challenges encountered.

Chapter 7 compares the efficiency and engine-out pollutants of optimised dual-fuel combustion to those of conventional diesel combustion using identical engine operating conditions. The expected GHG emissions reduction is also analysed. Finally, Chapter 8 summarises the primary findings of this research and presents recommendations for future studies.

Chapter 2

Literature Review

2.1 Introduction

The energy needs for the transport sector accounts for approximately 20% of global energy demand and is expected to increase by 25% from 2015 to 2040 [12], as shown in Figure 2.1. This is primary a result of a projected rise in the number of cars and heavy-duty vehicles as well as the increased demand for other commercial transportation (e.g. airplanes, ships, and trains) driven by economic growth. Moreover, the vast majority of the energy used to support transportation is met by fossil fuels [13], and represents 55% of the worldwide oil consumption [12].

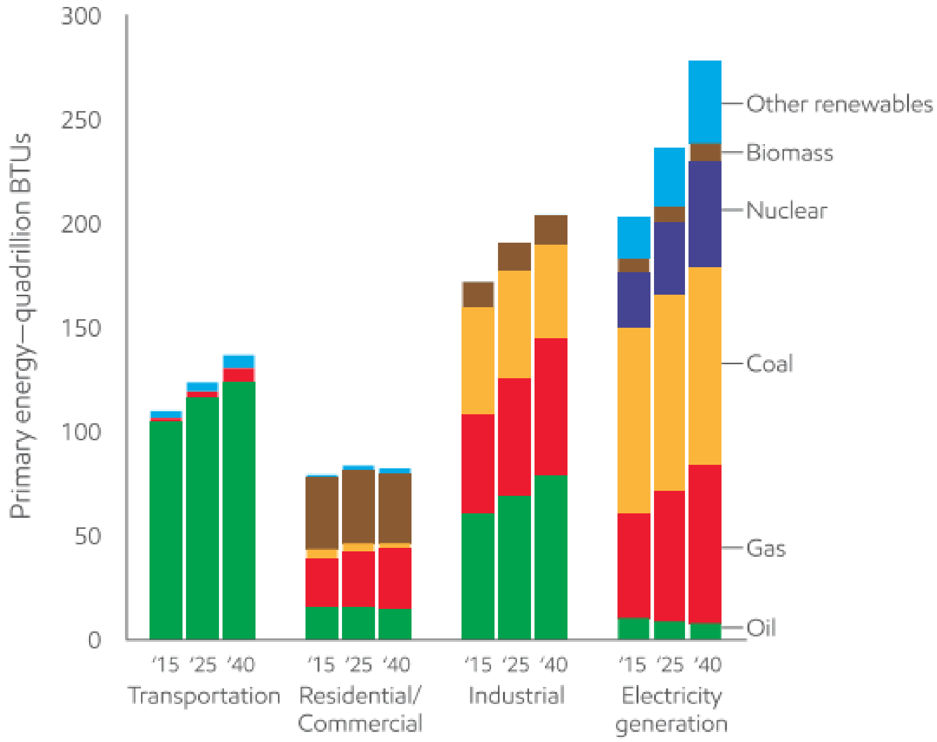

Figure 2.1 – Global energy demand by sector and source. Adapted from [12].

According to the Intergovernmental Panel on Climate Change (IPCC) [14], the combustion of fossil fuels has greatly affected the atmospheric concentration of heat-trapping or greenhouse gases, such as CO_2 and methane (CH_4). Figure 2.2 shows a substantial increase in the concentration of CO_2 emissions in the atmosphere since the 1950s, which is extremely likely to have been the dominant cause of the measured global warming over the last 35 years, as shown in Figure 2.3.

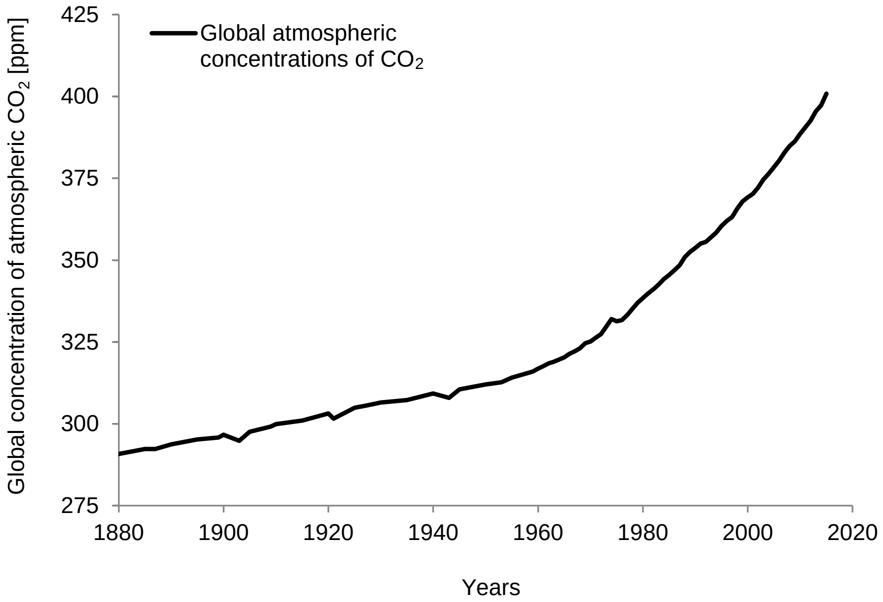

Figure 2.2 – Global concentration of atmospheric CO_2 in parts per million (ppm) based on recent direct measurements and indirect measurements reconstructed from ice cores over time. Source: United States Environmental Protection Agency [15].

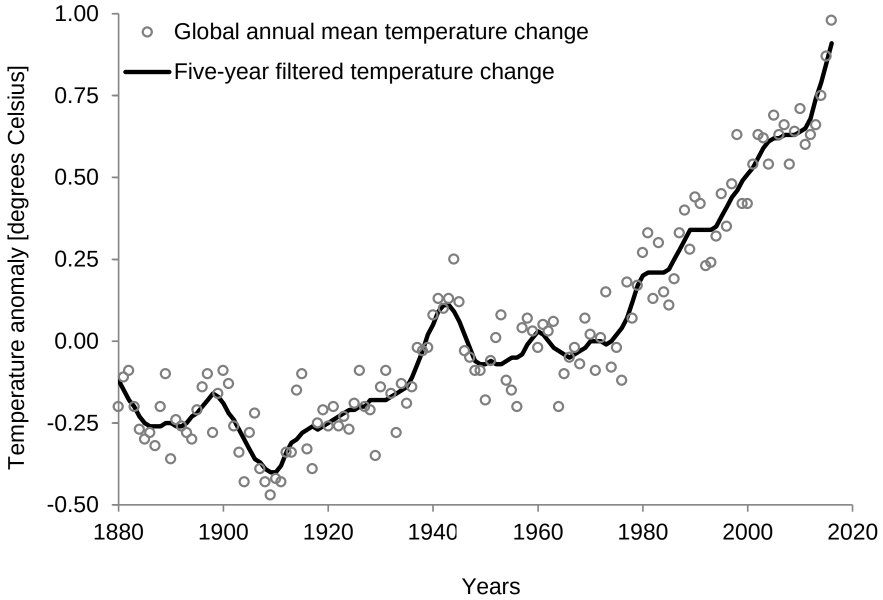

Figure 2.3 – Global annual mean surface air temperature change based on land and ocean data over time with base period 1951–1980. Source: GISTEMP Team [16].

The future fuel energy demand and resulting anthropogenic GHG emissions will largely determine the severity of the global warming. By the end of the 21st century, the global mean surface air temperature can increase by up 4.8 degrees Celsius relative to the period between 1986 and 2005 [14]. This variation can change depending on the projected emissions scenario.

A higher average surface air temperature can cause irreversible climate changes and negatively impact the health of living organisms across the globe [14]. Substantial and continuous reduction in fossil fuel energy use and GHG emissions must be achieved and combined with adaptation and mitigation strategies to address the impact on the environment.

Recently, 152 of the 197 parties to the United Nations Framework Convention on Climate Change [17] have ratified the Paris Agreement to combat climate change and accelerate the actions and investments for a sustainable low carbon future. The goal is to keep a global temperature rise well below 2 degrees Celsius above pre-industrial levels by the end of this century and urge efforts to limit the temperature increase to 1.5 degrees Celsius [18].

The introduction of measures to reduce energy use and decarbonise the supply is necessary in every major sector, particularly in transportation and electricity generation. Figure 2.4 shows the results of a lifecycle analysis used to assess the overall GHG impacts of fossil fuels from the extraction to combustion. The International Council on Clean Transportation reported that the global transport sector released 23% of the total anthropogenic lifecycle CO_2 emissions from economic sectors in 2010 [19].

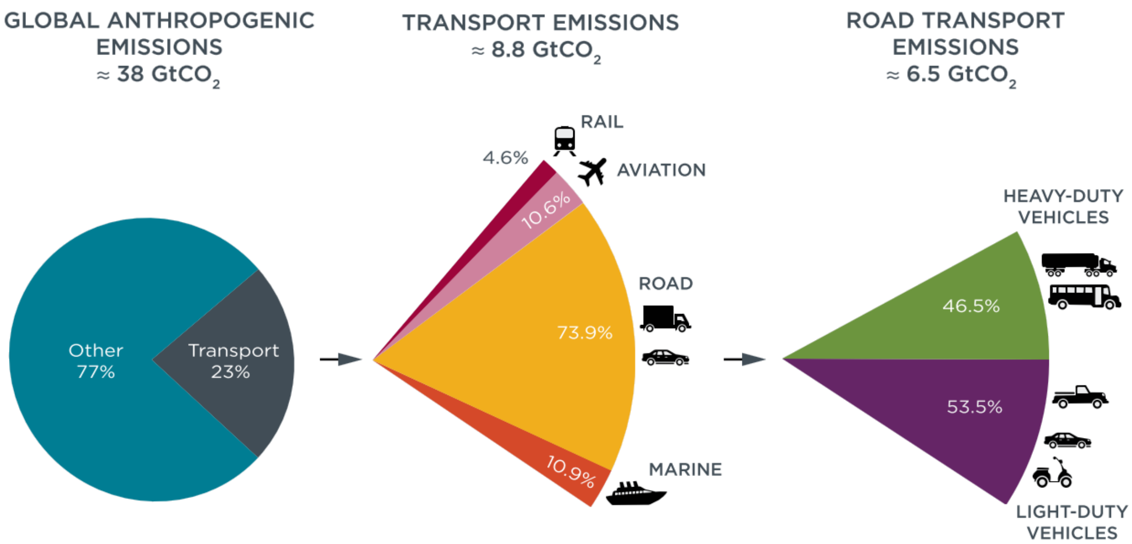

Figure 2.4 – Global anthropogenic lifecycle CO_2 emissions from economic sectors in 2010. Adapted from [19].

Heavy-duty (HD) vehicles contributed to almost half (46.5%) of road transport CO_2 emissions and were responsible for approximately one-third of the GHGs emitted by the total transportation sector [19]. This is equivalent to 8% of the global anthropogenic CO_2

emissions. The high environmental impact is highlighted by the fact the HD fleet represents only 11% of the world motor vehicles [20].

Therefore, more research into HD vehicles emissions and fuel efficiency has to be carried out in order to curb GHG emissions and minimise the sector's disproportionate contribution to climate change. The use of renewable fuels and the development of new engine technologies have the potential to reduce oil dependency and help meet emissions reduction targets.

2.2 Emission and fuel efficiency regulations

Stringent fuel efficiency and emission regulations have been implemented to limit the flow of GHG emissions into the atmosphere as well as the emissions of other pollutants such as particulate matter (PM) and nitrogen oxides (NOx) of the global transport sector. PM and NOx are linked to millions of premature deaths caused by cardiovascular and respiratory diseases [21,22] and harmful effects on climate [23].

Regulating fuel consumption and emissions of the HD fleet is more challenging because of the diversity of vehicle use compared to the light-duty sector [19]. The certification of exhaust emissions from HD vehicles is usually performed on an engine dynamometer and reported in units of mass of pollutant per unit of brake power (e.g. g/kWh) [24]. This allows for comparisons between different engine applications and duty cycles.

In Europe, the Euro VI standards for on-road HD vehicles have been brought in by Regulation 595/2009 [25] and implemented by Regulation 582/2011 [26] of the European Parliament and the Council of the European Union (EU). Further amendments are contained in Regulation 133/2014 [27]. European manufacturers have been required to ensure compliance with the Euro VI emission limits depicted in Table 2.1 since 2013 for new type-approvals and 2014 for all registrations [28].

The limitation of tailpipe emissions for EU's compression (CI) and positive ignition (PI) engines must be guaranteed under the World Harmonized Transient Driving Cycle (WHTC) and the World Harmonised Steady state Cycle (WHSC) specified in Regulation No 49 [29]. A limit was also set for ammonia (NH_3) in order to control excess injection of aqueous urea solution into the exhaust stream, which is often used for NOx reduction in Selective Catalytic Reduction (SCR) aftertreatment systems [30]. Moreover, the EU is setting up a system for monitoring and reporting CO_2 emissions and fuel consumption of

HD vehicles [31]. Other countries like Canada, China, Japan, and United States (US) have already defined their GHG/fuel efficiency standards [20,32].

Table 2.1 – Euro VI emission limits for different on-road HD engines and vehicles. Source: Regulation No 49 [27].

Pollutant	Unit	WHSC (CI)	WHTC (CI)	WHTC (PI)
Nitrogen oxides (NOx)	g/kWh	0.40	0.46	0.46
Carbon monoxide (CO)	g/kWh	1.50	4.00	4.00
Total unburnt hydrocarbons (HC)	g/kWh	0.13	0.16	n/a
Non-methane hydrocarbons (NMHC)	g/kWh	n/a	n/a	0.16
Methane (CH_4)	g/kWh	n/a	n/a	0.50
Particulate matter (PM) mass	g/kWh	0.010	0.010	0.010
Particulate number (PN)	#/kWh	$8.0x10^{11}$	$6.0x10^{11}$	$6.0x10^{11}$
Ammonia (NH_3)	ppm	10	10	10

In the US, the National Highway Traffic Safety Administration (NHTSA) and Environmental Protection Agency (EPA) have been defining the legal framework for type-approval of motor vehicles with respect to their fuel consumption and emission performance. The Phase 2 program [33] builds upon the initial Phase 1 [34] that have covered model years 2014 to 2018. The regulations encourage the development of new and advanced cost-effective technologies to improve fuel efficiency and reduce GHG emissions of medium- and heavy-duty vehicles in model years through 2027.

EPA's CO_2 emission limits and NHTSA's fuel consumption standards are defined for four categories of on-road HD vehicles: (1) combination tractors; (2) trailers pulled by combination tractors; (3) heavy-duty pickup trucks and vans; and (4) vocational vehicles, which include buses, refuse trucks, and cement mixers. Testing must be conducted over a ramped-modal steady state cycle called Supplemental Emissions Test (SET) and a transient cycle called Federal Test Procedure (FTP) [33]. The weighting factors for the test points of the SET cycle are identical to those of the European Stationary Cycle (ESC13) [35] and should be used for the purpose of pollutant emission testing. An additional set of weighting factors was introduced by the Phase 2 program to address the effect of engine down-speeding on CO_2 emissions, as manufacturers are configuring drivetrains to operate at lower speeds to reduce friction losses.

By 2027, Phase 2 requirements for HD diesel engines will bring up 5% reduction in CO_2 emissions and fuel consumption compared to a baseline model year 2017 [36]. The CO_2 emissions limit from heavy heavy-duty (HHD) engines installed in Class 8 tractors will be reduced from 616.9 g/kWh to 579.3 g/kWh over the SET cycle. This will result in 12% improvement relative to the 657.1 g/kWh from 2010 HHD engines [34].

Limits for non-CO_2 GHG emissions such as CH_4 and nitrous oxide (N_2O) have also been applied for model year 2014 and later compression ignition engines [33,34]. This is a result of the high global warming potential (GWP) of CH_4 and N_2O, which are equivalent to 25 and 298 times that of CO_2 over a 100 year lifetime [37,38]. N_2O emissions can be produced in urea SCR systems during periods of warm-up [34].

Table 2.2 shows the emission standards for CH_4 and N_2O as well as for other pollutants from HD engines set by the US EPA 40 CFR 86.007-11 for new 2007 and later models [39]. US NOx limit is lower but soot and CO emissions are more flexible than those of the Euro VI regulation.

Table 2.2 – Current US EPA emission limits for on-road HD engines and vehicles. Source: Phase 2 program [33] and 40 CFR 86.007-11 [39].

Pollutant	Unit	SET cycle	FTP cycle
Nitrogen oxides (NOx)	g/kWh	0.27	0.27
Carbon monoxide (CO)	g/kWh	20.79	20.79
Non-methane hydrocarbons (NMHC)	g/kWh	0.19	0.19
Methane (CH_4)	g/kWh	n/a	0.134
Particulate matter (PM) mass	g/kWh	0.013	0.013
Nitrous oxide (N_2O)	g/kWh	n/a	0.134

2.3 Heavy-duty engine and vehicle technologies

To help meet the standards over transient cycles, HD vehicle manufacturers have been improving internal combustion engine, transmission, driveline, and aerodynamic design [33]. Moreover, low rolling resistance tires, idle management, and other accessory/electrification technologies are likely to be introduced to the HD sector [33,36,40]. Engine down-speeding and down-sizing might be required as a result of the changes in vehicles load capacity, total weight, and frontal area.

HD vehicles are highly dependent on diesel engines due to their high torque capability, reliability, as well as superior fuel conversion efficiency [41]. Manufacturers are incorporating new engine design elements and in-cylinder strategies to achieve GHG reduction targets and comply with emission standards.

Some examples of improvements and technologies introduced to HD diesel engines are high efficiency turbocharging and air handling, flexible diesel injection capability with higher injection pressures, combustion optimisation, variable valve actuation, cooled exhaust gas recirculation (EGR), increased peak in-cylinder pressure limit, waste heat recovery (e.g. turbo-compound and Rankine-cycle), friction reduction, and reduced parasitic loads [30,31,33,36,42–44].

To some extent, the combination of in-cylinder measures like high diesel injection pressure, improved air management, and EGR can simultaneously reduce emissions and improve thermal efficiency through better fuel-air mixing and lower combustion temperatures [7]. Nevertheless, there is special concern over future HD engine efficiency standards due to a strong trade-off between fuel consumption and engine-out NOx emissions. A fuel efficiency improvement of 1% could increase the levels of NOx from 10 g/kWh to 14 g/kWh [42]. On the other hand, very low engine-out NOx emissions can adversely affect the engine performance and lead to excessive PM (e.g. soot) due the different formation mechanisms [45,46].

Despite the benefits of new in-cylinder control strategies and vehicle technologies, additional pollutant and fuel consumption reductions require the incorporation of exhaust aftertreatment devices to help control the levels of pollutants from the exhaust gas stream [46].

2.4 Exhaust aftertreatment technologies

Costly aftertreatment systems have been widely used in HD engines to meet stringent emission regulations [30] and optimise the trade-off between pollutants and overall fuel efficiency (e.g. total fluid consumption) [24,45]. These technologies have been combined with advanced engine management strategies and vehicle modifications, as described in the previous section.

The primary aftertreatment technologies installed in modern HD diesel engines are diesel oxidation catalyst (DOC), diesel particulate filter (DPF), and SCR system [47]. Figure 2.5 shows an example of an aftertreatment system, highlighting the exhaust gas flow and the main chemical reactions that occur in each device.

The reduction of engine-out PM is achieved by means of wall-flow filtration in the DPF, as soot accumulates in a ceramic honeycomb monolith. The device requires periodical "active" and/or "passive" regeneration to burn off the trapped soot and prevent it from blocking [48]. The DOC oxidises hydrocarbons, carbon monoxide, and organic fractions of PM produced by incomplete combustion and fuel injected into the exhaust gas during "active" DPF regeneration. Depending on the engine-out NOx to PM ratio, a "passive" filter cleaning process is achieved through the heat and NO_2 produced by the engine and chemical reactions in the DOC [40,47].

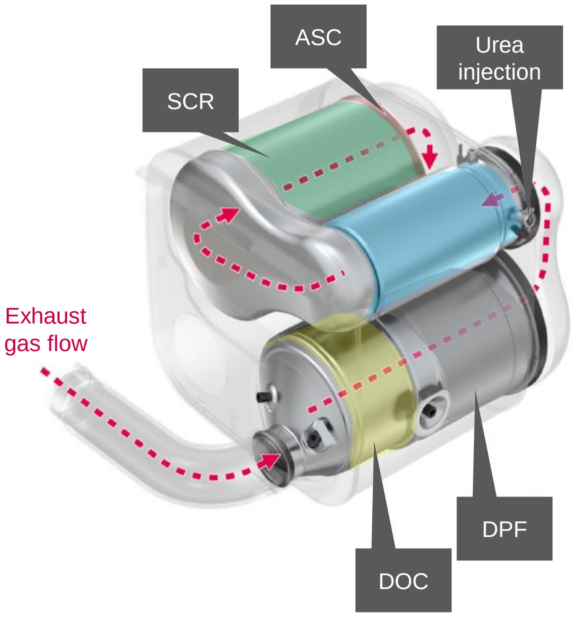

Diesel oxidation catalyst (DOC)

$2\ NO + O_2 \rightarrow 2\ NO_2$
$2\ CO + O_2 \rightarrow 2\ CO_2$
$C_nH_{2m} + (n + m/2)\ O_2 \rightarrow n\ CO_2 + m\ H_2O$

Diesel particulate filter (DPF)

$C + 2\ NO_2 \rightarrow CO_2 + 2\ NO_2$
$C + O_2 \rightarrow CO_2$
$2\ NO + O_2 \rightarrow 2\ NO_2$

Selective catalytic reduction (SCR)

$4\ NH_3 + 4\ NO + O_2 \rightarrow 4\ N_2 + 6\ H_2O$
$2\ NH_3 + NO + NO_2 \rightarrow 2\ N_2 + 3\ H_2O$

Ammonia slip catalyst (ASC)

$4\ NH_3 + 5\ O_2 \rightarrow 4\ NO + 6\ H_2O$
$4\ NH_3 + 4\ NO + O_2 \rightarrow 4\ N_2 + 6\ H_2O$

Figure 2.5 – Exhaust gas flow and chemical reactions in the aftertreatment system of a modern HD diesel engine. Adapted from [49].

The SCR system is typically composed of an SCR catalyst, a reducing agent injection system, NOx sensors, and ammonia slip catalyst (ASC) [30]. The reducing agent is a mixture of 32.5% of urea ($CO(NH_2)_2$) in demineralised water, which is marketed under the names 'AdBlue' in Europe and 'diesel exhaust fluid' (DEF) in North America. The urea converts to NH_3 and CO_2 in the exhaust stream at temperatures above 573 K [48,50]. The NH_3 reacts with NOx over the SCR catalyst to form harmless nitrogen gas (N_2) and water vapour (H_2O).

The consumption of aqueous urea solution in the SCR system typically ranges between 2% and 5% of the diesel fuel use [10,48,51,52], which adversely affects the total cost of ownership. The ASC removes traces of NH_3 slip via oxidation, leading to the formation of N_2, NO, and N_2O [52]. The only products desired downstream of the SCR system are N_2 and H_2O.

Recent research have been focused on reduced pressure drop across exhaust aftertreatment system, increased NOx conversion efficiency, and lower NH_3 and N_2O slip [53,54]. Studies have also been exploring the SCR catalyst properties, such as volume, effective temperature range, thermal stability, exhaust NO_2 to NOx ratio sensitivity, N_2O emissions, and sulphur tolerance [30,47]. These characteristics vary significantly with the catalytic coating applied to the SCR honeycomb substrate. Moreover, the use of cooled EGR along with an SCR catalyst have been investigated to minimise aqueous urea solution consumption in the SCR system and reduce the NOx conversion efficiency requirements [3,46,55]. Further investigation is required to improve the effectiveness of the SCR system under relatively low temperature conditions [33,50], such as engine start-stops and low load operation.

2.5 Alternative combustion strategies

Conventional diesel combustion (CDC) usually occurs with excess of air, resulting in an overall lean engine operation. However, the diesel combustion process incurs a wide range of local in-cylinder fuel/air equivalence ratio and temperature [56,57]. NOx is mainly formed in near-stoichiometric high temperatures regions close to the diffusion flame [58]. Soot formation occurs in high fuel/air equivalence ratio and intermediate temperature zones within the diesel spray [41,59].

Several alternative combustion technologies have been developed to optimise the combustion process, arising from costly aftertreatment systems and stringent fuel efficiency and emissions regulations [60]. These combustion concepts are generally centred on lower local fuel/air equivalence ratios and reduced combustion temperatures to avoid in-cylinder conditions that can lead to NOx and soot formation, as shown in Figure 2.6. This is usually referred to as Low Temperature Combustion (LTC) [60].

Among the LTC strategies proposed is Homogeneous Charge Compression Ignition (HCCI), which is characterised by early fuel injections promoting a fully premixed charge, long ignition delays, and short combustion durations. However, the lack of direct control of ignition timing and combustion phasing, particularly under transient conditions, is still the major drawback. It also exhibits elevated combustion losses, combustion noise, and sensitivity to temperature [61–63].

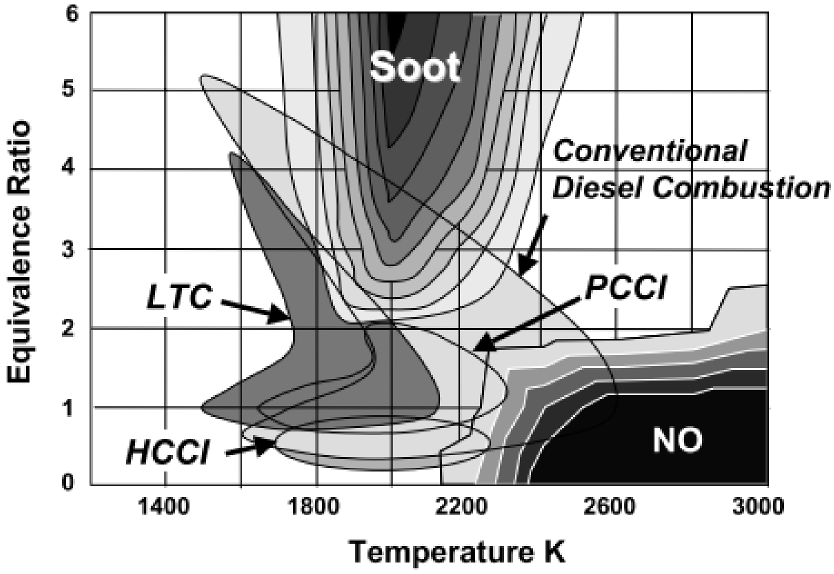

Figure 2.6 – Theoretical in-cylinder fuel/air equivalence ratio versus temperature range for CDC and LTC strategies such as HCCI and PPCI. The grey-scale areas represent approximate soot and NOx formation regions. Adapted from [64]

In comparison, some slightly more heterogeneous combustion concepts have been developed. Premixed Charge Compression Ignition (PCCI) [65,64,66,67], Partially Premixed Charge Compression Ignition (PPCI) [58], Modulated Kinetics (MK) [68], and Uniform Bulky Combustion System (UNIBUS) [69] name a few. These allow a higher degree of combustion phasing control at light and medium engine loads while maintaining low soot and NOx emissions. However, these less premixed combustion modes tend to suffer from lower indicated efficiency, increased unburnt HC and CO emissions, and limited load range due to high EGR and boost requirements.

Gasoline Direct Injection Compression Ignition (GDCI) [70,71] and Partially Premixed Combustion (PPC) [72–74] are some alternatives to diesel LTC. They expand the high efficiency window and achieve very low NOx emissions operating up to full load with moderate-high EGR rates. As these concepts utilise gasoline, they do not reduce the dependence on liquid fossil fuels. They also require engine hardware modifications such as different piston and injection system, and ignition or lubricant improvers depending on the fuel selected. Some drawbacks regarding soot levels at higher loads accompanied with high CO and HC emissions at low loads were also reported [74].

Recent PPC studies with renewable fuels, including ethanol, have demonstrated high thermal efficiency and soot reductions [75–77]. However, high acoustic noise and elevated peak heat release rates have been experienced due to a fast premixed combustion. This required the use of lower intake air pressures and larger amounts of EGR, which reduced combustion efficiency [78].

Alternatively, the dual-fuel combustion strategy has been developed to overcome the majority of the previously mentioned issues [79–81] and has been demonstrated as an effective means of utilising alternative low carbon fuels in conventional diesel engines [41].

2.6 Dual-fuel engine operation

The dual-fuel operation can be achieved by the installation of a low cost port fuel injection system in the intake manifold for the formation of a low reactivity mixture of air and fuel, such as NG, gasoline, or ethanol [79]. The stock diesel combustion and fuel injection systems can be retained in the dual-fuel engine. Direct injected diesel fuel usually serves as the ignition source for the premixed charge [82]. Once the right conditions for compression ignition (i.e. temperature and pressure) are achieved, the ignition of the more reactive fuel occurs and the charge is sequentially consumed from the more to the less reactive zones [41]. Fuel properties as well as variations in the diesel injection timing and substitution ratio (e.g. energy fraction of each fuel) can change the dual-fuel combustion characteristics, emissions, and efficiency.

2.6.1 Potential of the dual-fuel operation

Optimised dual-fuel combustion allows for better mixture preparation and lower NOx and soot emissions than CDC [5–7]. In particular, significant soot reduction can be achieved at elevated EGR rates [83,84]. Improvements in efficiency are also achievable [3,6,85] as a result of lower heat transfer losses introduced by reduced combustion temperatures and shorter burn duration [57].

Studies have also demonstrated the potential of a dual-fuel LTC combustion referred to as Reactivity Controlled Compression Ignition (RCCI) to achieve ultra-low NOx and soot emissions and increase engine efficiency [57,79,80,86]. The RCCI combustion relies on the in-cylinder fuel blending to generate fuel reactivity gradients that result in control over the combustion event [57,87,88]. Early diesel injections and high levels of EGR are often employed. The drawback of RCCI combustion is the high sensitivity to variations in the intake air temperature and pressure, as the strategy is sufficiently premixed and governed by chemical kinetics [79]. Nevertheless, dual-fuel engine operation can represent a more cost-effective solution to achieve emissions compliance and high efficiency targets than diesel-only combustion and conventional LTC strategies. Moreover, the partial substitution of diesel by low carbon fuels such as ethanol and NG can minimise CO_2 emissions while diversifying the fuel energy supply.

2.6.2 Limitations of the dual-fuel operation at low engine loads

Relatively high levels of CO and unburnt HC emissions are usually reported at low loads of less than 25% of the full load torque [89–93]. This is a result of non-uniform mixing and lower local combustion temperatures [88]. Kokjohn et al. [57] performed computational fluid dynamics modelling to show that unburnt HC and CO are typically found in the centre of the combustion chamber as well as in the crevice and liner regions, as shown in Figure 2.7.

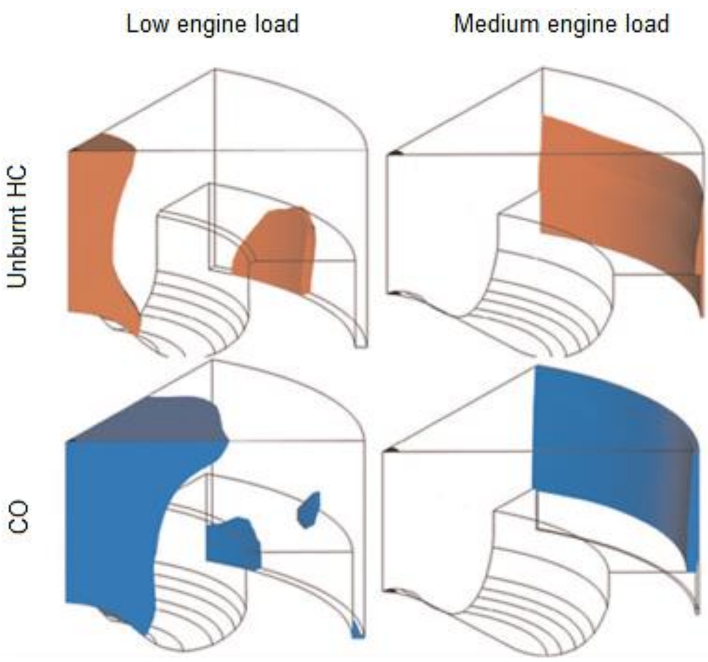

Figure 2.7 – Iso-volumes of unburnt HC and CO at concentrations greater than 4000 ppm for low and mid-load dual-fuel operation at 40 crank angle degrees (CAD) after firing top dead centre (ATDC). Adapted from [57].

The non-conversion of fuel combined with a fast heat release can lead to relatively low charge temperature later in the cycle. If the resulting exhaust gas temperature (EGT) is not high enough, the effectiveness of the DOC may be compromised [94]. Split diesel injections can be adopted to help enhance the mixture preparation and accelerate the occurrence of autoignition in high reactivity zones, minimising the combustion losses [6,7].

In addition, improvements in combustion efficiency [88] and elevation of the EGT [88,95] can be influenced by the intake charge temperature. However, rapid temperature increase of the inlet mixture may not be feasible in real world applications, particularly during cold start and transient operating conditions.

Higher fuel/air equivalence ratios achieved via intake throttling also showed potential to increase EGT at the expense of higher fuel consumption and NOx emissions [96]. These drawbacks can be attributed to higher peak combustion temperatures and elevated heat transfer losses [97].

Other effective means for increasing in-cylinder and exhaust gas temperatures is to retain hot residuals from the previous cycle [5]. This strategy is generally called internal exhaust gas recirculation (iEGR) [98]. The residual gas fraction (RGF) can be defined as the burnt gas mass divided by the total in-cylinder mass (burnt and unburnt) prior to the start of combustion (i.e. at intake valve closing).

The amount of exhaust gas trapped inside the cylinder depends on factors such as the valve timing, engine speed, and pressure differentials [8]. Means of adjusting the RGF generally rely on mechanisms such as two-stage cam-lift [98–100], camshaft phasing [101], variable valve actuation [102–106], and fully variable valve actuation [107–109]. There are several valve timing strategies utilised to aid the combustion process and consequently the aftertreatment system, including:

- Early exhaust valve opening (EEVO). This approach increases the EGT and reduces the catalyst light-off time, enhancing the CO and unburnt HC conversion in the oxidation catalyst [110]. However, the utilisation of EEVO results in lower engine efficiency due to the reduction in the effective expansion ratio and the higher fuelling needed to maintain the load output [109,111].

- Exhaust valve re-opening (2EVO) or rebreathing during the intake stroke. This strategy allows for the return of the burnt gases from the exhaust manifold into the combustion chamber. The utilisation of a 2EVO can help the autoignition of the in-cylinder charge and to achieve the catalyst light-off temperature [99]. Improvements in thermal efficiency and combustion efficiency were also reported as a result of a more appropriate combustion phasing [106]. The drawbacks of the 2EVO strategy are the reduction of the intake air flow rate and influence on in-cylinder mixture motion [112], as well as the increase of RGF and temperature stratification, which can shorten the ignition delay and increase NOx and soot emissions [113].

- Intake valve re-opening (2IVO) or rebreathing during the exhaust stroke. In this case, residuals are pushed into the intake port and re-inducted into the cylinder during the intake stroke [114]. A 2IVO strategy may result in relatively colder and higher RGF than a 2EVO strategy, further reducing NOx emissions [100] while lowering CO and HC emissions [113].

- Negative valve overlap (NVO). This strategy typically relies on a symmetrical interval to firing top dead centre (TDC) from an early exhaust valve closing (EEVC) to a late intake valve opening (LIVO). The EEVC increases the RGF and the in-cylinder gas temperature by reducing the scavenging process [104]. The use of NVO can result in lower net indicated efficiency due to higher heat transfer losses during the recompressions and reduced gas exchange efficiency compared to the 2EVO strategy [108].

Therefore, more research is required to simultaneously maximise fuel conversion efficiency, reduce overall emissions, and increase EGTs of low load dual-fuel operation.

2.6.3 Limitations of the dual-fuel operation at mid-loads

Experimental analyses on mid-load dual-fuel combustion have been performed with constant combustion phasing [90,115] or fixed diesel injection timing [116], resulting in non-optimised engine efficiency and exhaust emissions. It is important to note that mid-loads were defined as the region of the engine map between 25% and 75% of the full load torque.

The use of a constant start of injection can lead to over-retarded dual-fuel combustion and misfiring at high substitution ratios [117]. Non-optimised diesel injection timings can also limit the premixed fuel fraction as a result of high pressure rise rates, as shown in the experimental work of Sarjovaara and Larmi [118]. The authors reported the autoignition of a mixture of 85% ethanol content in gasoline (E85) during the premixed combustion phase, which increased the in-cylinder pressure rise rates (PRR) and limited the maximum E85 energy fraction to 0.34. This was possibly driven by the high intake air temperatures. Further investigations at the same load [95] revealed that lower charge temperatures can minimise the autoignition of the premixed fuel and delay the combustion phasing, allowing for the use of a higher E85 fraction of 0.74.

Another means of reducing excessive PPR and extending the operating range for dual-fuel combustion is the introduction of large amounts of EGR into the engine [89,90]. However, high EGR rates might not be practical due to a great demand (e.g. high pressure ratio) on the boosting system to maintain a reasonable air/fuel ratio and avoid excessive smoke as well as fuel efficiency penalty. Additionally, the maximum EGR rate and boost pressure are limited by the peak in-cylinder pressure of the engine [119].

In an attempt to decrease the EGR requirements, Asad et al. [120] demonstrated that ethanol fuel can be used in place of EGR to reduce NOx emissions for diesel LTC operation. Moreover, Hanson et al. [55] revealed that relatively low EGR rates can still reduce NOx emissions while minimising the consumption of aqueous urea solution in the SCR system and the impact on efficiency of a natural gas-diesel dual-fuel engine.

Thus, optimisation of the dual-fuel combustion using lower diesel energy fractions, optimum injection timings, and reduced EGR rates is needed to balance out NOx reduction capability, PRR, and running costs of SCR equipped vehicles.

2.6.4 Limitations of the dual-fuel operation at high engine loads

Dual-fuel engine operation at high load conditions (e.g. more than 75% of the full load torque) have been proved extremely challenging due to peak in-cylinder pressure [121] and/or PRR limitations [122,123]. As a result, the amount of low reactivity fuel injected is restricted to very low percentages. A number of studies have investigated combustion control strategies to allow for high load dual-fuel operation, such as the Direct Dual Fuel Stratification (DDFS) [124–126] and dual-fuel LTC [83,90,127–129].

DDFS and dual-fuel LTC often require relatively complex engine hardware modifications and/or high levels of EGR and boost pressure. The later can increase fuel consumption if higher pressure differential is needed across the cylinder to drive the requested amounts of EGR. Consequently, the dual-fuel combustion benefits might be partially or completely lost in comparison with optimised CDC operation.

Experimental research has also focused on the use of a lower compression ratio than the stock diesel combustion system to decrease the in-cylinder gas pressure and temperature during the compression stroke [85,130]. This delays the ignition of the fuel and allows for longer fuel-air mixing process.

The reduction in the compression ratio is typically attained via a modified piston [86]. High load gasoline-diesel dual-fuel combustion has been achieved on a medium-duty diesel engine using a piston with a lower geometric compression ratio (GCR) of 12.75:1 [131]. Despite the improvement, it is unlikely simultaneous high levels of boost pressure and EGR can be attained at a low intake charge temperature of 293 K in a production engine. In addition, experiments and computational optimisations performed on a HD engine with a GCR of 12:1 showed that controlling the dual-fuel combustion process at high loads can be quite demanding due to the sensitivity to fluctuations in the EGR rate [132]. Furthermore, the introduction of a low GCR piston can impair the efficiency of the dual-fuel engine at light load conditions [131].

Alternatively, the effective compression ratio (ECR) can be varied via an earlier or later intake valve closing event while retaining the stock piston and compression ratio. The strategy is commonly known as Miller cycle and also reduces the in-cylinder charge temperature at the end of the compression stroke [133,134]. The approach allows for a more flexible combustion control if the valve timings can be varied according to the engine operating condition. However, Miller cycle decreases the in-cylinder mass trapped at a constant intake manifold air pressure, which can result in higher average combustion temperatures, increased heat transfer losses, and lower cycle efficiency [135].

Previous research with an early intake valve closing (EIVC) strategy showed that gasoline-diesel dual-fuel combustion can be used over the entire engine speed-load map while maintaining the NOx emissions below 0.4 g/kWh [130]. The maximum engine load was increased from 1.2 MPa to 2.2 MPa break mean effective pressure (BMEP) when the ECR was reduced from 14.4:1 to 11:1, although the study relied on the use of high EGR rates. This likely placed a greater demand on the boosting system in order to supply enough air for lean and efficient engine operation.

The introduction of premixed fuels with high knock resistance such as ethanol and NG potentially allows for the use of relatively higher GCR/ECRs as well as lower EGR and boost requirements. The substitution of gasoline for E85 extended the dual-fuel operating range from 1.16 MPa to 1.9 MPa BMEP [136]. This was accomplished on a HD diesel engine with a GCR of 14:1 using an E85 mass fraction of 0.90 and an EGR rate of 41%. Goldsworthy [122] fumigated wet ethanol mixtures on a HD diesel engine with a GCR of 17.2:1. In this case, the experiments were carried out without EGR at high loads of 1.7 and 2.0 MPa BMEP. However, wet ethanol energy fractions were limited to approximately 0.30 due to rapid premixed combustion and excessive PRRs. Similarly, Hanson et al. [137] achieved 2.2 MPa BMEP on a HD diesel engine with a GCR higher than 17:1 using a NG mass fraction of 0.29 without the need for EGR.

This review of high load dual-fuel operation shows that further investigation is necessary to maximise the use of low carbon fuels while minimising EGR requirements and fuel efficiency penalty.

2.7 Ethanol as an alternative fuel

Diesel fuel is likely to continue dominating as primary energy source for the HD sector as a result of the high energy density, which allows for long range and rapid refuelling. However, economic growth projections have been predicting an increase in the demand for petroleum and other energy sources [138]. This may result in elevated prices for liquid fossil fuels and compromise their cost competitiveness, opening opportunities for improved sustainability and GHG emissions reduction via biofuels [139].

Biofuels are gaseous or liquid fuels produced from biomass, which is the biodegradable fraction of municipal and industrial waste as well as products, waste, and residues from agriculture, forestry, and related industries [140]. The energy and GHG emissions savings are heavily dependent on the fuel production process. The use of co-products for energy generation can minimise the actual levels of CO_2, although N_2O emissions from agriculture can impair the GHG balance.

The Joint Research Centre (JCR) of the European Commission, European Council for Automotive R&D (EUCAR), and CONCAWE consortium [141,142] estimated the energy use and GHG emissions in the production of a fuel and its use in a vehicle. Slightly different levels of GHGs is specified in the Directive 2009/28/EC of the European Parliament and the Council of the European Union [143]. Nevertheless, ethanol produced from sugar cane results in lower overall carbon footprint when compared against the life cycle GHG intensity of fossil fuels specified in Directive 2015/652 [144].

The carbon intensity calculation includes the overall GHG emissions associated with the CO_2, CH_4, and N_2O emitted during the extraction or cultivation of raw materials, processing, transport, and distribution of fuels. The resulting GHG emissions are expressed as grams of CO_2 equivalent (CO_{2eq}) emissions per MJ of fuel (g/MJ) due to the different GWP for CH_4 and N_2O compounds, as described in Section 2.2.

The impact of indirect land-use change (iLUC) can also be considered in the overall GHG emissions calculation, given that current biofuels are usually produced from crops grown on existing agricultural land [145]. The diversion of agricultural land and pasture previously destined for the food and feed markets to the production of biofuels might result in the use of non-agricultural land. This change occurs when the intensification of the current production is not sufficient to satisfy the non-fuel demand. However, cautiousness is needed as the levels of GHG associated with iLUC are estimated using modelling and can vary significantly depending on the data input into the calculation, as reported by the International Food Policy Research Institute (IFPRI) [146].

Other than the CO_{2eq} and iLUC analysis, the well-to-wheels (WTW) analysis is often used to examine the energy use and emissions associated with fuel production and distribution (well-to-tank) as well as those linked to vehicle operation (tank-to-wheels). The WTW analysis typically excludes the CO_2 emitted when burning biofuels, as these emissions can be absorbed by the crops during photosynthesis [141].

Figure 2.8 shows that ethanol produced by fermentation of sugar cane provides low overall CO_{2eq} emissions, being significantly less carbon intensive than fossil diesel fuel. Ethanol produced from wheat straw, biodiesel from waste vegetable or animal oil, as well as biogas from wet manure allow for the highest CO_{2eq} emissions savings with low risk of causing iLUC. The WTW analysis revealed that the use of biodiesel produced from soybean is likely to result in higher GHG emissions than those of the fossil fuel baseline.

2.8 The use of ethanol in internal combustion engines

Despite the GHG emissions reduction, the use of a low carbon fuel in IC engines is coupled with the availability of its feedstock, the complexity of the production process, and distribution infrastructure. It is also linked with the global oil price [138] and development and implementation of advanced combustion technologies [147].

Blending mandates, supply obligations, emission legislations, and financial incentives act as drivers for the rapid growth in the use of such fuels [148]. In the EU, biofuels can be blended with conventional fuels in small fractions, such as 10% of ethanol in gasoline [149]. Spark ignition (SI) engines compatible with E85 are already available in Sweden, France, Germany, and the Netherlands [147]. In the United States, ethanol is blended with gasoline to make E10, which is comprised of 10% ethanol and 90% gasoline in a volume basis (v/v). E85 has also been utilised in US, but is not as widespread in its use [150].

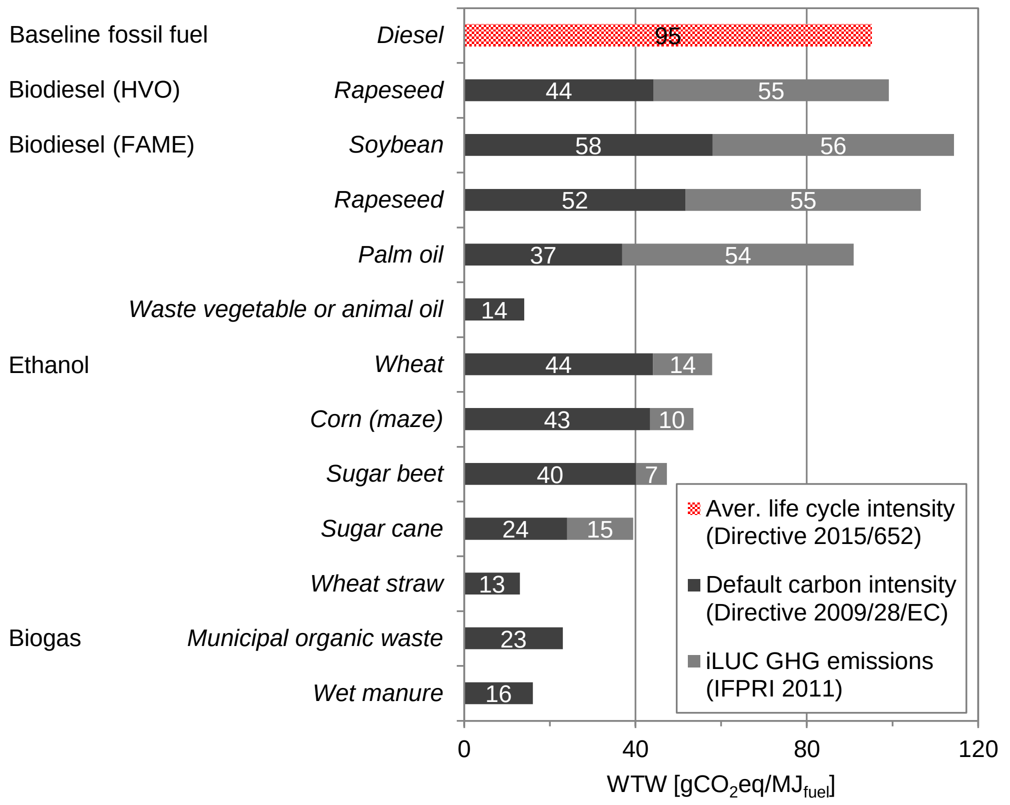

Figure 2.8 – CO_{2eq} emissions for different biofuels. HVO is hydrotreated vegetable oil and FAME is fatty acid methyl ester. Adapted from [151]. Sources: Directive 2009/28/EC [143], Directive 2015/652 [144], and IFPRI [146].

In particular, bioethanol is widely available in Brazil as the country is second largest producer, behind the US [152]. As a result, approximately 88% of all new light-duty vehicles are powered by SI flexible-fuel engines [153]. The technology allows the engine to operate either on hydrous ethanol containing up to 5.5% v/v of water [154], on gasoline with 27% of anhydrous ethanol [155], or on any mixture of them in between.

The high knock resistance of ethanol allows for the development of IC engines with higher compression ratios as well as the use of increased boost pressures [133]. Ethanol also has a higher latent heat of vaporisation than gasoline and diesel [8], which can help reduce the in-cylinder charge temperature and possibly NOx emissions. Moreover, early dual-fuel research in an optical engine showed that ethanol can suppress soot formation in high temperature regions of the conventional diesel combustion chamber [156].

The downside of ethanol is the lower heating value of 26.9 MJ/kg, which is equivalent to approximately 62% of the gasoline and diesel energy contents [8]. The lower energy density increases the volumetric fuel consumption and can impact the engine operational cost depending on fuel prices [3].

Studies have been exploring the effects of wet ethanol in different IC engines, as high water content ethanol can potentially minimise the fuel production costs [122,157–163]. This is attributed to a reduction in the energy spent for the distillation and dehydration phases of anhydrous ethanol, allowing for higher net energy efficiency and lower carbon footprint [164,165]. Researchers have demonstrated successful use of wet ethanol in conventional SI engines [157–159] as well as in HCCI engines with high intake air temperatures [160,161]. Recent wet ethanol research has also been conducted on dual-fuel engines [122,162,163], revealing potential NOx reduction and efficiency advantages.

2.9 Summary

This chapter revealed that changes in climate and higher levels of air pollution require a cleaner and more sustainable transport sector. This can be achieved through the development of high efficiency vehicles and use of low carbon fuels. Heavy-duty diesel engine and vehicle technologies implemented to meet stringent exhaust emission and fuel consumption regulations have been described. Alternative combustion strategies used to simultaneously reduce exhaust emissions and increase the fuel conversion efficiency have been presented.

The primary pros and cons of dual-fuel engines were accessed while the potential GHG emissions reduction promoted by biofuels has been discussed. Overall, ethanol-diesel dual-fuel combustion can help reduce the transport sector’s carbon footprint as well as minimise petroleum dependency. However, research and development works are needed to identify engine control techniques and optimise the combustion process to overcome the challenges encountered by current dual-fuel engines. Further investigations should also assess the effect of dual-fuel operation on total cost of ownership and GHG emissions of heavy-duty diesel engines equipped with complex and costly aftertreatment systems.

Chapter 3

Experimental methodology

3.1 Introduction

This chapter describes the setup of the research engine and test cell facilities. In addition, data acquisition and analysis are presented. Modifications were conducted to the fuel injection system in order to allow for the dual-fuel operation.

3.2 Experimental setup

Figure 3.1 shows a picture of the engine test cell. A battery supplied the current to an electric starter motor in order to initiate the engine operation. The engine speed governor in the engine control unit (ECU) automatically adjusted the diesel flow rate for a fixed load. A Froude Hofmann AG150 eddy current dynamometer (Dyno) was used to absorb the power produced by the engine. A Texcel V4-EC controller adjusted the load by varying the magnetic field generated by coils. The resulting electrical power was dissipated as heat by external cooling water.

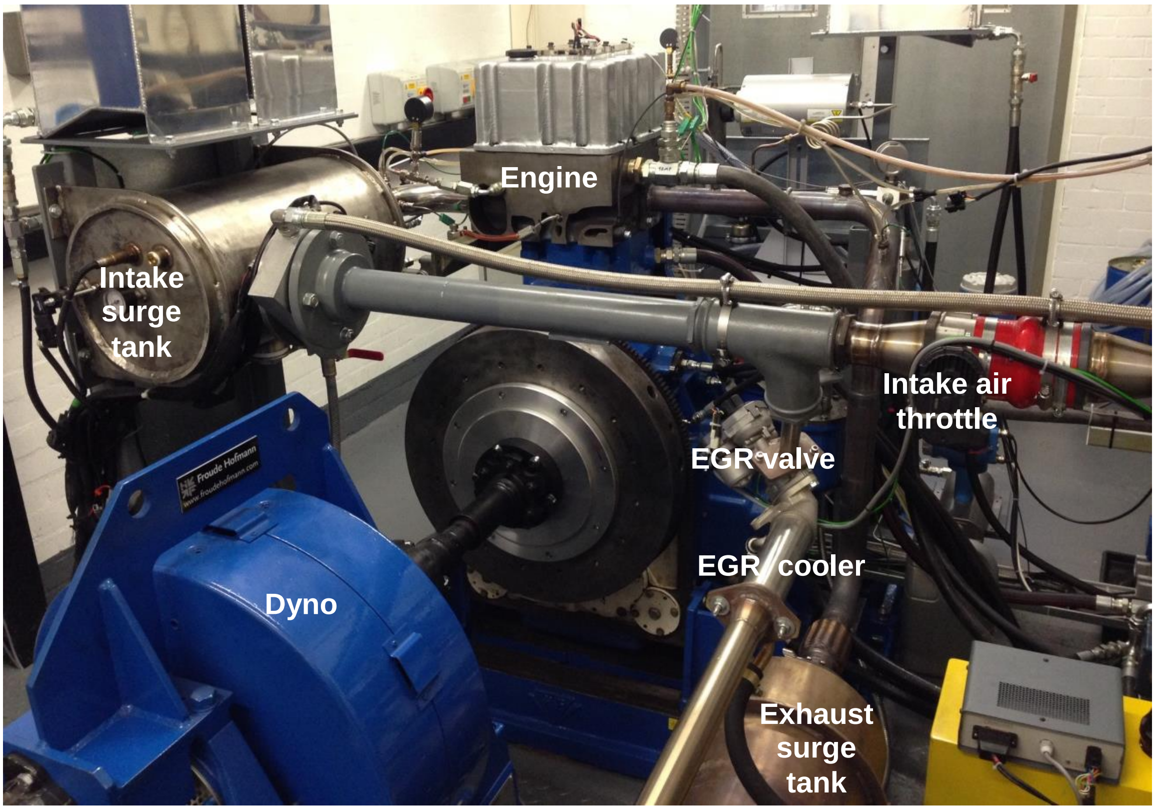

Figure 3.1 – Overview of the engine test bed and experimental facilities.

A schematic diagram of the test cell is depicted in Figure 3.2. Fresh intake air was either naturally aspirated or supplied to the engine via an AVL 515 sliding vanes compressor with a closed loop control for the boost pressure. The compressor can achieve a maximum air flow rate of 300 m^3/h and absolute pressure of 320 kPa. A water-to-air heat exchanger and an electric heater were used to control the intake manifold air temperature.

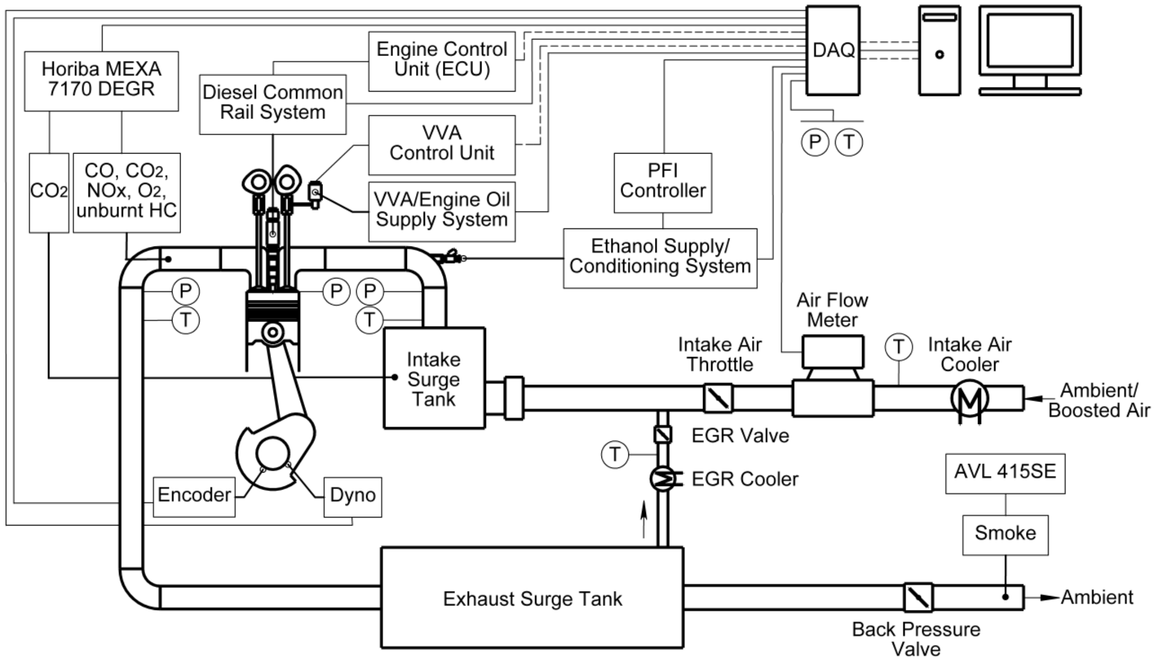

Figure 3.2 – Schematic diagram of the engine experimental setup.

An intake throttle valve located upstream of a 24 dm^3 surge tank provided fine control over the intake manifold air pressure. The fresh air flow rate ($\dot{m}_{air}$) was measured with an Endress+Hauser Proline t-mass 65F thermal mass flow meter. The measuring principle relied on the heat drawn from a heated element when air flow past. A PT100 temperature sensor was used to measure the current gas temperature as a reference. A second sensor was heated to maintain a constant temperature differential relative to the first sensor at the initial condition without air flow. Higher mass flow rates led to greater cooling effect, requiring higher electric current to maintain the temperature differential.

A 54 dm^3 surge tank was installed in the exhaust manifold to damp out pressure fluctuations prior to the EGR circuit. An electronically controlled butterfly valve located downstream of the exhaust surge tank was used to set the required exhaust manifold pressure. In some test conditions, high-pressure loop cooled external EGR was supplied to the engine intake system by an EGR valve.

Coolant and oil pumps were not coupled to the engine and were driven by separate electric motors. Engine coolant and oil temperatures were set to 353 ± 3 K. The oil pressure was held at 450 ± 10 kPa throughout the experiments. External EGR, coolant, and oil temperatures were controlled using water cooled heat exchangers. Measurement device specifications are given in Appendix A.

3.2.1 Engine specifications

The studies were carried out on a single cylinder HD diesel engine, representing the engine of a modern heavy goods vehicle (i.e. long-haul truck). Base hardware specifications are depicted in Table 3.1. The combustion system was composed of a swirl-oriented cylinder head with 2 intake and 2 exhaust valves and a stepped-lip piston bowl design based on the Yuchai YC-6K engine. The bottom end was AVL-designed with two counter-rotating balance shafts.

Table 3.1 – Single cylinder HD diesel engine specifications.

Parameter	Value
Stroke (S)	155 mm
Bore (B)	129 mm
Connecting rod length (l)	256 mm
Crank radius (a)	77.5 mm
Displaced volume (V_d)	2.026 dm^3
Clearance volume (V_c)	0.128 dm^3
Geometric compression ratio (GCR)	16.8:1
Maximum in-cylinder pressure	18 MPa
Piston type	Stepped-lip bowl
Number of valves	4
Intake valve diameter	43.9 mm
Exhaust valve diameter	40.4 mm
Exhaust valve opening (EVO)	144 CAD ATDC (at 0.5mm valve lift)
Exhaust valve closing (EVC)	360 CAD ATDC (at 0.5mm valve lift)
Engine coolant	50% of water and 50% of ethylene-glycol
Engine oil	Comma TransFlow SD 15W-40
Max. continuous operation speed	1900 rpm

The engine is equipped with a prototype lost-motion variable valve actuation (VVA) system on the intake camshaft produced by Jacobs Vehicle Systems. The system incorporates a hydraulic collapsing tappet on the valve side of the rocker arm [105], as shown in Figure 3.3. This enabled the adjustment of the intake valve lift profile via a normally open high-speed solenoid valve assembly and a special intake cam design.

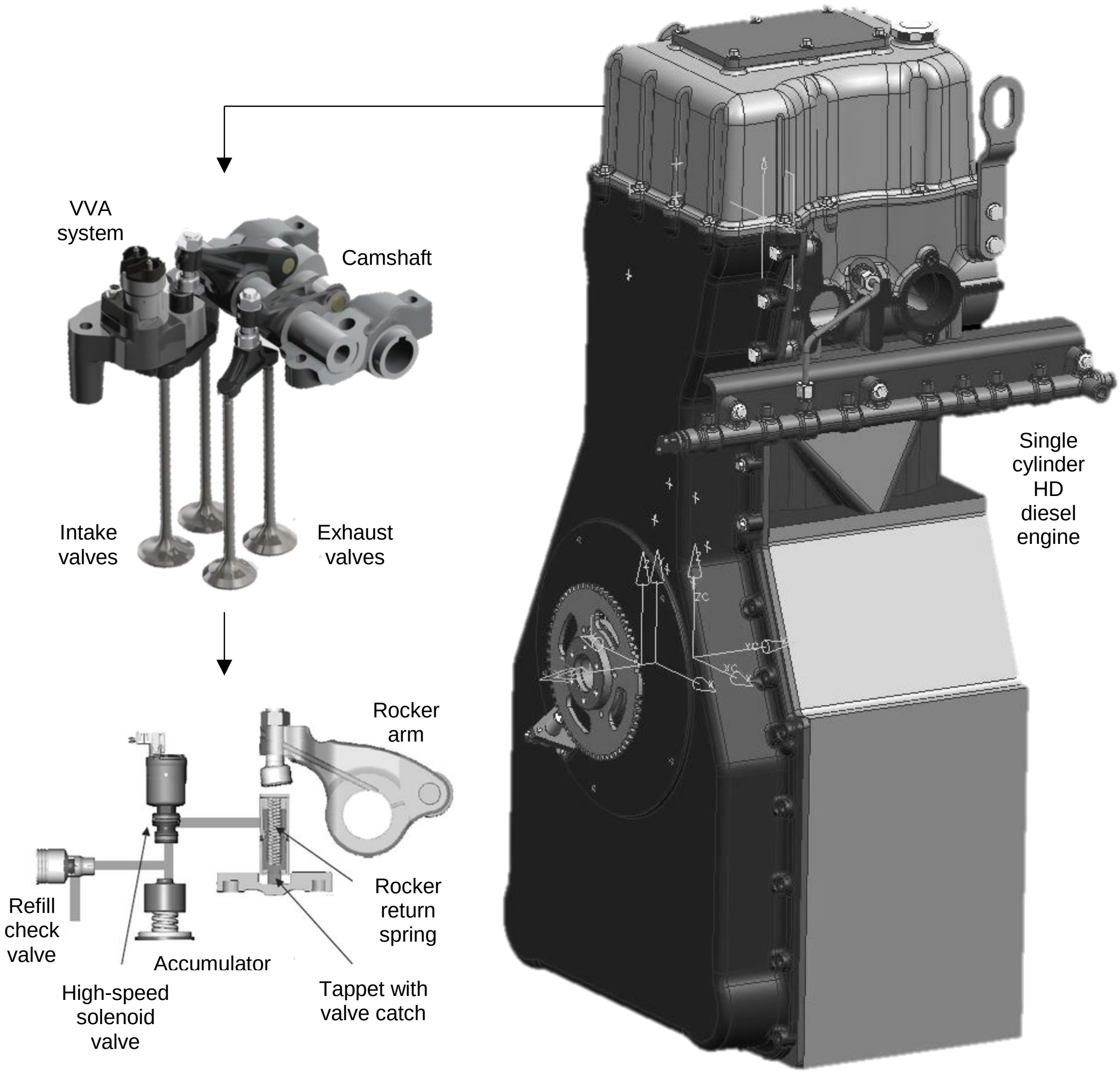

Figure 3.3 – Single cylinder HD diesel engine and the VVA system. Adapted from Schwoerer et al. [105] and Jacobs Vehicle Systems [166].

Figure 3.4 depicts an overview of the variable intake valve lift and fixed exhaust valve lift curves. The VVA system allows for the modification of the effective compression ratio (ECR) via delayed intake valve closing (IVC) events. In addition, an intake valve re-opening (2IVO) strategy can be used during the exhaust stroke for the purposes of introducing iEGR.

Unless otherwise stated, the main intake valve opening (IVO) event was set at 366 ± 1 CAD ATDC, as determined at 0.5mm valve lift. This was necessary in order to minimise the positive overlap period between the intake and exhaust processes, ensuring no premixed fuel was short-circuiting the combustion chamber and ending-up in the exhaust. A mechanical failsafe partial intake valve lift of ~9.6 mm is attained when the system is turned-off or the solenoid valve is held open.

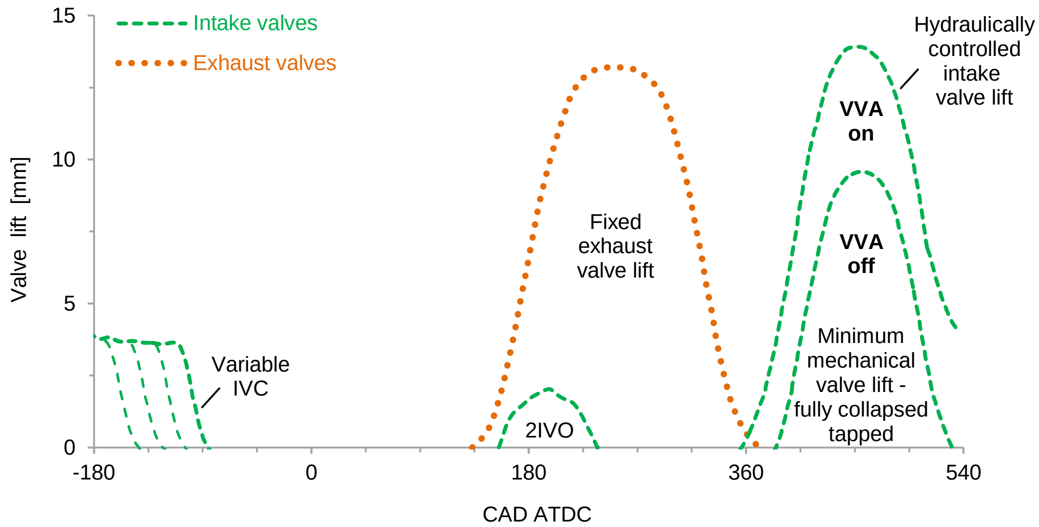

Figure 3.4 – Overview of the variable intake valve lift and fixed exhaust valve lift curves.

3.2.2 Fuel properties and delivery

The relevant properties of the fuel used in this work are listed in Table 3.2. More information can be found in Appendixes B, C, and D. Diesel fuel was supplied to the engine using a Bosch high pressure common rail injection system. The diesel injection characteristics were controlled via a CR.8 ECU supplied by Engine Control Electronics (ECE) GmbH. The communication between the device and a personal computer was performed using ECE's Application Program AP 2.0 and an USB-CAN interface.

Table 3.2 – Fuel properties.

Property	Red diesel (gas oil)	Anhydrous ethanol
Supplier	Advance Fuels	Haymankimia
Product/standard specification	BS 2869 Class A2	Absolute ethanol (F203227)
Density at 293 K (ρ)	0.827 kg/dm^3	0.790 kg/dm^3 [167]
Cetane number	> 45	n/a
Research octane number (RON)	n/a [8]	~107 [8]
Alcohol content	n/a	99.9% (> 99.5%)
Fatty acid methyl ester content	< 7.0%	n/a
Water content	< 0.20 g/kg [29]	1.7 g/kg [167] (< 8.2 g/kg)
Sulphur content	< 0.01 g/kg	n/a
Heat of vaporisation	270 kJ/kg [8]	840 kJ/kg [8]
Carbon mass content ($\%C_{fuel}$)	86.6%	52.1% [8]
Hydrogen mass content ($\%H_{fuel}$)	13.2%	13.1% [8]
Oxygen mass content ($\%O_{fuel}$)	0.2%	34.8% [8]
Normalised molecular composition	$CH_{1.825}O_{0.0014}$	$CH_3O_{0.5}$
Lower heating value (LHV_{fuel})	42.9 MJ/kg	26.9 MJ/kg [8]

Table 3.3 depicts the specifications of the diesel injector while Figure 3.5 shows a schematic diagram of the diesel fuel injection system. Two Endress+Hauser Promass 83A Coriolis flow meters were used to determine the diesel mass flow rate ($\dot{m}_{diesel}$) by measuring the total fuel supplied to and from the diesel high pressure pump and injector. This method reduced the pressure drop across the suction line and improved the consistency of the diesel flow measurements.

Table 3.3 – Diesel injector specifications.

Parameter	Value
Injector	Bosch CRIN3-22 (0446B00482)
Number of holes / Hole diameter	8 holes / 176 µm
Type	Solenoid, mini-sac hole (1x1), ks
Included spray angle	150 degrees
Operating rail pressure	25-220 MPa
Static flow rate	1600 cm^3/min at 10 MPa

The Coriolis principle is based on the oscillation of a measuring tube, through which the fuel flows. Additional twisting (phase shifting) is imposed on this oscillation as the fluid flows through the tube. Two sensors detect changes in time and space, which are proportional to the mass flow. The fuel density is determined from the oscillation frequency of the measuring tubes. The temperature of the measuring tube is also registered to compensate thermal influences.

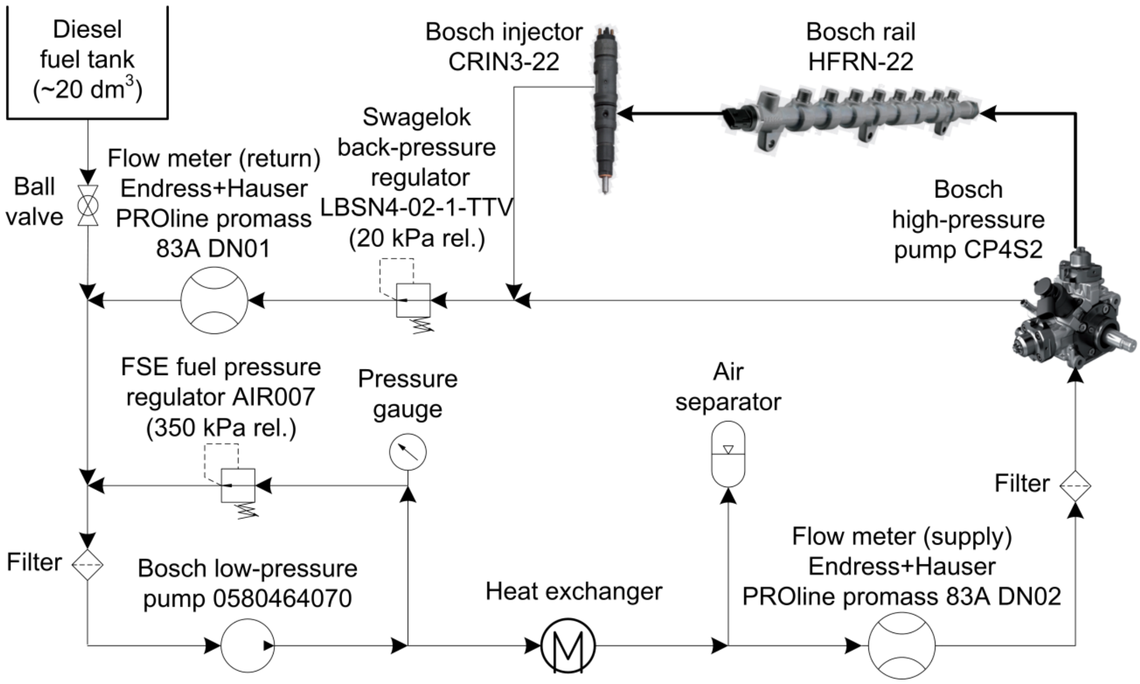

Figure 3.5 – Diesel fuel injection system.

In order to enable dual-fuel operation, an ethanol fuel injection system was designed and fitted to the engine. Ethanol was injected through a port fuel injector (PFI) installed in the intake manifold, as shown in Figure 3.6. The fuel spray was directed towards the intake valves.

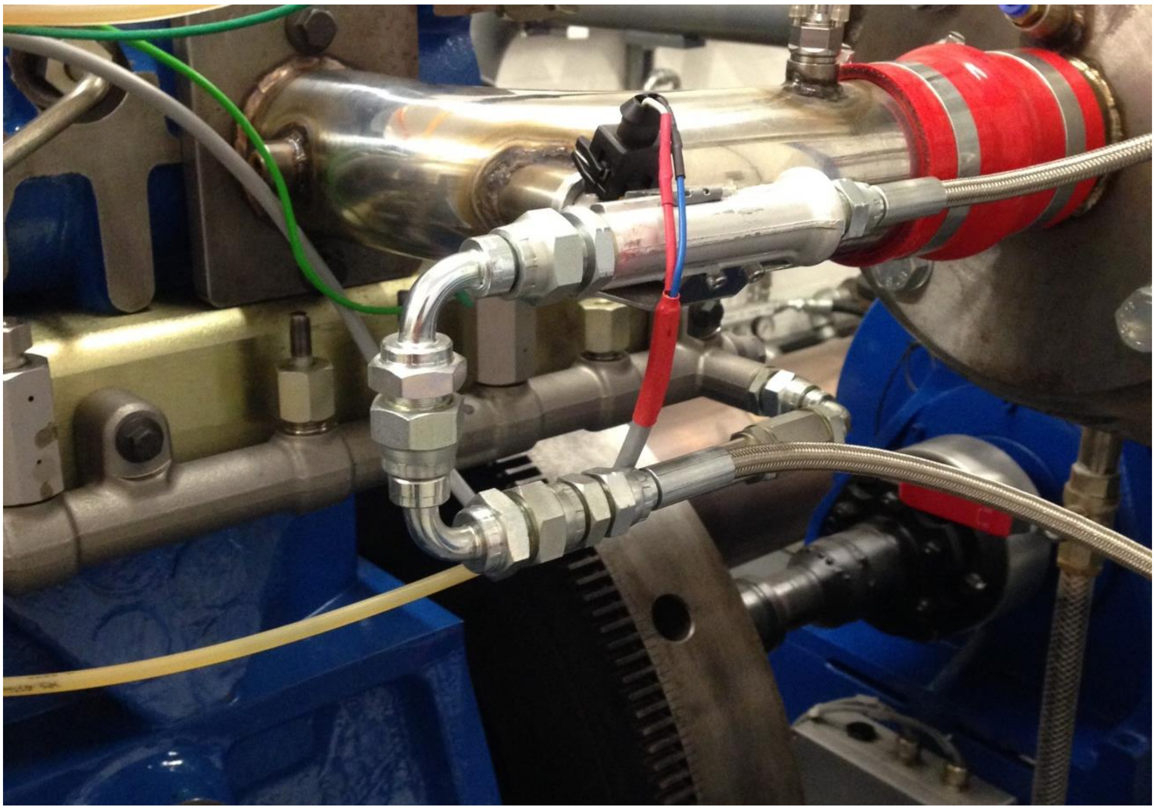

Figure 3.6 – Ethanol injector installed in the intake manifold.

The PFI specifications are depicted in Table 3.4. The start of ethanol injection was set to the TDC to maximise the time for the mixture preparation prior to the intake valve opening event.

Table 3.4 – Ethanol injector specifications.

Parameter	Value
Injector	Marelli IWP069
Number of holes	Single
Type	Saturated
Included (80%) spray angle	15 degrees
Maximum fuel pressure	500 kPa
Static flow rate	491 cm^3/min at 400 kPa (*)

(*) For n-heptane, density of 0.684 kg/dm^3 at 293 K.

Figure 3.7 shows a schematic diagram of the PFI system. An in-house injector driver controlled the injector pulse width, which was adjusted according to the desired ethanol energy fraction. The injection pressure was continuously monitored, so that a constant relative pressure of 300 kPa could be maintained across the injector. A heat exchanger held the ethanol temperature at 293 ± 5 K.

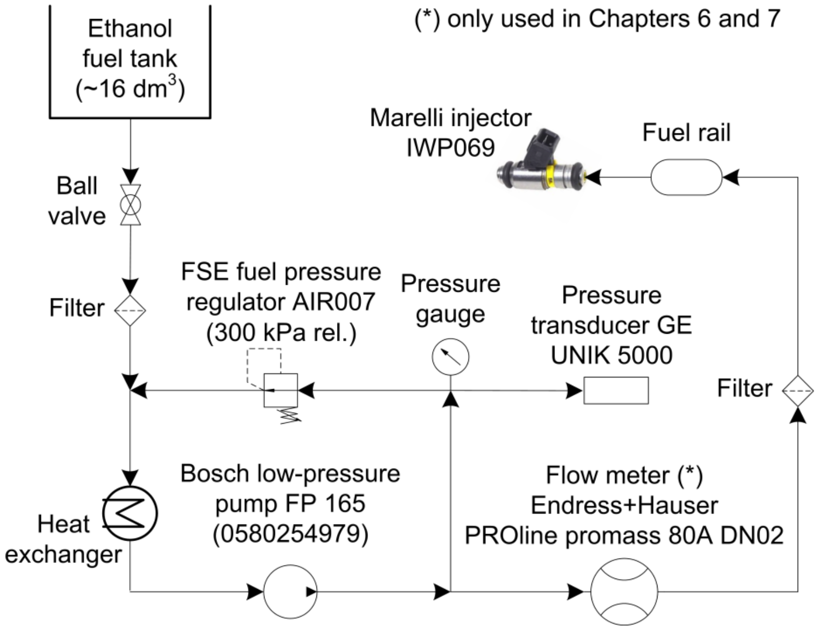

Figure 3.7 – Ethanol fuel injection system. Flow meter only used at high engine loads.

In Chapter 4 and Chapter 5, the mass of anhydrous ethanol injected ($m_{ethanol/cycle}$) was obtained from the injector calibration curve shown in Figure 3.8. The PFI calibration process was performed using a 12.0 ± 0.2 V power supply at an ambient pressure of 102 kPa. The ethanol was supplied to the rail at 293 K. The fuel was injected in a small partially enclosed container and weighted with a Sartorius Research R200D Electronic semi-microbalance with an accuracy of ± 0.1 mg. The mass of ethanol injected for a given pulse width was equivalent to the average of three samples collected over 60 seconds. Despite the sensitivity to changes in fuel density, the method has the merit of simplicity and the calibration can provide measurements similar to that of an average gravimetric fuel flow meter, with an accuracy of ~1% [168]. Equation (3.1) was used convert $m_{ethanol/cycle}$ to ethanol mass flow rate in kg/h ($\dot{m}_{ethanol}$).

$$\dot{m}_{ethanol} = \frac{60\ m_{ethanol/cycle}\ N}{2} \times 10^{-6} \tag{3.1}$$

where N is the engine speed.

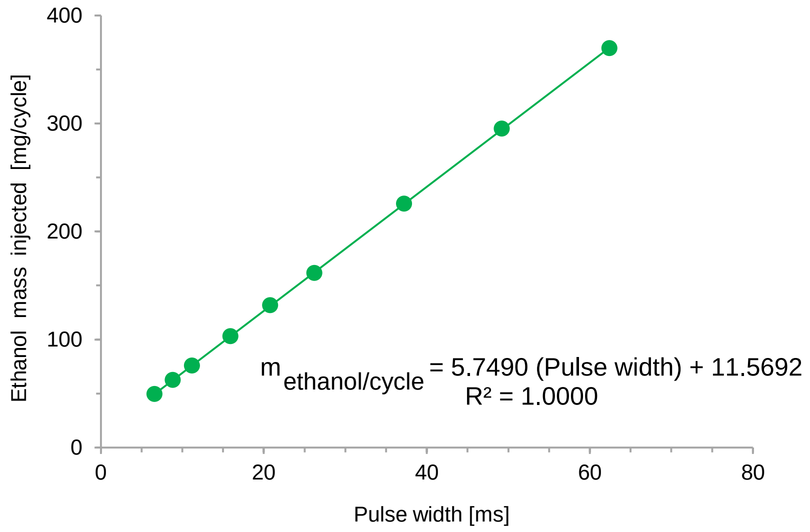

Figure 3.8 – PFI calibration curve for anhydrous ethanol at 300 kPa.

In Chapter 6 and Chapter 7, the ethanol mass flow rate was measured using an Endress+Hauser Proline Promass 80A Coriolis flow meter, allowing for measurements with a higher accuracy of 0.15%. The calibration of all fuel flow meters was carried out by the manufacturer to ensure that measurements were accurate.

3.2.3 Exhaust emissions measurement

Gaseous emissions such as CO, CO_2, NOx, unburnt HC, and oxygen (O_2) were taken using a Horiba MEXA-7170 DEGR emission analyser. The external EGR rate was determined by calculating the ratio of the intake to the exhaust CO_2 concentration measured by the same device. The analyser was calibrated before every engine test using span gases to ensure emissions measurement linearity. A high pressure module allowed for high-pressure sampling upstream of the exhaust back pressure valve while a heated line maintained a gas temperature of ~464 K to prevent water condensation. The communication between the analyser and a personal computer was performed via Ethernet ports.

A non-dispersive infrared detector (NDIR) measured the concentrations of CO and CO_2. The operating principle was based on the infrared absorption of these molecules and the use of a no dispersing element to resolve detailed spectral lines. A magneto-pneumatic detector (MPA) was used to measure the O_2 concentration in the exhaust. The analysis was based on a magnetic field applied on a gas cell. The resulting pressure difference caused by the collection of oxygen in the sample at a magnetic pole was detected by a microphone.

NOx emissions were the sum of nitrogen oxide (NO) and the nitrogen dioxide (NO_2) measured by a heated chemiluminescence detector (HCLD). An exhaust gas sample passes through a catalyst to convert NO_2 to NO. The operating principle relied on a chemical reaction between the resulting NO and ozone to produce NO_2 at an excited state, which emitted light in the 800 to 2500 nm range [169] when returning to a ground state. The amount of light emitted was proportional to the concentration of NO.

The measurement of the total unburnt HC was performed on a wet basis (e.g. with H_2O) by a heated flame ionisation detector (FID). The introduction of hydrocarbons into a hydrogen flame produced, in a complex process, electrons and positive ions. The ions generated were detected in the form of an electric current between two electrodes. The flow of electric charge was proportional to the number of carbon atoms in the exhaust gas.

However, the hydrocarbon emissions measured with the FID can lead to misinterpretation of unburnt HC as a result of the relative insensitivity of the device towards alcohols and aldehydes [170,171]. Therefore, the FID response was corrected by the method developed by Kar and Cheng [170] to account for the oxygenated organic species resultant from ethanol combustion. The calculation is described in the next section.

An AVL 415SE smoke meter was used for soot emission measurements. A sampling time of 30 seconds was selected to obtain 5 dm^3 of exhaust gas drawn through a filter paper. Paper blackening due to soot was detected by an optical reflectometer head. A Filter Smoke Number (FSN) of 10 was assigned to a filter paper with no reflection while an FSN of zero corresponded to a clean filter paper.

3.2.4 Data acquisition and control

Two National Instruments data acquisition (DAQ) cards and a personal computer were used to acquire the signals from the measurement device. A USB-6251 high speed DAQ card received the crank angle resolved data synchronized with an EB-58 optical encoder of 0.25 CAD resolution. A USB-6210 DAQ card acquired the low frequency engine operation conditions. These data were displayed live by a DAQ program and combustion analyser developed by Dr Yan Zhang. Figure 3.9 shows a similar screen to that provided by the software, which recorded the measurements in sets of 100 cycles.

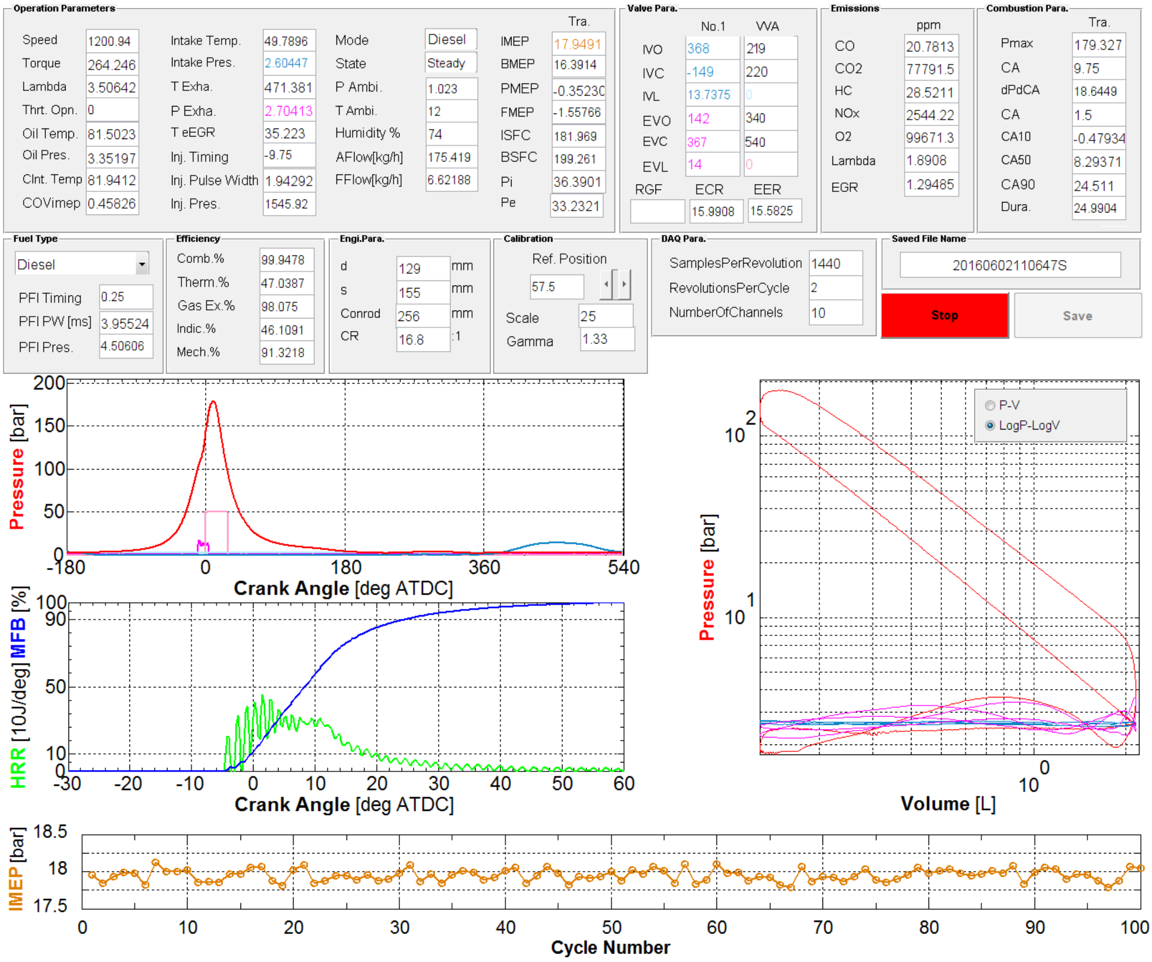

Figure 3.9 – Data acquisition program and combustion analyser.

Engine speed was taken by the dynamometer through an electromagnetic pulse pick up and a toothed wheel mounted on the shaft half coupling hub. Brake torque was measured by a Sherborne Sensors U4000 strain gauge load cell connected to the dynamometer. Intake and exhaust pressures were measured by two Kistler 4049A water cooled piezoresistive absolute pressure sensors coupled to Kistler 4622A amplifiers. Ethanol and engine oil pressures were monitored by GE UNIK 5000 pressure transducers. Temperatures and pressures at relevant locations were measured by K-type thermocouples and pressure gauges, respectively.

The in-cylinder pressure was measured by a Kistler 6125C piezoelectric pressure sensor. Under mechanical load, a crystal in the sensor produced an electrostatic charge (-0.3122 pC/kPa), which was converted into an electric potential difference by means of an AVL FI Piezo charge amplifier. The device was configured with a cyclic drift compensation mode in order to eliminate zero point drift, effects on amplitude and phase, and the need for reset prior to each measurement. In addition, a filter of 100 kHz was used to prevent phase shift errors.

The cylinder pressure signal was referenced (e.g. pegged) every cycle with the average intake manifold pressure over a window of the six crank angle degrees around inlet bottom dead centre. The amplitude and phasing of the motored peak in-cylinder pressure was verified after every test. A trigger signal (REF) was used to adjust the position of the TDC. The maximum pressure of ~4.1 MPa occurred between -1.0 and -0.5 CAD ATDC, and was very close to the peak pressure estimated from the compression ratio and polytropic coefficient [168].

The required intake valve timings were set in the DAQ program and sent to the VVA control unit using an analogue output channel in the high speed DAQ card. The resulting intake valve lift profile was obtained by measuring the displacement of the valve spring retainer with a LORD MicroStrain DEMOD-DVRT temperature compensated signal conditioner and an S-DVRT-24 displacement sensor. The curve was post-processed using a delay of 0.56 ms (-4 CAD at 1200 rpm). IVO and IVC events were determined at 0.5 mm valve lift.

An LEM PR30 current probe was used to acquire the electric current signal sent from the ECU to the diesel injector solenoid. The signal was corrected by adding the respective energising time delay (ET) shown in Table 3.5, which was previously measured by Dr Ian May in a constant volume chamber [172]. The resulting diesel injector current signal allowed for the determination of the actual start of diesel injection (SOI) or actual start of main diesel injection (SOI_2) in the case of a split injection strategy. The diesel injection pressure was monitored by a Bosch RDS4.5 high-pressure sensor. The ethanol injection timing and pulse width were collected directly from the PFI driver.

Table 3.5 – Energising time delay at different rail pressures. Source: May [172].

Rail pressure	ET	ET at 1200 rpm
50 MPa	0.406 ms	2.92 CAD
75 MPa	0.364 ms	2.62 CAD
90 MPa	0.358 ms	2.58 CAD
100 MPa	0.354 ms	2.55 CAD
110 MPa	0.349 ms	2.51 CAD
120 MPa	0.344 ms	2.48 CAD
140 MPa	0.344 ms	2.48 CAD
180 MPa	0.344 ms	2.48 CAD

3.3 Data analysis

The data acquired by the DAQ program were logged twice to record 200 consecutive cycles for every engine test point. The results were imported to an Excel spreadsheet. Post-processing was performed using the equations and considerations described below.

3.3.1 Heat release analysis

The method of analysis which yields the rate of release of the fuels' chemical energy starts with the first law of thermodynamics for an open system. The energy balance is given as

$$\frac{dQ}{dt} - p\,\frac{dV}{dt} + \sum_{x} \dot{m}_x\, h_x = \frac{dU}{dt} \tag{3.2}$$

where dQ/dt is the heat transfer rate across the system boundary into the combustion chamber walls, $p(dV/dt)$ is the rate of work transfer done by the system due to boundary displacement, $\dot{m}_x$ is the mass flow rate into the system across the system boundary at location x, h_x is the enthalpy of flux x leaving or entering the system, and U is the sensible internal energy of the cylinder contents.

There is a number of complications in the application of Equation (3.2) because of difficulties in dealing with the fuel injected into the cylinder ($\dot{m}_f$), unknown and non-uniform composition of the burnt gases, prediction of heat transfer, and presence of gas in the crevice regions.

A simplified method provided an approximate result by omitting the crevice flow effects and assuming that the cylinder contents are at a uniform temperature at each instant in time during the combustion event (single zone). Equation (3.2), therefore, becomes

$$\frac{dQ}{dt} - p\,\frac{dV}{dt} + \dot{m}_f\, h_f = \frac{dU}{dt} \tag{3.3}$$

If h_f is taken to be the sensible enthalpy of the injected fuel, the term $\dot{m}_f h_f \approx 0$ [8]. As a result, dQ/dt becomes the apparent net heat release (dQ_n/dt), representing the difference between the chemical energy released by the combustion of the fuel and the heat transfer to the system. When modelling the contents of the cylinder as an ideal gas, Equation (3.3) can be converted to

$$\frac{dQ_n}{dt} = p\ \frac{dV}{dt} + m\ c_v\ \frac{dT}{dt} \tag{3.4}$$

According to Heywood [8], neglecting changes in gas constant (R) in the ideal gas law ($pV = mRT$) allows for the calculation of the heat release rate (HRR) as

$$HRR = \frac{dQ_n}{dt} = \frac{\gamma}{\gamma - 1}\ p_i\ \frac{dV}{dt} + \frac{1}{\gamma - 1}\ V_i\ \frac{dp}{dt} \tag{3.5}$$

where γ is the ratio of specific heats, p_i is the in-cylinder gas pressure at any crank angle position θ, and dt is the encoder resolution of 0.25 CAD. Since the absolute value of the heat released is not as important to this study as the bulk shape of the curve with respect to crank angle, a constant γ of 1.33 was assumed throughout the engine cycle. The cylinder volume at any crank angle position θ was given by

$$V_i = V_c + \frac{V_d}{2}\left\{\left(\frac{l}{a}\right) + 1 - \cos\theta - \left[\left(\frac{l}{a}\right)^2 - \sin^2\theta\right]^{1/2}\right\} \tag{3.6}$$

The mass fraction burnt (MFB) was given by the ratio of the integral of the HRR and the maximum cumulative heat release. Combustion phasing (CA50) was determined by the crank angle of 50% MFB. Combustion duration (CA10-CA90) was represented by the period of time between the crank angles of 10% (CA10) and 90% (CA90) cumulative heat release. Ignition delay was defined as the period of time between the SOI or SOI_2 and the start of combustion (SOC), set to 0.3% MFB point of the average cycle.

Combustion noise is often a result of knock or high in-cylinder pressure rise rates (PRR). The PRR was represented by the average of the maximum pressure variations of 200 cycles of cylinder pressure versus crank angle as

$$PRR = \sum_{n=1}^{200} PRR_{max} \Big/ n = \sum_{n=1}^{200} \left(\frac{dp}{dt}_{max}\right) \Big/ n \tag{3.7}$$

Finally, the average in-cylinder pressure and HRR curves were post-processed using a third order Savitzky-Golay filter with a window size of five data points to remove signal noise.

3.3.2 Overall engine performance parameters

The net indicated work delivered to the piston over the entire four-stroke cycle ($W_{c,ind}$) was calculated with Equation (3.8), where a zero crank angle position was defined as the firing TDC.

$$W_{c,ind} = \int_{-180}^{540} p_i \, dV \tag{3.8}$$

The engine load at a given condition was represented by net indicated mean effective pressure (IMEP), which was obtained by the relation between $W_{c,ind}$ and the swept volume as

$$IMEP = \frac{W_{c,ind}}{V_d} \tag{3.9}$$

The engine net indicated power (P_{ind}) in kW was related to the $W_{c,ind}$ by

$$P_{ind} = \frac{W_{c,ind} \, N}{2 \times 60} \times 10^3 \tag{3.10}$$

The ratio of the work done to the rate of fuel energy supplied to the engine was represented by the net indicated efficiency as

$$Net\ Indicated\ Efficiency = \left[\frac{3.6 \, P_{ind}}{(\dot{m}_{diesel} \, LHV_{diesel}) + (\dot{m}_{ethanol} \, LHV_{ethanol})}\right] \times 100 \tag{3.11}$$

The work transfer between the piston and cylinder gas during the gas exchange process (e.g. intake and exhaust strokes) allowed for the calculation of the pumping mean effective pressure (PMEP). PMEP is typically a negative value that is reduced if the work transferred to the cylinder gas increases.

$$PMEP = \int_{180}^{540} p_i \, dV / V_d \tag{3.12}$$

A reduction in PMEP decreases the gas exchange efficiency, which represents the ratio of the available work by the gross work delivered to the piston (e.g. over the compression and expansion strokes).

$$Gas\ Exchange\ Efficiency = \left[\frac{IMEP}{(IMEP - PMEP)}\right] \times 100 \tag{3.13}$$

Combustion and in-cylinder flow stability were monitored by the coefficient of variation of IMEP (COV_IMEP) over the 200 sampled cycles as

$$COV\_IMEP = \left[\sqrt{\sum_{n=1}^{200} \frac{\left(IMEP - IMEP_{average}\right)^2}{n-1}} \Bigg/ IMEP_{average}\right] \times 100 \tag{3.14}$$

A relevant parameter for the dual-fuel operation was the ethanol energy fraction (EF), which was defined as the ratio of the energy content of the ethanol to the total fuel energy by

$$EF = \frac{\dot{m}_{ethanol}\, LHV_{ethanol}}{(\dot{m}_{diesel}\, LHV_{diesel}) + (\dot{m}_{ethanol}\, LHV_{ethanol})} \tag{3.15}$$

In addition, the ratio of the mass of ethanol to the total fuel mass injected allowed for the calculation of the ethanol mass fraction (MF) as

$$MF = \frac{\dot{m}_{ethanol}}{(\dot{m}_{diesel} + \dot{m}_{ethanol})} \tag{3.16}$$

3.3.3 Combustion stoichiometry

Figure 3.10 shows the equations used to calculate the molar carbon to carbon ratio (x), molar hydrogen to carbon ratio (y), and molar oxygen to carbon ratio (z) for a given MF. The approximation was based on the conservation of mass of each chemical element in the reactants shown in Equation (3.17) [8], and the normalised molecular composition of ethanol ($CH_3O_{0.5}$) and diesel ($CH_{1.825}O_{0.0014}$).

$$C_xH_yO_z + \left(x + \frac{y}{4} - \frac{z}{2}\right)(O_2 + 3.773N_2) \rightarrow xCO_2 + \frac{y}{2}H_2O + 3.773\left(x + \frac{y}{4} - \frac{z}{2}\right)N_2 \tag{3.17}$$

where $C_xH_yO_z$ is the normalised molecular composition of the in-cylinder fuel mixture.

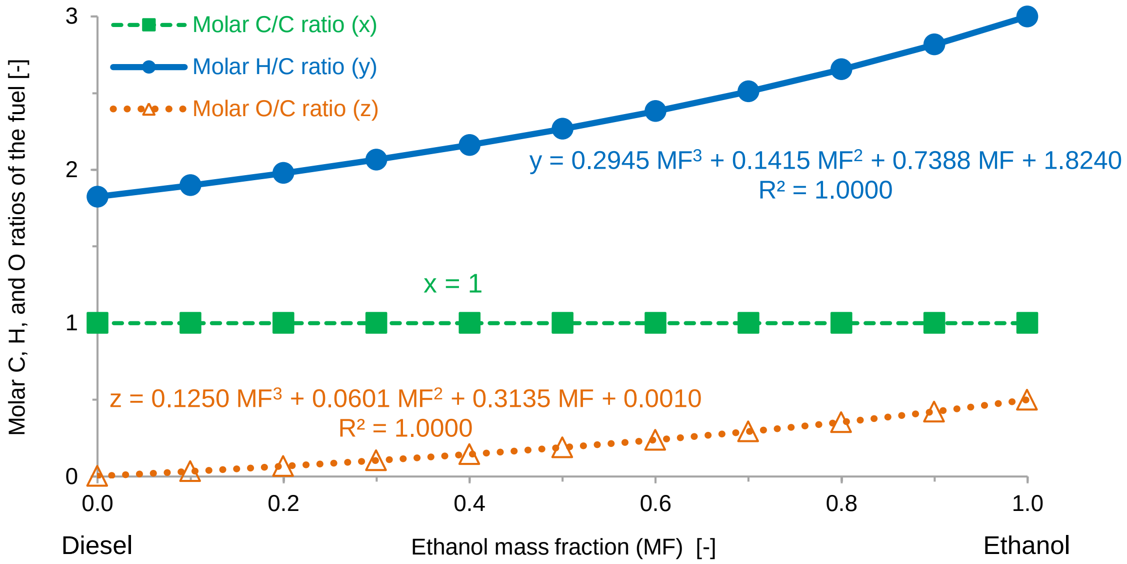

Figure 3.10 – Formulation of the molar H/C (y) and O/C ratios (z) for the actual in-cylinder fuel mixture as a function of the MF.

The determination of x, y, and z for the actual in-cylinder fuel mixture allowed for the calculation of the stoichiometric air/fuel ratio $(A/F)_{stoich}$ as

$$(A/F)_{stoich} = \frac{\left(x + \frac{y}{4} - \frac{z}{2}\right)\left(M_{O_2} + 3.773\ M_{N_2}\right)}{(12.011\ x + 1.008\ y + 15.999\ z)} \tag{3.18}$$

where M_{O_2} is the molar mass of oxygen of 31.9988 g/mol [29] and M_{N_2} is molar mass of nitrogen of 28.011 g/mol [29].

The stoichiometric air/fuel ratio for ethanol-diesel dual-fuel operation was validated using the $(A/F)_{stoich}$ for diesel (14.5) and ethanol (9.0) fuels as inputs to Equation (3.19):

$$(A/F)_{stoich} = 14.5 \times \frac{\dot{m}_{diesel}}{(\dot{m}_{diesel} + \dot{m}_{ethanol})} + 9.0 \times \frac{\dot{m}_{ethanol}}{(\dot{m}_{diesel} + \dot{m}_{ethanol})} \tag{3.19}$$

Finally, the excess of fuel in the exhaust was given by the global fuel/air equivalence ratio (Φ), which was calculated as the inverse of the relative air/fuel ratio (λ) by

$$\phi = \lambda^{-1} = \frac{(A/F)_{stoich}}{\dot{m}_{air}/(\dot{m}_{diesel} + \dot{m}_{ethanol})} = \frac{(14.5\ \dot{m}_{diesel}\ + 9.0\ \dot{m}_{ethanol})}{\dot{m}_{air}} \tag{3.20}$$

3.3.4 Mean in-cylinder gas temperature

The mean in-cylinder gas temperature at any crank angle position θ was computed using the ideal gas law [8] as

$$T_{cyl,i} = \frac{p_i \, V_i \, M_b}{m_{total/cycle} \, \tilde{R}} \tag{3.21}$$

where $\tilde{R}$ is the universal gas constant of 8.31432 J/mol.K [8]. The term M_b is the molecular weight of the burned gas in g/mol, which was calculated as

$$M_b = \frac{m_{RP}}{n_b} \tag{3.22}$$

where m_{RP} is the mass of mixture (burnt or unburnt) per mole of O_2 in the mixture and n_b is the number of moles of burnt gas. These parameters were calculated using Equations (3.23), (3.24), and (3.25) found in Heywood [8].

$$m_{RP} = 32 + 4\,\phi\,\zeta\,\left(1 + \frac{8}{4+y}\right) + 28.16\ \times 3.773\,\zeta\,\left(1 - \frac{4\,z}{8+2y}\right) \tag{3.23}$$

$$n_b = \phi\,\zeta\,\left(1 - \frac{4}{4+y}\right) + 1 + 3.773\,\zeta\,\left(1 - \frac{4\,z}{8+2y}\right) \tag{3.24}$$

$$\zeta = \frac{2}{2 - \frac{4\,z}{4+y}(1-\phi)} \tag{3.25}$$

The term $m_{total/cycle}$ in Equation (3.21) is the total in-cylinder mass per cycle given by

$$m_{total/cycle} = m_{air/cycle} + m_{fuel/cycle} + m_{rg/cycle} \tag{3.26}$$

where $m_{air/cycle}$ is the mass of fresh air inducted per cycle and $m_{fuel/cycle}$ is the mass of fuel injected per cycle (e.g. ethanol, diesel, etc.). The term $m_{rg/cycle}$ is the mass of residual gas trapped at IVC, which was calculated as

$$m_{rg/cycle} = \frac{p_{EVC}\,V_{EVC}\,M_b}{EGT\,\tilde{R}} \tag{3.27}$$

where p_{EVC} is the in-cylinder gas pressure at EVC, V_{EVC} is the in-cylinder volume at EVC, and EGT is the average exhaust gas temperature measured by a K-type thermocouple. This calculation is valid for cases without positive valve overlap.

It is important to note that engine experiments with an intake valve re-opening (2IVO) strategy required the use of a correlated one-dimensional (1D) engine model to estimate the $m_{rg/cycle}$. This was necessary because of the nature of the gas flow across the cylinder, where residual gas is expelled back into the intake port during the exhaust stroke and recirculated into the cylinder during the intake stroke.

In either case the in-cylinder residual gas fraction (RGF) was given by

$$RGF = \left(\frac{m_{rg/cycle}}{m_{total/cycle}}\right) \times 100 \tag{3.28}$$

3.3.5 Exhaust emissions analysis

The concentration of a given gas was measured by the Horiba emissions analyser in ppm. The measurements were converted to specific exhaust gas emissions using the methodology described in the Regulation number 49 of the Economic Commission for Europe of the United Nations [29]. Net indicated specific emissions of CO, NOx, and unburnt HC, in g/kWh, were calculated using the Equations (3.29), (3.30), and (3.31).

$$ISCO = \frac{\dot{m}_{CO}}{P_{ind}} = \frac{u_{CO}\,[CO\,]\,\dot{m}_{exh}\,k_{w,r}}{P_{ind}} \tag{3.29}$$

$$ISNOx = \frac{\dot{m}_{NOx}}{P_{ind}} = \frac{u_{NOx}\,[NOx]\,\dot{m}_{exh}\,k_{w,r}\,k_{h,D}}{P_{ind}} \tag{3.30}$$

$$ISHC = \frac{\dot{m}_{HC}}{P_{ind}} = \frac{u_{HC}\,[HC]\;\dot{m}_{exh}}{k_{FID}\,P_{ind}} \tag{3.31}$$

where $\dot{m}_{gas}$ is the flow rate of a given component in g/h, [gas] is the concentration of the component in the exhaust gas in ppm, and $\dot{m}_{exh}$ is the exhaust mass flow rate in kg/h given by

$$\dot{m}_{exh} = \dot{m}_{air} + \dot{m}_{diesel} + \dot{m}_{ethanol} \tag{3.32}$$

The term u_{gas} is the tabulated ratio between the component and exhaust gas density, which varies according to the fuel used as depicted in Table 3.6.

Table 3.6 – Raw exhaust gas (u_{gas}) for diesel and ethanol [29].

Raw exhaust gas	$u_{gas,\ diesel}$	$u_{gas,\ ethanol}$ (*)
u_{CO}	0.000966	0.000980
u_{NOx}	0.001586	0.001609
u_{HC}	0.000482	0.000780

(*) The characteristics for ethanol were given by those of a mixture of ethanol and 5% ignition improver (ED95).

The actual raw exhaust gas ($u_{gas,\ mix}$) for the dual-fuel operation was calculated from the contribution of the ethanol fuel to the total in-cylinder fuel mixture by

$$u_{gas,\ mix} = \frac{\dot{m}_{diesel}\, u_{gas,\ diesel} + \dot{m}_{ethanol}\, u_{gas,\ ethanol}}{\dot{m}_{diesel} + \dot{m}_{ethanol}} \tag{3.33}$$

The concentrations of CO and NOx were converted to a wet basis by applying a dry/wet correction factor for the raw exhaust gas ($k_{w,r}$), which varied with the in-cylinder fuel mixture composition. The calculation was adapted from [29] as follows:

$$k_{w,r} = 1.008 \left[1 - \frac{1.2442\left(H_f + H_a\right) + 111.19\, C_{\%} \left(\frac{\dot{m}_{diesel} + \dot{m}_{ethanol}}{\dot{m}_{dry\ air}}\right)}{773.4 + 1.2442\left(H_f + H_a\right) + k_{f,w}\left(\frac{\dot{m}_{diesel} + \dot{m}_{ethanol}}{\dot{m}_{dry\ air}}\right) \times 10^3} \right] \tag{3.34}$$

where $k_{f,w}$ is a fuel specific factor of wet exhaust calculated as

$$k_{f,w} = 0.055594\, H_{\%} + 0.0070046\, O_{\%} \tag{3.35}$$

The determination of the actual in-cylinder fuel mixture components $\%C_{mix}$, $\%H_{mix}$, and $\%O_{mix}$ were given by Equations (3.36), (3.37),and (3.38).

$$\%C_{mix} = \frac{\dot{m}_{diesel}\, \%C_{diesel} + \dot{m}_{ethanol}\, \%C_{ethanol}}{\dot{m}_{diesel} + \dot{m}_{ethanol}} \tag{3.36}$$

$$\%H_{mix} = \frac{\dot{m}_{diesel}\, \%H_{diesel} + \dot{m}_{ethanol}\, \%H_{ethanol}}{\dot{m}_{diesel} + \dot{m}_{ethanol}} \tag{3.37}$$

$$\%O_{mix} = \frac{\dot{m}_{diesel}\ \%O_{diesel} + \dot{m}_{ethanol}\ \%O_{ethanol}}{\dot{m}_{diesel} + \dot{m}_{ethanol}} \tag{3.38}$$

The term H_f in Equation (3.34) represents the humidity introduced by the water-in-fuel content ($\dot{m}_{H_2O}$), which was only applied for a dual-fuel operation with wet ethanol injection in Chapter 6. H_f was calculated in g of water per kg of dry air by

$$H_f = \frac{\dot{m}_{H_2O}}{\dot{m}_{dry\ air}} \times 10^3 \tag{3.39}$$

The term H_a in Equation (3.34) is the intake air humidity in g of water per kg of dry air, which was calculated as

$$H_a = \left(\frac{M_{H_2O}}{M_{dry\ air}}\right) \frac{p_{vapour}}{\left(p_{amb} - p_{vapour}\right)} \times 10^3 \tag{3.40}$$

where M_{H_2O} is the molar mass of water of 18.01534 g/mol [29], $M_{dry\ air}$ is the molar mass of dry air of 28.965 g/mol [29], and p_{amb} is the ambient air pressure. The p_{vapour} is the partial pressure of water vapour in the air derived from the relative humidity in ambient air (RH) by

$$p_{vapour} = p_{sat} \frac{RH}{100} \tag{3.41}$$

where p_{sat} is the saturation pressure of water vapour, in Pa, calculated from the formulation developed by Wexler [173]:

$$p_{sat} = e^{F(7)\ \ln(T_{amb}) + \sum_{j=0}^{6} F(j)\ (T_{amb})^{(j-2)}} \tag{3.42}$$

where $F(0)$ is -0.29912729×10^4, $F(1)$ is -0.60170128×10^4, $F(2)$ is $+0.1887643854 \times 10^2$, $F(3)$ is $-0.28354721 \times 10^{-1}$, $F(4)$ is $+0.17838301 \times 10^{-4}$, $F(5)$ is $-0.84150417 \times 10^{-9}$, $F(6)$ is $+0.44412543 \times 10^{-12}$, $F(7)$ is $+0.28584870 \times 10^1$, and T_{amb} is the ambient air temperature in K.

The term $\dot{m}_{dry\ air}$ in Equations (3.34) and (3.39) is the intake air mass flow rate on a dry basis, which was obtained by subtracting the humidity from the measured air flow rate by

$$\begin{aligned} \dot{m}_{dry\ air} &= \dot{m}_{air} - \dot{m}_{humidty} \\ &= \dot{m}_{air} - \left(\frac{\dot{m}_{dry\ air}\, H_a}{10^3}\right) \\ &= \frac{\dot{m}_{air}}{(1 + H_a \times 10^{-3})} \end{aligned} \tag{3.43}$$

In particular, the NOx concentration was also corrected with a humidity correction factor ($k_{h,D}$) for compression-ignition engines [29] given as

$$k_{h,D} = \frac{15.698\, H_a}{10^3} + 0.832 \tag{3.44}$$

The k_{FID} in Equation (3.31) is a correction factor used to calculate the actual concentration of unburnt HC emissions $[HC]_{actual}$ in the exhaust gas from the $[HC]$ measured by the FID [170] by

$$k_{FID} = 1 - [(1 - \alpha)(0.608\, VF^2 + 0.092\, VF)] \tag{3.45}$$

where α is an updated response factor of 0.68 for the ethanol constituent [171], and VF is the current volumetric fraction of ethanol in the total fuel injected calculated as

$$VF = \frac{\dot{m}_{ethanol}/\rho_{ethanol}}{(\dot{m}_{diesel}/\rho_{diesel}) + (\dot{m}_{ethanol}/\rho_{ethanol})} \tag{3.46}$$

The FID correction factor resulted in 20.9% higher $[HC]_{actual}$ than the measured $[HC]$ for the highest ethanol energy fraction of 0.80 used in the dual-fuel experiments (e.g. VF of 0.87). An ethanol-only operation would require a k_{FID} of 0.776, increasing the levels of unburnt HC emissions by 28.9%.

The calculation of the net indicated specific emission of soot (ISsoot) was slightly different from that of the other exhaust gases, and was given by

$$ISsoot = \frac{[soot\,]\, \dot{m}_{exh}}{\rho_{exh}\, P_{ind}} \times 10^3 \tag{3.47}$$

where $[soot\,]$ is the concentration of soot in mg/m^3 calculated from the smoke measurements in filter smoke number ($[FSN]$) and corrected to a standard condition of 273.15 K using the Equation (3.48) provided by AVL [174].

$$[soot] = \frac{5.32\,[FSN]\,e^{0.3062\,[FSN]}}{0.405} \times \frac{298}{273.15} \tag{3.48}$$

The term ρ_{exh} in Equation (3.47) is the exhaust gas density calculated from an equation based on the Regulation number 49 [29] as follows:

$$\rho_{exh} = \frac{10^3 + \left(H_f + H_a\right) + \left(\frac{\dot{m}_{diesel} + \dot{m}_{ethanol}}{\dot{m}_{dry\ air}}\right) \times 10^3}{773.4 + 1.2434\left(H_f + H_a\right) + k_{f,w}\left(\frac{\dot{m}_{diesel} + \dot{m}_{ethanol}}{\dot{m}_{dry\ air}}\right) \times 10^3} \tag{3.49}$$

Combustion efficiency calculations were based on the emissions products not fully oxidised during the combustion process except soot by

$$Combustion\ Efficiency = \left\{1 - \frac{P_{ind}}{10^3}\left[\frac{(ISCO\ LHV_{CO}) + (ISHC\ LHV_{mix})}{(\dot{m}_{diesel}\ LHV_{diesel}) + (\dot{m}_{ethanol}\ LHV_{ethanol})}\right]\right\} \times 100 \tag{3.50}$$

where LHV_{CO} is equivalent to 10.1 MJ/kg [8], and LHV_{mix} is the actual lower heating value of the in-cylinder fuel mixture given by

$$LHV_{mix} = \frac{(\dot{m}_{diesel}\ LHV_{diesel}) + (\dot{m}_{ethanol}\ LHV_{ethanol})}{\dot{m}_{diesel} + \dot{m}_{ethanol}} \tag{3.51}$$

3.4 Engine testing

The investigations were carried out at the engine speed of 1200 rpm and loads varying from 0.3 MPa IMEP to 2.4 MPa IMEP. Figure 3.11 shows that the selected test points are located over high residency areas in the WHSC [29] and SET [33] test cycles. The characteristic speeds were based on the speed of maximum power obtained from the full load curve [29,35]. The relative weight of each test point over a given test cycle is proportional to the size of the circle.

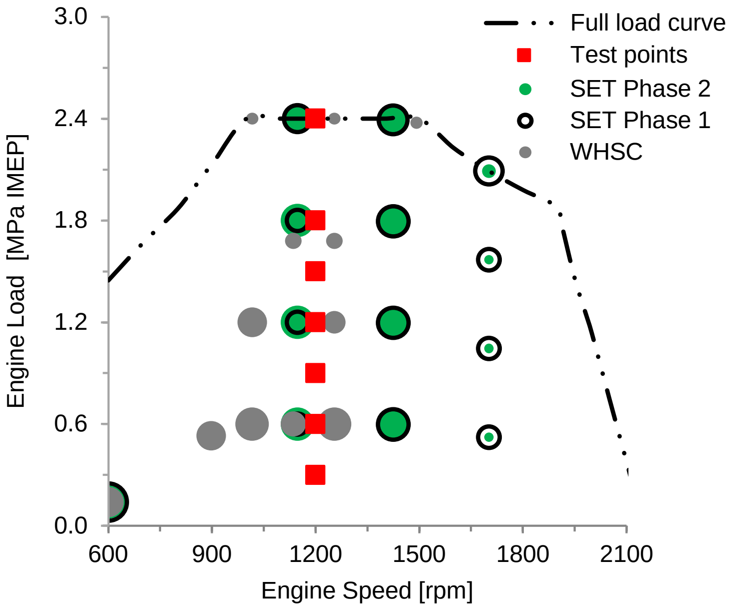

Figure 3.11 – The selected test points, and the WHSC [29] and SET [33] test cycle points over an estimated HD diesel engine speed-load map.

3.5 Summary

In this chapter, the research engine and test cell facilities employed were described alongside the measurement device specifications. The installation of the ethanol port fuel injection system was presented. The equations and assumptions required for data acquisition and post-processing analysis were defined. Methods and formulations used to determine the combustion heat release, engine performance, and exhaust emissions were presented. Finally, the engine speed and loads chosen for the dual-fuel studies were revealed and compared to modern HD engine test cycles.

Chapter 4

Dual-fuel combustion at low engine loads

4.1 Introduction

At light loads, the dual-fuel operation is adversely affected by incomplete combustion and poor thermal efficiency. In addition, the low exhaust gas temperatures at such conditions can reduce the effectiveness of the exhaust aftertreatment system, which is necessary to meet stringent emissions standards. Elevation of in-cylinder gas temperature and relatively higher fuel/air equivalence ratio are desirable in order to minimise CO and unburnt HC emissions and hence improve fuel conversion efficiency at low engine loads [5].

This chapter investigates fuel injection and engine control strategies to achieve high efficiency low load dual-fuel operation. Experimental studies have been carried out using different diesel injection strategies, internal exhaust gas recirculation, intake throttling, and external exhaust gas recirculation. Figure 4.1 shows where the low load region is located over an estimated speed and load map of a HD diesel engine.

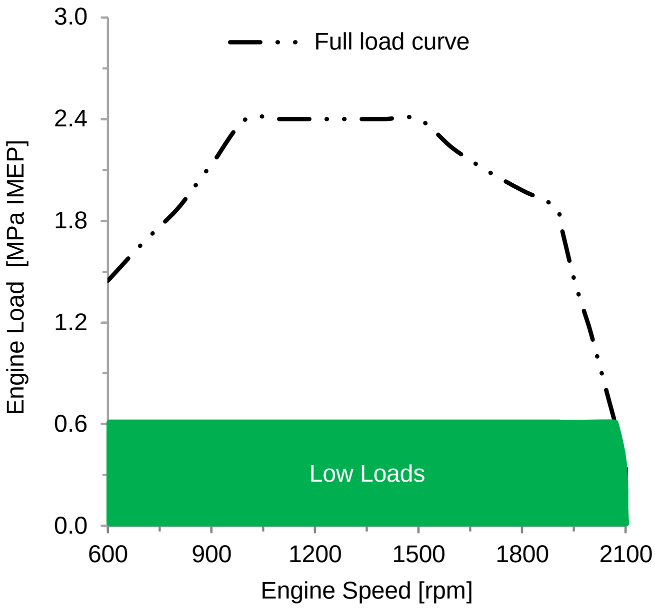

Figure 4.1 – Low load region over an estimated HD diesel engine speed-load map.

4.2 The effect of diesel injection timing on low load dual-fuel operation

Initially, experiments were carried out to demonstrate the effect of diesel start of injection (SOI) on the dual-fuel combustion process at 1200 rpm and 0.3 MPa IMEP. This test point represents an engine operating condition with high combustion losses, low exhaust gas temperatures, and possibly reduced aftertreatment efficiencies.

4.2.1 Experimental test procedure

Table 4.1 summarises the engine operating conditions. The diesel SOI was swept at a constant injection pressure of 50 MPa. The ethanol mass flow rate ($\dot{m}_{ethanol}$) was held constant and set to the minimum pulse width provided by the injector driver. The resulting ethanol energy fraction (EF) varied as the net indicated efficiency changed. No external EGR was used in this initial test to reduce the complexity of the test. PRR and COV_IMEP were limited to 2.0 MPa/CAD and 5%, respectively.

Table 4.1 – Engine operating conditions during a sweep of diesel SOI.

Parameter	Value
Speed	1200 rpm
Load	0.3 MPa IMEP
Diesel injection pressure	50 MPa
Diesel SOI	Varied between -40 and 0 CAD ATDC
$m_{ethanol/cycle}$ (*)	34.5 mg/cycle
EF (*)	Varied between 0.48 and 0.57
Intake air temperature	298 ± 2 K
Intake pressure	103 kPa
Exhaust pressure	104 kPa
EGR rate	0%

(*) Only for the dual-fuel testing modes.

4.2.2 Overview of the dual-fuel operation at a light load

Upon using a single diesel injection near firing top dead centre (TDC), the dual-fuel combustion had limited operating range due to relatively low fuel conversion efficiency and high PRRs. Figure 4.2 shows a comparison between conventional diesel combustion (CDC) and dual-fuel operation using constant diesel SOI at -10.3 CAD ATDC. Lower in-cylinder pressures were observed during the compression stroke due to the evaporation of the ethanol in the dual-fuel mode. The charge cooling effect and low reactivity of the ethanol retarded the start of combustion (SOC), allowing for a longer fuel-air mixing period and faster premixed combustion phase. The dual-fuel strategy with a late single diesel injection led lower net indicated efficiencies than the diesel-only operation. Therefore, this dual-fuel approach would not be a cost-effective alternative for partially replacing diesel with ethanol in heavy-duty engines. Alternatively, an early diesel fuel injection at -38.8 CAD ATDC reduced the levels of PRR, leading to lower peak heat release and improved fuel conversion efficiency, as depicted in Figure 4.3.

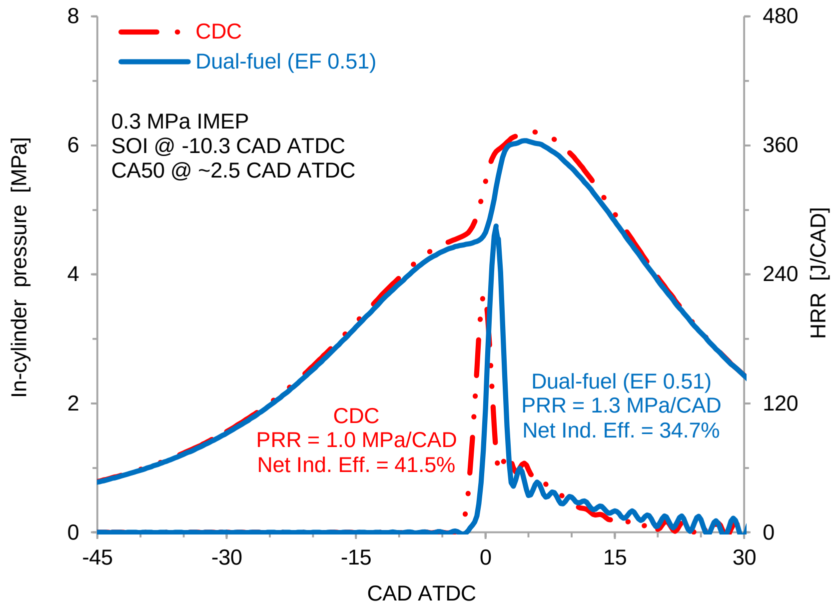

Figure 4.2 – In-cylinder pressure and HRR for CDC and dual-fuel combustion modes.

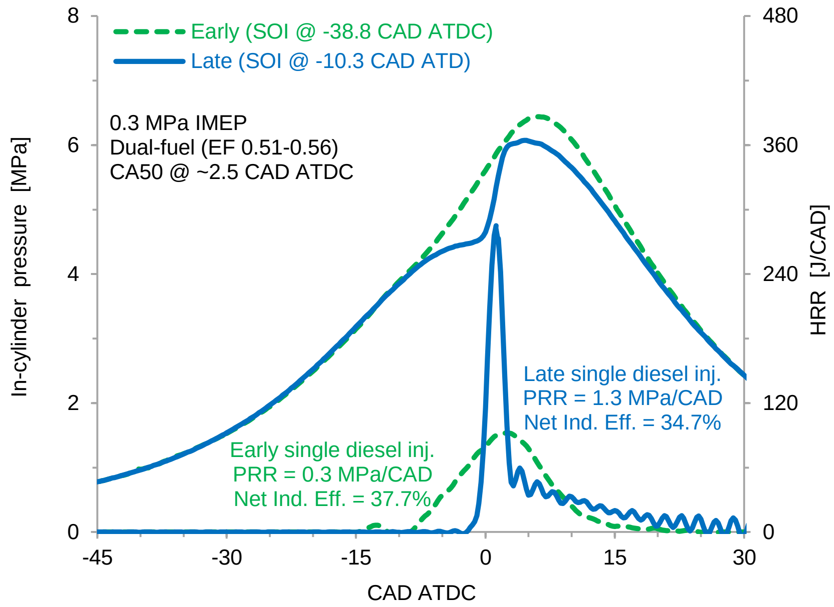

Figure 4.3 – In-cylinder pressure and HRR for dual-fuel operation with early and late diesel injection timings.

4.2.3 Combustion characteristics

Figure 4.4 shows the effects introduced by early and late diesel injections on the dual-fuel combustion process. SOIs between approximately -25 and -12.5 CAD ATDC could not be tested due to excessive PRRs, as indicated by the region of light grey dotted line. To the right of this region with late injections near TDC, it was observed that the ignition delay from SOI to SOC rises slightly for more advanced diesel injections. The combustion phasing (CA50) was shifted linearly towards the expansion stroke while the combustion duration (CA10-CA90) remained nearly constant for late SOIs. There was a reversal of the trend for early diesel injection timings. The CA50 position was advanced and the burn rate was shortened as the SOI was retarded from -40 to -25 CAD ATDC. The differences between the strategies were mainly a result of the degree of fuel stratification, which becomes more pronounced with the later injections. Extremely advanced and retarded SOIs effectively reduced the levels of PRR. The use of diesel injections within the grey dotted region would lead to unacceptable combustion noise.

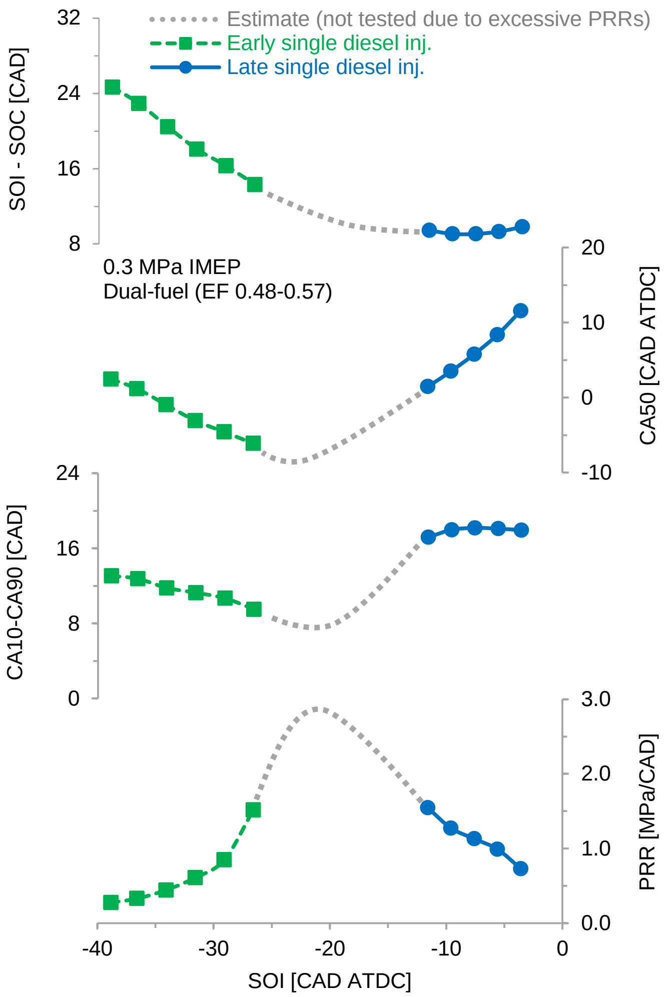

Figure 4.4 – Combustion characteristics for dual-fuel operation with early and late SOIs.

4.2.4 Engine-out emissions and performance

Figure 4.5 depicts the exhaust emissions as the diesel SOI was varied. Unburnt HC, soot, and NOx emissions were effectively reduced with early SOIs. This was due to longer ignition delays and improved mixture preparation, which resulted in more homogeneous and leaner in-cylinder charge and less high temperatures zones. However, the low temperature combustion led to a sharp increase in CO emissions. Nevertheless, Figure 4.6 shows that combustion efficiency was increased when using early single diesel injections, which is supported by the significant reduction in unburnt hydrocarbons.

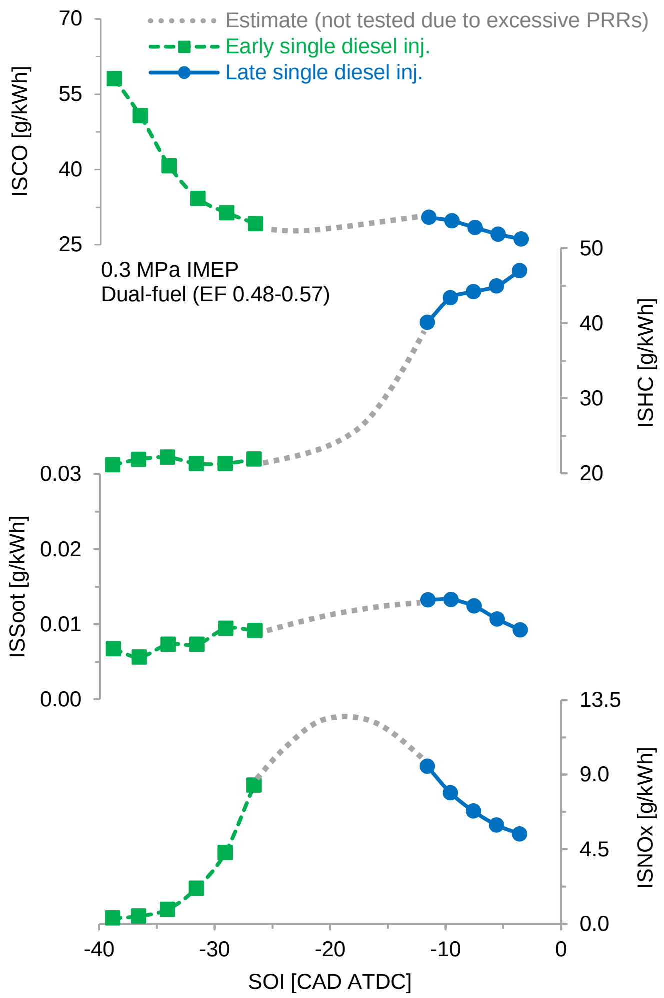

Figure 4.5 – Net indicated specific emissions for dual-fuel operation with early and late SOIs.

The reduction in the levels of incomplete combustion combined with a relatively faster burn rate allowed for higher net indicated efficiency when operating the engine with early SOIs, as depicted in Figure 4.6. Despite the relatively lower exhaust gas temperatures

(EGT), early diesel injection timings will be employed when exploring the effects of iEGR and intake throttling on low load dual-fuel combustion.

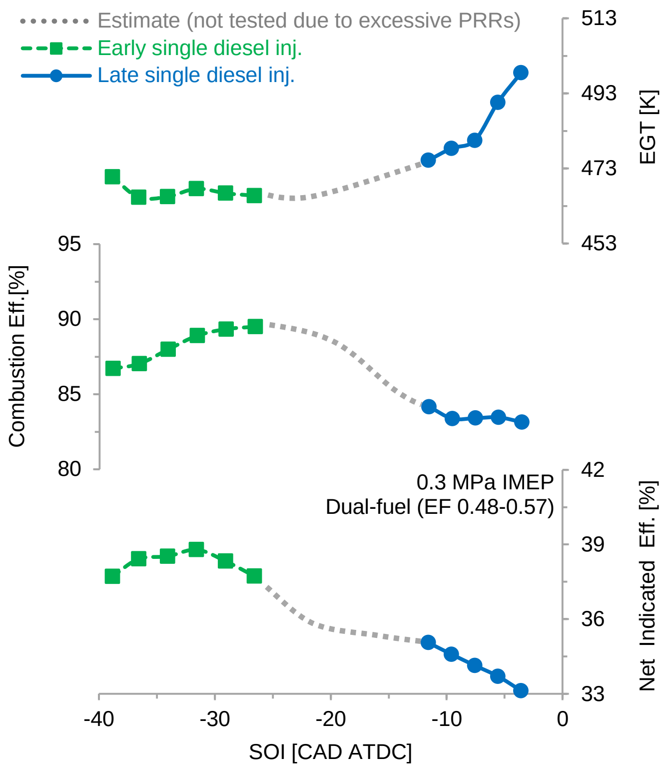

Figure 4.6 – Exhaust gas temperature and efficiencies for dual-fuel operation with early and late SOIs.

4.3 The effect of iEGR and intake throttling on low load dual-fuel operation

The effects of the internal exhaust gas recirculation (iEGR) and intake throttling on combustion, emissions, and efficiency of the dual-fuel operation have been investigated at 1200 rpm and 0.32 MPa IMEP. The iEGR was introduced using an intake valve re-opening (2IVO) provided by the variable valve actuation (VVA) system. The retention of hot residuals was used to enhance the mixture preparation and accelerate the occurrence of autoignition in high reactivity zones. Intake throttling was used to increase the global fuel/air equivalence ratio and elevate mean in-cylinder gas temperatures during combustion. This effect can help improve the combustion efficiency. One-dimensional (1D) engine simulation was used to estimate the in-cylinder residual gas fraction (RGF) and the mean in-cylinder gas temperature.

4.3.1 Experimental test procedure

Table 4.2 summarises the engine operating conditions. In this subsection, the diesel SOI was swept at a constant injection pressure of 50 MPa in order to determine the CA50 which achieved the highest net indicated efficiency. The $\dot{m}_{ethanol}$ was held constant and set to the minimum pulse width provided by the injector driver. The resulting ethanol energy fraction (EF) varied as the net indicated efficiency changed. No external EGR was used in this phase to reduce the complexity of the test. PRR and COV_IMEP were limited to 1.0 MPa/CAD and 5%, respectively.

Table 4.2 – Engine operating conditions for the different dual-fuel testing modes.

Parameter	Value
Speed	1200 rpm
Load	0.32 MPa IMEP
Diesel injection pressure	50 MPa
Diesel SOI	Varied between -55 and -25 CAD ATDC
$m_{ethanol/cycle}$	34.5 mg/cycle
EF	Varied between 0.53 and 0.56
Intake air temperature	298 ± 2 K
EGR rate	0%

The main intake valve opening (IVO) and closing (IVC) events were set at 367 and -151 CAD ATDC, respectively, as determined at 0.5mm valve lift. The maximum main intake valve lift was 14 mm. The intake valve re-opening during the exhaust stroke had its peak lift at around 195 CAD ATDC. When required, the 2IVO strategy opening and closing timings were set at the earliest (160 CAD ATDC) and latest positions (230 CAD ATDC), respectively. This configuration allowed for the maximum lift of 2 mm and highest residual gas fraction achieved by the current intake cam design. Figure 4.7 shows the resulting intake and 2IVO valve lift profiles as well as the fixed exhaust camshaft timing.

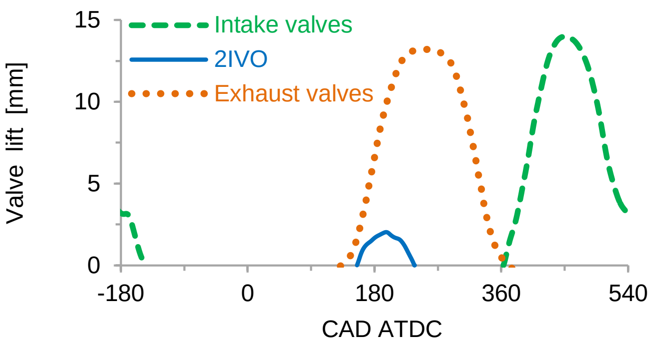

Figure 4.7 – Valve lift profiles based on crank angle position relative to firing TDC.

Table 4.3 depicts the three dual-fuel testing modes explored: baseline, iEGR, and throttled. The baseline represents wide open throttled engine operation. The iEGR mode utilised the 2IVO strategy to achieve internal exhaust gas recirculation. The intake manifold air pressure was held constant at 103 kPa while the exhaust pressure was gradually increased from 104 kPa to 134 kPa using the back pressure valve to obtain higher RGF. The throttled mode was operated with reduced intake air pressure of 90 kPa, 80 kPa, and 69 kPa while the back pressure was maintained at 104 kPa.

Table 4.3 – The dual-fuel testing modes.

Testing modes	Case number	Intake pressure	Exhaust pressure
Baseline	-	103 kPa	104 kPa
iEGR (with 2IVO)	1	103 kPa	104 kPa
	2		114 kPa
	3		125 kPa
	4		134 kPa
Throttled	1	90 kPa	104 kPa
	2	80 kPa	
	3	69 kPa	

4.3.2 Engine modelling

A 1D engine model was created with Ricardo Wave® 2015.1 simulation software to estimate the residual gas fraction and the mean in-cylinder gas temperature with different intake cam designs. The software uses the finite difference method to solve the unsteady compressible flow equations governing the conservation of mass, momentum, and energy. The simulation uses detailed thermodynamic gas properties, including equilibrium composition for the burnt gases, and enables the characterisation of the pulsating flows that occur in the engine. The later allows the determination of the RGF by computing the mass flow rates through the valves and due to fuel injection.

Figure 4.8 shows a snapshot of the single cylinder engine model. The inlet and exhaust piping were accurately measured from the engine test cell and modelled accordingly. Oscilloscopes were placed in the same locations as the experimental in-cylinder, intake, and exhaust pressures transducers. The geometric data of the cylinder head was obtained from the computer-aided design model provided by Yuchai. Experimental data, such as temperatures, initial intake and exhaust pressures, fuel flow rates, injection locations and timings, and heat release profile, were imposed in the model. Ethanol was injected in the intake port (PFI) while diesel was direct injected into the cylinder (DI).

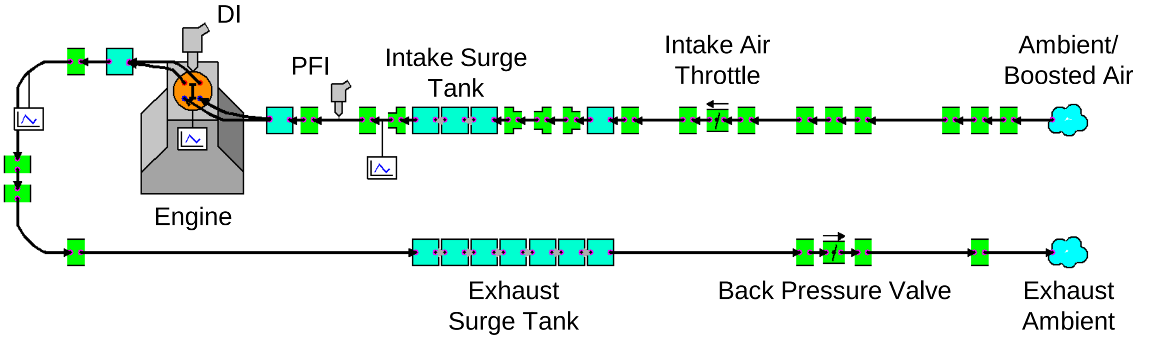

Figure 4.8 – 1D model of the single cylinder HD engine.

Port and valve flow coefficients (CF) were provided by the engine supplier and tuned using the engine simulation software. The coefficients compare the actual air flow rate through the poppet valves against the performance of theoretical ports without any restriction. The calculation of the CFs uses the ideal gas velocity and valve throat cross-sectional area. The reference diameters (D) were obtained from the valves inner seats, which were equivalent to 39.2 mm for the intake side and 35.8 mm for the exhaust side. Figure 4.9 shows the resulting CFs for the intake and exhaust ports as a function of valve lift (L).

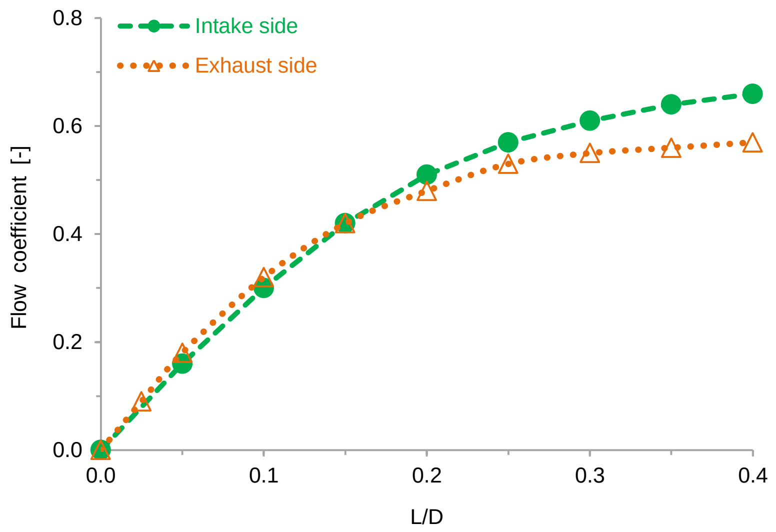

Figure 4.9 – Flow coefficient as a function of valve lift for the intake and exhaust ports.

In terms of discretisation, the software suggests a minimum length of 58 mm for the intake side and 71 mm for the exhaust system calculated as a function of the engine bore diameter. The discretisation sizes were refined to 20 and 30 mm, respectively, in order to achieve better resolution of changes in the calculated state of the fluid (e.g. pressure waves) and optimise the model. However, the two pipes connected to intake and exhaust ambient required a discretisation size of 200 mm, as they were 600 and

10000 millimetres long. This was necessary to obtain a trade-off between computational time and high accuracy.

Each engine operating case was started with the initial conditions set by the user and was simulated for 80 cycles. If the convergence criteria was met before the end of simulation duration, the current case would run one additional cycle before was stopped. The standard tolerance for convergence was set to 0.1% of the computational cells' pressure and velocity for three consecutive cycles. The maximum time step was set to 0.25 CAD. A user-imposed multiplier of 0.7 was introduced to shorten the time step size and improve stability.

The engine conduction sub-model used a more detailed pre-defined thermal network with components to represent the cylinder liner, head, piston, intake valves, exhaust valves, valve seats, and ports. Initial gas side surface temperatures were set to the default values of 385 K and 500 K for the intake and exhaust sides, respectively. Coolant temperature at different piston, liner and cylinder head locations was set to 380 K using the corresponding heat transfer coefficient obtained from an example of a multi-cylinder diesel engine provided by the simulation software.

The combustion process was based on empirical functions provided by the 1D code, similar to the correlations determined by Watson et al. [175]. Diesel-only combustion simulations were carried out using a multi-component Wiebe combustion model for a single fuel. In the dual-fuel cases, a multi-fuel multi-component Wiebe combustion sub-model with up to four superimposed curves was used to better fit the MFB profile calculated from the experimental in-cylinder data.

Figure 4.10 shows the sum of three Wiebe curves superimposed to re-create the experimental or "target" burn rate for a dual-fuel operation. Each Wiebe function was defined using a specified crank angle position corresponding to a burnt mass fraction of 50%, burn duration, Wiebe exponent, and relative ratio of fuel mass consumed. The total burn rate profile was scaled by the experimentally determined combustion efficiency to account for incomplete combustion, as shown in Figure 4.11.

A Woschni heat transfer sub-model [176] calculated the amount of heat transferred to and from the charge by assuming a uniform convective heat flow coefficient and velocity on all surfaces of the cylinder. The correlation included a load compensation term to adjust for the characteristic velocity used in the heat transfer coefficient calculation. This term represents the sum of the mean piston speed and a combustion-related velocity, which is affected by the in-cylinder pressure.

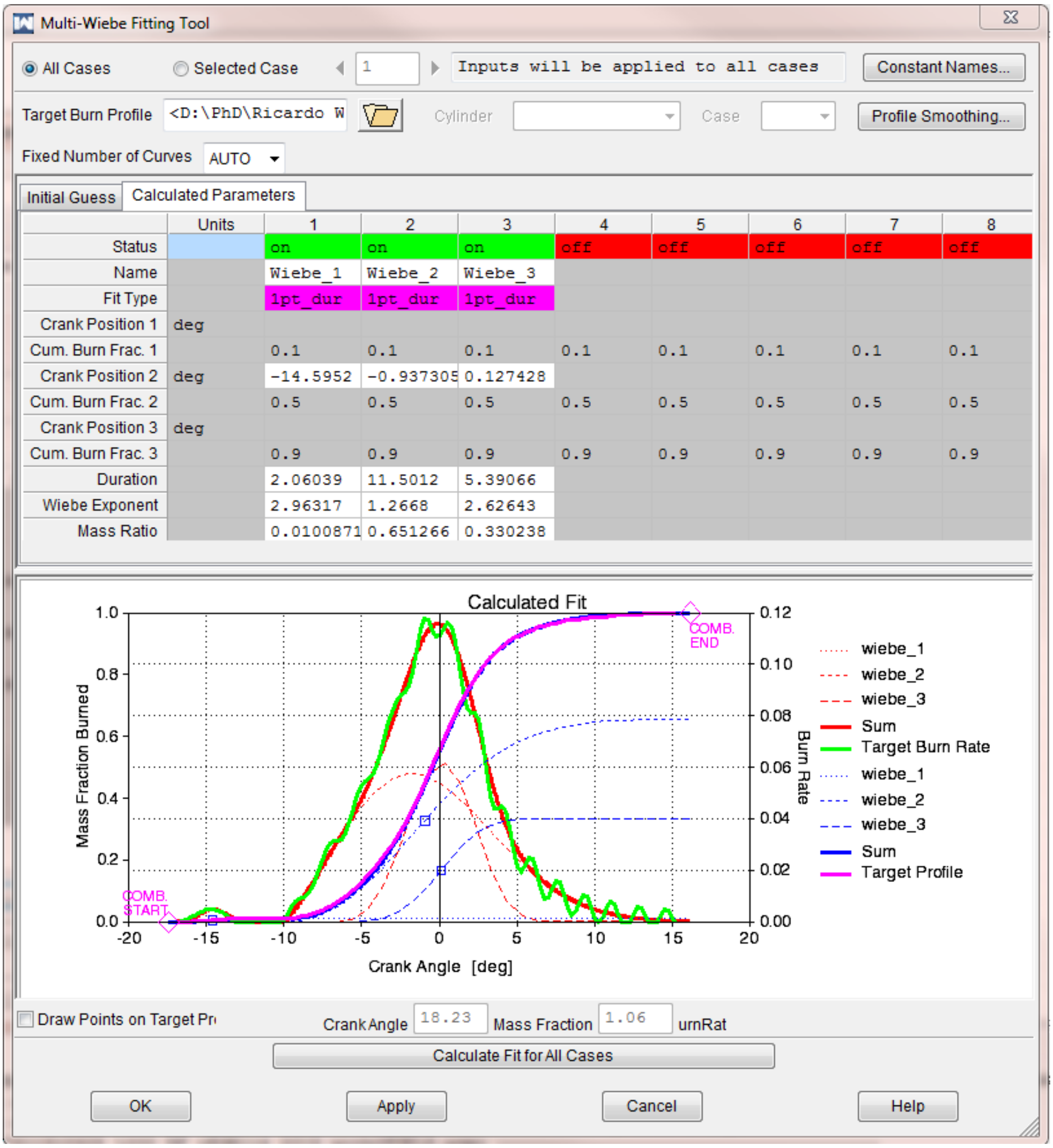

Figure 4.10 – Ricardo Wave's multi-Wiebe fitting tool panel.

Multipliers of the convective heat transfer coefficient were set between 1.2 and 1.6 during the intake valve open period, and between 0.9 and 1.2 during closed period. Heat transfer multipliers were also imposed at the intake and exhaust ports and were set to 1.5 and 2.0, respectively. These values were determined empirically in order to optimise the model. Wall friction multipliers were not used.

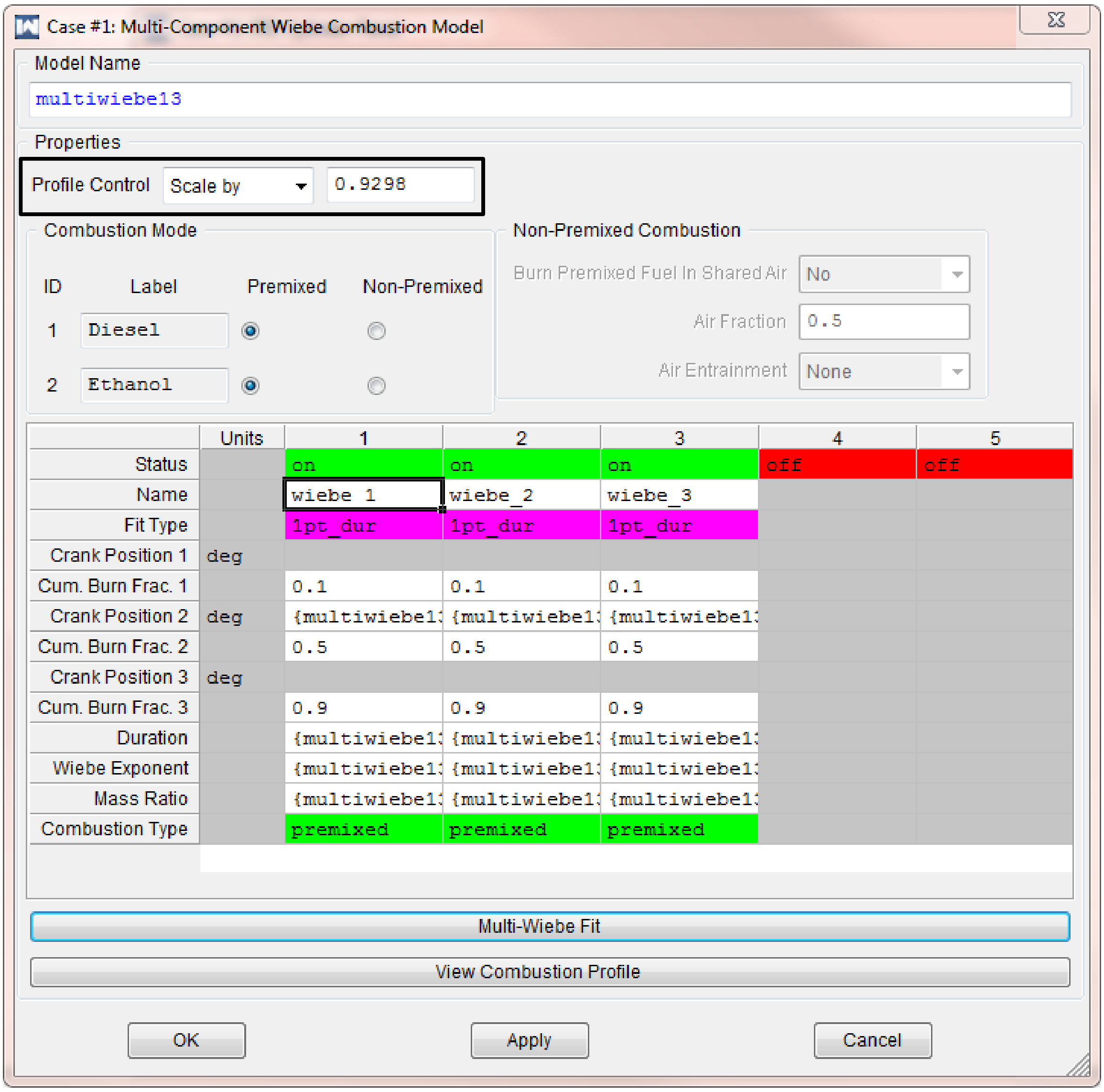

Figure 4.11 – Ricardo Wave's multi-fuel multi-component Wiebe combustion panel.

The cylinder thermodynamic state was calculated through a two zone model, comprised of unburnt and burnt zones. The unburnt zone contains air, fuel vapour, and residual gases, while the burnt zone contains all of the mass that has been consumed by the combustion. In the real engine, diesel starts to burn as it achieves thermal ignition, reached when favourable chemical kinetics (i.e. temperature and equivalence ratio) are attained [88]. The prediction of this phenomenon would require the modelling of the heat released by the non-premixed diesel fuel and the determination of the fraction of air utilised. In order to simplify the dual-fuel combustion model, the diesel fuel was set as premixed prior to the start of combustion, respecting the diesel injection timing and fuelling rate. This simplification has an effect on the resulting burnt gas temperature, which was not used in this study.

Nevertheless, the mean in-cylinder gas temperatures determined by the thermodynamic model via the equation of state resulted in coherent trends. In addition, the residual gas fraction, which is strongly related to the valve strategy, compression ratio, and instantaneous pressures, was in agreement with the literature [100,114].

4.3.3 Validation of the 1D engine model

In all cases, the intake air mass flow and the maximum in-cylinder gas pressure (P_{max}) were validated to within 3% of the experimental data. The modelled and experimental values for average intake and exhaust manifold pressures and IMEP were computed to be within 1.5% and 5.0%, respectively. The accuracy allowed for the use of the 1D model to estimate the RGF and the mean in-cylinder gas temperature.

Figure 4.12 provides a comparison between experimental and modelled instantaneous in-cylinder pressure for Case 4 of the iEGR mode depicted in Table 4.3. The diagram shows the model predicts lower in-cylinder pressures during the second half of the compression stroke. This is likely to be a result of over-predicted heat transfer and the fact the modelled in-cylinder pressure is insensitive to the simulated diesel injection pressure.

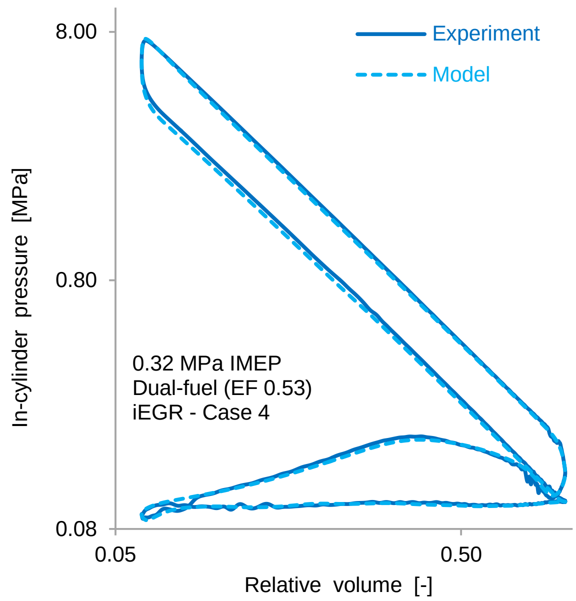

Figure 4.12 – Experimental and modelled log P-V diagram of Case 4 of the iEGR mode.

However, there was excellent agreement between the experimental and modelled gas exchange process, as supported by the pumping loop in Figure 4.12 as well as the intake and exhaust manifold pressures in Figure 4.13.

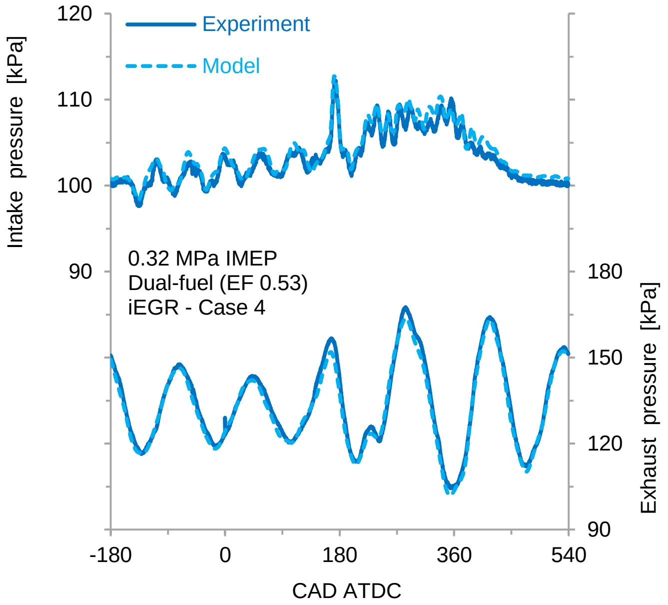

Figure 4.13 – Experimental and modelled instantaneous intake and exhaust manifold pressures of Case 4 of the iEGR mode.

4.3.4 Overview of the iEGR and throttled dual-fuel modes

Figure 4.14 shows the effect of varied diesel injection timings on CA50 position and combustion stability as measured by the COV_IMEP. The early single diesel injection strategy ensured sufficient mixing time and allowed an almost linear combustion phasing control with low overall COV_IMEP. A low COV_IMEP is important to minimise the combustion instability associated with misfiring cycles and partial burning of the fuel [8].

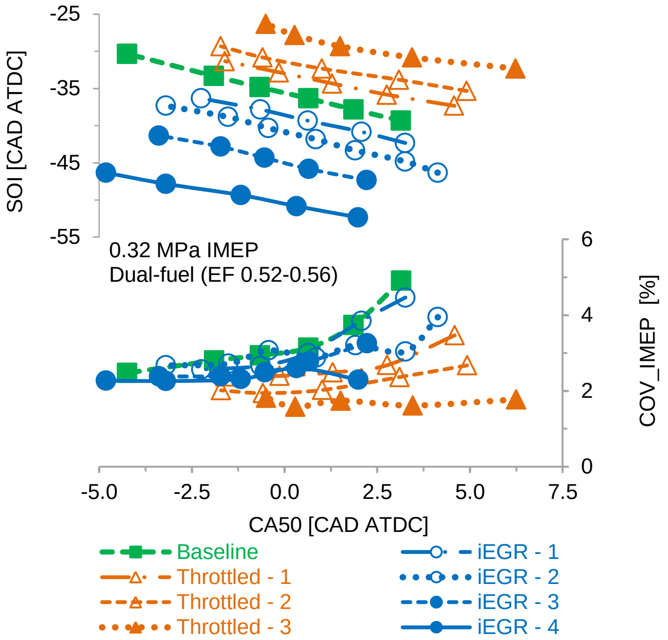

Figure 4.14 – The effect of diesel SOI on dual-fuel combustion phasing and COV_IMEP.

Relatively later diesel injections resulted in the production of higher fuel/air equivalence ratio regions in the piston bowl [177]. This higher degree of stratification increased local in-cylinder temperatures, advancing the CA50 positions and reducing the COV_IMEP. In comparison, advanced SOI allowed for more uniform equivalence ratio and ignition delay distribution [177], yielding opposite effects to later SOI.

The use of the 2IVO strategy combined with higher back pressures in the iEGR mode elevated the RGF. Higher levels of hot residuals increased the mean in-cylinder gas temperature, which accelerated the evaporation and combustion processes and reduced the cycle-to-cycle variability. As a result, advanced SOIs were required to control charge reactivity. The use of a constant SOI would lead to over-advanced burn rates triggered by the more reactive mixture with iEGR, as show in Figure 4.15.

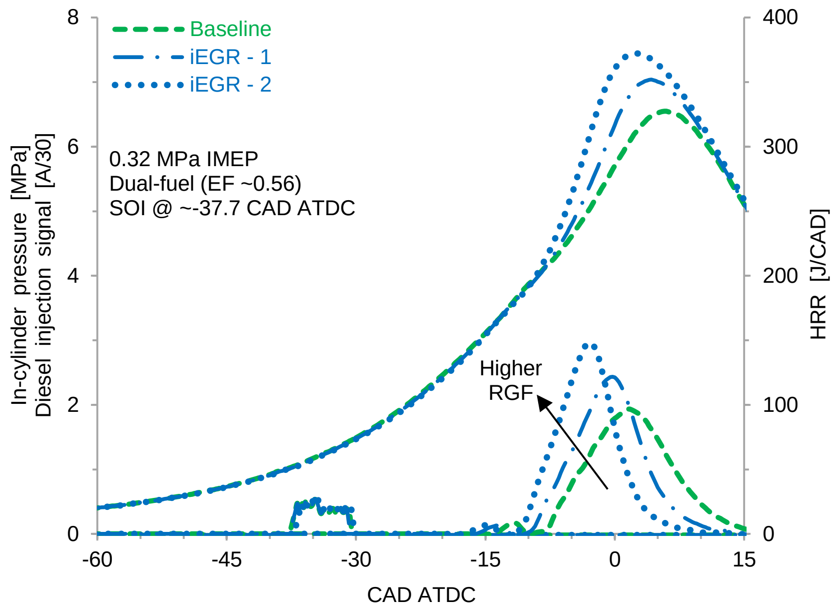

Figure 4.15 – The effect of higher iEGR on dual-fuel combustion with constant early diesel injection timing.

Interestingly, the throttled operation required relatively later diesel injections to increase fuel stratification and advance the SOC. This different behaviour is probably a result of lower in-cylinder pressures, which impaired the ignition of the diesel fuel for a constant SOI in Figure 4.16. Retarded injection timings led to higher local and global fuel/air equivalence ratios, which likely increased peak mean in-cylinder gas temperatures during combustion. The hotter combustion process accelerates the reaction rates [178], which can shorten the burn rate and lower the COV_IMEP.

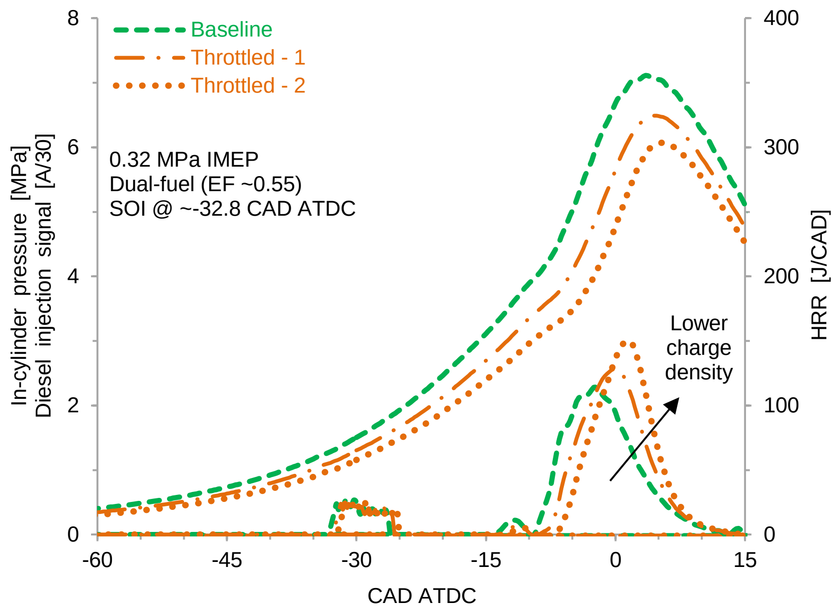

Figure 4.16 – The effect of intake throttling on dual-fuel combustion with constant early diesel injection timing.

The dual-fuel operation with a similar CA50 position at ~0.5 CAD ATDC showed that the iEGR and throttled modes were characterised by shorter combustion process and higher peak heat release than the dual-fuel baseline. Figure 4.17 depicts the in-cylinder pressure, diesel injection signal, and HRR for the baseline, Case 4 of the iEGR mode, and Case 3 of the throttled mode.

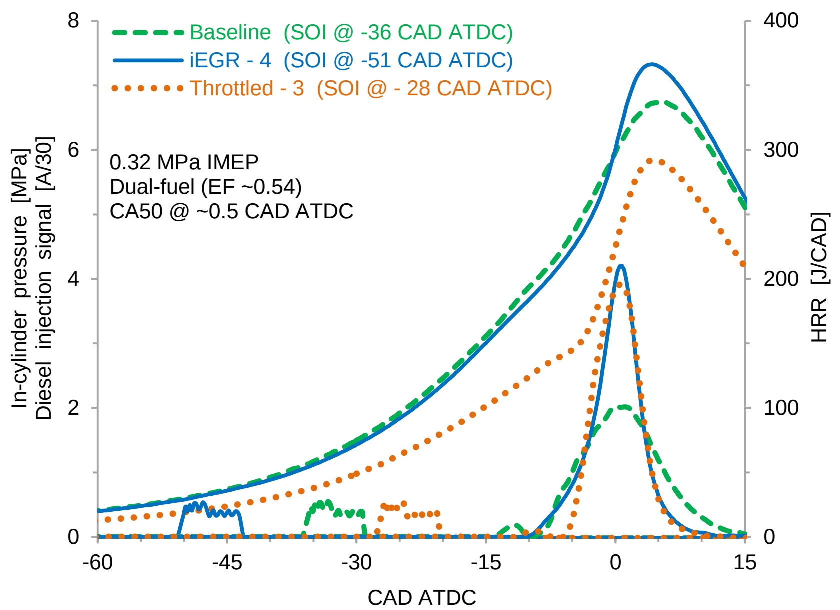

Figure 4.17 – In-cylinder pressure, diesel injection signal, and HRR for the baseline, Case 4 of the iEGR mode, and Case 3 of the throttled mode at similar CA50 position.

Figure 4.18 depicts the log P-V diagram for the same operating points showed in Figure 4.17. The plot reveals a larger pumping loop area for the iEGR and throttled modes compared to the dual-fuel combustion baseline.

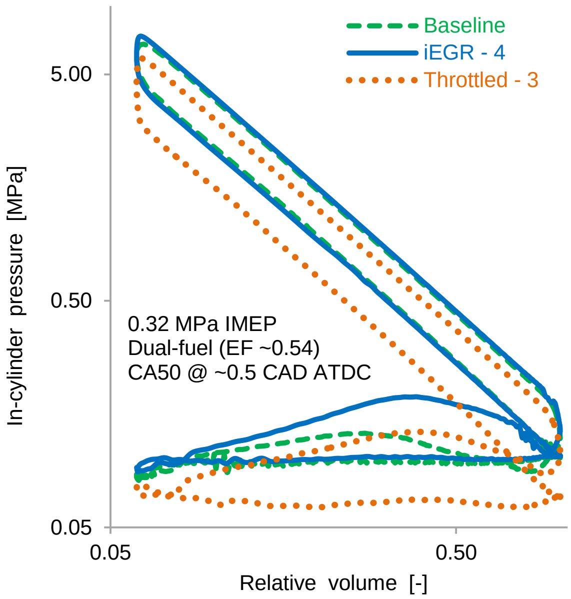

Figure 4.18 – Log P-V diagram of the baseline, Case 4 of the iEGR mode, and Case 3 of the throttled mode at similar CA50 position.

Figure 4.19 complements the information given above by showing the resulting gas exchange efficiency and the global fuel/air equivalence ratio (Φ) for the most efficient operating points of each dual-fuel case (see Table 4.3). The baseline achieved the highest gas exchange efficiency and leaner combustion process due to the most efficient scavenging process.

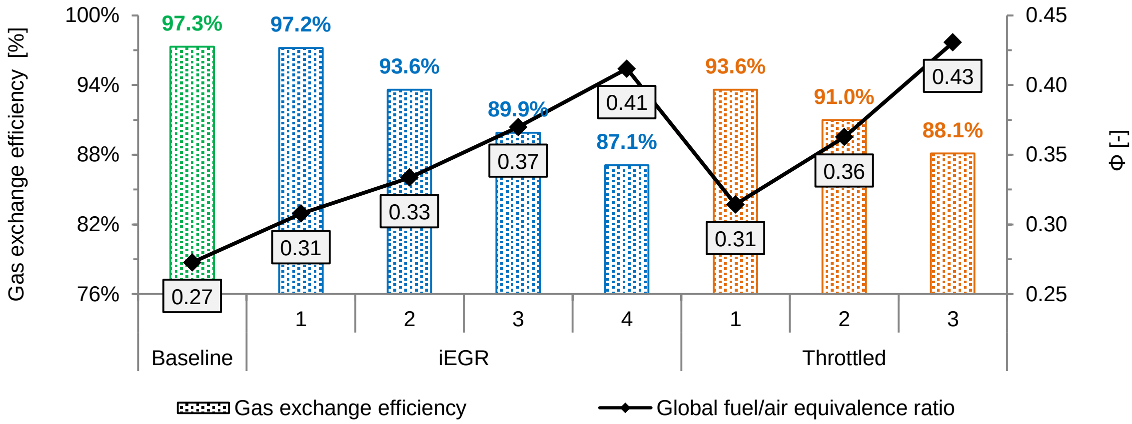

Figure 4.19 – Gas exchange efficiency and Φ for the most efficient operating points of each dual-fuel case.

There were minor effects with regard to pumping losses when using the 2IVO strategy and maintaining the same exhaust pressure of the baseline (Case 1 of the iEGR mode). The higher pressure ratio between the exhaust and intake manifolds in the Cases 2-4 of the iEGR mode lowered the gas exchange efficiency and allowed for higher RGF up to 26.2%. The introduction of hot residuals into the intake manifold increased the specific volume of the inlet charge and decreased the amount of fresh air inducted, resulting in higher Φ. Alternatively, intake throttling resulted in lower inlet charge density and increased Φ than the baseline via a reduction in intake manifold air pressure. The lower overall in-cylinder pressure resulted in higher pumping mean effective pressure (PMEP) and lower gas exchange efficiency.

Figure 4.20 shows the in-cylinder gas temperature at IVC (T_{IVC}), the peak mean in-cylinder gas temperature, and RGF obtained from the 1D engine model for the most efficient operating points of each dual-fuel case. The larger amount of hot residual gases raised the initial charge temperature T_{IVC} of the iEGR mode. The hotter charge combined with higher Φ increased mean in-cylinder gas temperatures during the combustion process. In the throttled mode, the RGF slightly increased from 3.7% to 4.5% due to lower pressure ratios between the cylinder and manifolds. The T_{IVC} remained nearly constant with the decrease of intake air pressure. However, peak mean in-cylinder gas temperatures progressively increased due to higher Φ, reaching temperatures of 1890 K.

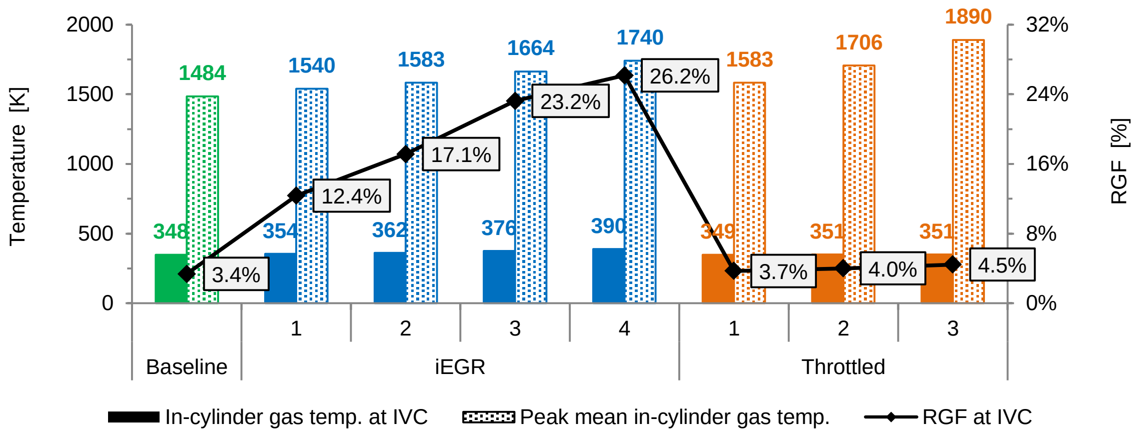

Figure 4.20 – In-cylinder gas temperatures and RGF for the most efficient operating points of each dual-fuel case obtained from the 1D engine model.

4.3.5 Combustion characteristics

The mapping established in Subsection 4.3.4 helped determine the SOI that provides the highest net indicated efficiency for each case of the testing modes showed in Table

4.3. Earlier combustion processes resulted in higher compression work and possibly higher heat losses. Later combustion events lowered the engine efficiency due to higher combustion losses and decreased expansion work.

Figure 4.21 and Figure 4.22 show the optimum diesel injection timings and the resulting heat release characteristics. The analysis was performed on a global fuel/air equivalence ratio basis, as the higher RGF of the iEGR mode and the lower charge density of the throttled mode effectively increased the value of Φ.

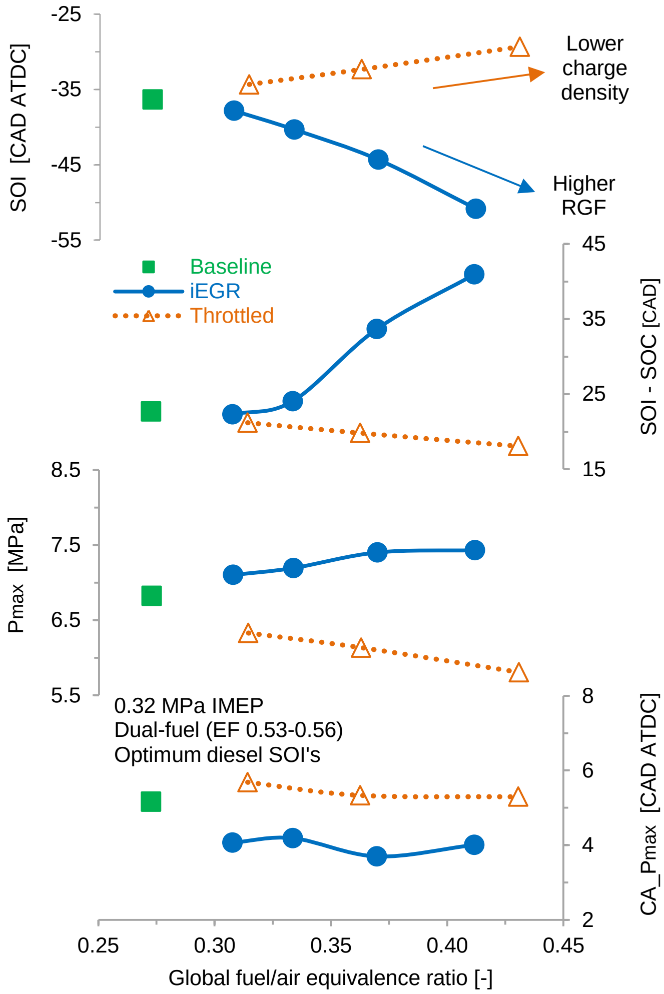

Figure 4.21 – Optimum diesel injection timing, ignition delay from SOI to SOC, P_{max}, and CA_P_{max} for the different dual-fuel testing modes.

In the iEGR mode, the optimum SOI was advanced from -37.8 CAD ATDC to -50.8 CAD ATDC as the RGF and Φ increased in order to avoid too advanced combustion [179]. The earlier injections lengthened the ignition delays, as the SOC and CA10 took place almost at the same crank angle. In addition, the iEGR mode required different combustion phasing for maximum efficiency than the baseline and throttled modes.

According to Caton [180], shorter burning rates and relatively lower heat losses allow for more advanced CA50 and higher maximum in-cylinder pressure (P_{max}). This is the case of the iEGR mode, where peak combustion temperatures (i.e. burnt zone) and heat transfer are likely to be reduced by the dilution and higher heat capacity introduced by higher RGFs [181]. The more advanced and faster combustion process resulted in higher P_{max} at around 4 CAD ATDC.

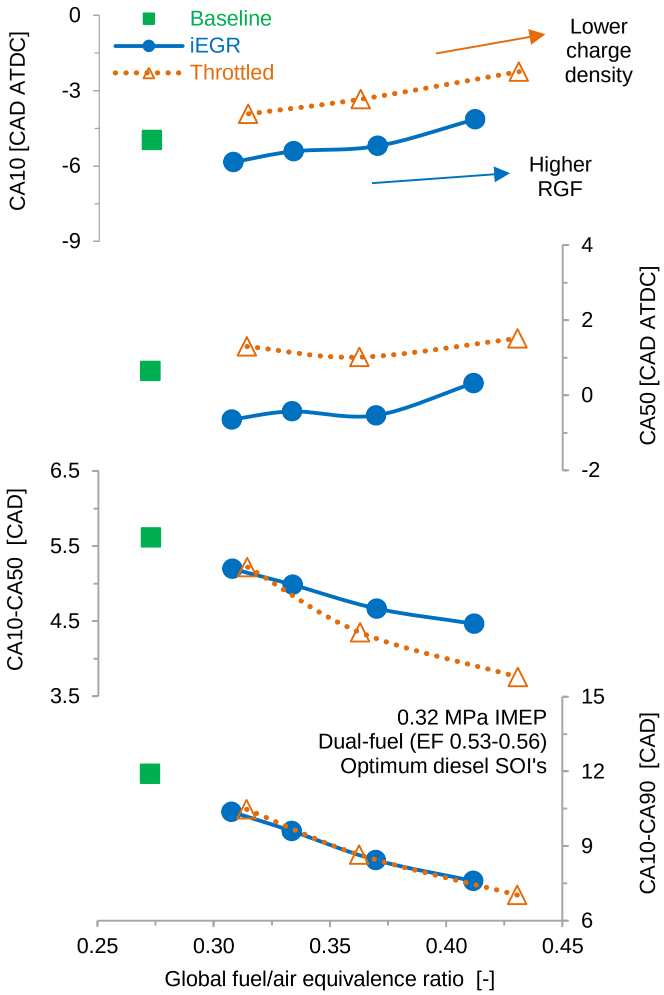

Figure 4.22 – CA10, CA50, CA10-CA50, and CA10-CA90 for the different dual-fuel testing modes.

In the throttled mode, the reduced in-cylinder charge density decreased the in-cylinder pressures and adversely affected the compression ignition process [182]. Consequently, SOI was retarded from -34.3 CAD ATDC to -29.3 CAD ATDC when the charge temperature is higher, shortening ignition delay. Once ignition occurred, the combustion rapidly progressed in the relatively high reactivity and high equivalence ratio zones, as shown in the optical experiments performed by Kokjohn et al. [183] using iso-octane and n-heptane. This fast progression is demonstrated by the shorter period of CA10-CA50 at higher Φ conditions. The rapid initial heat release combined with low RGF resulted in higher mean combustion temperatures, leading to later optimum CA50 and crank angle of P_{max} (CA_P_{max}) than the dual-fuel baseline and iEGR mode. Combustion duration was shortened at higher Φ, independently of the dual-fuel combustion mode.

4.3.6 Engine-out emissions and performance

Figure 4.23 depicts the engine-out emissions produced by the three dual-fuel testing modes shown in Table 4.3. Net indicated specific emissions of unburnt HC, CO, NOx, and soot are given by ISHC, ISCO, ISNOx, and ISsoot, respectively. The use of the iEGR and throttled modes to achieve higher Φ were shown effective in reducing unburnt HC and CO emissions. NOx and soot emissions demonstrated completely different trends as the air flow rate was reduced. The lowest values were achieved in the iEGR mode.

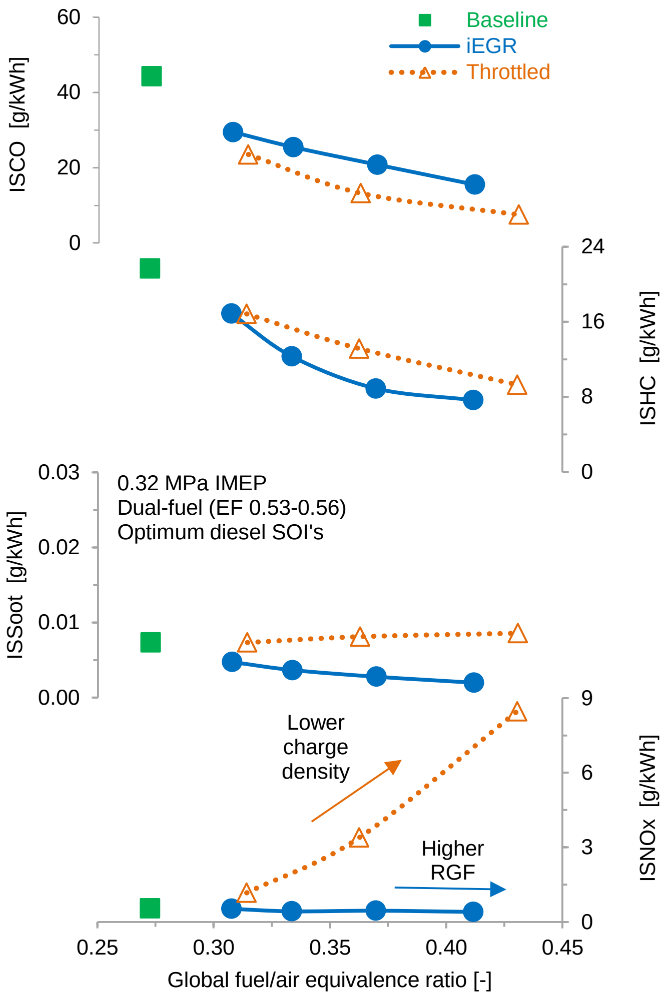

Figure 4.23 – Net indicated specific emissions for the different dual-fuel testing modes.

Higher back pressures pushed more burnt gases into the intake manifold in the iEGR mode, increasing the initial RGF of 3.4% in the baseline up to 26.2% in Case 4. The higher amount of hot residuals elevated the T_{IVC} by 42 K (see Figure 4.20). The hotter charge and higher Φ led to peak mean in-cylinder gas temperatures of 1740 K. The warmer combustion process reduced the CO and unburnt HC emissions to 15.5 g/kWh and 7.6 g/kWh, respectively – nearly a third of the baseline results. Further reduction in CO and unburnt HC emissions was possibly limited by a decrease in oxygen availability, as demonstrated by Kawasaki et al. [106] using an exhaust valve re-opening (2EVO) strategy in a natural-gas HCCI engine. Another hypothesis is that lower local combustion temperatures combined with a stock diesel combustion system not designed for premixed fuel operation hampered the complete oxidation of the fuels [57]. The dilution and higher heat capacity of the in-cylinder charge decreased the levels of NOx emissions from 0.54 g/kWh in the baseline to 0.40 g/kWh. Soot emissions decreased from 0.007 g/kWh to 0.002 g/kWh due to longer ignition delay and hence better mixing of the diesel fuel.

In the throttled mode, the faster HRR and lower in-cylinder mass increased mean in-cylinder gas temperatures during combustion, reducing the ISCO and ISHC to 7.5 g/kWh and 9.3 g/kWh, respectively. The unburnt HC emissions were relatively higher in the throttled mode than in the iEGR mode when considering the same Φ. This is likely a result of lower initial charge temperatures and shorter ignition delays in the throttled mode, which also led to relatively higher soot levels of 0.009 g/kWh. The combination of a more stratified in-cylinder charge promoted by later diesel injections and the oxygen availability sharply increased NOx formation.

Figure 4.24 shows the PMEP, EGT, combustion efficiency, and net indicated efficiency. Higher back pressures in the iEGR mode reduced the PMEP from -9 kPa to -48 kPa. In addition, lower intake air pressures in the throttled mode increased the pumping losses to -44 kPa as compared with -9 kPa in the baseline. Hotter combustion processes elevated the EGT up to 600 K in the throttled mode, which is sufficiently high to initiate the catalyst light-off and enhance its conversion efficiency [94]. The dilution of the in-cylinder charge with residual gases and lower local in-cylinder gas temperatures limited the exhaust gas temperatures of the iEGR mode to 531 K. Relatively higher mean combustion temperatures with increased global fuel/air equivalence ratio enhanced the oxidation process of HC and CO. As a result, combustion efficiencies increased from 87.7% in the baseline dual-fuel case to almost 96% in the iEGR and throttled modes. This improvement would have increased the net indicated efficiency if PMEP had been maintained, which is supported by the results for Case 1 of the iEGR mode. However, the engine efficiency dropped from 39.4% to 37.2% as the exhaust manifold pressure was elevated from 104 kPa to 134 kPa. This reduction was a result of the higher pumping losses as well as a lower γ value for the mixture with higher RGF and Φ.

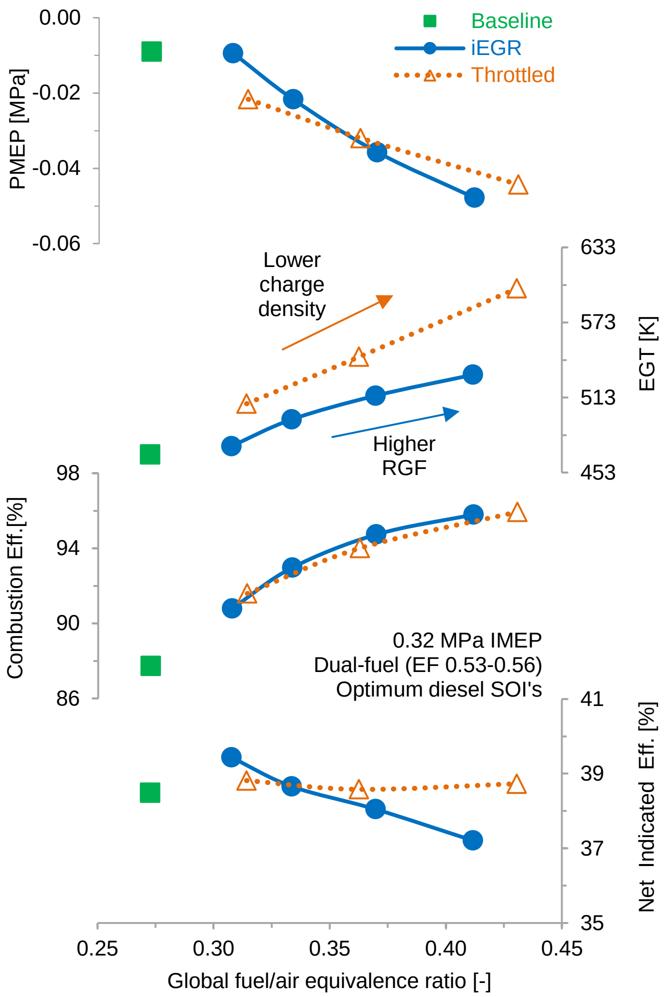

Figure 4.24 – Overall engine performance for the different dual-fuel testing modes.

The reduced charge density in the throttled mode allowed for higher mean in-cylinder gas temperatures during combustion, which increased the amount of fuel converted. The higher fuel conversion combined with an optimised combustion phasing and shorter CA10-CA90 maintained the net indicated efficiency at near constant value. Therefore, the increase in pumping losses introduced by the intake throttling was offset by the improvement in combustion efficiency and the more thermodynamically optimum heat release. Nevertheless, the iEGR testing mode with a constant exhaust back pressure was considered the optimum dual-fuel strategy for further investigations at low engine loads as a result of the low overall emissions and higher net indicated efficiency achieved.

4.4 The effect of engine load on dual-fuel operation with iEGR

Experimental studies were carried out using iEGR at 1200 rpm at engine loads that varied from 0.3 MPa IMEP to 0.6 MPa IMEP. The later represents a high residency area in the WHSC engine test cycle. The objective of this section was to explore the dual-fuel operating range with higher RGF. The alternative dual-fuel combustion process with iEGR was compared to a dual-fuel baseline (e.g. without a 2IVO) and CDC.

4.4.1 Experimental test procedure

Table 4.4 depicts the main engine operating conditions. Three testing modes were explored: dual-fuel baseline, dual-fuel combustion with iEGR (via a 2IVO strategy), and conventional diesel combustion.

Table 4.4 – Engine operating conditions and testing modes.

Parameter	Value			
Speed	1200 rpm			
Load	0.3 MPa IMEP	0.4 MPa IMEP	0.5 MPa IMEP	0.6 MPa IMEP
Diesel inj. pressure	50 MPa	60 MPa	70 MPa	80 MPa
$m_{ethanol/cycle}$ (*)	35.7 mg/cycle	42.7 mg/cycle	49.5 mg/cycle	57.5 mg/cycle
EF(*)	0.59-0.62	0.60-0.62	0.58-0.60	0.59-0.60
Intake air temp.	297 ± 2 K			
Intake pressure	103 kPa			
Exhaust pressure	104 kPa			
EGR rate	0%			
Testing modes	Dual-fuel baseline, dual-fuel with iEGR, and CDC			

(*) Only for the dual-fuel testing modes.

The back pressure was maintained 104 kPa while the intake manifold air pressure was kept at 103 kPa as the load was increased. The diesel SOI was swept to obtain the CA50 with the highest net indicated efficiency. The dual-fuel strategies used an ethanol energy fraction of ~0.60 and an early single diesel injection between -50 CAD ATDC and -30 CAD ATDC. Conventional diesel combustion was characterised by a single diesel injection close to firing TDC. Rail pressure was increased progressively to minimise soot emissions. The PRR limit was increased to 2.0 MPa/CAD to allow the use of higher diesel injection pressures. COV_IMEP was limited to 5%. The main intake valve timings and intake valve re-opening profile were the same as those employed in Section 4.3.

4.4.2 Overview of the engine operating modes

The comparison with the diesel-only mode enabled a clear analysis of the benefits and challenges for low load dual-fuel operation with and without iEGR. Figure 4.25 shows the in-cylinder pressure and HRR curve for the three combustion strategies at 0.5 MPa IMEP. Figure 4.26 depicts the resulting mean in-cylinder gas temperatures.

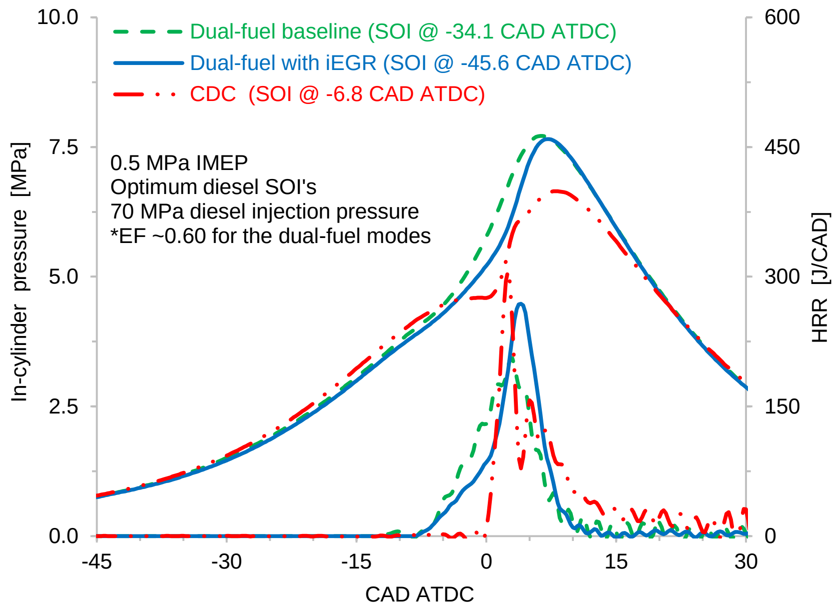

Figure 4.25 – In-cylinder pressure and HRR for the three testing modes at 0.5 MPa IMEP.

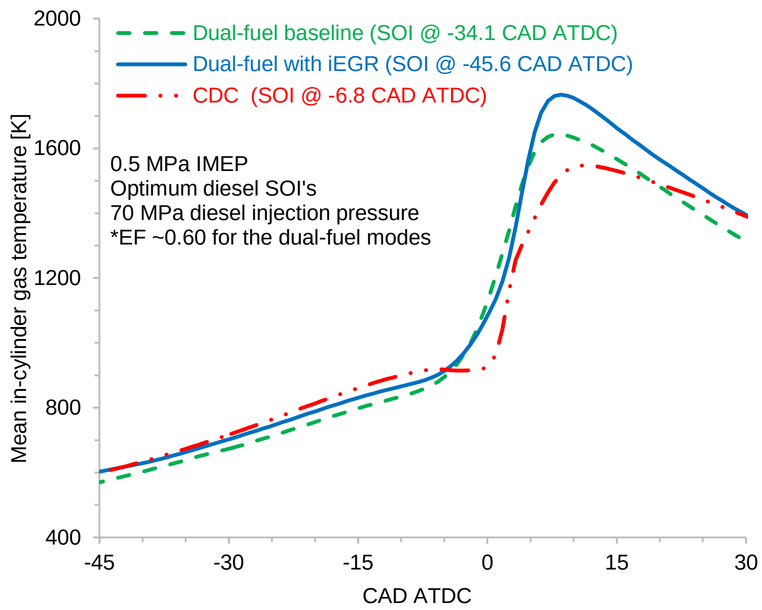

Figure 4.26 – Mean in-cylinder gas temperature for the three testing modes at 0.5 MPa IMEP.

After a short fuel-air mixing period, the CDC operation resulted in a high peak heat release during the premixed combustion phase, followed by a mixing-controlled combustion [8]. The later SOC and longer burn rate of the diesel-only mode decreased the P_{max} and led to lower mean in-cylinder gas temperature during combustion, as shown in Figure 4.26. Despite of this apparent improvement, the diesel diffusion flame presents locally rich and lean high temperature regions [57].

4.4.3 Combustion characteristics

Figure 4.27 depicts the main combustion characteristics of the three modes of operation. The highest net indicated efficiencies and thus optimum operating conditions were attained using later combustion phasing as the engine load was increased. This delay was necessary due to increased heat transfer losses and different start- and end-of-combustion timings. In the CDC, the SOI was retarded as the load was elevated since the diffusion flame directly controls the CA50 position. Relatively longer burn rates were also obtained as a result of greater amount of diesel injected and burnt in the mixing controlled combustion.

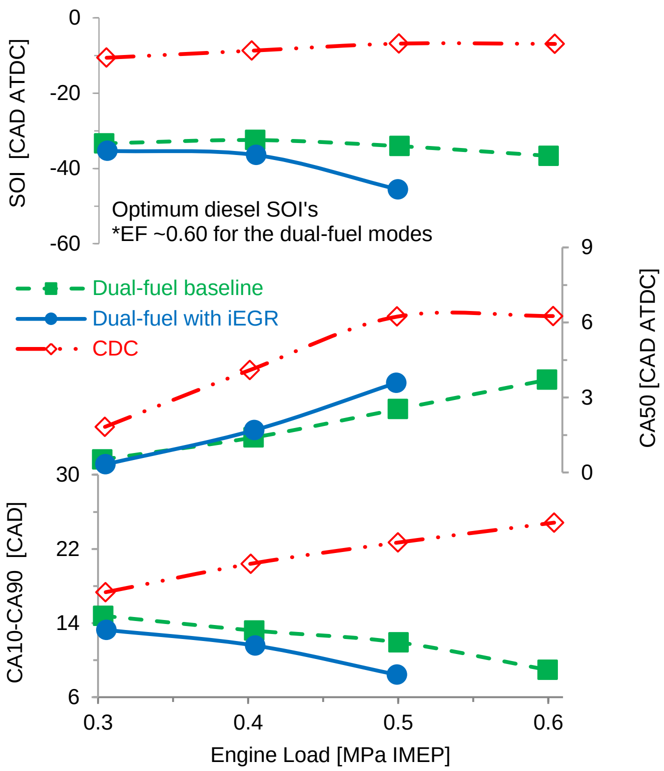

Figure 4.27 – Combustion characteristics for the three testing modes at different loads.

In contrast, the dual-fuel baseline and iEGR modes required earlier diesel injections due to increased equivalence ratio and charge reactivity at higher engine loads. The use of advanced diesel injections resulted in more homogeneous in-cylinder charge, which helped retard the combustion event. When comparing the combustion phasing, optimum dual-fuel operation was achieved with earlier CA50s than those of the conventional diesel combustion. This was attributed to lower local combustion temperatures [57] produced by its more progressive heat release and well-distributed fuel reactivity.

The use of a 2IVO strategy under the iEGR mode allowed for slightly more advanced combustion phasing at 0.3 MPa IMEP. However, shorter CA10-CA90 and increased amounts of fuel converted required earlier SOIs and retarded CA50s at 0.4 and 0.5 MPa IMEP, as shown in Figure 4.28.

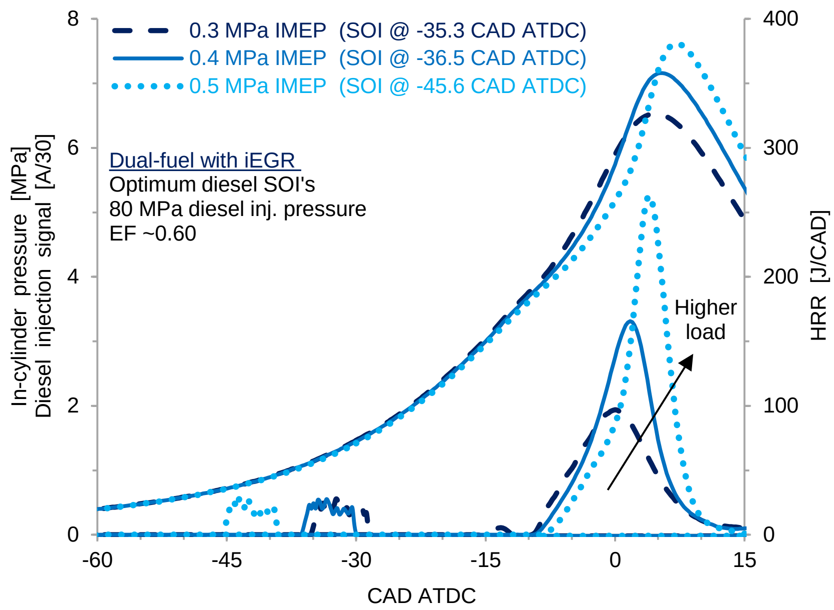

Figure 4.28 – The effect of engine load on dual-fuel operation with iEGR.

The increase of the engine load to 0.6 MPa IMEP was not possible with iEGR due to uncontrolled early autoignition of the charge and severe knock, as revealed in Figure 4.29. This was mainly a result of elevated in-cylinder gas temperatures and Φ introduced by the 2IVO strategy, as the RGF remained nearly constant at ~12.9% (Figure 4.30). Advanced single diesel injections did not have an effect on controlling combustion at this particular load, limiting the range of the dual-fuel mode with iEGR to a maximum load of 0.5 MPa IMEP.

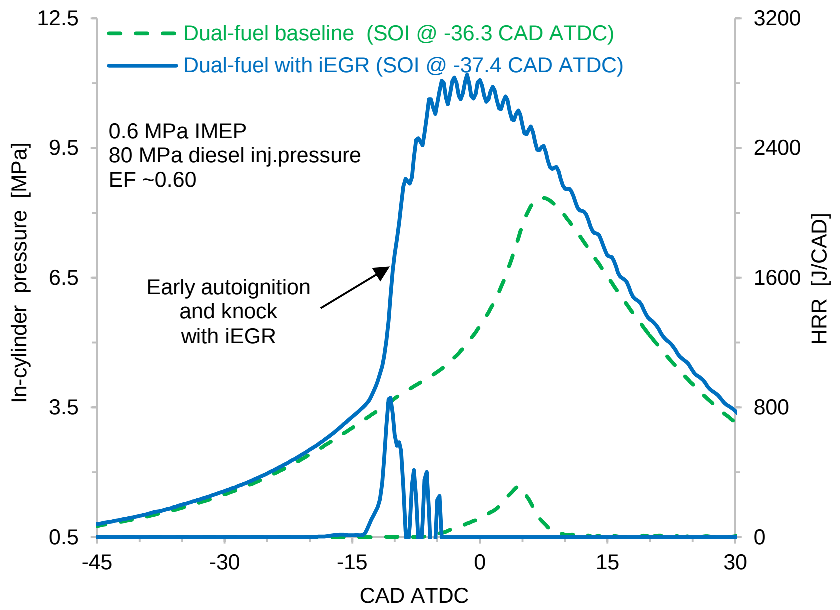

Figure 4.29 – The effect of iEGR on dual-fuel combustion at 0.6 MPa IMEP.

Unlike conventional diesel combustion, the low reactivity of the in-cylinder charge combined with an early single diesel injection used in both dual-fuel modes allowed for longer ignition delays. As the ignition occurred, combustion sequentially progressed from high reactivity to low reactivity zones [88]. The relatively better distribution of the reactivity zones in the cylinder resulted in shorter CA10-CA90. Higher engine loads and a higher RGF in the iEGR mode shortened the dual-fuel combustion processes. These effects were produced by the elevation of the global fuel/air equivalence ratio and increased mean in-cylinder gas temperatures (Figure 4.30).

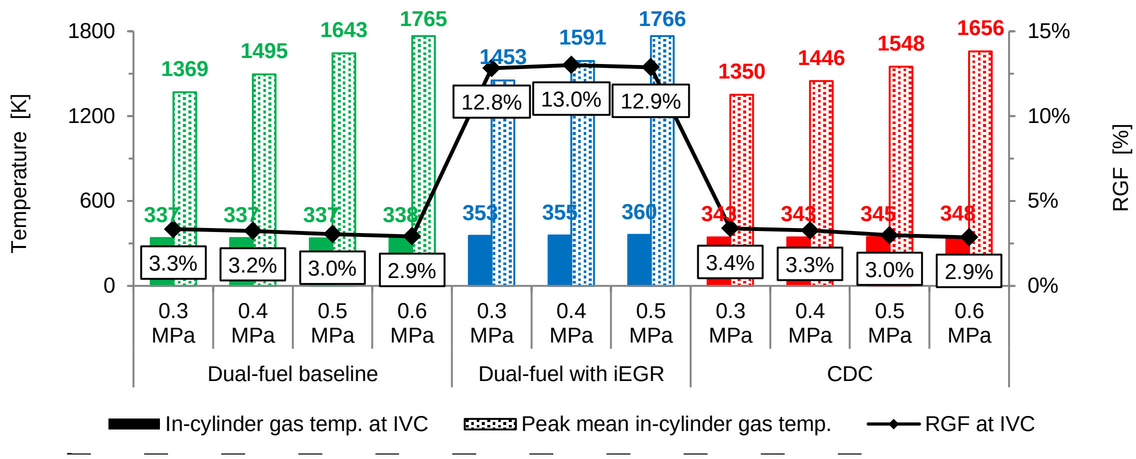

Figure 4.30 – In-cylinder gas temperatures and RGF for the three testing modes at different loads.

4.4.4 Engine-out emissions and performance

Figure 4.31 shows the net indicated specific emissions while Figure 4.32 depicts the overall engine performance.

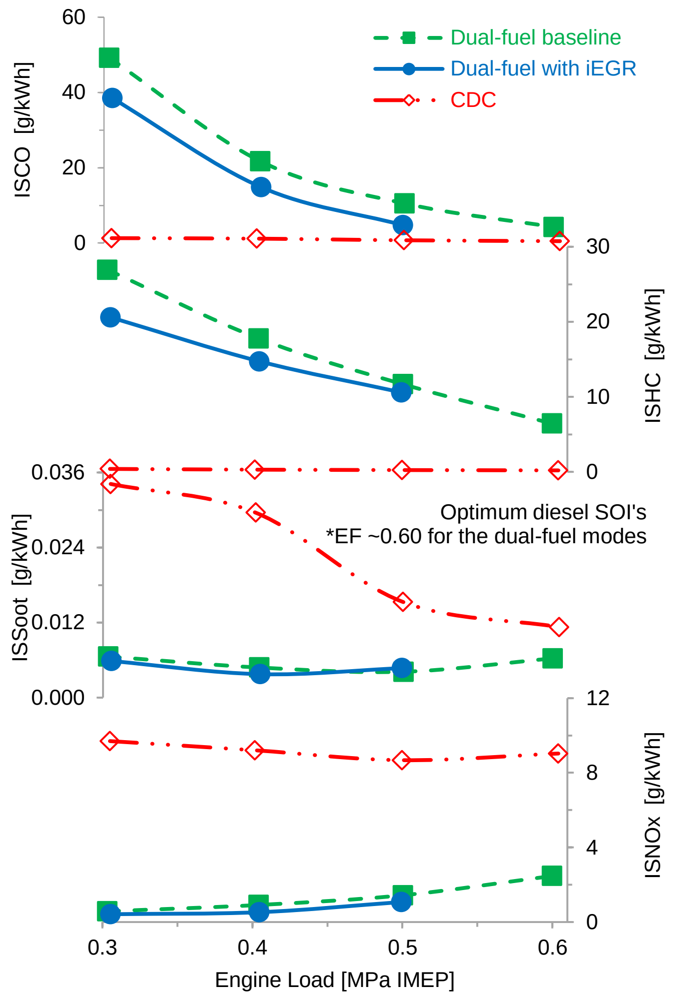

Figure 4.31 – Net indicated specific emissions for the three testing modes at different loads.

Conventional diesel combustion emitted very low levels of CO and unburnt HC emissions, leading to combustion efficiencies above 99.6%. Diesel-only mode also showed the highest EGT as a result of longer and delayed combustion processes towards the expansion stroke. Net indicated efficiencies in the CDC mode were limited at 45.4% due to the imposed and relatively low intake air pressure of 103 kPa. Higher boost pressures could increase the net indicated efficiency via lower combustion temperatures, higher ratio of specific heats (γ), and lower heat transfer losses [184].

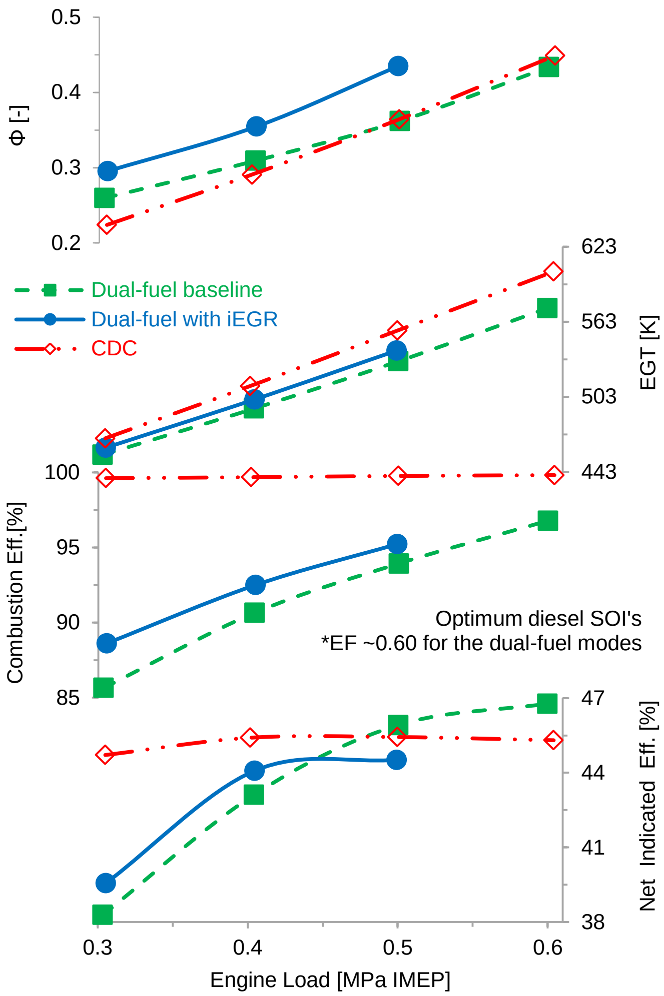

Figure 4.32 – Overall engine performance for the three testing modes at different loads.

Shorter ignition delays and higher local in-cylinder gas temperatures resulted in significant amounts of soot and NOx emissions for the diesel-only mode. Soot levels decreased at elevated loads mainly due to the use of higher injection pressures. NOx emissions remained at 9.2 g/kWh, on average. The combination of external EGR, higher intake air pressures, and increased rail pressures can effectively minimise NOx emissions while maintaining reasonable levels of soot [7]. However, this is beyond the scope of the present study.

The dual-fuel baseline allowed for lower local combustion temperatures, mitigating NOx formation at the expense of higher CO and unburnt HC emissions (Figure 4.31). Unburnt fuel is likely to be trapped in the crevice and squish volumes of the stock combustion system. Desantes et al. [88] showed that the combustion of the high reactivity fuel may not progress from the squish to the crevice regions, limiting the complete oxidation of the CO in this region. In addition, simulations performed by Kokjohn et al. [57] revealed that unburnt fuel can also be found in the centreline of the combustion chamber due to the presence of overly lean regions at lower loads. Dual-fuel combustion efficiencies remained between 85.7% and 96.8%, as shown in Figure 4.32. As the load increased, CO and unburnt HC levels rapidly decreased but were crevice volume limited. The reduction was attributed to higher Φ and elevated mean in-cylinder gas temperatures during the combustion process.

At 0.6 MPa IMEP, ISCO and ISHC were equivalent to 4.2 g/kWh and 6.5 g/kWh, respectively. Soot emissions of the dual-fuel baseline were maintained under 0.007 g/kWh throughout the sweep of load. The level of NOx emissions increased with load from 0.57 g/kWh to 2.47 g/kWh as a result of shorter burn durations and higher peak combustion temperatures. Nevertheless, it represents a substantial reduction compared to the NOx levels emitted by conventional diesel combustion. EGT was 13 K to 29 K lower than in diesel-only mode due to the rapid and more advanced heat release. The increase in Φ at 0.3 MPa IMEP and 0.4 MPa IMEP was attributed to lower net indicated efficiency when compared against the conventional diesel combustion.

The dual-fuel operation with iEGR was effective in reducing CO and unburnt HC emissions of the dual-fuel combustion baseline. Hotter combustion processes and improved flammability of the charge helped elevate the combustion efficiency. At 0.3 and 0.4 MPa IMEP, higher combustion efficiencies increased the net indicated efficiency by 3.3% and 2.3%, respectively.

In addition, higher CO_2 concentration introduced by the RGF curbed NOx formation and maintained ISNOx between 0.42 g/kWh and 1.07 g/kWh, despite the elevation of mean in-cylinder gas temperature. Earlier diesel injections maintained soot emissions slightly lower than the baseline up to 0.4 MPa IMEP. At 0.5 MPa IMEP, the further advanced SOI at -46 CAD ATDC likely resulted in impingement of the diesel spray upon the cylinder liner [59], as suggested in Figure 4.33. This is supported by the flattening of the improvements in unburnt HC emissions and efficiencies. Global fuel/air equivalence ratios increased by 16.2%, on average, when compared to those of the dual-fuel baseline, elevating the EGT by up to 9 K.

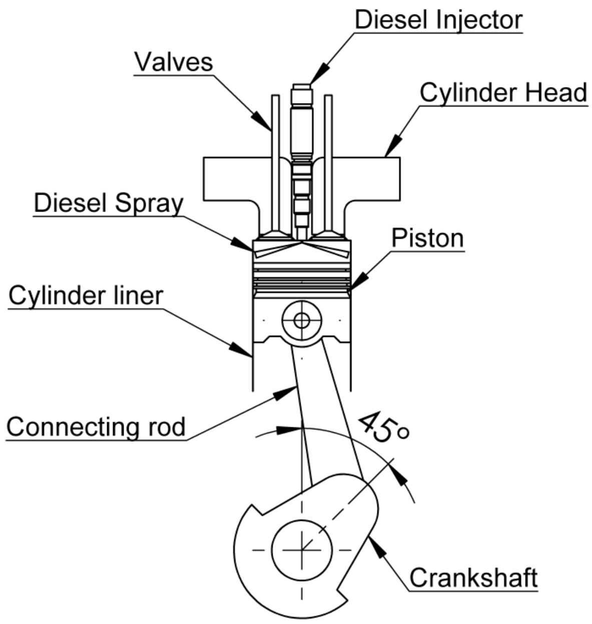

Figure 4.33 – Schematic diagram of the estimated impingement of the diesel spray upon the cylinder liner for an SOI at -45 CAD ATDC.

4.5 The effect of external EGR on low load dual-fuel operation

The previous section revealed that the dual-fuel combustion with iEGR exhibits a limited operating range due to relatively lower fuel conversion efficiency at 0.5 MPa IMEP and knock at 0.6 MPa IMEP. Therefore, experiments were carried out to determine whether external EGR has the potential to improve the performance of the dual-fuel combustion process. The investigation was performed at a low engine load of 0.31 MPa IMEP in order to prevent excessive PRRs while understanding the effects of the EGR.

4.5.1 Experimental test procedure

Table 4.5 summarises the engine operating conditions. An early single diesel injection was swept at a constant injection pressure of 50 MPa. The $\dot{m}_{ethanol}$ was held constant and the resulting ethanol energy fraction varied slightly as the net indicated efficiency changed. The use of external EGR rate of 24.5% was compared to a dual-fuel baseline without EGR. PRR and COV_IMEP were limited to 1.0 MPa/CAD and 5%, respectively.

Table 4.5 – Engine operating conditions for the investigation with EGR.

Parameter	Value	
Speed	1200 rpm	
Load	0.31 MPa IMEP	
Diesel injection pressure	50 MPa	
Diesel SOI	Varied between -43 and -34 CAD ATDC	
$m_{ethanol/cycle}$	36.3 mg/cycle	
EF	Varied between 0.54 and 0.57	
Intake air temperature	300 ± 2 K	
Intake pressure	115 kPa	
Exhaust pressure	125 kPa	
EGR rate	0%	24.5 ± 0.1%
EGR temperature	n/a	332 ± 5 K

4.5.2 Overview of the dual-fuel operation with EGR

Figure 4.34 shows the effect of EGR on the dual-fuel combustion with constant diesel SOI. Adding EGR delayed the combustion into the expansion stroke and increased the combustion duration, successfully reducing NOx emissions.

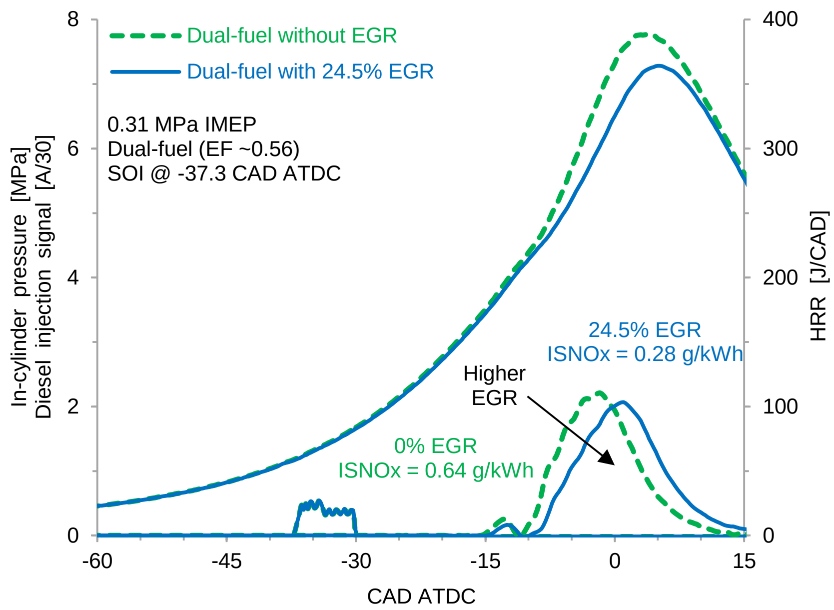

Figure 4.34 – The effect of EGR on dual-fuel combustion with constant early diesel injection timing.

Alternatively, comparisons can be made on a CA50 basis, as depicted in Figure 4.35. The analysis showed that the SOI was retarded with EGR in order to increase the charge reactivity and phase the burn rate closer to the combustion phasing of the 0% EGR case. The resulting dual-fuel operation displayed similar combustion characteristics with and without EGR when assuming a constant γ of 1.33. However, the actual peak heat release is likely to be lower in the EGR case due to lower combustion temperatures and slightly higher γ [185].

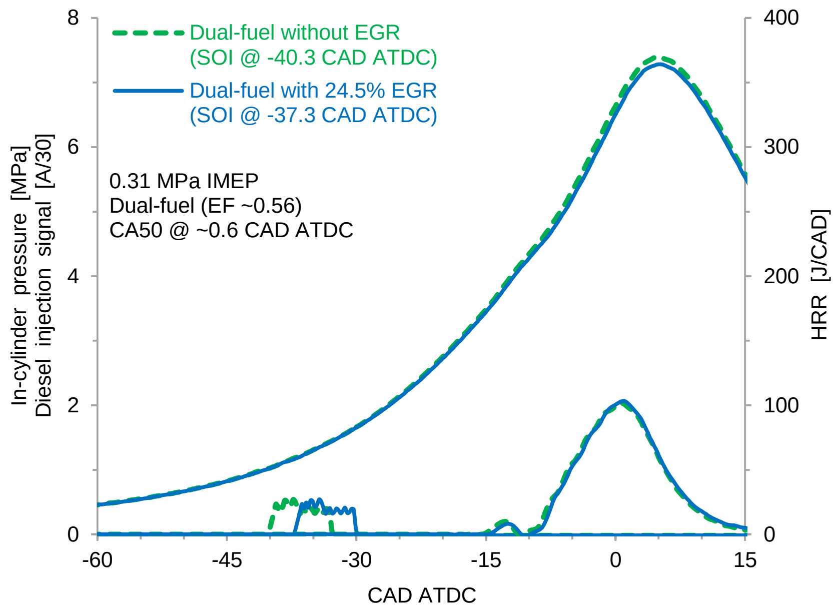

Figure 4.35 – The effect of EGR on dual-fuel combustion with constant CA50.

4.5.3 Engine-out emissions and performance

Figure 4.36 presents the exhaust emissions for the dual-fuel operation with 0% and 24.5% EGR. The results highlight the CO and NOx emissions' strong dependence on CA50 position and thus CA_P_{max}. At a given combustion phasing, the introduction of EGR required relatively shorter ignition delays via later diesel injection timings. Retarded SOIs likely increased local temperatures, improving the oxidation of CO and soot emissions. In addition, a higher global fuel/air equivalence ratio achieved with EGR possibly helped minimise overly lean regions, curbing CO and unburnt HC emissions. This is supported by the findings shown in Section 4.3. However, the fuel stratification and elevation of local in-cylinder gas temperatures slightly increased NOx formation at a constant CA50.

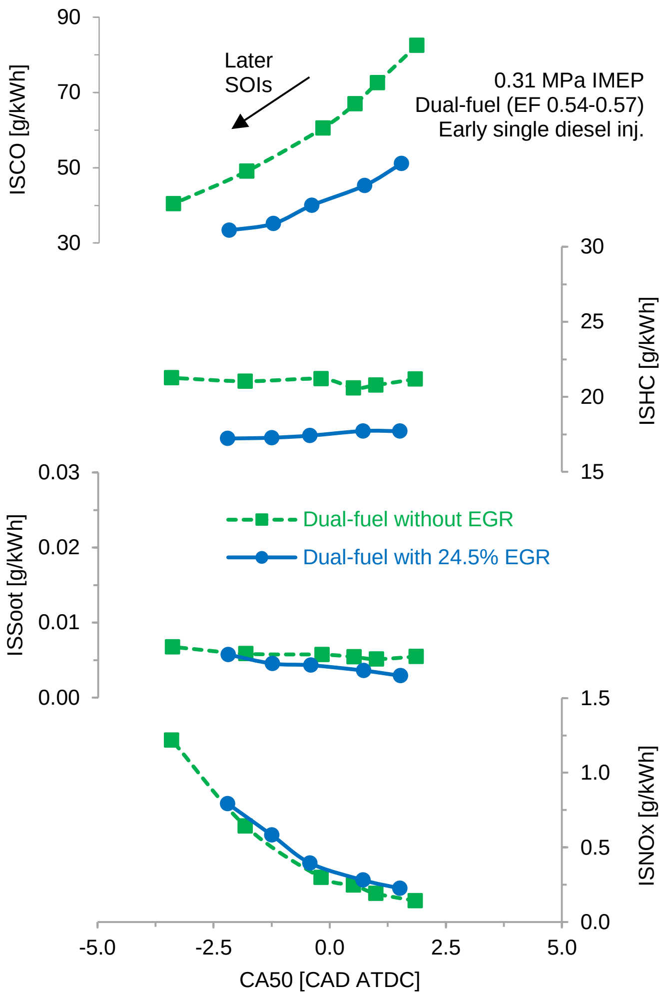

Figure 4.36 – Net indicated specific emissions for dual-fuel operation with and without EGR.

Figure 4.37 shows Φ and EGT's little sensitivity to changes in combustion phasing. This is because of the overly lean mixture at 0.31 MPa IMEP. However, the use of EGR increased the exhaust gas temperature by 5 K, on average. Higher combustion and net indicated efficiencies were also attained with a more diluted premixed charge. Therefore, external exhaust gas recirculation represents an effective in-cylinder strategy to enhance the dual-fuel engine performance at loads where iEGR needs to be avoided, such as 0.5 and 0.6 MPa IMEP.

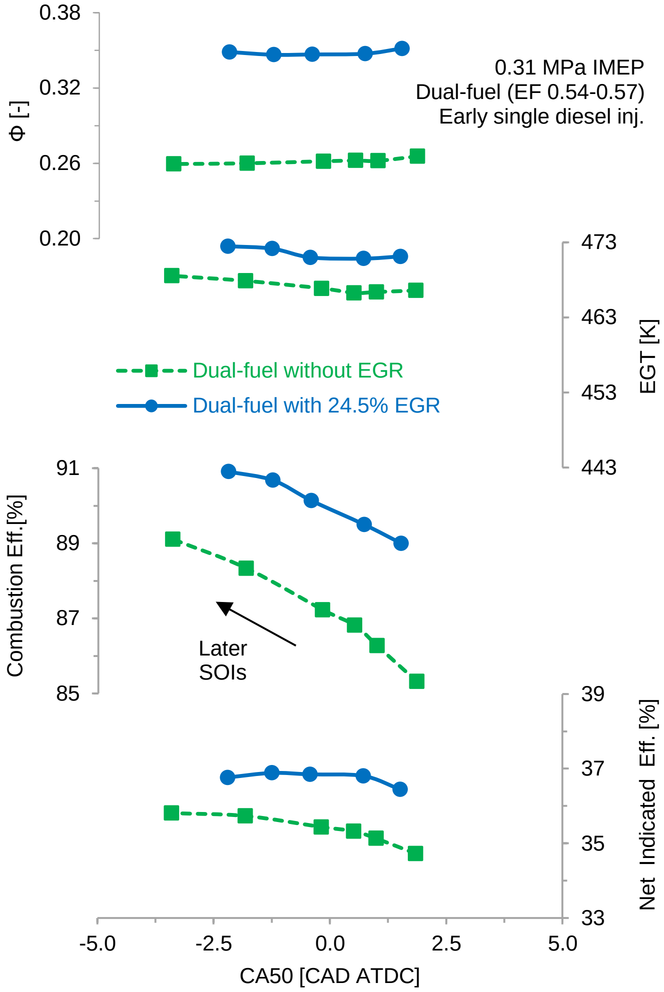

Figure 4.37 – Overall engine performance for dual-fuel operation with and without EGR.

4.6 The effect of diesel injection strategy on low load dual-fuel operation

The objective of this study was to experimentally characterise the dual-fuel combustion process using two alternative diesel injection strategies to an early single shot: an early split and a late split injection. Split diesel injections were adopted to help adjust the mixture flammability and promote in-cylinder reactivity gradients. The ethanol energy fraction was also varied from 0.44 to 0.80 in order to explore the resulting effects on combustion control, performance, and emissions. The investigation was performed at 1200 rpm and 0.6 MPa IMEP. The optimum diesel injection strategy and ethanol percentage for minimal exhaust emissions and maximum efficiency were identified.

4.6.1 Experimental test procedure

Table 4.6 summarises the engine operating conditions. The CA50 was kept at 2.00 ± 0.25 CAD ATDC by advancing or retarding the diesel injection timing (i.e. second injection in the case of split injections). This combustion phasing was chosen to increase combustion temperatures, reduce combustion instability, and minimise combustion inefficiencies typically encountered at light loads. More advanced CA50s would lead to excessive NOx emissions. An external EGR rate of ~25% was used to help improve the combustion efficiency, as the introduction of iEGR via a 2IVO strategy causes knock at this particular load. The main IVO and IVC events were set at 366 and -152 CAD ATDC, respectively, as determined at 0.5mm valve lift. PRR and COV_IMEP limits were 2.0 MPa/CAD and 5%, respectively.

Table 4.6 – Engine operating conditions for a dual-fuel operation with different diesel injection strategies.

Parameter	Value
Speed	1200 rpm
Load	0.6 MPa IMEP
Diesel injection pressure	90 MPa
$m_{ethanol/cycle}$	Varied between 48 and 81 mg/cycle
EF	Varied between 0.44 and 0.80
Intake air temperature	309 ± 4 K
Intake pressure	125 kPa
Exhaust pressure	135 kPa
EGR rate	24.8 ± 1%
EGR temperature	358 ± 8 K

Table 4.7 depicts the main characteristics of the diesel injection strategies used in this dual-fuel investigation. The split ratio calculation was based on the ratio of the energising time of each injection to the total energising time.

The **single injection** strategy had one early cycle shot (e.g. at -35 CAD ATDC) to increase the charge reactivity and trigger the ignition. This concept is slightly different from a dual-fuel operation with a late single diesel injection near TDC (e.g. at -10 CAD ATDC) [83,84,89,129,186,187], as shown in Section 4.2. The **early split injection** strategy targeted the squish and the bowl regions of the combustion chamber. The first injection (SOI_1) ensured high reactivity fuel in the outer portion of the combustion chamber, while the second shot (SOI_2) acted as an ignition source [57,79,81]. Finally, the SOI_1 of the **late split injection** strategy helped adjust mixture flammability while the SOI_2 allowed more direct control over the combustion phasing due to the proximity to TDC [7,121].

Table 4.7 – Main characteristics of the diesel injection strategies.

Diesel injection strategy	SOI_1	SOI_2	Split ratio
(Early) single	Varied from -59 to -18 CAD ATDC	n/a	n/a
Early split	-60 CAD ATDC	Varied from -39 to -24 CAD ATDC	50/50
Late split	-36.5 CAD ATDC	Varied from -16 to -5 CAD ATDC	53/47

Figure 4.38 depicts the characteristic energising profiles of the diesel injection strategies. The average split ratios were estimated as 50/50 for the early split and 53/47 for the late split strategy. A more equalised split ratio with early injections allowed for an optimum trade-off between controllability and exhaust emissions. Alternatively, late split injections displayed higher combustion efficiencies and lower NOx emissions when running with slightly more diesel in the first shot. For the sake of brevity, the split ratio sweeps have not been included in the thesis.

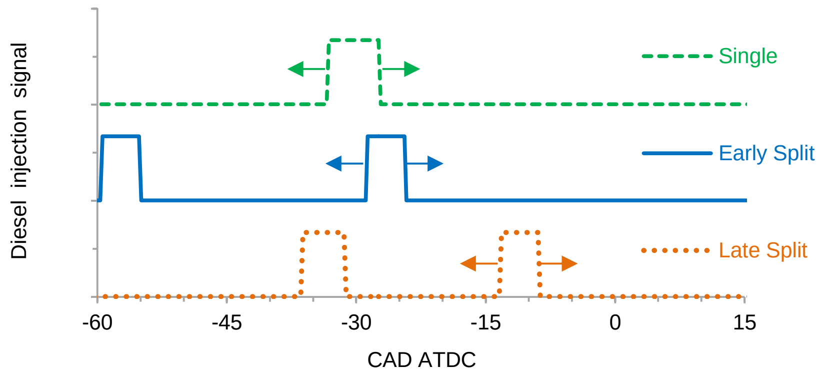

Figure 4.38 – Characteristic energising profile for each diesel injection strategy.

4.6.2 Overview of the diesel injection strategies for low load dual-fuel operation

Figure 4.39 illustrates the heat release process for a dual-fuel operation with different diesel injection strategies at an ethanol energy fraction of 0.65. The use of a single injection resulted in higher peak heat release and P_{max} than those obtained with an early split strategy, although the SOC was taking place almost at the same crank angle. This can be explained by the difference in the diesel fuel distribution. Early split strategy is likely to have lower local equivalence ratios [85], leading to different thermal ignition sites depending on their fuel reactivity [188]. At this substitution ratio, the single injection strategy probably resulted in high reactivity and high equivalence ratio regions confined to the piston bowl, shortening the combustion process. The two heat release peaks measured with late split injections could be readily explained by the reduced mixing time and individual combustion events following the shorter ignition delay.

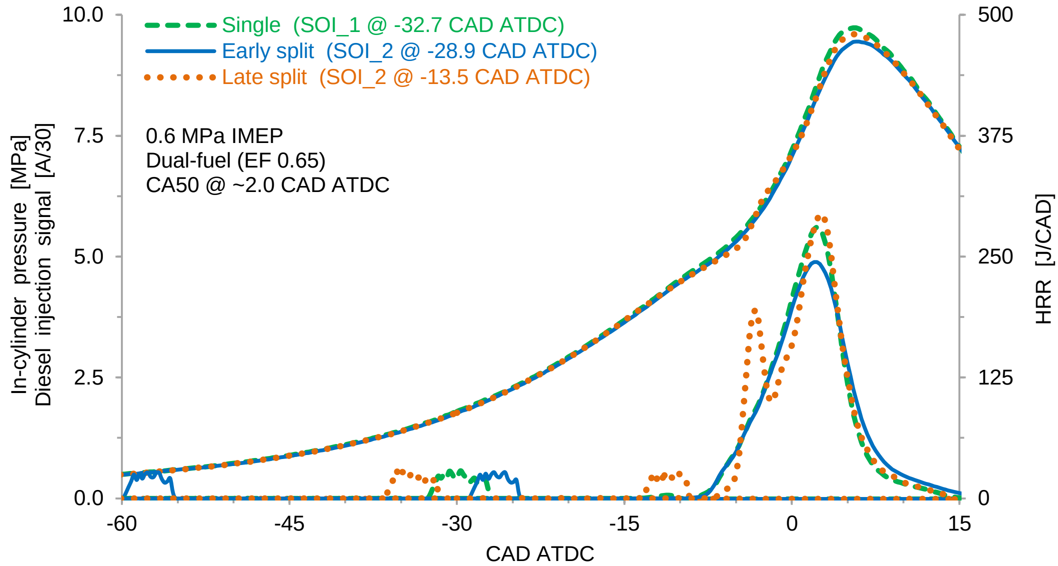

Figure 4.39 – The effect of different diesel injection strategies on dual-fuel combustion with an ethanol energy fraction of 0.65.

Figure 4.40 shows the in-cylinder pressure, diesel injection signal, and HRR for dual-fuel combustion with different diesel injection strategies and varied ethanol energy fraction. The use of early single and early split injection strategies resulted in more progressive combustion processes than that achieved with the late split injections. Additionally, the burn rate changed significantly with the ethanol percentage for a late split injection strategy. The use of ethanol energy fractions up to 0.53 led to a heat release process likely characterised by slow diffusion combustion of the first diesel injection and burning of the premixed charge, followed by the combustion of the second diesel injection. As the EF was increased to 0.59, the effect of the first injection was reduced, leading to longer ignition delay and shorter combustion duration. Further increase of the ethanol fraction considerably reduced the charge reactivity and created two distinct high temperature heat release events. The first peak may represent the ignition of the diesel injections in the piston bowl and entrained low reactivity fuel, while the second spike probably indicates the combustion of the remaining premixed charge.

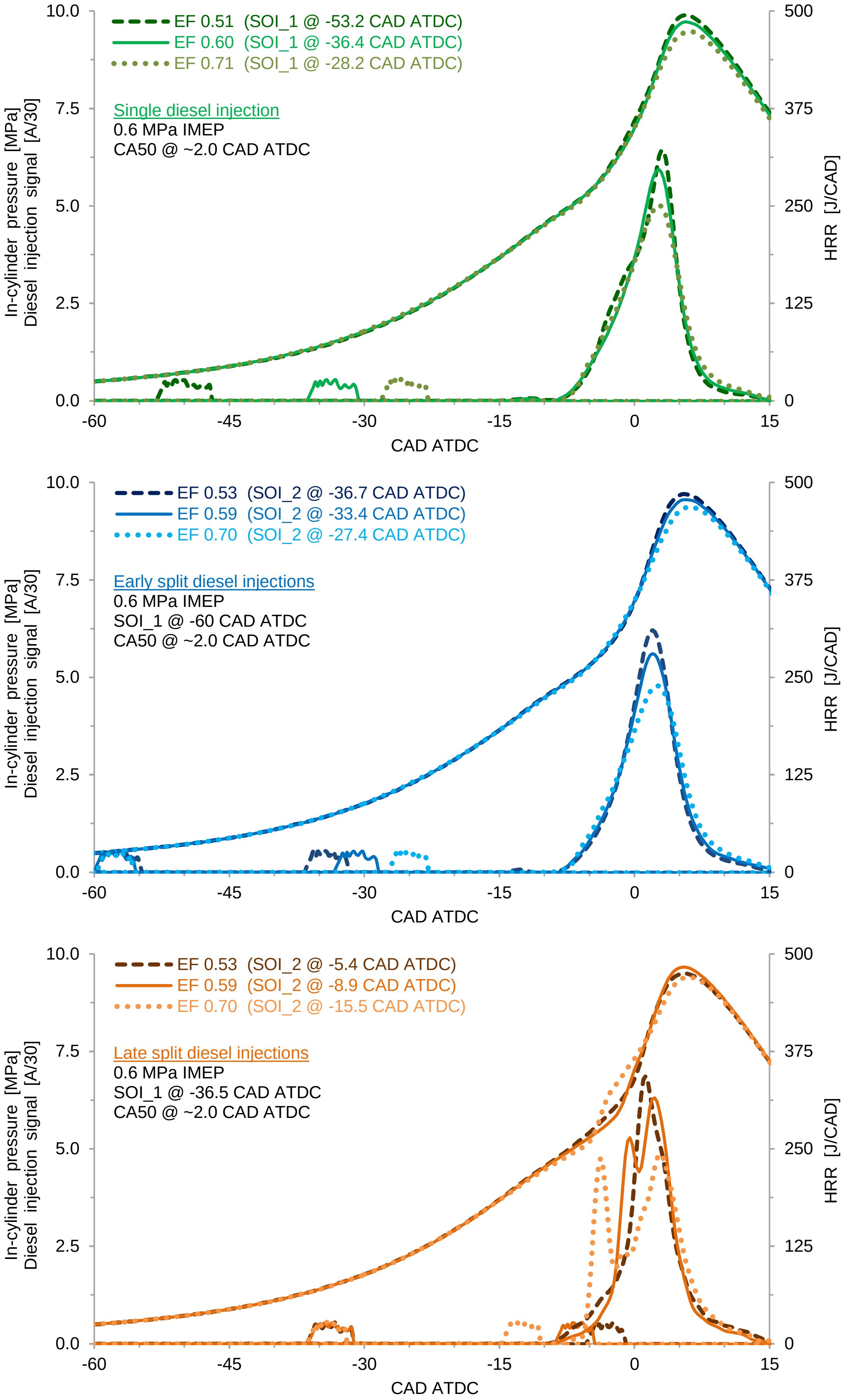

Figure 4.40 – The effect of ethanol energy fraction on dual-fuel combustion with different diesel injection strategies.

4.6.3 Combustion characteristics

Figure 4.41 displays the main SOIs (i.e. SOI_2 for split injections) used to keep the CA50 at ~2 CAD ATDC and the resulting heat release characteristics. Late and early split injection strategies presented a limited operating range, as the CA50 could only be held constant at the desired value when the EF was kept between ~0.50 and 0.70.

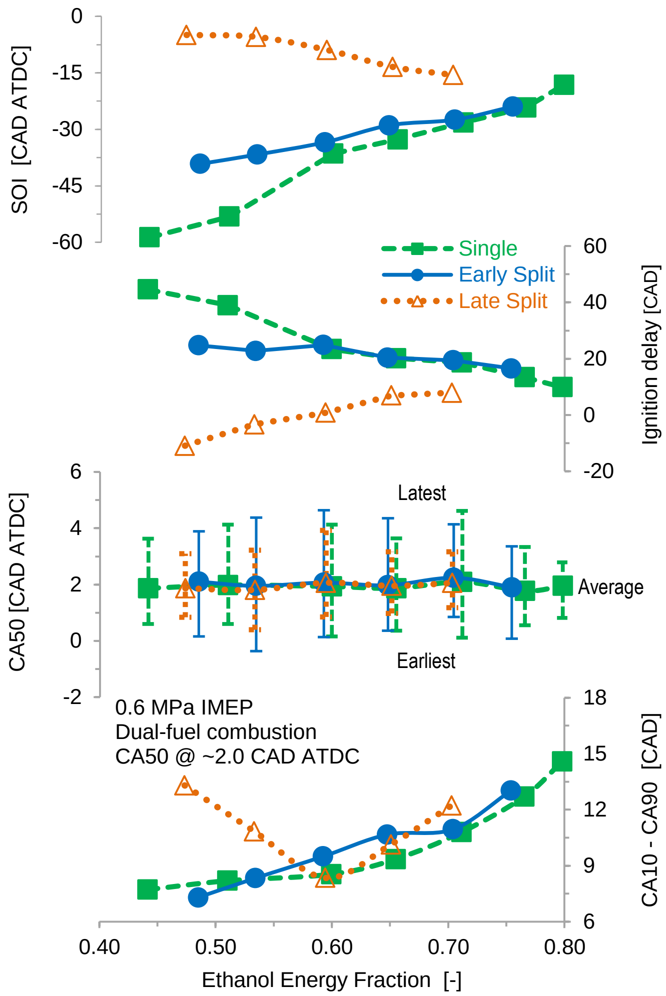

Figure 4.41 – Main diesel injection timings and the resulting heat release characteristics for dual-fuel operation with different diesel injection strategies.

The single injection strategy could be applied to a wider range of ethanol percentages due to the presence of in-cylinder regions relatively richer in diesel. However, there was a slight change in the injection timing trend as the ethanol energy fraction was increased from 0.51 to 0.60. For the conditions with EFs between 0.44 and 0.51, the majority of the single diesel injection was probably targeting the outside the piston bowl, as shown in Figure 4.33. The use of ethanol fractions higher than 0.60 required a diesel injection likely constrained within the bowl region.

The results also reveal that single and early split injection strategies displayed similar controllability over combustion phasing. As more ethanol was injected, more of a premixed charge was formed, and the later was the required main injection timing to increase the charge reactivity. This was necessary in order to avoid delayed CA50 positions at higher ethanol energy fractions, as supported by the comparison in Figure 4.42 for a dual-fuel operation with constant early split injection timings. The first diesel injection of the early split strategy had little effect on increasing the reactivity and initiating the combustion prior to the SOI_2. This is probably attributed to the lower in-cylinder gas temperature and over dilution of the diesel injected at -60 CAD ATDC. Therefore, the second injection had the dominant effect on the ignition timing due to hotter in-cylinder conditions and relatively higher degree of stratification.

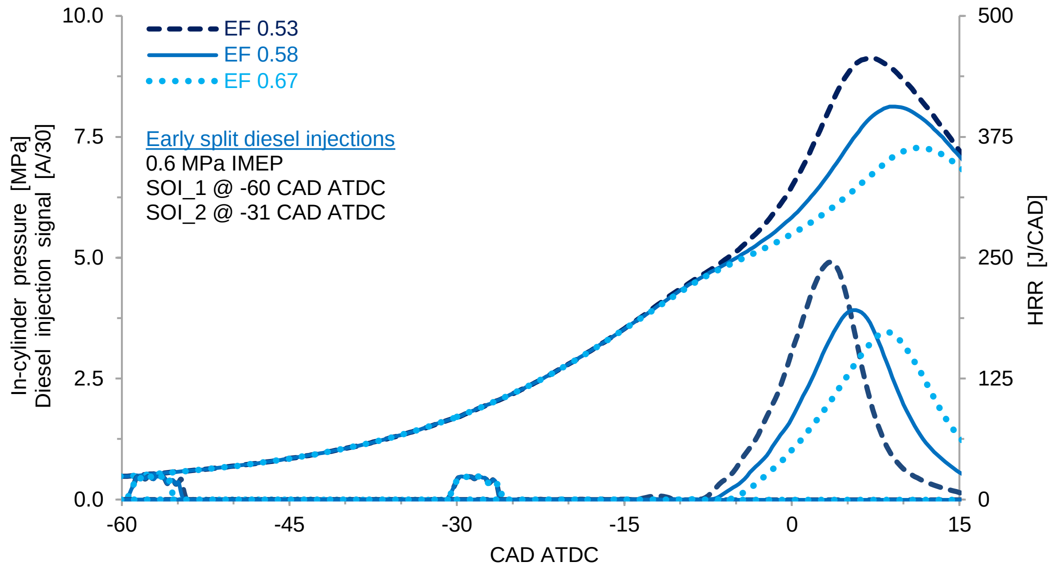

Figure 4.42 – The effect of ethanol energy fraction on dual-fuel combustion with constant early split injection timings.

In comparison with early diesel injections, a late split strategy allowed for more direct control over CA50 as a result of shorter ignition delay, which was defined as the period of time between the start of main diesel injection (i.e. SOI_2 for split injections) and SOC. However, advanced SOI_2s were used to maintain CA50 constant at higher ethanol energy fractions due to relatively longer ignition delays.

Overall, lower in-cylinder charge reactivity and higher fuel stratification required with increased ethanol percentage led to longer burn durations. Late oxidation of diesel fuel extended the CA10-CA90 when operating the engine with a late split strategy and low ethanol energy fractions of 0.47 and 0.53.

Figure 4.43 shows the combustion stability as measured by the COV_IMEP and PRR. An early single diesel injection led to reduced combustion stability at the lowest and highest ethanol percentages. This was likely a result of the fuel-air mixing process introduced by very advanced or retarded diesel injection timings. The early split strategy allowed for the formation of a more homogenous charge, yielding the lowest PRRs at the expense of some of highest but still relatively small COV_IMEP, under 2%. Finally, late split injections produced low overall COV_IMEP after shorter ignition delays and small variations between the earliest and latest CA50 positions. However, the more heterogeneous in-cylinder charge led to the highest levels of PRR.

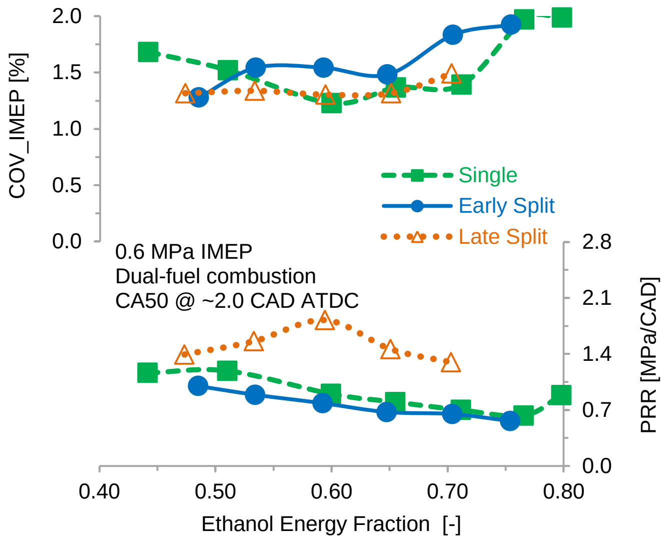

Figure 4.43 – COV_IMEP and PRR for dual-fuel operation with different diesel injection strategies.

4.6.4 Engine-out emissions and performance

Figure 4.44 depicts the resulting exhaust emissions. The levels of ISCO and ISHC were quite similar between the different diesel injection strategies. Combustion modelling performed by Kokjohn et al. [189] showed the majority of late cycle unburnt HC is located in the piston-to-liner crevices, and that the bulk of the CO resides near the liner and the crevice regions. This phenomenon was exacerbated as more ethanol was used due to the higher amount of fuel trapped in the squish and crevice volumes. In addition, unburnt HC and CO are probably found in the centreline of the combustion chamber as a result of overly lean regions at low load conditions [57]. The lack of high reactivity fuel in the piston bowl could possibly explain the relatively higher HC emissions for the early split strategy at ethanol energy fractions between 0.53 and 0.70.

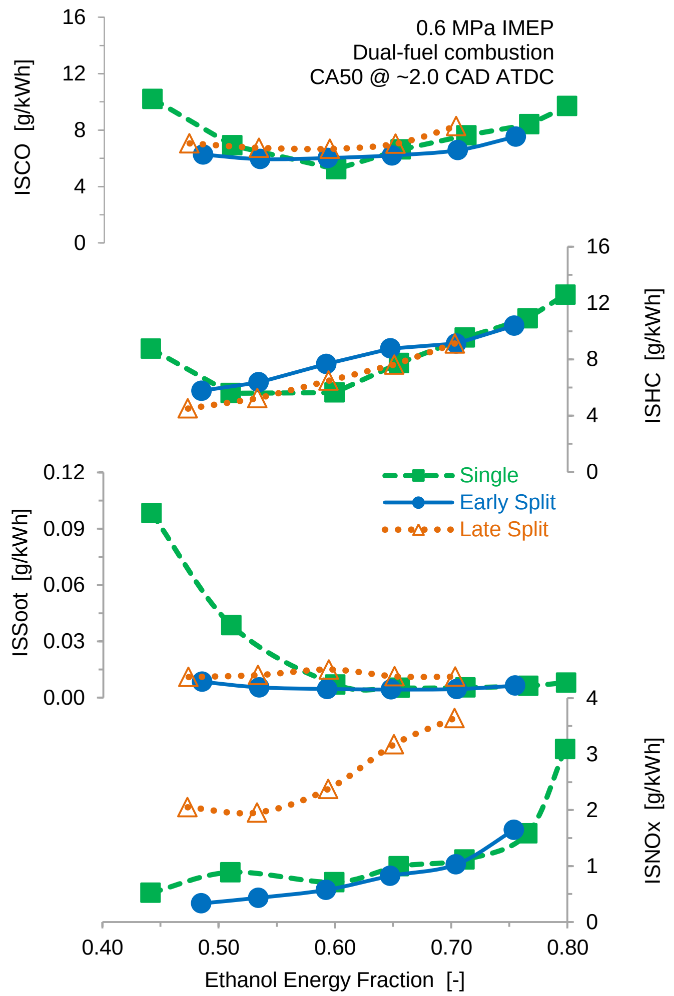

Figure 4.44 – Net indicated specific emissions for dual-fuel operation with different diesel injection strategies.

The increase in ISCO and ISHC levels for a single injection strategy at low ethanol energy fractions (e.g. 0.44) was likely a result of impingement of the diesel spray upon the cylinder liner, as injections prior to -50 CAD ATDC were required to keep CA50 constant at 2 CAD ATDC. This is supported by the higher soot emissions and lower net indicated efficiencies (Figure 4.45) at this specific condition, which confirms the trend revealed by Iwabuchi et al. [59].

Soot emissions were consistently low for the other strategies, mostly under 0.015 g/kWh, indicating minimal fuel-rich zones at intermediate temperatures. The lowest levels of soot were obtained by early split injections due to a more uniform charge distribution prior to the SOC. Late split injections showed relatively higher soot emissions caused by increased diffusion combustion of diesel after shorter ignition delays.

The in-cylinder charge stratification introduced by the main diesel injection timing was the primary reason for the increase in NOx emissions at higher ethanol energy fractions. This is supported by the less homogenous in-cylinder charge obtained for a dual-fuel operation with late split injections, which significantly increased the levels of ISNOx. Nevertheless, the use of a single or early split diesel injection strategy helped minimise NOx emissions. This was a result of a better mixture preparation and lower local in-cylinder gas temperatures.

Regardless of the diesel injection strategy and ethanol percentage, combustion efficiency was maintained above 94% throughout the experiments, as shown in Figure 4.45. Reasonable 97.1% was achieved with a single diesel injection at an ethanol energy fraction of 0.60. Higher combustion efficiencies combined with a reduction in high temperature zones [57] allowed for high net indicated efficiencies. The EGTs were consistently high at 565 ± 4 K. Differences were mostly attributed to variations in fuel conversion efficiency as well as intake air and EGR temperatures.

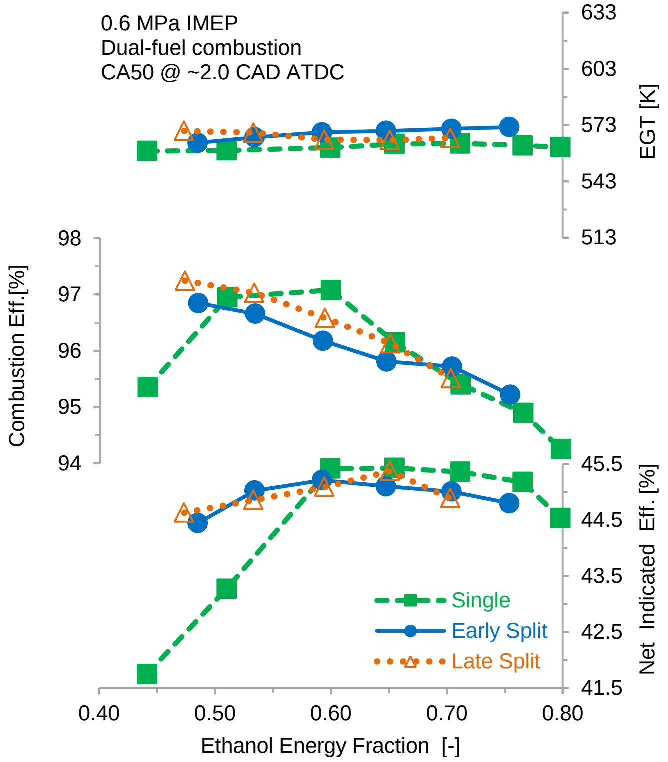

Figure 4.45 – Performance for dual-fuel operation with different diesel injection strategies.

The most efficient operating point was achieved under a single diesel injection strategy at an ethanol energy fraction of 0.65. This was a result of appropriate charge reactivity and mixing time combined with a high degree of constant volume heat release. Early and late split injection strategies exhibited slightly lower but similar net indicated efficiencies. The optimum operating point in terms of engine-out emissions was attained with an early split injection strategy at an EF of 0.53, yielding an ISNOx of 0.43 g/kWh.

4.7 Summary

In this chapter, advanced engine control and fuel injection strategies were investigated in order to reduce the levels of CO and unburnt HC emissions and improve the fuel conversion efficiency of low load dual-fuel operation. Experiments were performed at a constant engine speed of 1200 rpm and loads that varied from 0.3 to 0.6 MPa IMEP. A 1D engine model was used to calculate the in-cylinder residual gas fraction and the mean in-cylinder gas temperature.

The main findings of the ethanol-diesel dual-fuel operation with different diesel injection strategies can be summarised as follows:

- The optimum combustion control changes according to the diesel injection strategy selected and ethanol percentage.
- Dual-fuel combustion with a single diesel injection close to TDC has a limited operating range as a result of high PRRs and low net indicated efficiency.
- The use of an early single diesel injection appears as an attractive solution for low load dual-fuel operation. The strategy ensured sufficient fuel-air mixing time while leading to an almost linear combustion phasing control. In addition, high net indicated efficiencies and relatively low engine-out emissions were attained at ethanol energy fractions higher than 0.60. Higher combustion inefficiencies were generally observed as the ethanol percentage was increased.
- Early split injections resulted in a more homogeneous charge, yielding low overall emissions and low levels of PRR. However, a more sophisticated method of combustion control would likely be required due to higher combustion instability.
- A less premixed charge promoted by late split diesel injections allowed for more direct control over the CA50 at the expense of increased PRRs as well as higher NOx and soot emissions than the other diesel injection strategies.

The primary findings of the dual-fuel operation with iEGR, intake throttling, and external EGR were as follows:

- The alternative dual-fuel operating modes with iEGR and intake throttling are characterised by shorter burn durations and higher peak heat release than the dual-fuel baseline.
- The utilisation of higher RGF in the iEGR mode and lower charge density in the throttled mode increased the mean in-cylinder gas temperature during combustion. The hotter combustion process resulted in lower CO and unburnt HC emissions, and increased exhaust gas temperature. At a low load of 0.32 MPa IMEP, the combustion efficiency was increased from 87.7% in the dual-fuel baseline to ~96% in the iEGR and throttled modes. In addition, a maximum EGT of 600 K was achieved while throttling the engine, which is beneficial to oxidation catalyst operation.
- In the iEGR mode, the lower oxygen concentration and higher heat capacity of the in-cylinder charge curbed NOx formation. However, net indicated efficiency was reduced when increasing the exhaust back pressure (e.g. used to achieve higher RGF). In addition, the iEGR mode needed to be switched off to avoid a decrease in net indicated efficiency and knock as the load reached 0.5 MPa IMEP.
- Although a throttled operation minimised combustion inefficiencies while maintaining net indicated efficiency nearly constant, the increase in NOx emissions may limit the minimum intake air pressure (e.g. maximum Φ).
- Alternatively, external EGR can be used to help increase the combustion efficiency via a relatively richer burn, improving the net indicated efficiency of the dual-fuel engine at light loads.

Overall, the results show that the optimised ethanol-diesel dual-fuel combustion of high ethanol concentration can be achieved at low load by an early single diesel injection. Moreover, the combustion strategy produces lower NOx and soot emissions than conventional diesel combustion and competitive fuel conversion efficiencies. The CO and unburnt HC emissions can be reduced and combustion efficiency further improved at very low load by either iEGR, intake throttling, or external EGR.

Chapter 5

Dual-fuel combustion at medium engine loads

5.1 Introduction

The dual-fuel combustion needs to be controlled to achieve the trade-off between NOx emissions and fuel conversion efficiency. In this chapter, an experimental study has been carried out to explore the potential of the dual-fuel operation at mid-loads, where combustion efficiency and maximum in-cylinder pressure limit are less likely to affect engine performance [121]. Figure 5.1 shows where the medium load region is located over an estimated speed and load map of a HD diesel engine.

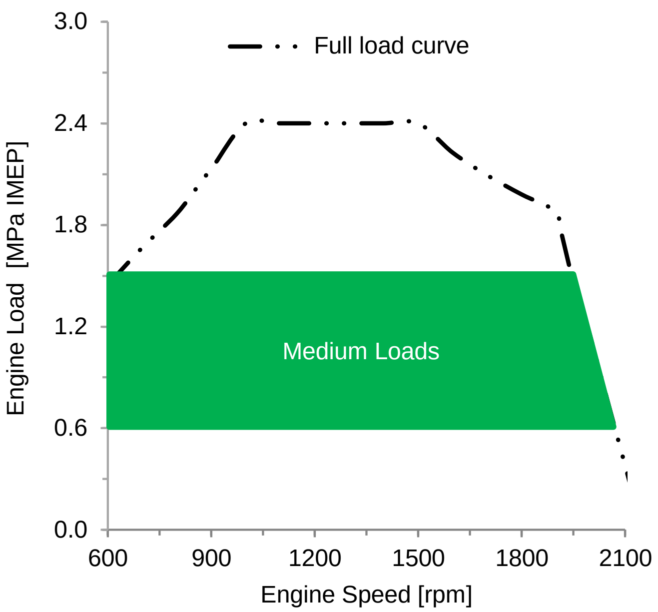

Figure 5.1 – Medium load region over an estimated HD diesel engine speed-load map.

The effects of different diesel injection strategies, ethanol energy fractions, intake air temperatures, and EGR rates have been investigated. A cost-benefit and overall emissions analysis was also carried out to determine the effectiveness of the use of ethanol and EGR on a HD diesel engine in terms of emissions, efficiency, and operational cost. The consumption of aqueous urea solution was estimated and the sensitivity of dual-fuel combustion to different SCR conversion efficiencies and fuel prices analysed.

5.2 Assessment of the optimum diesel injection strategy for mid-load dual-fuel operation

Initially, experiments were carried out to demonstrate the effect of different diesel injection strategies on the dual-fuel combustion process at medium loads. The optimum approach was selected for further emissions and performance analysis.

5.2.1 Experimental test procedure

Engine tests were performed at engine loads between 0.7 and 1.5 MPa IMEP at a constant speed of 1200 rpm. The main IVO and IVC events were set at 365 and -152 CAD ATDC, respectively, as determined at 0.5 mm valve lift. The pressure rise rate and COV_IMEP limits were 2.0 MPa/CAD and 5%, respectively

Table 5.1 summarises the diesel injection strategies investigated in this section. The diesel SOIs and rail pressure were swept when required. In addition, the mass and energy fraction of ethanol varied depending on the experiment. External EGR was employed in some cases. The use of an early single diesel injection led to excessive levels of pressure rise rate with low ethanol percentages, and high combustion instability with high ethanol energy fractions. Therefore, the results for this strategy were not recorded. A late single diesel injection also yielded high PRRs and was used during a short period of time.

Table 5.1 – Diesel injection strategies tested at mid-loads.

Diesel injection strategy	Load range	Observation
Early single	n/a	High COV_IMEP or high PRRs
Early split	0.7-1.0 MPa IMEP	Sensitive to load/temperatures
Late split	0.7-1.2 MPa IMEP	Sensitive to diesel injections
Late single	n/a	High PRRs
Pre- and main inj. near TDC	0.7-1.5 MPa IMEP	Shorter ignition delays

5.2.2 Dual-fuel combustion with early split diesel injections

The dual-fuel combustion with early split diesel injections can be controlled by, for example, varying the second diesel injection timing. However, this would likely require a more sophisticated method of combustion control during transient operation (e.g. as the engine load is increased). Alternatively, the diesel SOIs and split ratio can be held constant as long as the ethanol energy fraction is adjusted. This is usually referred to RCCI combustion, where the reactivity gradients promoted by the in-cylinder fuel blending help control the combustion event [57,79,86–88]. Higher amounts of premixed ethanol fuel effectively delays the SOC, as discussed in Chapter 4.

Figure 5.2 shows the dual-fuel combustion characteristics during a sweep of engine load with constant diesel injection timings. The test conditions are depicted in Table 5.2. The ethanol energy fraction had to be increased with the IMEP in order to avoid early fuel ignition, which would lead to knock or low fuel conversion efficiency.

The SOC became more advanced as the load was increased, leading to higher peak heat release. This was likely a result of increased in-cylinder pressure and charge density [190], limiting the dual-fuel operating range to 1.0 MPa IMEP. Further increase in the engine load resulted in severe knock because the ECU removed the first diesel injection, as the energising time of the second shot became too short to be maintained. Lower diesel injection pressures could possibly help but were not investigated.

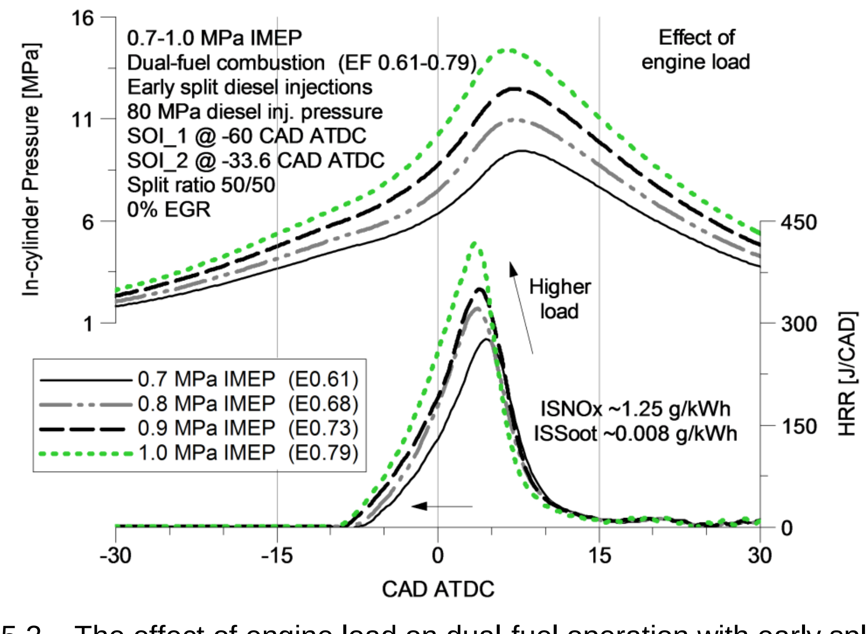

Figure 5.2 – The effect of engine load on dual-fuel operation with early split diesel injections.

Table 5.2 – Engine operating conditions for a sweep of load with early split diesel injections.

Parameter	Value			
Speed	1200 rpm			
Load	0.7 MPa IMEP	0.8 MPa IMEP	0.9 MPa IMEP	1.0 MPa IMEP
Diesel inj. pressure	80 MPa			
Diesel SOI_1	-60.0 CAD ATDC			
Diesel SOI_2	-33.6 CAD ATDC			
Diesel split ratio	50/50			
$m_{ethanol/cycle}$	70 mg/cycle	88 mg/cycle	104 mg/cycle	124 mg/cycle
EF	0.61	0.68	0.73	0.79
Intake air temp.	300 ± 2 K			
Intake pressure	122 kPa	139 kPa	158 kPa	177 kPa
Exhaust pressure	124 kPa	140 kPa	159 kPa	183 kPa
EGR rate	0%			
Φ	0.39-0.40			

Overall, the use of early split diesel injections between 0.7-1.0 MPa IMEP allowed for relatively low NOx and soot emissions of ~1.25 g/kWh and ~0.008 g/kWh, respectively. Despite the potential emissions reduction, this strategy was particularly sensitive to intake air temperature (IAT). An increase of 10 K was sufficient to cause early ignition of the fuel when operating without EGR, as depicted in Figure 5.3. This experiment was carried out at 0.9 MPa IMEP under similar conditions to Table 5.2 except for the use of a higher diesel injection pressure of 110 MPa and a slightly more retarded SOI_2.

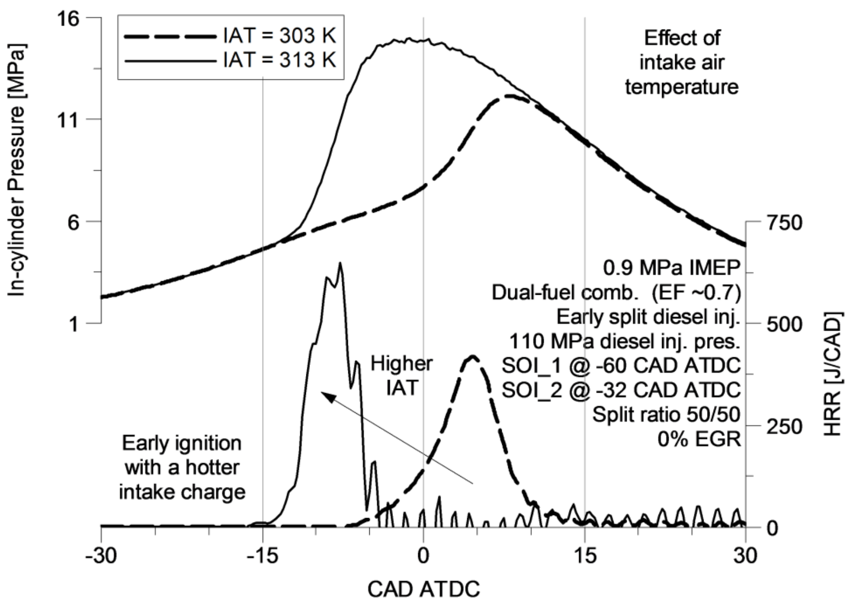

Figure 5.3 – The effect of IAT on dual-fuel operation with early split diesel injections.

The early fuel ignition with a hotter inlet charge was acquired during 19 cycles due to unacceptable levels of PRR of 6.6 MPa/CAD. In comparison, the dual-fuel operation with a lower IAT yielded a PRR of 1.4 MPa/CAD.

5.2.3 Dual-fuel combustion with late split diesel injections

Dual-fuel combustion with late split diesel injections allowed for a wider operating range than that obtained with early split injections. The maximum load achieved was 1.2 MPa IMEP. This was enabled by the relatively later introduction of diesel (e.g. high reactivity fuel) into the cylinder. EGR could be employed to minimise NOx emissions without early ignition of the in-cylinder charge. However, the use of ethanol was limited to energy fractions between 0.6 and 0.8 due to excessive PRRs at low EFs and a hardware limitation (e.g. minimum energising time for the diesel injector) at elevated EFs.

In addition, high sensitivities to variations in the first diesel injection timing and quantity were observed. A more advanced SOI_1 was required and less diesel fuel could be injected in the first shot as the load was increased. This limitation was attributed to an increase in in-cylinder gas temperature. To demonstrate the effect of diesel split ratio and SOI_1 on mind-load dual-fuel combustion, experiments were performed using the engine operating conditions shown in Table 5.3.

Table 5.3 – Engine operating conditions for a sweep of diesel split ratio and SOI_1.

Parameter	Value	
Speed	1200 rpm	
Load	0.9 MPa IMEP	
Diesel injection pressure	110 MPa	
Diesel SOI_1	-36.7 CAD ATDC	Varied
Diesel SOI_2	-1.5 CAD ATDC	-2.2 CAD ATDC
Diesel split ratio	Varied	~50/50
$m_{ethanol/cycle}$	94.3 mg/cycle	103.5 mg/cycle
EF	~0.65	~0.70
Intake air temperature	301 ± 1 K	317 ± 1 K
Intake pressure	155 kPa	
Exhaust pressure	165 kPa	
EGR rate	0%	25.0 ± 0.2%
EGR temperature	n/a	371 ± 7 K
Φ	~0.41	~0.61

During the sweep of split ratio, the amount of diesel injected in the first shot was varied while maintaining SOI_1 and SOI_2 constant at -36.7 and -1.5 CAD ATDC, respectively. These injection timings were based on experiments carried out at low engine loads.

Figure 5.4 shows that the mid-load dual-fuel combustion is much more sensitive to the diesel split ratio than a low load dual-fuel operation [7]. A small reduction in the split ratio from 51/49 to 49/51 effectively reduced the reactivity of the in-cylinder charge prior to the SOC and decreased the net indicated efficiency in 2%. This was attributed to later CA50 and longer burn duration.

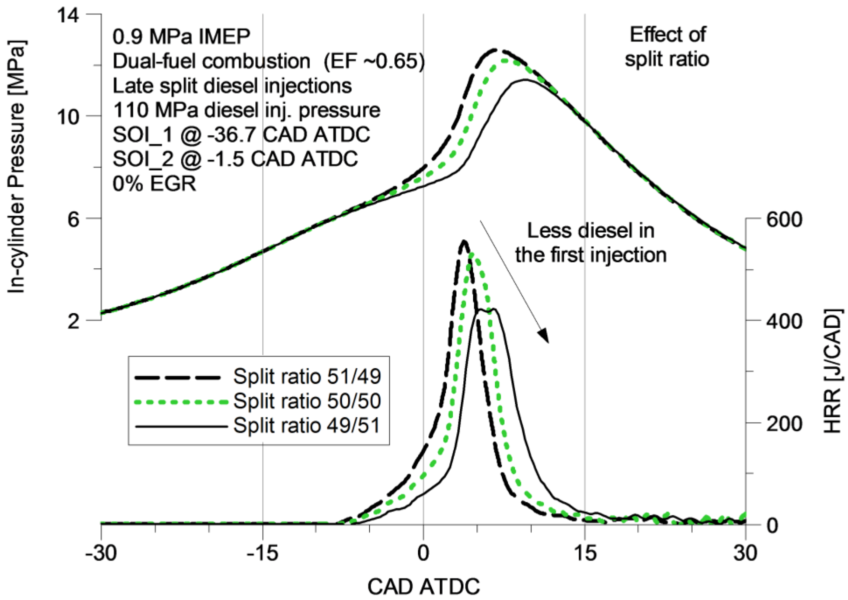

Figure 5.4 – The effect of split ratio on mid-load dual-fuel operation with late split diesel injections.

Alternatively, the sweep of SOI_1 was performed using a split ratio of ~50/50 and constant SOI_2 at -2.2 CAD ATDC. Table 5.3 shows that other boundary conditions were similar those of the split ratio sweep except for the use of an EGR rate of 25%, a higher EF of ~0.70, and a higher intake manifold air temperature of ~317 K. These parameters were modified to explore the limits of this dual-fuel strategy.

Figure 5.5 depicts the effect of varying the SOI_1 from -28.7 to -36.7 CAD ATDC. The use of earlier SOI_1 likely reduced fuel-rich zones within the piston bowl, yielding similar effects to lower diesel quantity in the first shot. The relatively less reactive mixture retarded the SOC and slowed down the combustion process, decreasing the net indicated efficiency by 3% in comparison with the combustion event with an SOI_1 at -28.7 CAD ATDC.

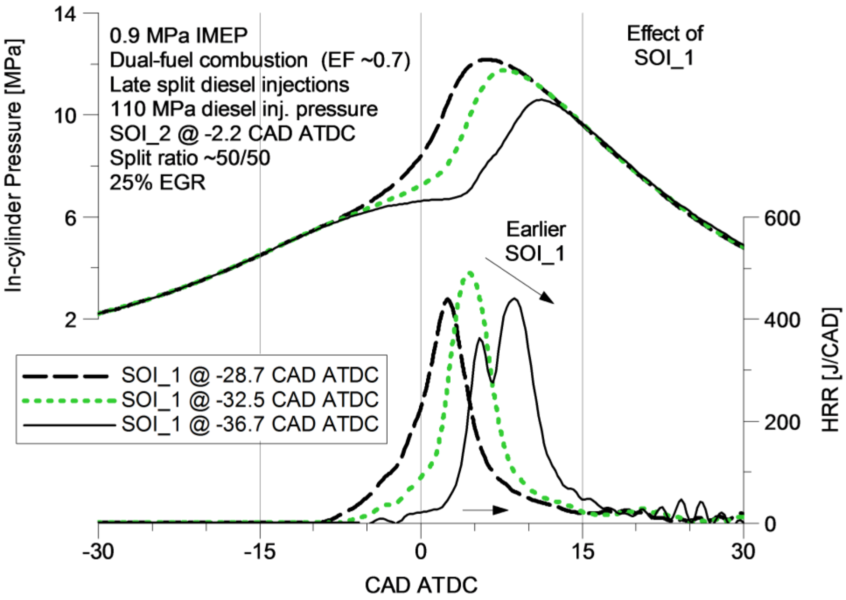

Figure 5.5 – The effect of SOI_1 on mid-load dual-fuel operation with late split diesel injections.

Despite the potential to achieve high efficiency and relatively low ISNOx levels, mid-load dual-fuel combustion with a late split strategy has been shown highly sensitive to the characteristics of the first diesel injection. As a result, an advanced fuel injection system would be required to precisely control the amount of diesel injected. In the next subsection, investigations were performed using a single diesel injection near TDC to simplify the dual-fuel engine operation and possibly extend the load range to 1.5 MPa IMEP.

5.2.4 Dual-fuel combustion with diesel injections near TDC

Initially, engine experiments explored dual-fuel combustion with a single diesel injection near firing TDC. The study was carried out at 1.2 MPa IMEP. Table 5.4 summarises the engine operating conditions. In this subsection, the average in-cylinder pressure traces were not filtered in order to highlight the pressure oscillations. The HRR curves were post-processed using the Savitzky-Golay filter with a window size of five data points.

Table 5.4 – Engine operating conditions for a dual-fuel operation with diesel injections near TDC.

Parameter	Value	
Speed	1200 rpm	
Load	1.2 MPa IMEP	
Diesel injection pressure	110 MPa	
$m_{ethanol/cycle}$	0.0 mg/cycle	162.7 mg/cycle
EF	0.00	0.83
Intake air temperature	317 ± 1 K	
Intake pressure	190 kPa	
Exhaust pressure	200 kPa	
EGR rate	20.1 ± 0.5%	
EGR temperature	392 ± 3 K	
Φ	~0.63	

Figure 5.6 shows a comparison between the conventional diesel combustion (CDC) and dual-fuel operation modes using a late single diesel injection strategy. Dual-fuel combustion led to longer ignition delay and higher levels of PRR than diesel-only combustion, despite the slightly retarded injection timing. In addition, considerably greater premixed combustion peak was observed in the dual-fuel mode, increasing the P_{max}. The HRR shape suggests simultaneous combustion of diesel and entrained ethanol fuel [90]. The faster and more prominent premixed combustion accelerated the autoignition of the remaining in-cylinder charge. The rapid burning resulted in ringing/knocking combustion and reached a PRR of 3.7 MPa/CAD. The high heat of vaporisation of ethanol helped reduce the in-cylinder charge temperature and the subsequent compression pressures prior to the SOC.

Alternatively, a small pre-injection prior to the main injection can be used to significantly reduce PRRs. Diesel-only investigations [3] revealed that the use of a diesel pre-injection extends the engine operating range, lowers the levels of PRR, and results in minimal impact on the soot/NOx trade-off when compared against a single injection strategy at 0.9, 1.2, and 1.5 MPa IMEP. The pre-injection of diesel had an estimated volume of 3 mm^3 and a constant dwell time of 1 ms between pre- and main injection events. This strategy used the lowest and closest pre-injected mass of diesel required to smooth the premixed combustion phase while minimising deviations to the setpoint and complying with hardware technical limitations.

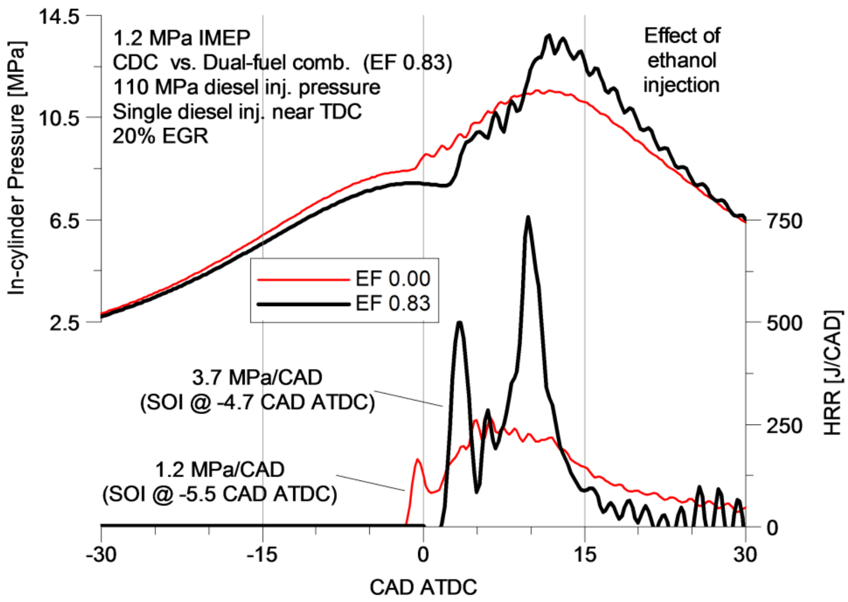

Figure 5.6 – The effect of ethanol injection on mid-load dual-fuel operation with a single diesel injection near firing TDC.

Figure 5.7 compares the effect of diesel pre-injection on reducing the rate of premixed combustion and the in-cylinder pressure oscillations of a dual-fuel case with an EF 0.83. The introduction of the pre-injection effectively reduced the PRRs from 3.7 MPa/CAD to 1.7 MPa/CAD. Therefore, this injection strategy was considered the optimum choice for exploring the potential of the dual-fuel combustion at mid-loads up to 1.5 MPa IMEP.

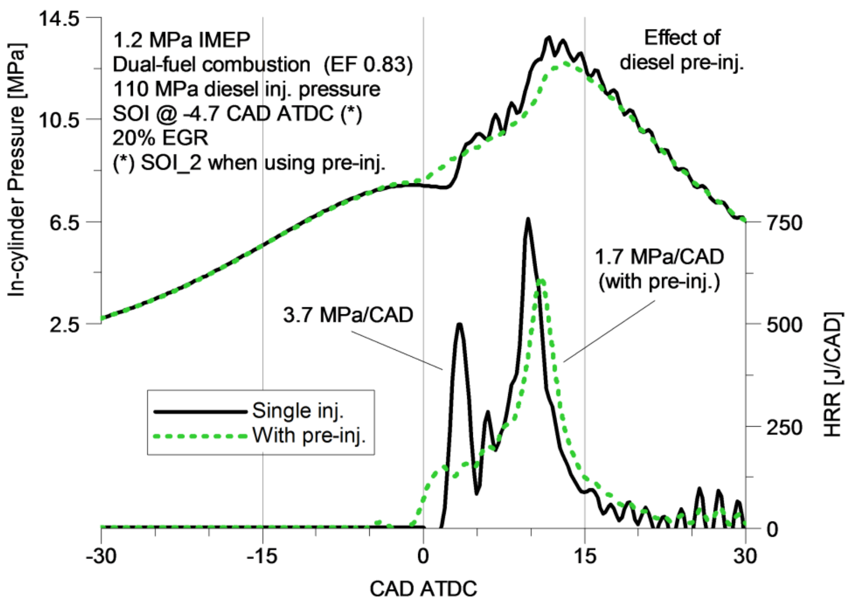

Figure 5.7 – The effect of diesel pre-injection on mid-load dual-fuel operation with constant main diesel SOI.

5.3 Characterisation of mid-load dual-fuel operation

This section characterises the effect of ethanol energy fraction, diesel injection timing, intake air temperature, and EGR on mid-load dual-fuel combustion with pre- and main diesel injections near TDC.

5.3.1 Experimental test procedure

Engine tests were performed at 1.2 MPa IMEP at a constant speed of 1200 rpm. The main IVO and IVC events were set at 365 and -152 CAD ATDC, respectively, as determined at 0.5 mm valve lift. PRR and COV_IMEP limits were 2.0 MPa/CAD and 5%, respectively. Table 5.5 summarises the main boundary conditions for the different sweeps performed.

Table 5.5 – Engine operating conditions during the characterisation of the dual-fuel combustion with pre- and main diesel injections near TDC.

Parameter	Value
Speed	1200 rpm
Load	1.2 MPa IMEP
Diesel injection pressure	Varied between 95 and 155 MPa
$m_{ethanol/cycle}$	Varied between 0.0 and 155.5 mg/cycle
EF	Varied between 0.00 and 0.81
Intake air temperature	Varied between 308 K and 326 K
Intake pressure	190 kPa
Exhaust pressure	200 kPa
EGR rate	Varied between 0% and 33%
EGR temperature	364 ± 8 K
Φ	Varied between 0.48 and 0.82

5.3.2 Overview of the dual-fuel operation at a medium load

The ignition of the pre-injected diesel fuel was advanced when operating in dual-fuel mode with the same diesel SOIs of a CDC case. Figure 5.8 shows that SOI_2 took place after combustion had already started. This was likely caused by the relatively richer premixed charge introduced by the port fuel injected ethanol. The heat release profile changed from typical mixing controlled combustion in the diesel-only mode to a shorter combustion process with higher heat release rates. The increase in the peak HRR indicates some degree of premixed combustion (e.g. ethanol autoignition).

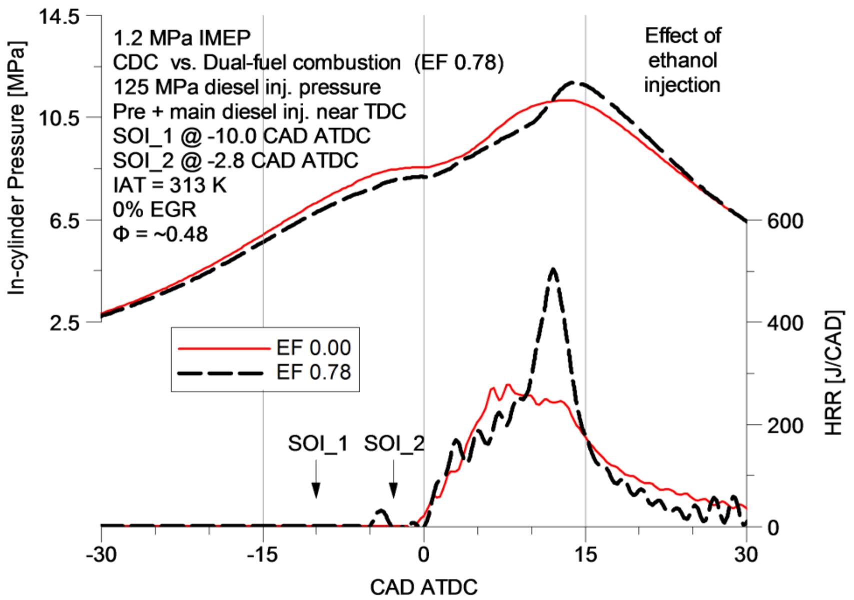

Figure 5.8 – The effect of ethanol injection on mid-load dual-fuel operation with constant pre- and main diesel injections near TDC.

Figure 5.9 reveals that earlier diesel SOIs linearly shifted the dual-fuel combustion towards TDC. This possibly increased the combustion temperatures, allowing for shorter burn durations and improved net indicated efficiencies at the expense of higher NOx emissions. However, the dual-fuel combustion was delayed as more ethanol was injected in order to maintain the maximum PRR below 2.0 MPa/CAD. Figure 5.10 shows that the diesel-only combustion allowed for more advanced heat release process.

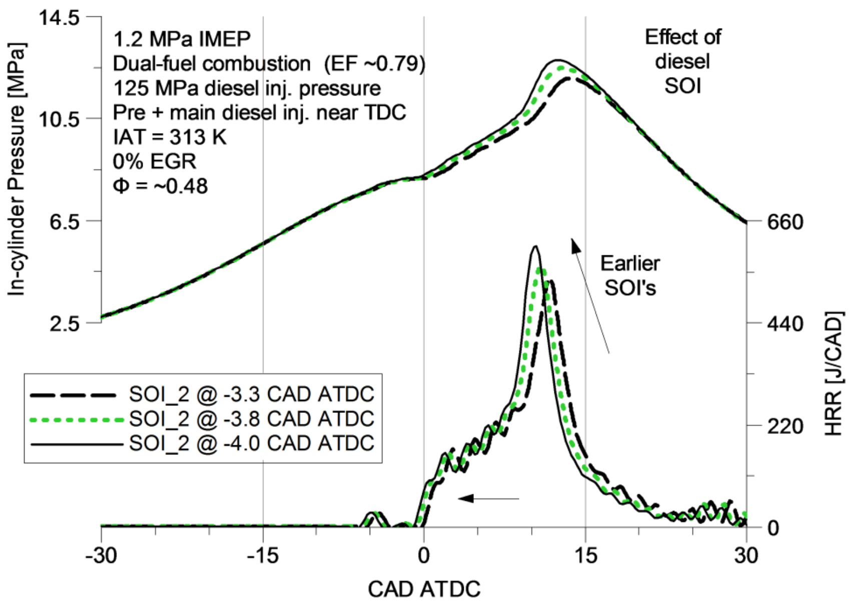

Figure 5.9 – The effect of diesel injection timing on mid-load dual-fuel operation.

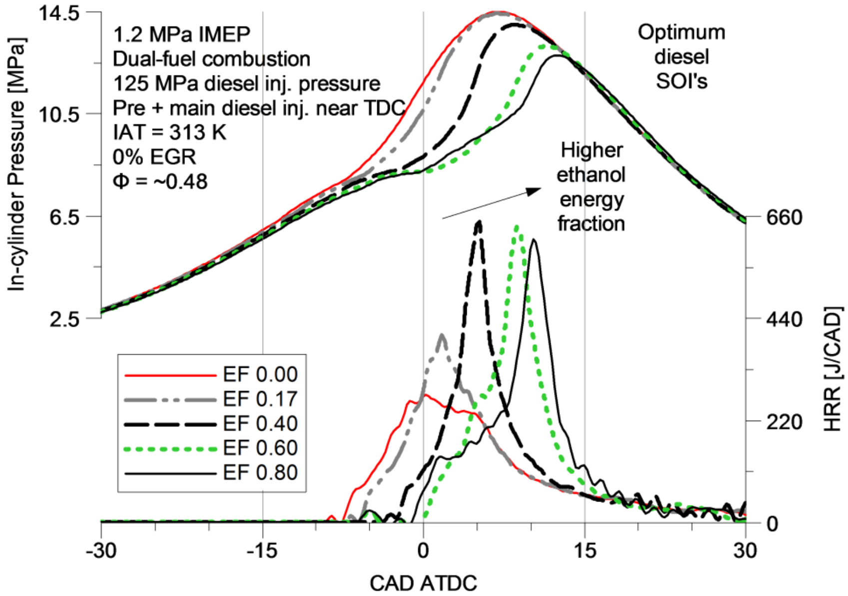

Figure 5.10 – The effect of ethanol energy fraction on mid-load dual-fuel operation with optimised diesel injections for the maximum net indicated efficiency.

5.3.3 The effect of intake air temperature on mid-load dual-fuel operation

The intake manifold air temperature was varied from 308 K to 318 K to explore the sensitivity to charge temperature. Figure 5.11 depicts the resulting in-cylinder pressure and HRR for the dual-fuel combustion with an EF of approximately 0.79.

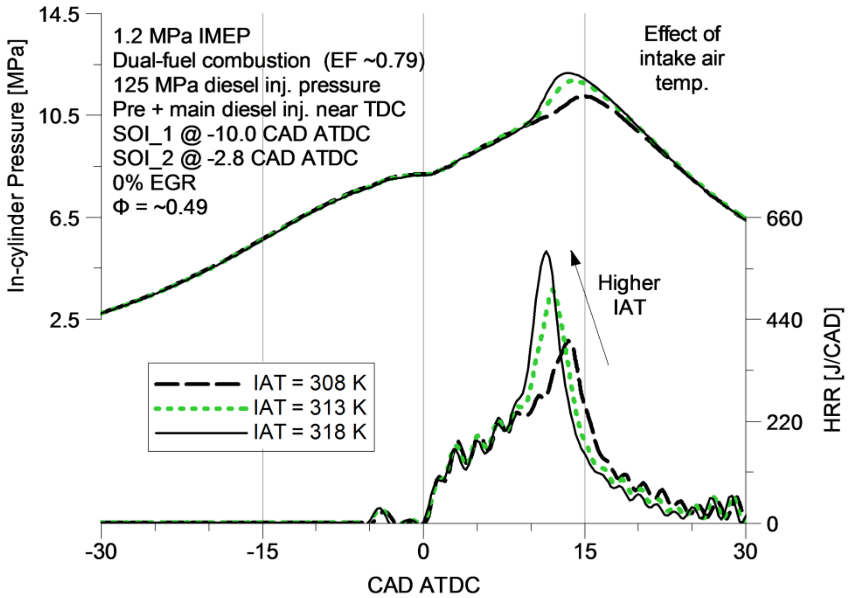

Figure 5.11 – The effect of IAT on mid-load dual-fuel operation.

A higher IAT had little impact on the SOC, advancing slightly the ignition of the pre-injected diesel. However, the increase of the end-gas temperature caused faster autoignition of the premixed charge, leading to higher peak heat release. Therefore, the use of a high IAT can limit the dual-fuel operating range due to excessive PRRs.

5.3.4 The effect of external EGR on mid-load dual-fuel operation

The use of EGR combined with an efficient SCR system can represent a cost-effective method for achieving NOx emissions compliance and high engine efficiency [10,55]. To give an example, the introduction of an EGR rate of 25% with constant diesel SOIs increased the ignition delay and resulted in longer combustion duration, as depicted in Figure 5.12. This was attributed to lower in-cylinder gas temperatures introduced by increased specific heat capacity of the in-cylinder charge (e.g. presence of CO_2 in the recycled gases) and reduced oxygen availability (or dilution effect) [119,181]. The levels of ISNOx were effectively reduced from 8.7 g/kWh to 1.3 g/kWh at the expense of a decrease of 1.7% in net indicated efficiency.

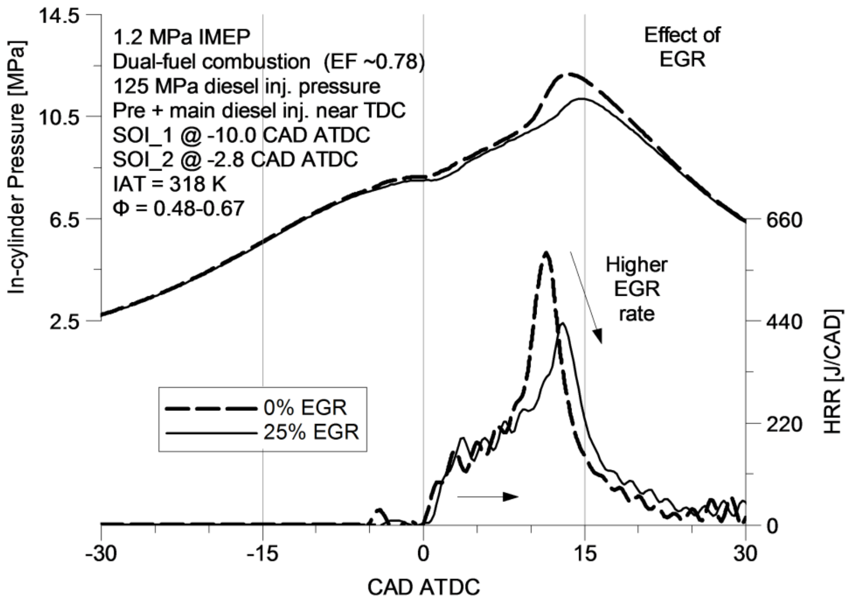

Figure 5.12 – The effect of EGR on mid-load dual-fuel operation.

To explore the trade-off between exhaust emissions and efficiency, a sweep of EGR was performed using optimised diesel SOIs for the maximum engine efficiency. Intake air temperature increased from 308 K for the non-EGR case up to 326 K for a dual-fuel operation with an EGR rate of ~33%.

Figure 5.13 shows that the use of EGR allowed for more advanced burn rates, despite the elevation of the IAT. Net indicated efficiency was slightly reduced by ~0.9% from 46.9% to 46.5%. NOx emissions were significantly reduced from 8.9 g/kWh to 0.6 g/kWh.

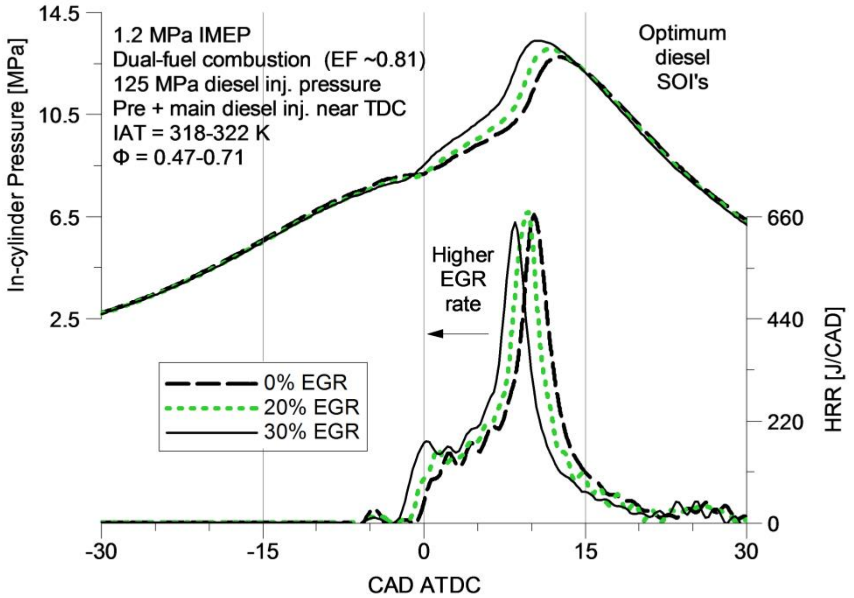

Figure 5.13 – The effect of EGR on mid-load dual-fuel operation with optimised diesel SOIs.

While comparing the dual-fuel combustion (EF of ~0.81) against the CDC, Figure 5.14 reveals that the use of a premixed charge of ethanol effectively reduced the levels of ISNOx independently of the EGR percentage. This is attributed to the formation of relatively more homogenous mixture and reduction of local combustion temperatures. Moreover, the dual-fuel operation resulted in higher net indicated efficiencies than a diesel-only combustion. However, slightly higher soot levels were measured at low EGR rates due to relatively lower in-cylinder gas temperatures and the 30 MPa lower diesel injection pressure selected for the dual-fuel mode. EGR fractions above 25% resulted in excessive smoke and deteriorated the efficiency in both combustion modes.

Therefore, an EGR rate of 25% was high enough to minimise NOx emissions while maintaining high engine efficiency and low soot emissions. The combination of external EGR with the dual-fuel strategy can potentially improve the total cost of ownership via reduction of the aqueous urea solution consumption in the SCR system.

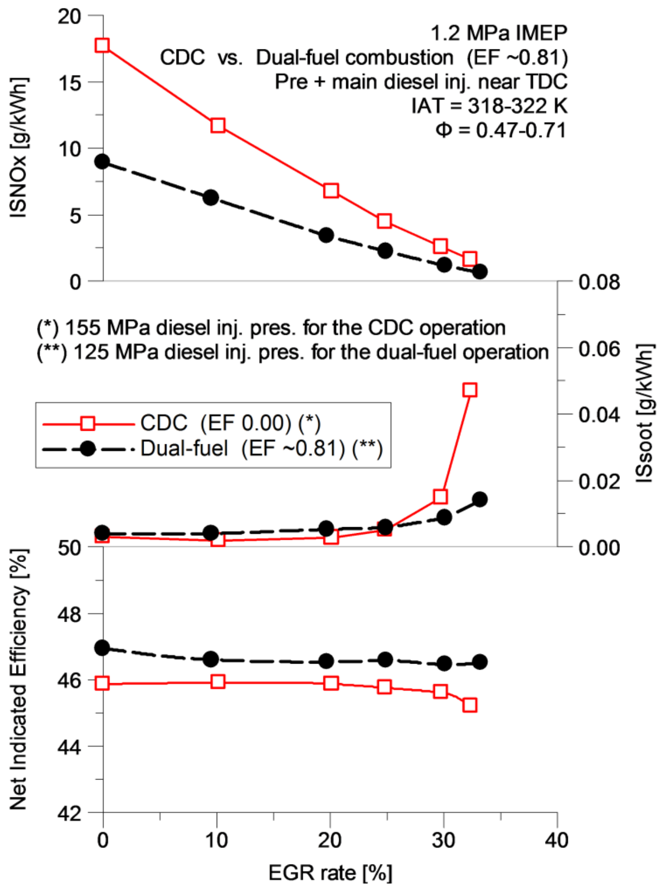

Figure 5.14 – The effect of EGR on emissions and net indicated efficiency of mid-load dual-fuel combustion with optimised diesel SOIs.

5.3.5 The effect of diesel injection pressure on mid-load dual-fuel operation

Mid-load dual-fuel operation employed lower diesel injection pressures than the CDC because of the higher levels of PRR. Figure 5.15 depicts the in-cylinder pressure and HRR for dual-fuel combustion with different rail pressures. While maintaining the diesel SOIs constant, the increase in the diesel injection pressure from 95 MPa to 155 MPa produced unacceptable combustion noise and a PRR of 2.9 MPa/CAD. This was a result of a shorter mixing-controlled combustion and higher rates of heat release.

The use of optimised diesel SOIs to maintain PRR below 2.0 MPa/CAD revealed that a higher rail pressure leads to insignificant improvements in net indicated efficiency and slightly higher NOx emissions. Thus, an intermediate diesel injection pressure (e.g. 125 MPa at 1.2 MPa IMEP) was selected for the dual-fuel operation in order to minimise the levels of smoke.

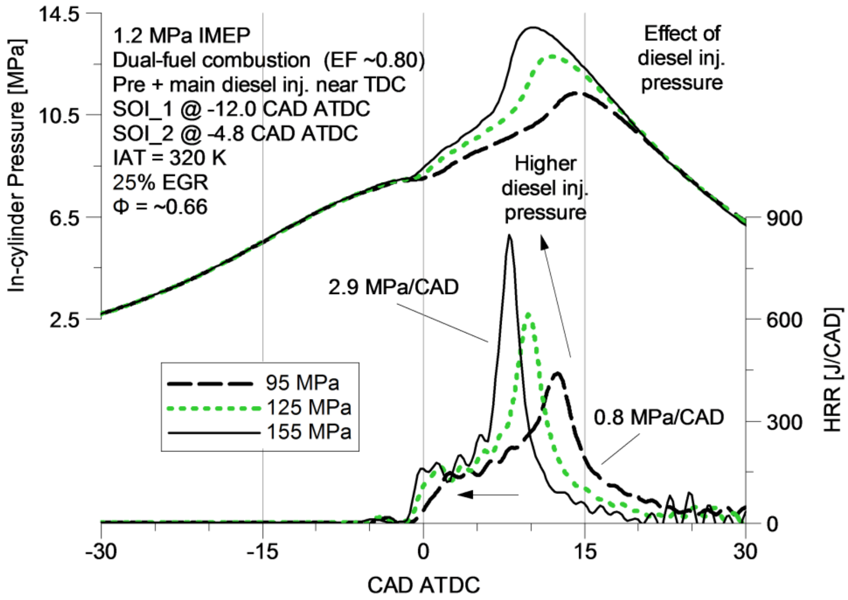

Figure 5.15 – The effect of diesel injection pressure on mid-load dual-fuel operation.

5.4 Exploring the potential of the dual-fuel operation with and without EGR

A systematic study was performed to optimise the use of ethanol as a partial substitute for diesel fuel. In addition, the investigation provides a better understanding of the trade-off between exhaust emissions, efficiency, and engine running costs for mid-load dual-fuel operation with and without EGR.

5.4.1 Experimental test procedure

Table 5.6 summarises the engine operating conditions. The experiments were performed at a constant engine speed of 1200 rpm and three loads of 0.9, 1.2, and 1.5 MPa IMEP using 0% and 25% EGR. The ethanol energy fraction was varied from 0.00 to 0.80. Diesel injection timings were optimised for maximum net indicated efficiency. A small pre-injection with an estimated volume of 3 mm^3 and a constant dwell time of 1 ms was employed to reduce the PRRs, which was limited to 2.0 MPa/CAD. The maximum in-cylinder pressure was limited to 18 MPa. Stable engine operation was quantified by a COV_IMEP below 3%.

Table 5.6 – Engine operating conditions for optimised mid-load dual-fuel combustion with pre- and main diesel injections near TDC.

Parameter	Value					
Speed	1200 rpm					
Load	0.9 MPa IMEP		1.2 MPa IMEP		1.5 MPa IMEP	
Diesel inj. pressure	110 MPa		125 MPa		140 MPa	
Diesel inj. strategy	Pre- and main injection near TDC					
$m_{ethanol/cycle}$	Varied from 0 to 189 mg/cycle					
EF	0.00-0.76		0.00-0.80		0.00-0.76	
Intake pressure	155 kPa		190 kPa		230 kPa	
Exhaust pressure	165 kPa		200 kPa		240 kPa	
EGR rate	0%	25%	0%	25%	0%	25%
Intake air temp.	308 K	317 K	313 K	318 K	319 K	323 K
EGR temperature	n/a	381 K	n/a	379 K	n/a	382 K

5.4.2 Combustion characteristics

Figure 5.16 shows the main diesel injection timings and in-cylinder pressure characteristics for ethanol-diesel dual-fuel combustion. Diesel-only operation (EF 0.00) was not PRR limited and allowed for the most advanced injection timings. The SOI_2 was retarded as more ethanol was injected to maintain the maximum PRR below 2.0 MPa/CAD. The dual-fuel operation with constant injection timing would result in excessive PRRs for early start of injections and inefficient combustion processes for late ones. The injection timing trend was reversed when running the engine with an ethanol energy fraction of 0.60-0.70. Relatively earlier injections were required as the ethanol percentage was increased due to a reduction in the reactivity of the in-cylinder charge (e.g. reduced amount of diesel).

Adding 25% EGR generally allowed for advanced injections due to longer burn rates and possibly lower local combustion temperatures. The use of a constant SOI with a higher EGR rate would likely lead to later combustion events [7]. The increase of the engine load yielded the opposite effects, limiting the maximum advance. The optimum SOIs with and without EGR were somewhat similar at 0.9 MPa IMEP as the combustion was more sensitive to higher intake charge temperature introduced by the recycled gases.

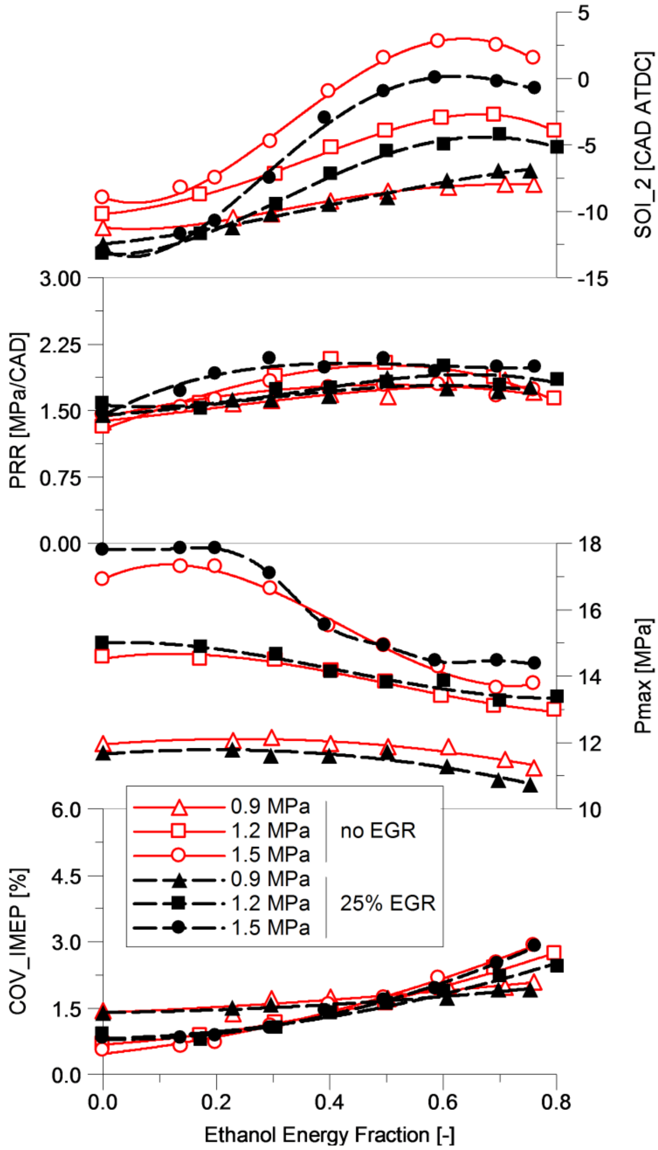

Figure 5.16 – Main diesel injection timings and combustion characteristics for optimised mid-load dual-fuel operation.

The maximum in-cylinder pressure increased with the engine load as a result of greater boost pressures and quantity of fuel injected/energy released. However, P_{max} was reduced by the use of higher ethanol fractions mainly due to later combustion events (see Figure 5.17). The limitation of peak pressure started to be an issue only when running with EGR and low ethanol percentages at the highest load of 1.5 MPa IMEP. The introduction of EGR typically allowed for earlier combustion phasing, leading to higher P_{max}. The exception occurred at the lightest load of 0.9 MPa IMEP, where the use of EGR increased the premixed combustion peak and limited the maximum injection timing advance. Consequently, P_{max} with EGR dropped in comparison with the cases without EGR. This was a result of relatively lower in-cylinder charge dilution (e.g. higher intake oxygen/nitrogen concentration) [119] and an increase of 9 K in the intake charge temperature.

COV_IMEP rose when the ethanol percentage was increased. This trend was attributed to the lower reactivity of the ethanol fuel and its dependence on the temperature rise introduced by the diesel fuel to initiate combustion. To some extent, higher engine loads and the use of EGR reduced the COV_IMEP due to increased fuel/air equivalence ratio. However, combustion instability with ethanol energy fractions above 0.60 was higher at 1.2 and 1.5 MPa IMEP than at 0.9 MPa IMEP. This is likely to be a result of the cyclic variability caused by the autoignition process of ethanol and is supported by a slight increase in the coefficient of variation of Pmax (not shown for brevity).

The analysis of the heat released showed that the ignition delay between the start of pre-injection (SOI_1) and SOC was always positive, which means combustion was controlled by the diesel injections. However, there were cases with negative ignition delay between SOI_2 and SOC, as depicted in Figure 5.17. This indicates that the combustion was starting prior to the main diesel injection timing. The shorter ignition delay was possibly a result of the higher fuel/air equivalence ratios obtained when the ethanol energy fraction and engine load were increased. Alternatively, the introduction of EGR led to slightly longer ignition delays. This was attributed to the higher heat capacity and dilution effect of the EGR that slowed down the onset of ignition and hampered the mixing between oxygen and fuel [181].

After the ignition occurred, the first part of the heat release process between CA10-CA50 became shorter as the ethanol percentage was increased. The ethanol fuel progressively burnt as the diffusion combustion took place. However, there was a reversal of the trend between the ethanol energy fractions of 0.40 and 0.60, depending on the engine load. For the conditions with higher levels of premixed ethanol, it is likely the fuel slowed the reaction rates due to its cooling effect and low reactivity. Despite the relatively longer CA10-CA50 period measured, it was still necessary to maintain or delay CA50 to avoid high PRR. The resulting CA50s depicted similar response to changes in diesel injection timings.

Higher ethanol percentages and elevated engine loads resulted in faster CA10-CA90. The greatest reduction in combustion duration occurred when using EGR at 1.2 MPa IMEP, where the CA10-CA90 was shortened from 30.7 CAD in diesel-only mode to 16.7 CAD in the dual-fuel combustion with an ethanol energy fraction of 0.80. The use of

EGR was effective in slowing down the combustion process, increasing the CA10-CA90 by up to 29%.

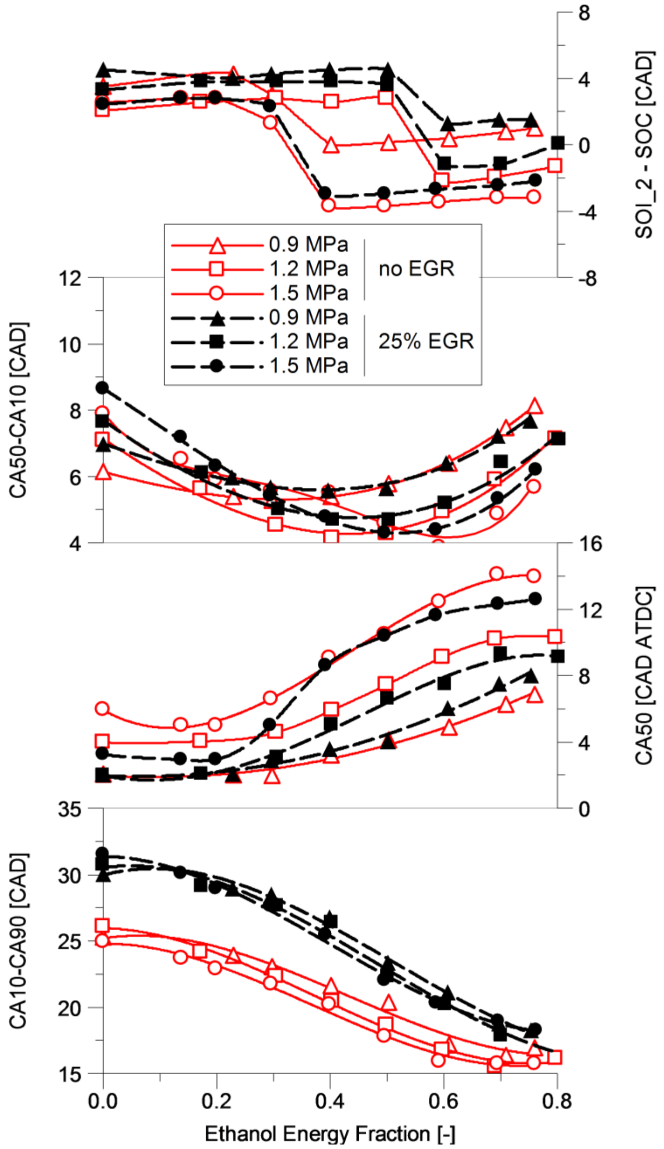

Figure 5.17 – Heat release characteristics for optimised mid-load dual-fuel operation.

5.4.3 Engine-out emissions and performance

Figure 5.18 shows the net indicated specific emissions for ethanol-diesel dual-fuel combustion. NOx emissions were reduced by 39-68% at the highest ethanol energy fractions. More homogeneous combustion with high ethanol percentages possibly helped minimise NOx production at the outer boundary of the diesel diffusion flame. Later combustion phasing and lower P_{max} also contributed to this improvement.

In one specific case at 0.9 MPa IMEP, ISNOx levels without EGR were decreased from 17.1 g/kWh in the diesel-only mode to 10.4 g/kWh in the dual-fuel combustion with an ethanol energy fraction of 0.76. The use of EGR and the increase of the engine load to 1.5 MPa IMEP allowed for further NOx reductions due to relatively lower oxygen availability [8]. On average, the introduction of the EGR dropped the NOx emissions by 80% while maintaining a similar trend to that of the cases where no EGR was used. This can be demonstrated by the decrease from 10.4 to 2.1 g/kWh when operating the engine with an EF of 0.76 at 0.9 MPa IMEP.

The smoke number was maintained under 0.1 FSN without EGR, which was equivalent to an ISsoot below 0.008 g/kWh, independent of ethanol percentage and load. Soot emissions slightly increased with the ethanol energy fraction due to the later combustion process and the decreasing gas temperatures as the expansion stroke continues [8]. To some extent, lighter loads tend to produce more soot emissions than higher loads as a result of lower rail pressures and reduced end-of-combustion temperatures [191].

The presence of EGR elevated levels of ISsoot due to reduced oxygen concentration and lower combustion temperatures. Ethanol energy fractions between approximately 0.40 and 0.60 resulted in an apparent “soot bump” associated with a rapid CA10-CA50 duration and thus shorter mixing time prior to the autoignition of ethanol. As the port fuel injected ethanol fraction increased towards 0.80, combustion became more homogenous and less diesel fuel was available for soot formation. As a result, the dual-fuel combustion with 25% EGR attained smoke levels between 0.006-0.011 g/kWh.

Diesel-only combustion yielded values under 0.5 g/kWh and 0.2 g/kWh for ISCO and ISHC, respectively, maintaining high combustion efficiencies throughout the sweep of load and EGR. In comparison, the port fuel injection of a low reactivity fuel usually leads to higher levels of late cycle CO and unburnt HC. This effect was shown by computational fluid dynamics modelling performed by Kokjohn et al. [57] and Desantes et al. [88], where it was revealed that fuel is trapped in the crevice and squish volumes of a stock diesel combustion system. Therefore, it would be generally accepted that the use of higher ethanol energy fractions would lead to increased unburnt HC emissions.

For the specific cases investigated in this study, engine load had little influence on unburnt hydrocarbon emissions for a constant ethanol percentage. The ISHC was slightly reduced at 1.2 MPa IMEP when compared to the levels measured at 0.9 MPa IMEP due to a higher Φ. However, ISHC increased at 1.5 MPa IMEP mostly as a result of delayed combustion processes and lower combustion temperatures (as supported by the NOx emissions). The introduction of EGR was beneficial to ISHC reduction because of the relatively higher fuel/air equivalence ratio of the premixed charge. ISHC was more susceptible to the low Φ obtained without EGR at 0.9 MPa IMEP.

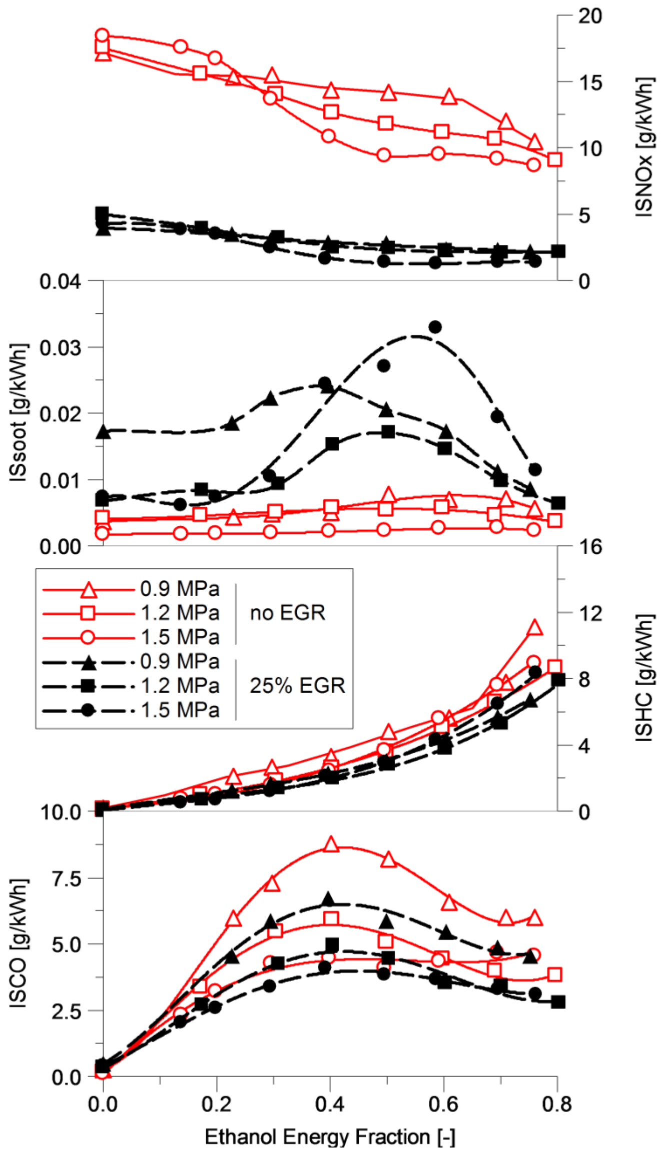

Figure 5.18 – Net indicated specific emissions for optimised mid-load dual-fuel operation.

The ISCO exhibited a different trend from ISHC. Carbon monoxide emissions increased rapidly as more diesel fuel was substituted with ethanol until it reached a peak at ethanol energy fractions of approximately 0.40. These conditions represent dual-fuel combustion processes with some of the shortest CA10-CA50 periods. The results are indicative of inappropriate mixing time and show a transition between stratified dual-fuel combustion and ethanol-dominated heat release [120].

CO emissions decreased as the ethanol fraction was increased from 0.40 towards 0.80. This was attributed to the lower in-cylinder gas temperatures and the reduction in partial oxidation of the premixed fuel (e.g. higher unburnt HC emissions). Relatively lower levels of ISCO at high ethanol percentages was also reported by Han et al. [83] over a sweep of intake oxygen concentration at 1.0 MPa IMEP. Higher engine loads and the use of EGR were effective in reducing CO emissions, mainly due to increased global fuel/air equivalence ratio.

Figure 5.19 depicts the overall dual-fuel engine performance at medium loads. Since combustion efficiency is determined by CO and unburnt HC emissions, its level gradually decreased with higher ethanol energy fractions and reached approximately 96% at the maximum substitution ratios. At the lightest load of 0.9 MPa, the dual-fuel operation without EGR led to lowest combustion efficiency of 95% as a result of reduced in-cylinder gas temperatures and Φ.

Net indicated efficiency is a dimensionless parameter that relates the indicated power to the amount of fuel energy delivered. Net indicated efficiency varied slightly with ethanol content and EGR at the three mid-loads investigated. This shows the efficiency was found to be affected by the combustion efficiency and heat transfer, as the pumping losses were kept approximately the same at a given load.

The best dual-fuel results were achieved at 1.2 MPa IMEP, where net indicated efficiency reached more than 47% using an ethanol energy fraction of 0.80. Peak in-cylinder pressure and PRR limitations combined with a high Φ (e.g. heat transfer loss) constrained improvements in engine performance at 1.5 MPa IMEP compared to the medium load of 1.2 MPa IMEP. The maximum net indicated efficiency for diesel-only combustion was 46.3%.

At 0.9 MPa IMEP, the overly lean in-cylinder charge somewhat degraded the efficiencies at low EF of 0.20-0.40. As the ethanol energy fraction was increased, net indicated efficiency was recovered by reduced heat transfer loss due to shorter combustion duration and lower peak in-cylinder pressures. Higher intake charge temperature and relatively longer ignition delay introduced by the use of EGR increased the premixed combustion peak and limited advanced combustion events at 0.9 MPa IMEP. As a result, net indicated efficiency was slightly reduced with 25% EGR.

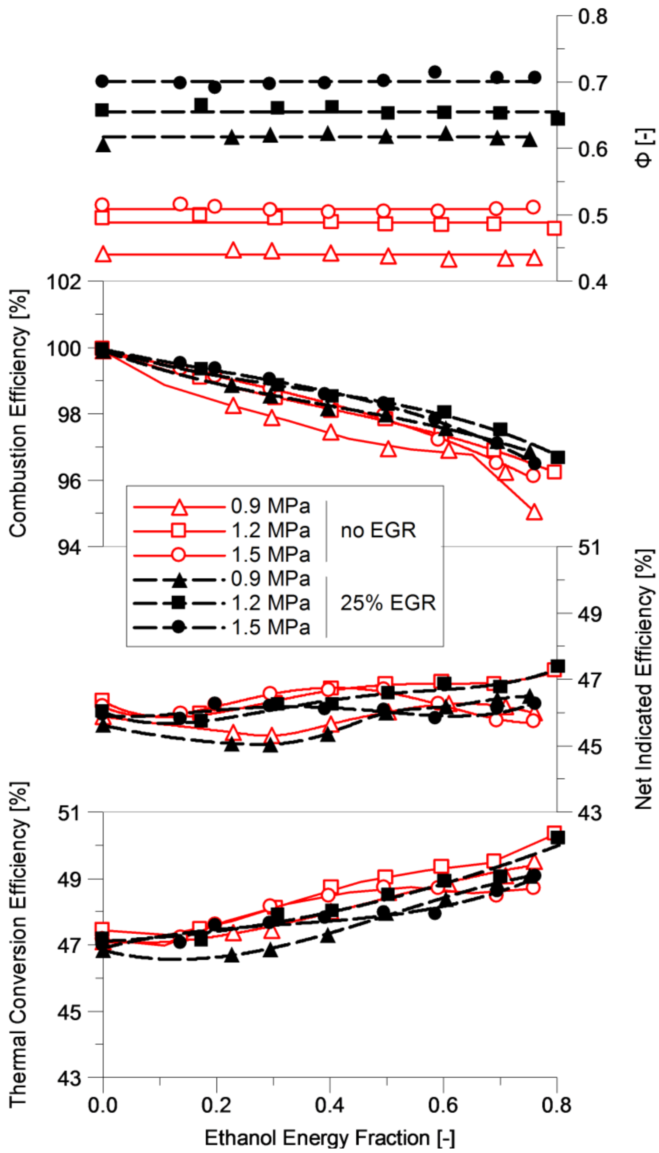

Figure 5.19 – Performance for optimised mid-load dual-fuel operation.

The thermal conversion efficiency was calculated to evaluate the maximum theoretical thermodynamic efficiency of the engine by subtracting the effects of combustion efficiency (e.g. partial oxidation) and gas exchange process (e.g. pumping losses) from the net indicated efficiency by

$$\begin{aligned} &Thermal\ Converison\ Efficiency \\ &= \frac{Net\ Indicated\ Efficiency}{Combustion\ Efficiency\ \times\ Gas\ Exchange\ Efficiency} \times 10^4 \end{aligned} \tag{5.1}$$

The analysis showed that the port fuel injection of ethanol in a heavy-duty diesel engine can lead to thermal conversion efficiencies of more than 50% with an ethanol energy fraction of 0.80 at the load of 1.2 MPa IMEP. This is likely attributed to a reduction in heat transfer losses introduced by lower local in-cylinder gas temperatures and optimum start- and end-of-combustion timings.

Improvements in thermal conversion efficiency with EGR were often counterbalanced by a higher global fuel/air equivalence ratio and longer combustion duration, despite the lower peak combustion temperatures. Therefore, ethanol-diesel dual-fuel combustion has the potential to simultaneously yield high thermal conversion efficiencies and low NOx emissions. The effectiveness of the alternative combustion strategy in terms of operational cost is discussed in the next subsection.

5.4.4 Cost-benefit and overall emissions analysis

The practical use of ethanol in a heavy-duty diesel engine is linked to several aspects, such as fuel prices, volumetric fuel consumption, engine performance, and exhaust emissions. Therefore, a cost-benefit and overall emissions analysis was carried out to determine the best way to utilise ethanol as a fuel.

Figure 5.20 shows the total fuel energy flow rate and the relative volumetric fuel flow rate at different engine operating conditions. The fuel energy consumption rose with load and remained practically constant when more ethanol and/or EGR were used. However, the ratio of the total volumetric fuel flow rate to the diesel flow rate in the diesel-only baseline cases increased with the ethanol percentage.

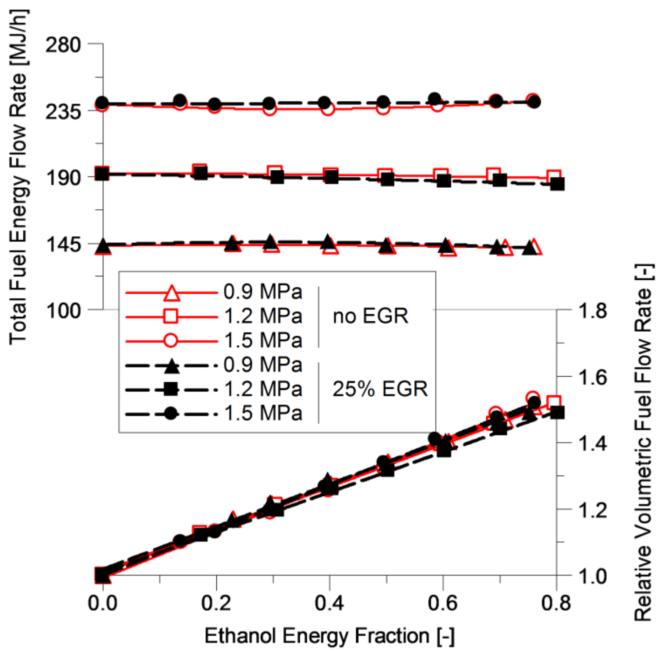

Figure 5.20 – Total fuel energy flow rate and relative volumetric fuel flow rate.

The dual-fuel combustion with ethanol energy fractions of 0.76-0.80 resulted in approximately 50% higher volumetric fuel consumption (e.g. dm^3/h) than the conventional diesel combustion. The increase in total volumetric fuel flow rate is attributed to the differences in densities and LHV between ethanol and diesel.

The fuel properties can be used to obtain an economic assessment of the maximum volumetric price ratio (VPR_{max}) between ethanol and diesel fuels, as shown in Equation (5.2). If one considers the fuel energy flow rate has been kept constant as more ethanol was injected at a given operating condition, the dual-fuel operation will be cost-effective when the relative price of one litre of anhydrous ethanol ($Price_{ethanol}$) is less than 60% of the cost of one litre of diesel ($Price_{diesel}$).

$$VPR_{max} = \left(\frac{Price_{ethanol}}{Price_{diesel}}\right)_{max} = \frac{\rho_{ethanol}\, LHV_{ethanol}}{\rho_{diesel}\, LHV_{diesel}} \approx 0.60 \tag{5.2}$$

In addition to fuel prices, the total cost of ownership will be affected by the operating cost of the aftertreatment system. The Euro VI emissions regulation applied for heavy-duty vehicles [29] limits the NOx and the particulate matter emissions to 0.4 g/kWh and 0.010 g/kWh, respectively. The regulation also sets maximum levels of CO and unburnt HC emissions equivalent to 1.5 g/kWh and 0.13 g/kWh, respectively.

The emissions standard limits were not fully met by the in-cylinder measures investigated in this work. Although the majority of the CO and unburnt HC emissions produced by dual-fuel combustion can be removed by a diesel oxidation catalyst [94], extremely high HC conversion efficiencies will be necessary to comply with the stringent tailpipe unburnt HC emissions of 0.13 g/kWh.

Relatively low levels of soot emissions were attained and can be further reduced with higher diesel injection pressures. Alternatively, smoke control can be achieved using diesel particulate filters typically required in heavy-duty diesel applications. However, it should be noted that the use of this aftertreatment system is associated with higher backpressure and involves periodic regenerations, resulting in fuel efficiency penalty [41,48,52].

NOx emissions still present a challenge depending on the engine calibration due to limited conversion efficiency of the SCR system and/or high aqueous urea solution usage (e.g. increased engine operational cost). The NOx conversion ($Conv.Eff$) of practical SCR aftertreatment systems typically ranges between 80% and 90% when the exhaust gas temperature is higher than 573 K [50,192]. Higher conversion of 97% is likely attained with optimised closed loop control of aqueous urea solution injection [52] or with the introduction of an additional flow-through SCR catalyst [193].

Figure 5.21 compares the estimated SCR-out NOx levels attained with different SCR conversion efficiencies when operating the engine with and without EGR at 1.2 MPa IMEP. The shaded areas represent the sensitivity of NOx emissions when the conversion efficiency was varied from 80% to 97%. The lines in between indicate the NOx emissions for an SCR system with 90% removal efficiency. The levels of ISNOx downstream of the SCR system were calculated as

$$SCR - out\ ISNOx = \left(\frac{100 - Conv.Eff.}{100}\right) ISNOx \tag{5.3}$$

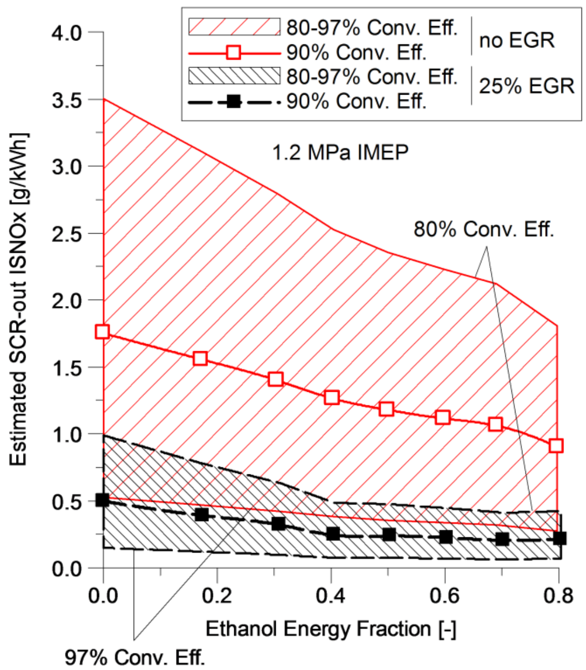

Figure 5.21 – Estimated ISNOx levels for different SCR conversion efficiencies.

The use of low ethanol energy fractions between 0.00 and 0.30 without EGR resulted in estimated SCR-out ISNOx higher than the Euro VI standard limit of 0.4 g/kWh, independent of the NOx removal efficiency. Later diesel injection timings are likely to be required at these particular conditions, which would adversely affect soot emissions and indicated efficiency.

Alternatively, the use of 25% EGR allowed for NOx emissions compliance when running with ethanol fractions above 0.20 and an SCR conversion efficiency of 90%. The combination of a high EF of 0.80 and EGR led to an ISNOx reduction of 88% compared with diesel-only combustion without EGR at a given SCR efficiency.

A decrease in ISNOx levels allows for operational cost savings as a result of lower aqueous urea solution consumption ($\dot{m}_{urea}$) in the SCR system. To determine the effectiveness of the use of ethanol and EGR in terms of running costs, the $\dot{m}_{urea}$ required to reduce the ISNOx levels to the Euro VI emissions standard limit was calculated as

$$\dot{m}_{urea} = 0.01\ (ISNOx - ISNOx_{Euro\ VI})\left(\dot{m}_{diesel} + \dot{m}_{ethanol}\ \frac{LHV_{ethanol}}{LHV_{diesel}}\right) \tag{5.4}$$

where $\dot{m}_{urea}$ is estimated at 1% of the diesel equivalent fuel flow rate per g/kWh reduction in NOx emissions [48,51,52,55,123]. Adding the estimated $\dot{m}_{urea}$ to the measured diesel fuel flow rate allowed for the calculation of the SCR corrected net indicated efficiency ($Net\ Indicated\ Eff._{SCR\ corrected}$), which was defined as

$$Net\ Indicated\ Eff._{SCR\ corrected} = \left[\frac{3.6\ P_{ind}}{(\dot{m}_{diesel} + \dot{m}_{urea})\ LHV_{diesel} + (\dot{m}_{ethanol})\ LHV_{ethanol}}\right] \times 100 \tag{5.5}$$

The aqueous urea solution was simulated to have the same cost and “properties” of the diesel fuel [55], as their relative prices vary according to region and purchase order quantity [52]. The estimated $\dot{m}_{urea}$ to meet the Euro VI heavy-duty NOx emissions target and the resulting $Net\ Indicated\ Eff._{SCR\ corrected}$ are shown in Figure 5.22. Diesel-only combustion and no EGR operation resulted in lower SCR corrected net indicated efficiency due to higher urea consumption. The use of ethanol and EGR minimised the NOx emissions and thus the $\dot{m}_{urea}$ required. This allowed for higher $Net\ Indicated\ Eff._{SCR\ corrected}$, effectively translating into lower running costs.

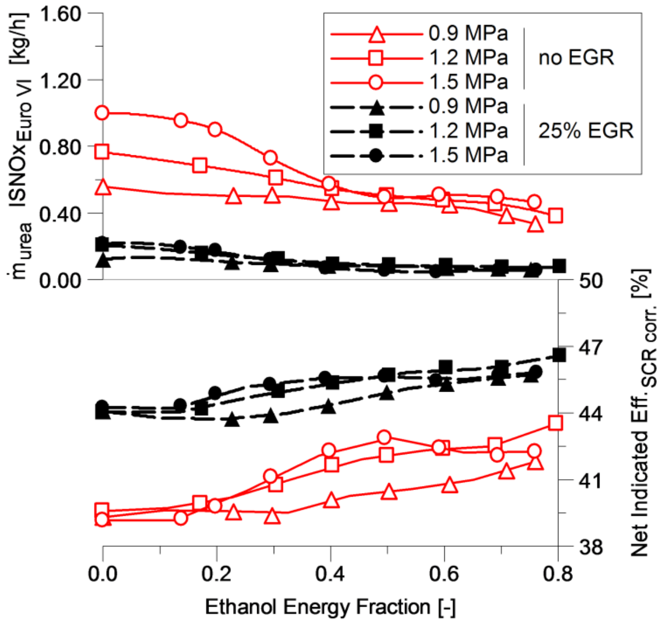

Figure 5.22 – Estimated aqueous urea solution flow rate to meet the Euro VI heavy-duty NOx emissions target and SCR corrected net indicated efficiency.

If the $\dot{m}_{urea}$ and fuel prices (per litre) are known, the engine operational cost ratio ($EOCR$) at a given load can be estimated using Equation (5.6). The result of this equation will characterise an increase or decrease in engine operational cost (e.g. $£/kW$) compared to those of a CDC operation baseline without an SCR system ($\dot{m}_{urea} = 0$). This condition was represented by the measured net indicated efficiencies for the diesel-only cases with and without EGR ($Net\ Indicated\ Efficiency_{baseline}$) showed in Figure 5.19.

$$EOCR = \left\{\left[\frac{Engine\ Operational\ Cost_{(SCR\ corrected)}}{Engine\ Operational\ Cost_{(CDC\ baseline)}}\right] - 1\right\} \times 100$$
$$= \left\{\left[\frac{\dfrac{\left(\dfrac{Price_{ethanol}}{\rho_{ethanol} LHV_{ethanol}}\right)(EF) + \left(\dfrac{Price_{diesel}}{\rho_{diesel} LHV_{diesel}}\right)(1 - EF)}{Net\ Indicated\ Eff._{SCR\ corrected}}}{\dfrac{\left(\dfrac{Price_{diesel}}{\rho_{diesel} LHV_{diesel}}\right)}{Net\ Indicated\ Efficiency_{baseline}}}\right] - 1\right\} \times 100 \qquad (5.6)$$
$$= \left\{\frac{Net\ Indicated\ Efficiency_{baseline}}{Net\ Indicated\ Eff._{SCR\ corrected}}\left[\frac{Price_{ethanol}}{Price_{diesel}}\left(\frac{\rho_{diesel}\ LHV_{diesel}}{\rho_{ethanol}\ LHV_{ethanol}}\right)(EF) + (1 - EF)\right] - 1\right\} \times 100$$

The use of the VPR_{max} and the actual volumetric price ratio (VPR) between ethanol and diesel fuels simplifies the Equation (5.6) into Equation (5.7). If $VPR = VPR_{max} \approx 60\%$, the $EOCR$ will rely exclusively on the net indicated efficiencies.

$$EOCR = \left\{ \frac{Net\ Indicated\ Efficiency_{baseline}}{Net\ Indicated\ Eff._{SCR\ corrected}} \left[\frac{VPR}{VPR_{max}}(EF) + (1 - EF) \right] - 1 \right\} \times 100 \quad (5.7)$$

Figure 5.23 shows the influence of the VPR on the engine operational cost ratio at 1.2 MPa IMEP. Lower $EOCR$ represents a reduced cost of ownership. The symbols indicate the sensitivity of the $EOCR$ to a VPR of 60% as the ethanol energy fraction was varied with and without EGR. The shaded areas depict the estimated $EOCR$ when the volumetric price ratio varies from 50% to 70%.

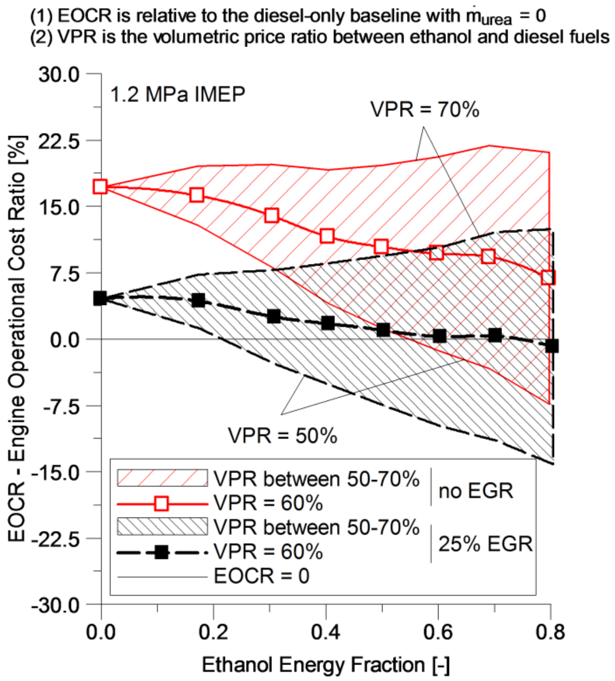

Figure 5.23 –Sensitivity of the $EOCR$ to different volumetric price ratios between ethanol and diesel fuels.

The results highlight the potential of high ethanol energy fractions and a moderate EGR rate to reduce the overall engine running costs via lower consumption of aqueous urea solution. This demonstrates the optimum balance between in-cylinder and aftertreatment control of NOx emissions. However, the effectiveness of dual-fuel combustion in terms of cost heavily depends on fuel prices, which vary according to availability of feedstock, production process, financial incentives, supply obligations, etc. Dual-fuel combustion will reduce the engine operational cost when the VPR between ethanol and diesel fuels is less than 60%. Higher relative prices can still be cost-effective depending on the EGR rate and ethanol fraction.

5.5 Summary

In this chapter, engine experiments were carried out to investigate the performance and emissions of ethanol-diesel dual-fuel combustion at medium loads (between 0.7 and 1.5 MPa IMEP). The study was performed using different diesel injection strategies, ethanol energy fractions, intake air temperatures, and EGR rates. In some cases, diesel injection timings were optimised for the maximum net indicated efficiency. Combustion characteristics, exhaust emissions, and performance were discussed. Cost-benefit ratio and overall exhaust emissions aspects of the utilisation of ethanol and EGR were introduced.

The primary findings of the mid-load dual-fuel operation can be summarised as follows:

- An early single diesel injection strategy led to low combustion stability at high ethanol energy fractions and excessive PRRs at low ethanol percentages. Similarly, the dual-fuel combustion with premixed ethanol fuel ignited by a single diesel injection near TDC yielded unacceptable combustion noise due to high levels of PRR during the premixed combustion phase.
- The use of early and late split diesel injections allows for high efficiency dual-fuel operation and relatively low NOx emissions. However, these strategies were extremely sensitive to variations in the intake charge temperature and characteristics of the first diesel injection diesel (e.g. split ratio and timing).
- The use of a pre-injection in conjunction with the main diesel injection reduced the levels of PRR and was a key enabler for achieving efficient mid-load dual-fuel combustion with ethanol energy fractions up to 0.80.
- The increase in engine load to 1.5 MPa IMEP in the dual-fuel mode advanced the ignition of the premixed ethanol fuel and shortened the combustion durations. This required retarded diesel injection timings to lower the in-cylinder pressure rise rates.
- Higher ethanol percentages also resulted in faster burn durations, requiring later diesel injection timings. Despite the retarded combustion, net indicated efficiency was maintained essentially constant due to the more thermodynamically optimum heat release.
- High ethanol energy fractions reduced the levels of ISNOx of the diesel-only operation at the expense of higher CO and unburnt HC emissions. Soot levels varied with different ethanol percentages.

- The use of 25% EGR and optimised diesel SOIs was effective in reducing NOx emissions by approximately 80% with negligible impact on the efficiency when compared to the cases without EGR at a given ethanol energy fraction.
- The results also indicate that the utilisation of an ethanol energy fraction of 0.80 combined with EGR has potential to achieve 88% NOx reduction compared against the diesel-only combustion baseline without EGR at 1.2 MPa IMEP.
- The engine operational cost is highly dependent on fuel prices (e.g. per litre) despite the significant NOx reduction capability and lower aqueous urea solution consumption attained with ethanol-diesel dual-fuel combustion.

Overall, high efficiency and low emissions mid-load dual-fuel combustion was achieved with EGR and a close-coupled pre-injection introduced shortly before the main diesel injection. However, the effectiveness of the dual-fuel operation relies on a maximum volumetric price ratio between ethanol and diesel fuels equivalent to 60%. Higher relative prices can still be cost-effective depending on the ethanol energy fraction and EGR rate used as a result of reduced aqueous urea solution consumption in the NOx aftertreatment system.

Chapter 6

Dual-fuel combustion at high engine loads

6.1 Introduction

Dual-fuel operation at high load conditions has proved extremely challenging as a result of the peak in-cylinder pressure [121] and/or PRR limitations [122,123], which restrict the amount of low reactivity fuel used to very low percentages. Figure 6.1 shows where the high load region is located over an estimated speed and load map of a HD diesel engine.

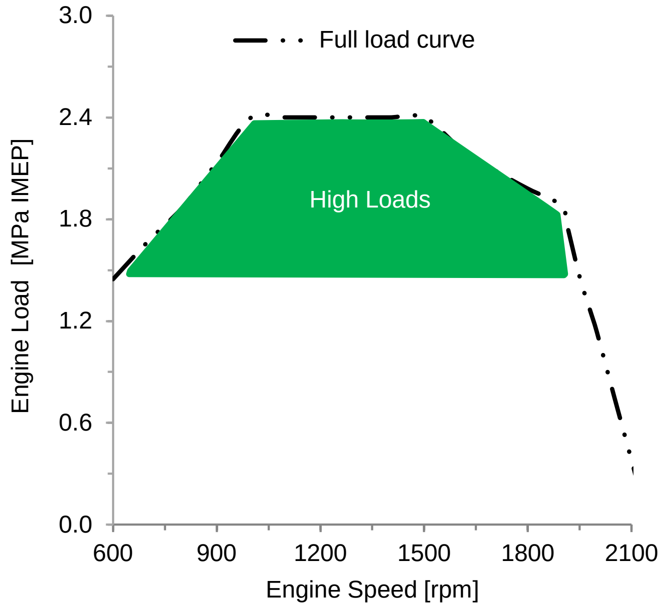

Figure 6.1 – High load region over an estimated HD diesel engine speed-load map.

At high load, dual-fuel engines often rely on exhaust gas recirculation (EGR) to avoid excessive in-cylinder pressure rise rates caused by the autoignition of the premixed fuel. This can adversely affect the net indicated efficiency depending on the resulting fuel/air equivalence ratio and pressure differential across the cylinder used to drive the requested amounts of EGR. In this chapter, an experimental analysis has been performed to investigate the characteristics of high load ethanol-diesel dual-fuel combustion and identify the optimum combustion control strategies for highly efficient engine operation.

Section 6.2 reveals the influence of different parameters on dual-fuel combustion at 1.8 MPa IMEP. Section 6.3 assesses the potential of Miller cycle via late intake valve closing events and charge air cooling via an air-to-water heat to minimise the EGR requirements and improve upon the net indicated efficiency. Combustion characteristics, exhaust emissions, and efficiencies were measured and discussed for different ethanol energy fractions. The trade-off between net indicated efficiency and NOx emissions has been discussed. Finally, Section 6.4 shows engine experiments performed to understand the effects of wet ethanol injection and Miller cycle on the dual-fuel operation at full load (2.4 MPa IMEP). Anhydrous ethanol and wet ethanol mixtures containing 20%, 35%, and 50% of water in a volume basis were explored as potential premixed fuels.

6.2 Characterisation of high load dual-fuel operation

This section will present and discuss the effect of ethanol energy fraction, EGR rate, global fuel/air equivalence ratio, pressure-based effective compression ratio (ECR), and intake manifold air temperature on high load dual-fuel operation.

6.2.1 Experimental test procedure

Table 6.1 summarises the baseline engine operating conditions and highlights the optimised parameters. Testing was performed at a constant engine speed of 1200 rpm and a high load of 1.8 MPa IMEP. The maximum in-cylinder gas pressure (P_{max}) and the pressure rise rate (PPR) limit were set at 18 MPa and 2.0 MPa/CAD, respectively. The PRR limit was relaxed to 3.0 MPa/CAD on a few cases to allow for the demonstration of a given trend. Stable engine operation was quantified by a COV_IMEP below 3%.

The ethanol energy fraction and diesel injection timings were varied when required. The exhaust back pressure was also varied when performing sweeps of intake pressure to maintain a constant pressure differential across the cylinder of 10 kPa and a comparable PMEP. Diesel fuel was introduced using a single injection near firing top dead centre (TDC). However, there were some cases where a small pre-injection of an estimated volume of 3 mm^3 and a constant dwell time of 1 ms (e.g. 7.2 CAD at 1200 rpm) between pre- (SOI_1) and main (SOI_2) diesel injection events was employed to reduce the levels of PRR, as revealed in [3] and discussed in Chapter 5.

Table 6.1 – Engine operating conditions during the characterisation of high load dual-fuel operation.

Parameter	Baseline	Sweeps
Speed	1200 rpm	
Load	1.8 MPa IMEP	
Diesel injection pressure	155 MPa	
Diesel injection strategy	Late single	Pre- and main injection near TDC
$m_{ethanol/cycle}$	0.0 mg/cycle	Varied between 0.00 and 88.1 mg/cycle
EF	0.00	Varied between 0.00 and 0.30
Intake air temperature	324 K	304 K without EGR and 328 K with EGR
Intake pressure	260 kPa	Varied between 240 kPa and 290 kPa
Exhaust pressure	270 kPa	Varied with the intake pressure
EGR rate	0%	15.7% and 21.2%
EGR temperature	n/a	383 ± 3 K
Intake valve closing (IVC)	-154 CAD ATDC	-126 and -108 CAD ATDC
Pressure-based ECR	16.8:1	15.7:1 and 14.4:1

6.2.2 Miller cycle and the pressure-based ECR calculation

The engine features a variable valve actuation (VVA) system on the intake camshaft, incorporating a hydraulic tappet on the valve side of the rocker arm [105]. This system allows for the use of Miller cycle via modification of the main intake valve closing (IVC) event. Some experiments were carried out using late intake valve closing (LIVC) events, where the intake valves were left open for longer in duration than those of the baseline intake valve lift profile. This decreased the actual in-cylinder mass trapped as the piston expelled part of the inducted mass back into the intake port.

The later initiation of the compression process resulted in a lower ECR, which can be calculated as the ratio of the instantaneous in-cylinder volume at IVC (e.g. 0.5 mm valve lift) to the clearance volume at TDC. However, this volume-based approach might not represent the actual compression ratio due to the flow resistance across the intake valves [194] and inertia of the gas in the intake port before the inlet valves are closed [8].

Therefore, a pressure-based ECR calculation was employed in order to better account for the gas exchange process. The method used the effective in-cylinder volume at IVC obtained from the intersection of the average intake manifold pressure and an extrapolated polytropic compression curve fitted to the experimental in-cylinder pressure (from -90 CAD to -25 CAD ATDC) [135,194].

Figure 6.2 depicts the method used for computation of the volume-based (A) and pressure-based (B) ECR for the three intake valve lift profiles used in this study. The analysis revealed that the effective volume at IVC (B) and thus the pressure-based ECR are higher than those obtained by the volume-based method using the instantaneous volume at IVC (A).

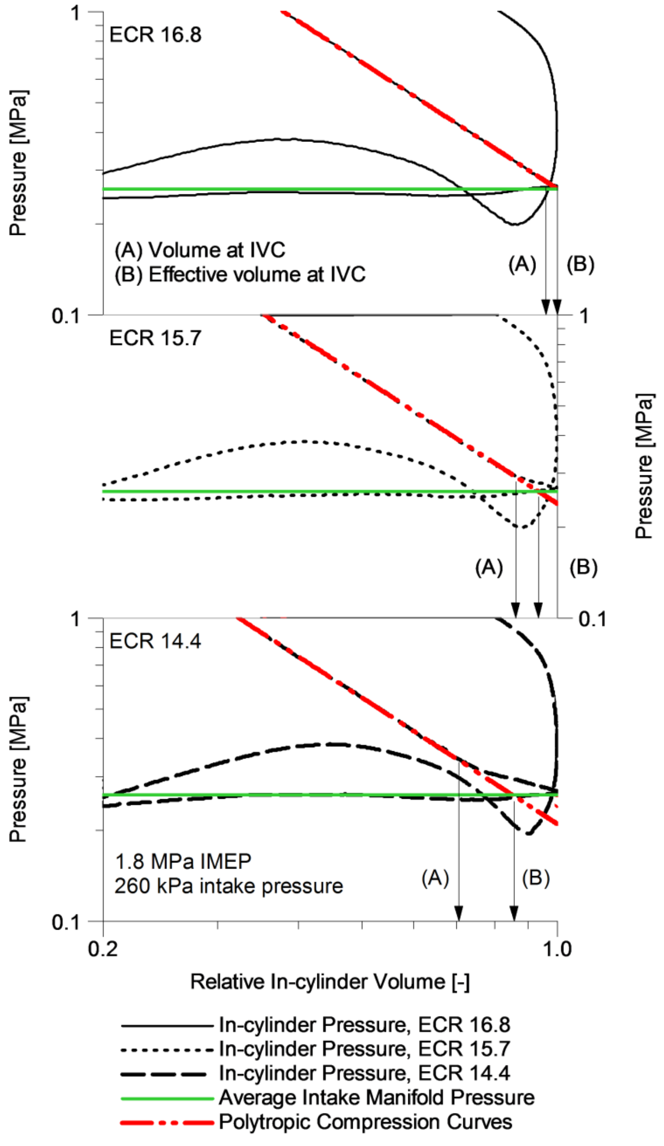

Figure 6.2 – In-cylinder pressure, average intake manifold pressure, and polytropic compression curve as a function of in-cylinder volume for three intake valve lift profiles.

Figure 6.3 shows the intake and exhaust valve lift profiles used in this study. The main IVO event was set at 366 CAD ATDC as determined at 0.5 mm valve lift, maintaining the maximum lift constant. The main IVC event was set at -154, -126, and -108 CAD ATDC, attaining pressure-based ECRs of 16.8:1, 15.7:1, and 14.4:1, respectively. The expansion ratio remained constant as a result of the fixed exhaust camshaft timing.

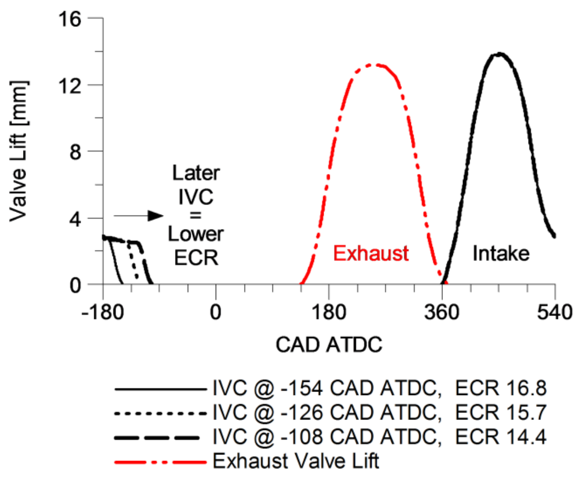

Figure 6.3 – Intake and exhaust valve lift profiles based on crank angle position relative to firing TDC.

6.2.3 The effect of ethanol energy fraction on high load dual-fuel operation

Initially, experiments were performed to characterise the ethanol-diesel dual-fuel combustion with the default intake valve timings. The engine was operated using the baseline condition showed in Table 6.1 with ethanol energy fractions that varied from 0.00 to 0.30. The diesel injection timing was held constant at 4.75 CAD ATDC to ensure the diesel-only baseline would have a complete compression process (without combustion) up to firing top dead centre. Any heat release before the diesel injection would be produced by the autoignition of ethanol in the dual-fuel mode.

Figure 6.4 shows that homogeneous charge compression ignition (HCCI) of the ethanol fuel occurred prior to the start of the diesel injection. The premixed peak heat release increased with the ethanol content, reaching a PRR of 2.2 MPa/CAD at the ethanol energy fraction of 0.30. The increase in the total in-cylinder mass trapped and cooling effect achieved with higher EFs helped decrease the compression temperatures. However, the port fuel injected ethanol autoignited prior to the direct injection of diesel because of the high mean in-cylinder gas temperatures, which were above 950 K after -10 CAD ATDC.

Fuel autoignition in internal combustion engines is predicted to take place between 900 and 950 K [190,195]. This is supported by Sjöberg and Dec's study [196], which revealed that the ethanol autoignition occurred as the mean in-cylinder gas temperature reached more than 900 K. The ignition is followed by the production of water and heat release due to the reaction between hydroxyl (OH) radicals and fuel molecules [197].

The OH radicals are rapidly produced by the thermal decomposition of hydrogen peroxide (H_2O_2) as the in-cylinder gas temperature approaches the autoignition temperature. The H_2O_2 is formed and accumulated by low and intermediate temperature kinetic pathways during the compression stroke [190].

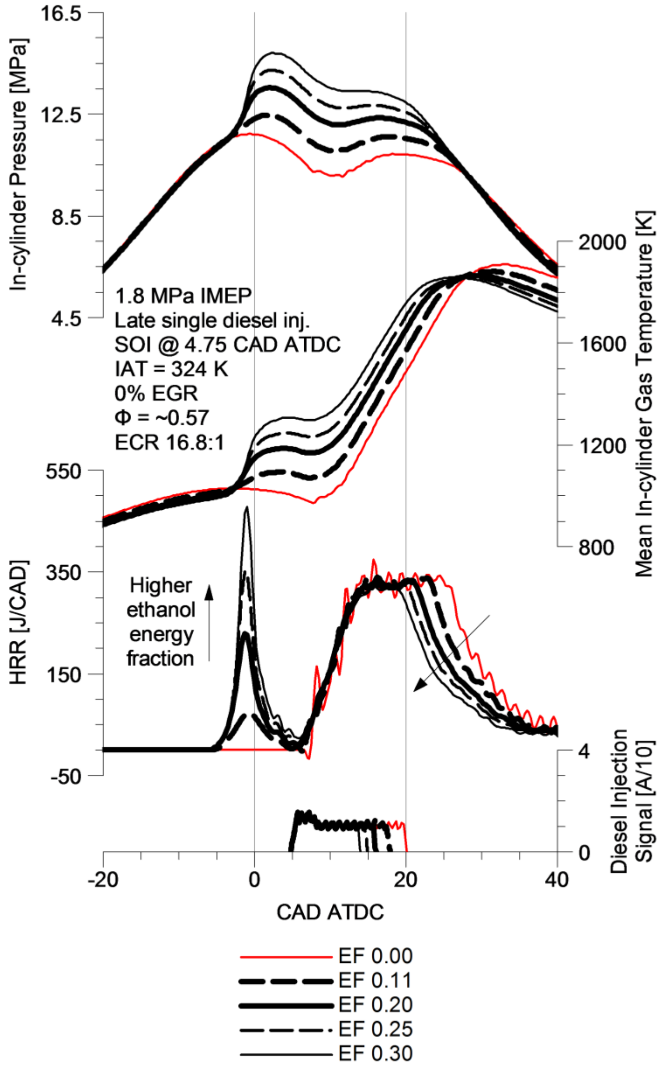

Figure 6.4 – The effect of ethanol energy fraction on high load dual-fuel operation with an ECR of 16.8:1.

6.2.4 The effect of EGR on high load dual-fuel operation

External EGR rate was varied from 0% to 21.2% in an attempt to delay the ethanol autoignition process. The intake and exhaust manifold pressures were held constant. Figure 6.5 demonstrates that increased EGR percentage delayed the SOC, lowered the peak heat release, and slowed the diesel mixing-controlled combustion. This was a result of the lower O_2 concentration and higher heat capacity of the in-cylinder charge with EGR rates of 15.7% and 21.2%, which delayed the early ignition of ethanol by 1.25 CAD and 1.50 CAD respectively when compared to the dual-fuel operation without EGR.

In a previous study by Sjöberg and Dec [196], it was shown that replacing inducted air with EGR and its different constituents could decrease the compression temperatures and slow down the intermediate-temperature heat-release rate (e.g. SOC-CA10) of the ethanol autoignition process.

However, in the present study the ignition of the ethanol fuel exhibited a relatively low sensitivity to variations in the in-cylinder O_2 concentration when using the actual engine EGR. This reduced sensitivity towards different levels of EGR can be partially attributed to the slightly higher intake charge temperatures. The use of recycled exhaust gas increased the intake manifold air temperature (IAT) by up to 4 K when operating with an EGR rate of 21.2%.

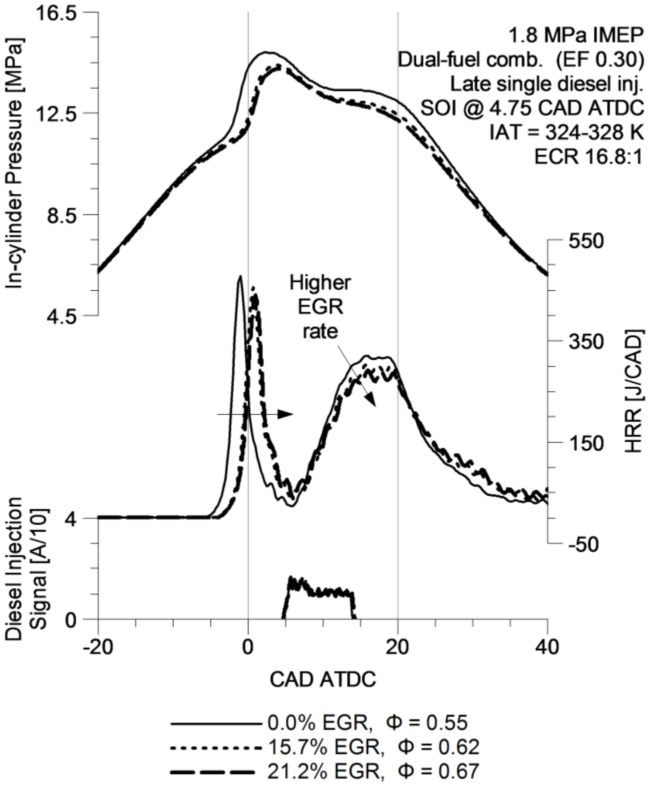

Figure 6.5 – The effect of EGR on high load dual-fuel operation with an ethanol energy fraction of 0.30.

6.2.5 The effect of global fuel/air equivalence ratio on high load dual-fuel operation

In this subsection, the effect of global fuel/air equivalence ratio (Φ) was characterised by varying the intake manifold pressure from 240 kPa to 290 kPa. External EGR was not used and the exhaust manifold pressure was adjusted so as to maintain a constant pressure differential across the cylinder of 10 kPa (with the exhaust being higher than the intake manifold pressure).

Figure 6.6 shows that the autoignition of ethanol was practically unaffected as the global fuel/air equivalence ratio was swept. This was attributed to the similar compression temperatures, which were sufficiently high to ignite the premixed charge despite the differences in compression pressure and Φ.

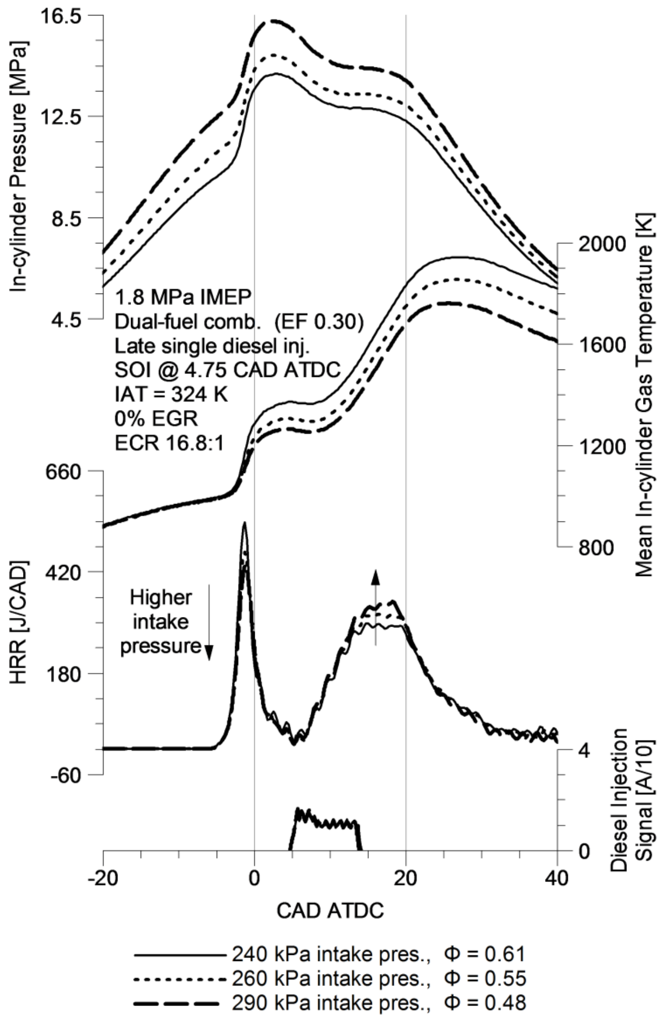

Figure 6.6 – The effect of global fuel/air equivalence ratio on high load dual-fuel operation with an ethanol energy fraction of 0.30.

The excess of air at highest intake manifold pressure of 290 kPa diluted the in-cylinder charge, decreased the first peak heat release, and reduced the mean in-cylinder gas temperature as the combustion progressed. However, the increased O_2 availability led to a faster oxidation of the diesel fuel, as supported by the higher second peak heat release. In comparison, the use of a lower intake manifold pressure of 240 kPa increased slightly the premixed peak heat release due the relatively higher in-cylinder gas temperatures during combustion at a Φ of 0.61.

6.2.6 The effect of Miller cycle on high load dual-fuel operation

The next approach aimed at retarding the autoignition timing was Miller cycle via an LIVC strategy. Figure 6.7 depicts the effect of different pressure-based ECRs on high load dual-fuel operation. The ethanol energy fraction was maintained at 0.30. The diesel injection timing was set at 4.75 CAD ATDC and the intake pressure was held constant at 260 kPa.

A reduction in ECR decreased the in-cylinder pressure as well as the mean in-cylinder gas temperature during the compression stroke. This successfully delayed the autoignition process of ethanol.

Figure 6.7 shows that the temperature prior to the SOC was reduced to less than 950 K at an ECR of 14.4:1. Despite the improvement and the later SOC, the premixed charge still autoignited just before the introduction of the diesel fuel. Engine experiments using ECRs lower than 14.4:1 were not performed due to low net indicated efficiencies at a constant intake manifold pressure.

6.2.7 The effect of intake manifold air temperature (IAT) on high load dual-fuel operation

This subsection investigates whether a colder intake manifold air is effective at delaying the ethanol autoignition process without EGR at an ECR of 16.8:1. The IAT was controlled using an air-to-water charge air cooler. The intake manifold pressure was held constant at 260 kPa. The ethanol energy fraction was set to 0.30 and the diesel injection timings were maintained at 4.75 CAD ATDC.

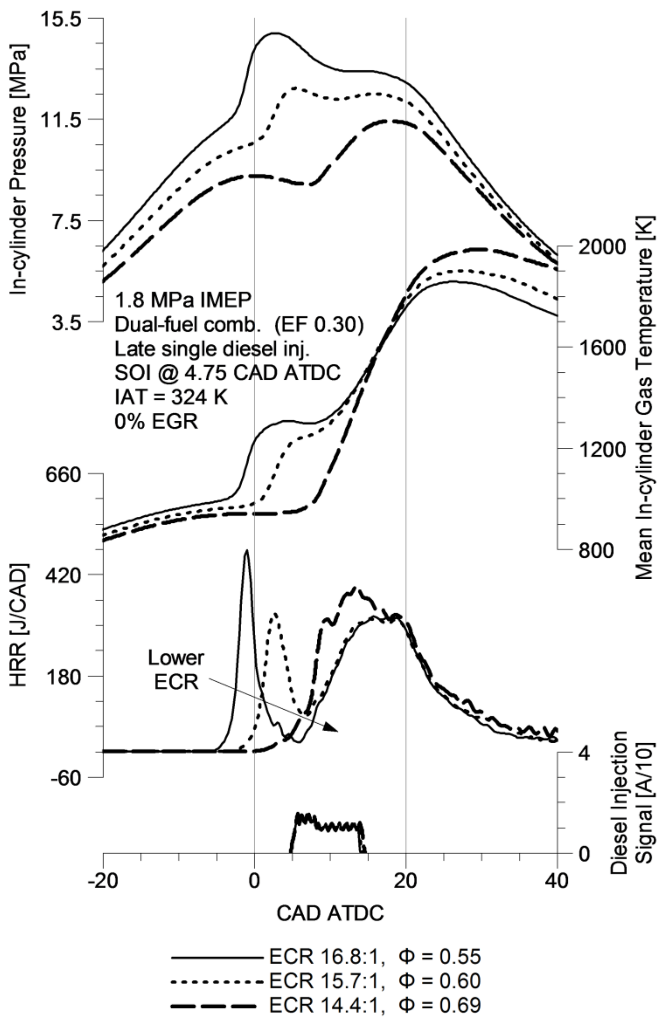

Figure 6.7 – The effect of Miller cycle on high load dual-fuel operation with an ethanol energy fraction of 0.30.

Figure 6.8 shows that a reduction in IAT from 324 K to 304 K decreased the mean in-cylinder gas temperature during the compression stroke and delayed the premixed fuel autoignition timing. The end-of-compression temperature and heat release process with a colder intake charge were comparable to the results attained with a higher IAT of 324 K at an ECR of 14.4:1. These similarities were attributed to the lower gas temperature and higher in-cylinder charge density at IVC for the case with an IAT of 304 K at an ECR of 16.8:1.

These findings highlight the sensitivity of high load dual-fuel operation to variations in IAT and in-cylinder gas temperature, as the ignition of the premixed fuel is mainly controlled by chemical kinetics [79].

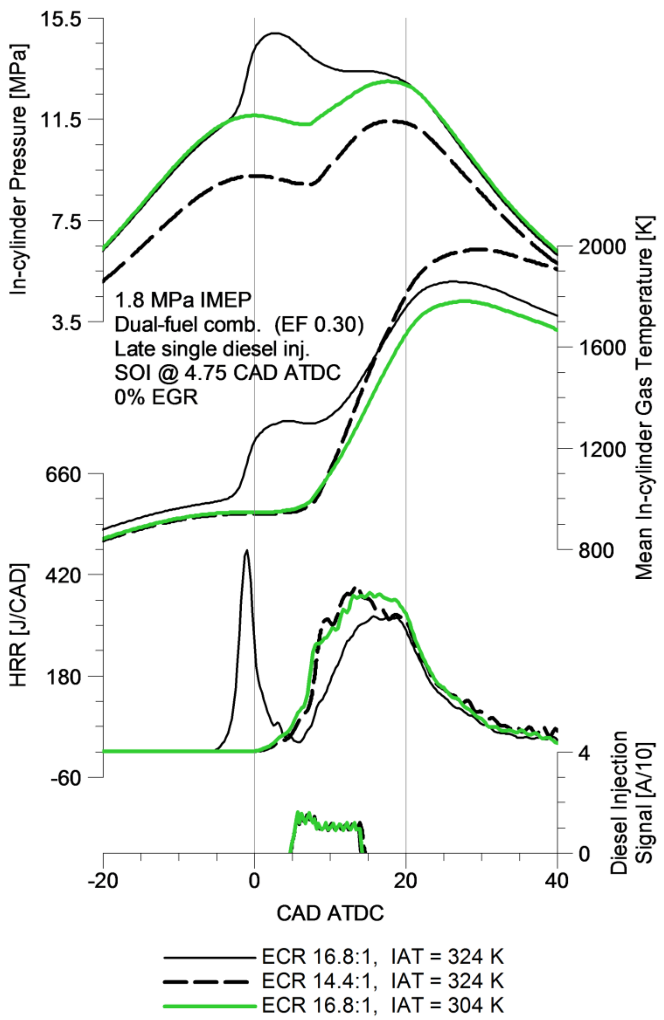

Figure 6.8 – The effect of intake air temperature on high load dual-fuel operation with an ethanol energy fraction of 0.30.

6.3 Exploring the high load potential of the dual-fuel operation with Miller cycle

The objectives of this subsection were to map the dual-fuel operation with Miller cycle at 1.8 MPa IMEP and optimise the dual-fuel combustion process for the maximum net indicated efficiency.

6.3.1 Experimental test procedure

The experiments were carried out without EGR while varying the ethanol energy fraction and diesel injection timings at different pressure-based ECRs of 16.8:1, 15.7:1, and 14.4:1. The most delayed CA50 was limited to 16 CAD ATDC due to relatively lower net indicated efficiencies.

Table 6.2 summarises the engine operating conditions. Diesel fuel was introduced using a late single injection. However, a pre-injection with an estimated volume of 3 mm^3 and a constant dwell time of 1 ms was employed to reduce the levels of pressure rise rate of some cases. PRR was limited to 2.0 MPa/CAD. P_{max} and COV_IMEP limits were set at 18 MPa and 3%, respectively.

Table 6.2 – Engine operating conditions for the mapping of the high load dual-fuel operation.

Parameter	Baseline
Speed	1200 rpm
Load	1.8 MPa IMEP
Diesel injection pressure	155 MPa
Diesel injection strategies	Late single and Pre- and main injection near TDC
$m_{ethanol/cycle}$	Varied between 0.00 and 225.8 mg/cycle
EF	Varied between 0.00 and 0.79
Intake air temperature	324 K
Intake pressure	260 kPa
Exhaust pressure	270 kPa
EGR rate	0%
Pressure-based ECRs	16.8:1, 15.7:1, and 14.4:1

6.3.2 Overview of the high load dual-fuel operating range with different ECRs

Figure 6.9 shows the ethanol-diesel dual-fuel operating range can be enlarged when using lower ECRs. At an ECR of 16.8:1, the maximum ethanol energy fraction was PRR limited to 0.26 and the most advanced CA50 was at 8 CAD ATDC. The reduction of the ECR to 15.7:1 allowed for higher ethanol fractions of 0.40. However, combustion phasing needed to be retarded because of the relatively longer ignition delay and faster premixed combustion phase. A single diesel injection strategy could only be used at the ECRs of 16.8:1 and 15.7:1 due to excessive PRRs at the ECR of 14.4:1.

The introduction of a pre-injection with an estimated volume of 3 mm^3 and a constant dwell time of 7.2 CAD to the main diesel injection shortened the ignition delay and effectively decreased the levels of PRR at the ECRs of 15.7:1 and 14.4:1. The combination of lower PRRs with lower compression temperatures at an ECR of 14.4:1 enabled the use of an ethanol energy fraction of 0.79.

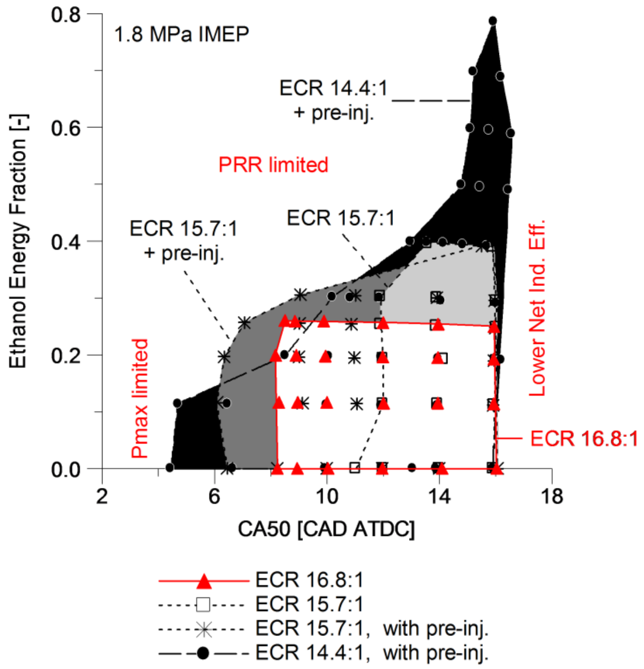

Figure 6.9 – High load operating range for ethanol-diesel dual-fuel combustion using different ECRs and ethanol energy fractions.

Therefore, the split diesel injection strategy was the key enabler for advancing the combustion process and allowing for more efficient dual-fuel operation at lower ECRs. The ratio of the volume of diesel pre-injection to the total volume of diesel injected per cycle varied from 2% to 9% due to changes in net indicated efficiency as well as ethanol energy fraction. Peak in-cylinder pressure was only a concern for the most advanced cases performed with low EFs.

6.3.3 Combustion characteristics

Figure 6.10 depict the diesel injection timings and combustion characteristics for the most efficient cases attained with varied EFs and diesel injection strategies at different ECRs. The optimum SOIs were delayed as the ethanol energy fraction was increased in order to control the levels of PRR within the limitation of 2.0 MPa/CAD.

The operation at the lowest ECR 14.4:1 was very sensitive to the start of injection. Slightly earlier diesel injection resulted in PRRs above the acceptable limit. This is the reason for the retarded SOI_2 and lower PRR when using ethanol energy fractions above 0.60.

The later combustion process at high EFs combined with a lower ECR of 14.4:1 can reduce the peak in-cylinder pressure, as shown in Figure 6.11. The heat release profile changed from typical mixing-controlled combustion in CDC to a shorter combustion process with higher peak heat release in the dual-fuel mode.

Figure 6.10 also revealed that higher amounts of premixed ethanol fuel increased the COV_IMEP. This was likely as a result of the autoignition process of ethanol, which seemed more sensitive to variations in the in-cylinder gas temperature than a diesel mixing-controlled combustion. The cycle-to-cycle variability was lower at the highest ECR of 16.8:1 due to the relatively higher compression temperatures and more stable ignition of ethanol and diesel fuels.

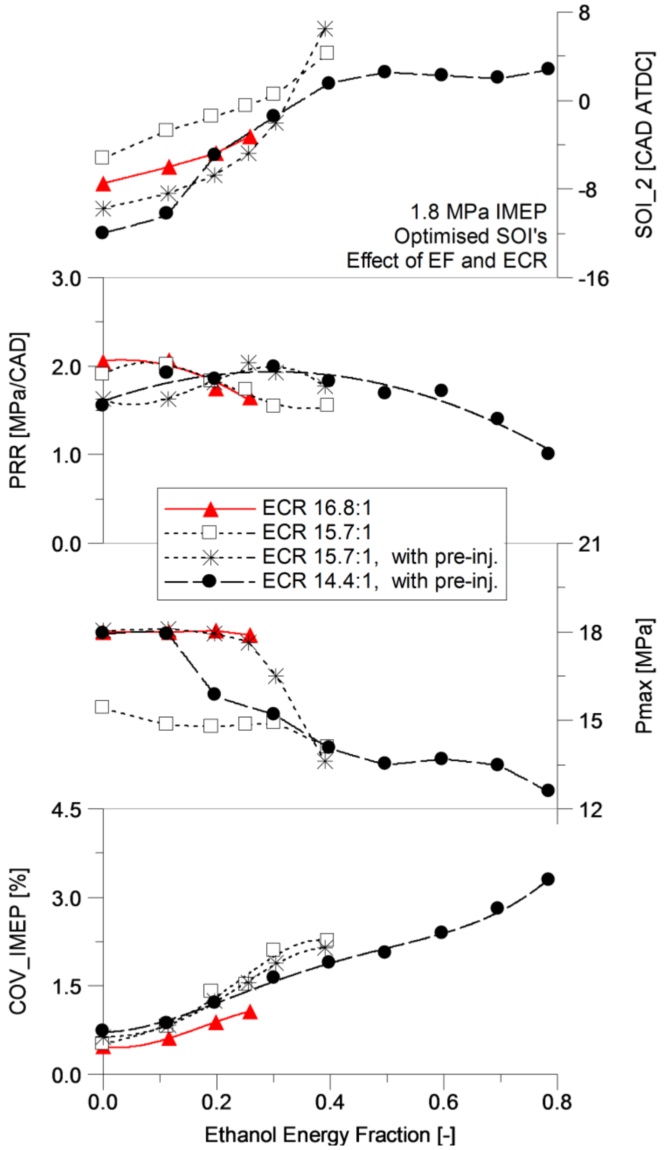

Figure 6.10 – Main diesel injection timings and combustion characteristics for optimised high load dual-fuel operation with different ECRs.

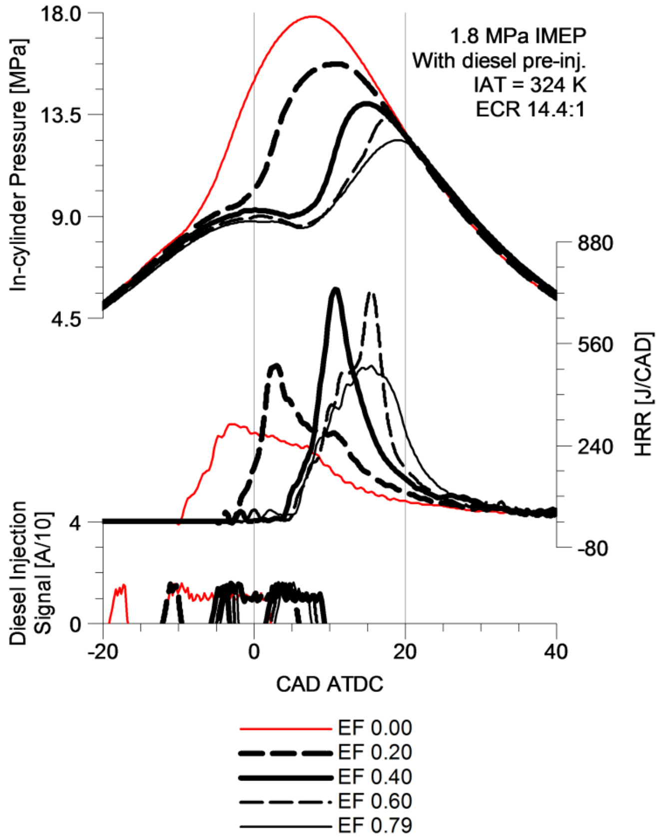

Figure 6.11 – Optimised high load dual-fuel operation with diesel pre-injection at an ECR of 14.4:1.

In dual-fuel mode, the period of time between the SOI_2 and SOC remained below the interval measured for the diesel-only cases, as shown in Figure 6.12. In addition, the ignition delay was shortened as the EF was increased towards 0.40, independent of the ECR. This was mainly a result of the early autoignition of ethanol when using a single diesel injection at the ECRs of 16.8:1 and 15.7:1. The introduction of a diesel pre-injection at the ECRs of 15.7:1 and 14.4:1 modified the trends slightly depending on the ethanol energy fraction. At an ECR of 14.4:1, the use of high EFs (e.g. above 0.40) yielded relatively longer ignition delays due to the low reactivity of the ethanol fuel.

The first part of the heat release process between CA10 and CA50 was affected by the ECR, ethanol energy fraction, and diesel injection strategy. The most noticeable change was observed at an ECR of 14.4:1, where the CA10-CA50 period became shorter as the EF was raised to 0.40. This was probably caused by rapid simultaneous combustion of diesel and ethanol fuels. However, there was a reversal of the trend as the ethanol energy fraction was increased to 0.79 due to charge cooling and slower reaction rates of the premixed fuel [3].

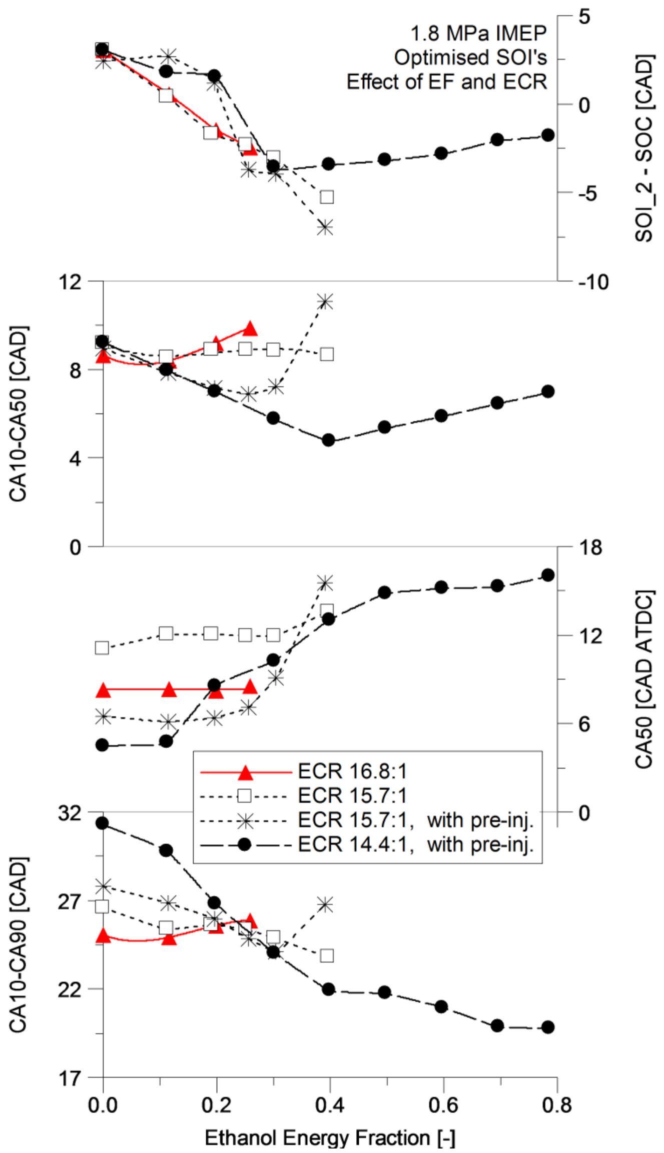

Figure 6.12 – Heat release characteristics for optimised high load dual-fuel operation with different ECRs.

Combustion phasing was retarded with the increase of ethanol energy fraction despite the partial recovery of the CA10-CA50 period at an ECR of 14.4:1. This was necessary to control the levels of PRR caused by the more homogenous combustion process in the dual-fuel mode, which is supported by shorter combustion duration (CA10-CA90) and higher peak heat release.

There were exceptions when more ethanol was used at an ECR of 16.8:1 and for the dual-fuel case with a diesel pre-injection and an EF of 0.39 at an ECR of 15.7:1. In the first condition, the early ignition of ethanol resulted in a practically constant CA50 position and slightly longer CA10-CA90 period. In the second case, the increase in combustion duration was due to the late diesel injection timings used to prevent the simultaneous combustion of the pre-injected diesel and premixed ethanol fuel.

6.3.4 Engine-out emissions and performance

Figure 6.13 depicts the net indicated specific emissions for the most efficient cases. The dual-fuel operation with a pre-injection of diesel and an ethanol energy fraction of 0.79 achieved 7.4 g/kWh of NOx at an ECR of 14.4:1. This is equivalent to an ISNOx reduction of 57% when compared against the 17.3 g/kWh produced by the diesel-only operation at an ECR of 16.8:1. This improvement was likely a result of the later CA50 position and more homogeneous combustion (e.g. lower local temperatures), as less diesel fuel was burnt during the mixing-controlled combustion phase. The use of a single diesel injection strategy delayed the optimum CA50s at an ECR of 15.7:1, attaining similar levels of NOx emissions to those measured with EFs between 0.20 and 0.40 at an ECR of 14.4:1.

Later diesel injection timings and thus delayed combustion process increased the soot emissions as the ethanol energy fraction was increased. Lower in-cylinder gas temperatures and shorter ignition delays at such conditions are probably linked to the elevation in the levels of smoke [198]. The highest ISsoot was 0.0024 g/kWh for an ethanol energy fraction of 0.79 at an ECR of 14.4:1, which is well below the Euro VI emission limit for particulate matter of 0.010 g/kWh [26].

The unburnt HC and CO emissions increased as more ethanol was injected, reaching ~3.6 g/kWh at an ethanol energy fraction of 0.79. This phenomenon likely occurs due to premixed fuel trapped in the crevice volumes of the stock diesel piston, as shown in the computational fluid dynamics modelling performed by Kokjohn et al. [57].

The use of Miller cycle via an LIVC strategy reduced the compression pressures, which possibly minimised the amount of ethanol fuel pushed into these crevice volumes Additionally, the adoption of a lower ECR at a constant intake manifold pressure increased the global fuel/air equivalence ratio and the mean in-cylinder gas temperature during combustion (see Figure 6.7). This allowed for higher combustion efficiencies than those achieved with the baseline ECR of 16.8:1, as shown in Figure 6.14.

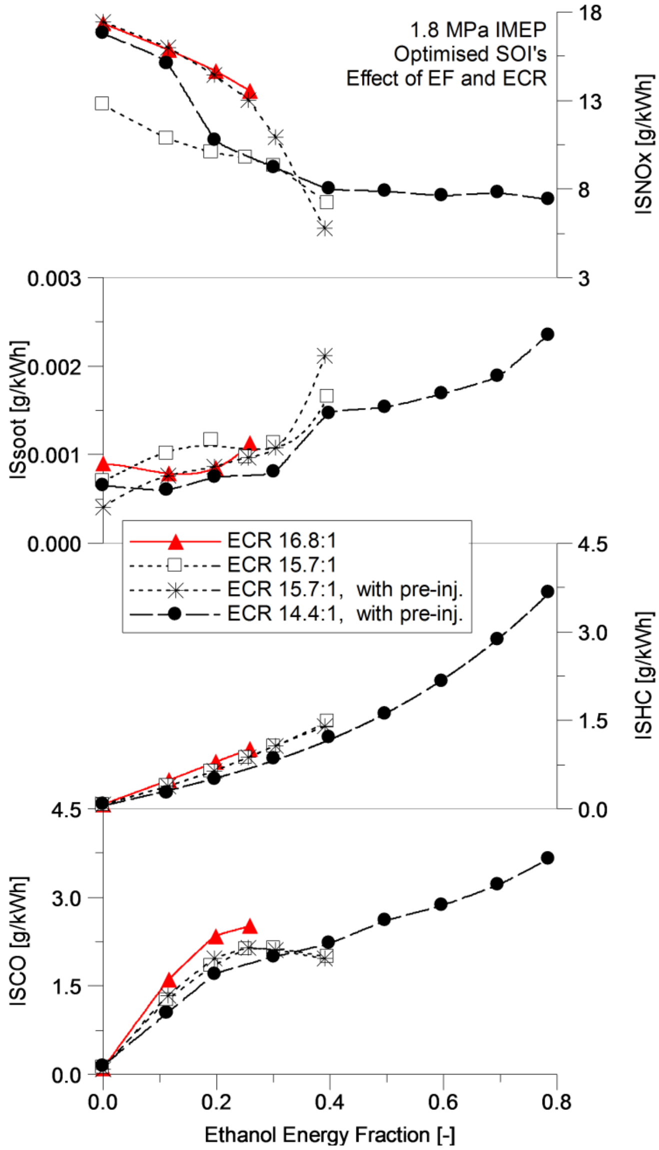

Figure 6.13 – Net indicated specific emissions for optimised high load dual-fuel operation with different ECRs.

The highest net indicated efficiency of 47.5% was attained by a dual-fuel operation with an EF of 0.25 at the baseline ECR of 16.8:1. This was likely a result of lower heat transfer losses [57], which increased net indicated efficiency by 2.9% when compared to the 46.1% achieved during the diesel-only operation at the same ECR of 16.8:1 (see red circle in Figure 6.14). However, a reduction in the ECR at a constant intake manifold pressure slightly decreased the net indicated efficiency for a given ethanol energy fraction. This was a result of the lower in-cylinder mass trapped and formation of a relatively richer mixture, which reduced the ratio of specific heats and probably increased the heat transfer and exhaust losses [97].

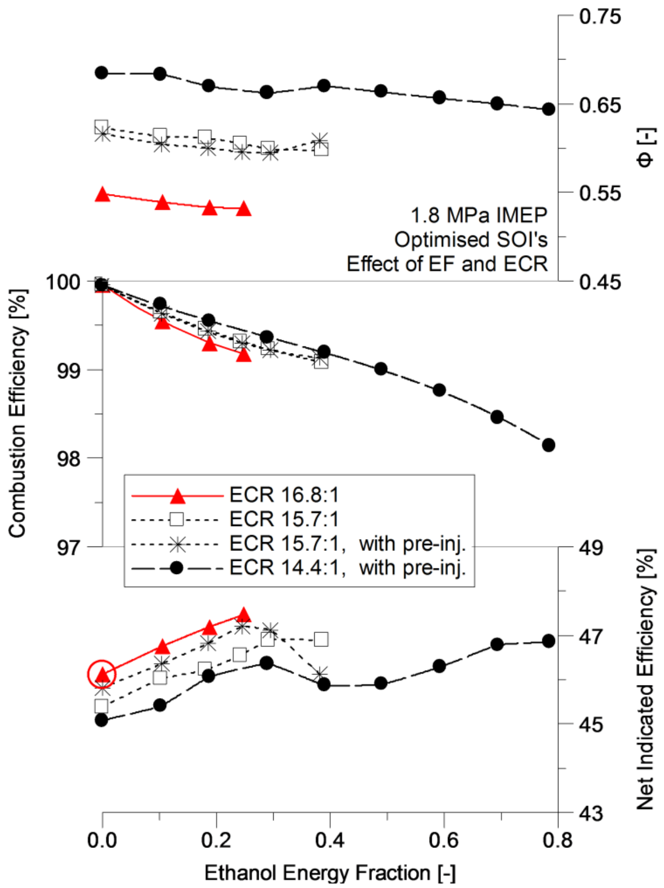

Figure 6.14 – Performance for optimised high load dual-fuel operation with different ECRs.

Despite the losses observed with Miller cycle, the use of an EF of 0.79 yielded a net indicated efficiency of 46.85% at an ECR of 14.4, which was 1.6% higher than that of the most efficient diesel-only operation at the baseline ECR of 16.8. This improvement was possibly attributed to a reduction in heat transfer/exhaust losses via shorter burn rate and lower local in-cylinder gas temperatures [57].

6.3.5 Improvements brought about by the high load dual-fuel operation with Miller cycle

This subsection includes a comparison of high load dual-fuel operation at an ECR of 14.4:1 and conventional diesel combustion at the baseline ECR of 16.8:1 with respect to net indicated efficiency and NOx emissions, as these factors can adversely affect the engine operational cost [3]. This helped determine the potential benefits brought about by the use of Miller cycle on a HD engine.

The variation in net indicated efficiency and NOx emissions were calculated as

$$Variation\ in\ Net\ Indicated\ Eff.\,[\%] = \left(\frac{Net\ Indicated\ Efficiency}{Net\ Indicated\ Efficiency_{baseline}} - 1\right) \times 100 \tag{6.1}$$

$$Variation\ in\ NOx\ emissions\ [\%] = \left(\frac{ISNOx}{ISNOx_{baseline}} - 1\right) \times 100 \tag{6.2}$$

where $Net\ Indicated\ Efficiency_{baseline}$ and $ISNOx_{baseline}$ are the net indicated efficiency and specific emissions of NOx of the most efficient CDC case at an ECR of 16.8:1. Negative values represent a decrease in net indicated efficiency or NOx emissions when utilising dual-fuel operation with Miller cycle over the diesel-only combustion at the baseline ECR.

Figure 6.15 and Figure 6.16 depict the variation in net indicated efficiency and NOx emissions when operating the engine with different EFs and CA50 positions. Combustion phasing was adjusted by performing sweeps of diesel injection timings with a constant dwell time between pre- and main diesel injections of 7.2 CAD.

The analysis revealed that high load dual-fuel operation at an ECR of 14.4 can achieve higher net indicated efficiencies and lower NOx emissions than CDC at an ECR of 16.8:1. The alternative combustion strategy increased the net indicated efficiency by up to 1.6% and decreased the levels of ISNOx by up to 60%. This is a significant improvement over a retarded diesel-only combustion at an ECR of 14.4:1, which reduced the NOx emissions by 50% at the expense of 5.5% lower net indicated efficiency.

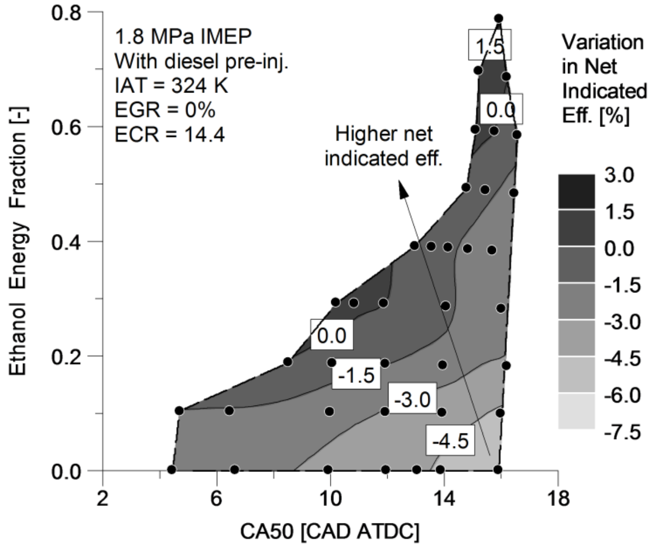

Figure 6.15 – Variation in net indicated efficiency of high load dual-fuel operation at an ECR of 14.4 over the most efficient CDC case at the baseline ECR of 16.8.

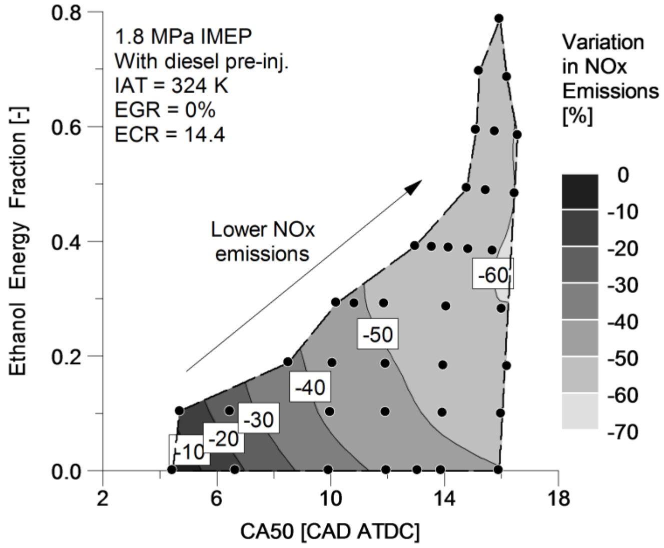

Figure 6.16 – Variation in NOx emissions of high load dual-fuel operation at an ECR of 14.4 over the most efficient CDC case at the baseline ECR of 16.8.

Figure 6.17 combines the two maps above to show the trade-off between the variation in net indicated efficiency and NOx emissions as the ethanol energy fraction and CA50 position were varied. The plot highlights the effectiveness of the dual-fuel operation with Miller cycle as a way to control engine-out NOx emissions and increase net indicated efficiency, particularly at high EFs. The reasoning behind the best overall performance and emissions was discussed in Subsection 6.3.4.

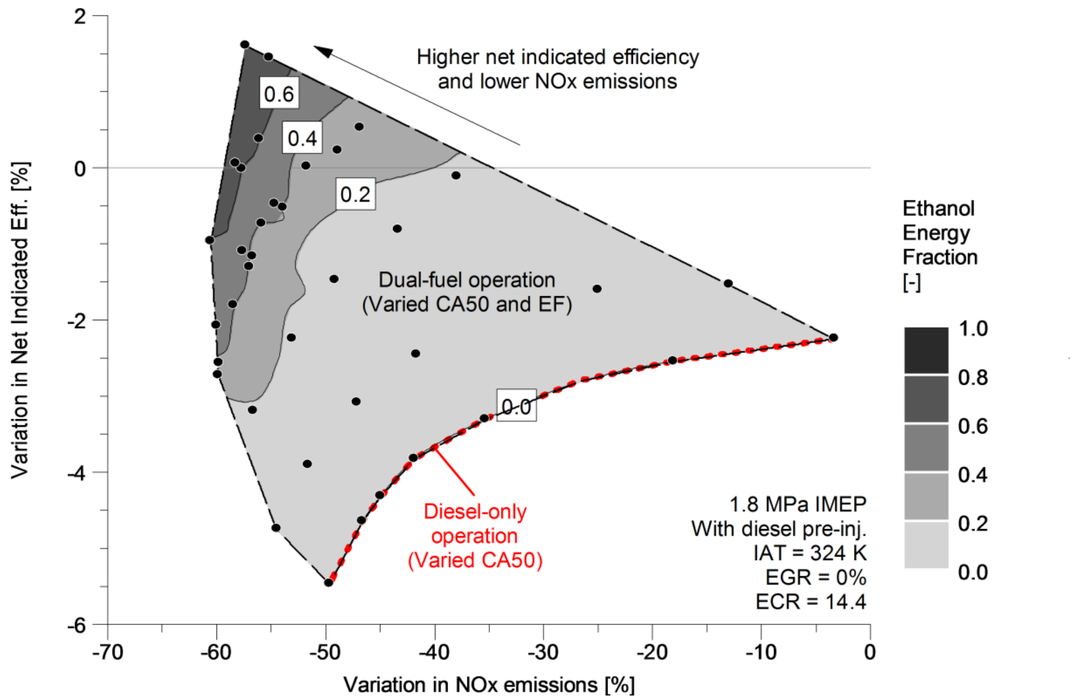

Figure 6.17 – Trade-off between the variation in net indicated efficiency and NOx emissions for high load dual-fuel operation with Miller cycle.

6.4 Exploring the high load potential of the dual-fuel operation with charge air cooling

A one-off test was carried out to determine whether charge air cooling has the potential to enable the use of a high EF of 0.65 at the baseline ECR of 16.8:1 while achieving the efficiency and emissions benefits of a dual-fuel operation with Miller cycle.

The investigation was performed with an increased water flow rate into the charge air cooler in order to reduce the intake manifold air temperature by 20 K to 304 K. The diesel injection timings were optimised for the maximum net indicated efficiency. A pre-injection of diesel was used to maintain the PRR within the limit of 2.0 MPa/CAD, as described in previous subsections. The intake pressure was held constant at 260 kPa and no cooled external EGR was used.

Figure 6.18 depicts a comparison between optimised dual-fuel operations with charge air cooling (EF of 0.65) and Miller cycle (EFs of 0.60 and 0.70). The earlier IVC/higher ECR and lower IAT of the dual-fuel case with charge air cooling resulted in a relatively longer compression process (e.g. higher ECR) and higher in-cylinder mass trapped, as supported by the lower global fuel/air equivalence ratio. This diluted mixture decreased the mean in-cylinder gas temperature during combustion despite the higher peak heat release when compared against the dual-fuel cases with Miller cycle (ECR of 14.4:1). Similar trend occurred with the decreasing of the global fuel/air equivalence ratio via higher intake manifold pressure in Subsection 6.2.5.

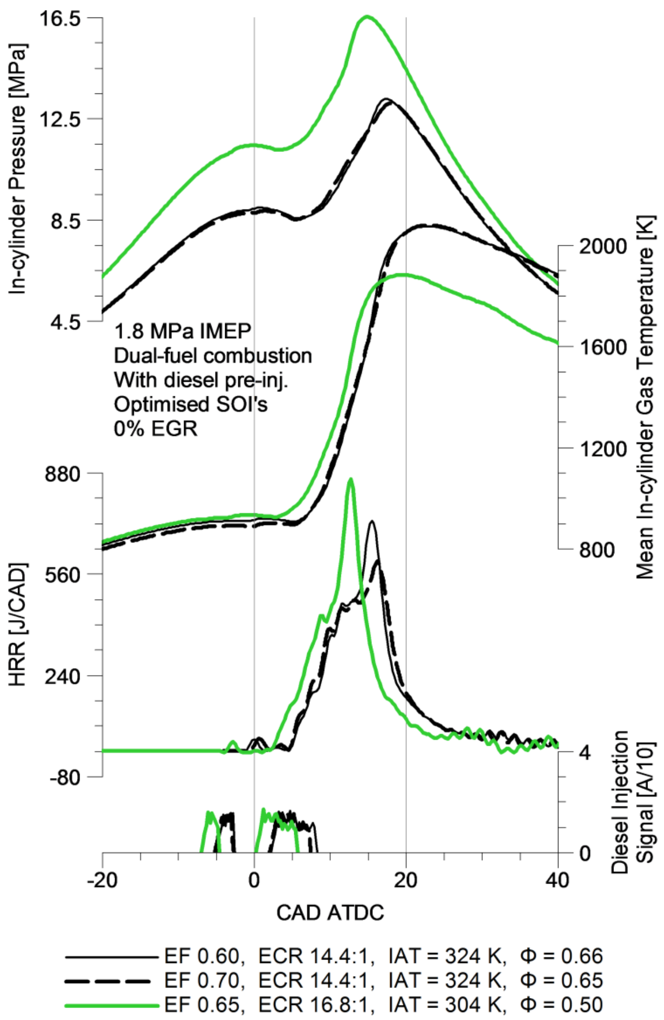

Figure 6.18 – Comparison between optimised high load dual-fuel operations with Miller cycle and charge air cooling.

The leaner dual-fuel combustion with an IAT of 304 K and an ECR of 16.8:1 allowed for more advanced burn rate and higher peak heat release. As a result, net indicated efficiency was increased from 46.3% and 46.8% in the dual-fuel cases with Miller cycle to 48% in the dual-fuel case with charge air cooling. Additionally, high load dual-fuel operation with an IAT of 304 K increased the net indicated efficiency by 4.1% over the most efficient conventional diesel combustion case (46.1%) at an ECR of 16.8:1. This improvement was probably attributed to lower heat transfer losses of the dual-fuel combustion.

ISsoot (0.003 g/kWh), ISCO (4.9 g/kWh), and ISHC (6.7 g/kWh) were increased in the dual-fuel operation with charge air cooling as a result of higher in-cylinder mass trapped (e.g. air dilution) and lower mean in-cylinder gas temperature. NOx emissions were also increased from 7.6 and 7.8 g/kWh in the Miller cycle cases to 9.7 g/kWh in the dual-fuel case with a lower IAT. This was attributed to the more advanced HRR (e.g. higher combustion/local temperatures) and lower global fuel/air equivalence ratio (e.g. higher O_2 availability). Nevertheless, optimised dual-fuel operation with charge air cooling effectively reduced the levels of NOx by 44% when compared against the 17.3 g/kWh of the diesel-only baseline.

Despite the relatively high net indicated efficiency and low NOx emissions brought about by the dual-fuel operation with charge air cooling, a further analysis was not performed as low IATs might not be achievable from a practical standpoint. Finally, it is important to bear in mind that high load dual-fuel operation with IATs higher than 324 K can potentially cause unacceptable combustion noise (e.g. knock) and low engine efficiency.

6.5 Assessment of the full load dual-fuel operation with wet ethanol injection and Miller cycle

This section characterised the ethanol-diesel dual-fuel combustion at full engine load. The study investigated the potential of wet ethanol injection to enable high efficiency and clean dual-fuel operation at full engine load, as the presence of water introduces helpful thermal and dilution effects. Exhaust emissions and net indicated efficiency were compared to those of a CDC baseline. The dual-fuel combustion characteristics were presented and discussed for anhydrous ethanol as well as wet ethanol containing up to 50% of distilled water in a volume basis. Three different ECRs achieved via LIVC events were explored during the analysis.

6.5.1 Experimental test procedure

Table 6.3 summarises the baseline engine operating conditions and highlights the parameters that were optimised. The $m_{ethanol/cycle}$ represents the actual mass of anhydrous ethanol injected per cycle. The $\dot{m}_{ethanol}$ represents the actual anhydrous ethanol mass flow rate and was calculated by subtracting the water mass flow rate from the total wet ethanol flow rate measured with a Coriolis flow meter. This methodology is slightly different from that used in the previous sections, where the ethanol mass flow rate was obtained from an injector calibration curve. The resulting ethanol energy fraction (EF) was calculated using the $LHV_{ethanol}$.

Table 6.3 – Engine operating conditions for full load dual-fuel operation.

Parameter	Baseline	Optimisation
Speed	1200 rpm	
Load	2.4 MPa IMEP	
Diesel injection pressure	180 MPa	
Diesel injection strategy	Late single injection	
$m_{ethanol/cycle}$	0.00 mg/cycle	Varied up to 102.4 mg/cycle
EF	0.00	Varied up to 0.26
Intake air temperature	318 K	
Intake pressure	300 kPa	
Exhaust pressure	290 kPa	
EGR rate	0%	
Pressure-based ECRs	16.8:1	15.7:1 and 14.4:1

Diesel fuel was introduced using a single injection that varied between -10 and 5 CAD ATDC. In some cases, a Miller cycle strategy via LIVC events was used to delay the initiation of the compression process and reduce the ECR from 16.8:1 to 15.7:1 and 14.4:1.

EGR was not employed in this study because the intake manifold and recycled exhaust gas temperatures could not be controlled with the current gas-to-water charge coolers setup. Stable engine operation was quantified by a COV_IMEP below 3%. A maximum PRR of 3.0 MPa/CAD was considered as the upper bound for calibration. Moreover, the maximum in-cylinder gas pressure (P_{max}) was limited to 18 MPa.

6.5.2 Fuel properties

The experiments were performed using anhydrous ethanol (E100) and wet ethanol containing 20%, 35%, and 50% of distilled water in a volume basis. These ethanol-water mixtures were named E80W20, E65W35, and E50W50, respectively. The water mass and volume fractions in the wet ethanol were determined using the fuel density measured by the flow meter and an alcoholometry table [167]. An alcoholmeter was used to confirm the water content. Fuel properties are shown in Table 6.4.

Table 6.4 – Fuel properties.

Property	Unit	Diesel	E100	E80W20	E65W35	E50W50
Density at 293 K	kg/m^3	827	790	859	898	930
Water Vol. Content	(v/v)	~0%	~0%	20%	35%	50%
Water Mass Content	(m/m)	~0%	~0%	26.5%	42.8%	57.6%
Heat of Vaporisation	kJ/kg	270	840	1216	1448	1658
$c_{p,v}$ (*)	kJ/kg.K	-	1.68	1.77	1.83	1.88

(*) Vapour specific heat capacity at 373 K [199].

6.5.3 The effect of Miller cycle and start of injection on emission and net indicated efficiency of full load CDC operation

Diesel-only combustion is characterised by an exhaust emissions/net indicated efficiency trade-off where lower NOx emissions are usually attained at the expense of higher smoke and reduced net indicated efficiency. Figure 6.19 depicts the ISsoot and ISNOx as well as the variation in net indicated efficiency for full load CDC operation with varied SOIs and ECRs. The $Net\ indicated\ efficiency_{baseline}$ was equivalent to 45.1% for the case with the most advanced SOI at an ECR of 16.8:1.

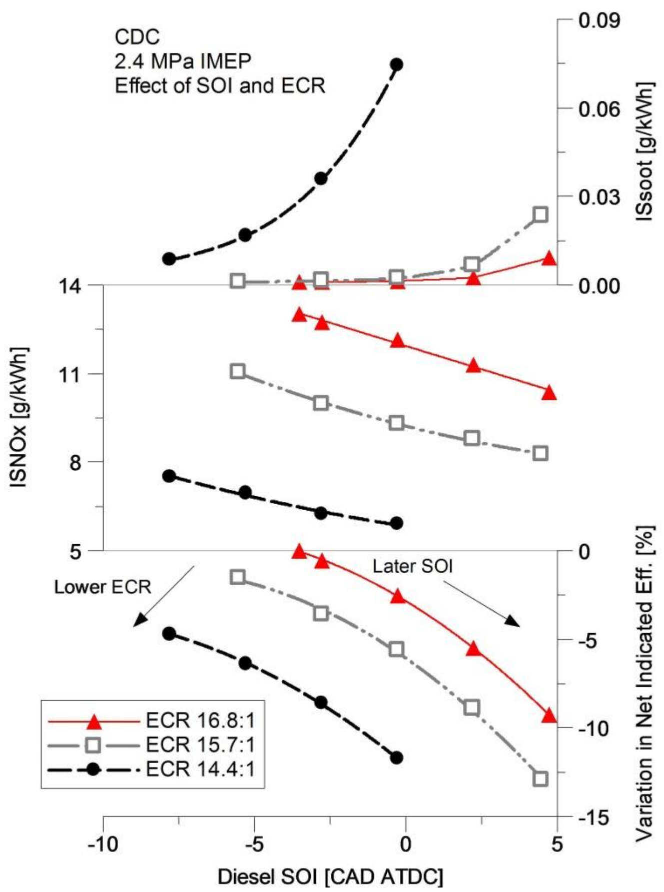

Figure 6.19 – ISsoot, ISNOx, and variation in net indicated efficiency for full load CDC operation with different SOIs and ECRs.

Later diesel injection timings and lower ECRs of 15.7:1 and 14.4:1 reduced NOx and increased soot emissions. At these conditions, the resulting ISsoot levels exceeded the Euro VI limit of 0.010 g/kWh [26]. This was possibly attributed to the lower combustion temperatures and oxygen availability [198]. At an ECR of 16.8:1, a delay of 8.25 CAD in the SOI reduced the net indicated efficiency by 9.3% for 20% lower NOx emissions. Alternatively, the most efficient case at an ECR of 14.4:1 decreased the net indicated efficiency in 4.7% for 42% reduction in ISNOx. This demonstrates the potential of Miller cycle to minimise NOx emissions with relatively lower fuel consumption than a retarded combustion process. However, the NOx emissions for the CDC operation remained considerably higher than the Euro VI emission target of 0.4 g/kWh [26]. This gives the opportunity of applying alternative combustion strategies such as the dual-fuel operation.

6.5.4 The effect of anhydrous ethanol injection on full load dual-fuel operation

Experiments were performed to explore the effect of anhydrous ethanol injection on combustion. The investigation was carried out using the baseline engine operating conditions showed in Table 6.3 except for the use of different EFs. The diesel injection timing was held at 4.75 CAD ATDC. Figure 6.20 shows that the anhydrous ethanol fuel autoignited prior to the diesel SOI. This was a result of the high in-cylinder gas temperatures and pressures at this particular load. Increased EF led to higher first peak heat release and shorter diesel mixing-controlled combustion, which elevated both the P_{max} and the levels of PRR. At the baseline ECR of 16.8:1, the dual-fuel operation with a constant diesel SOI was limited to an ethanol energy fraction of 0.19 and a PRR of 1.9 MPa/CAD. The pressure traces for the dual-fuel combustion with higher EFs were not recorded due to excessive PRRs.

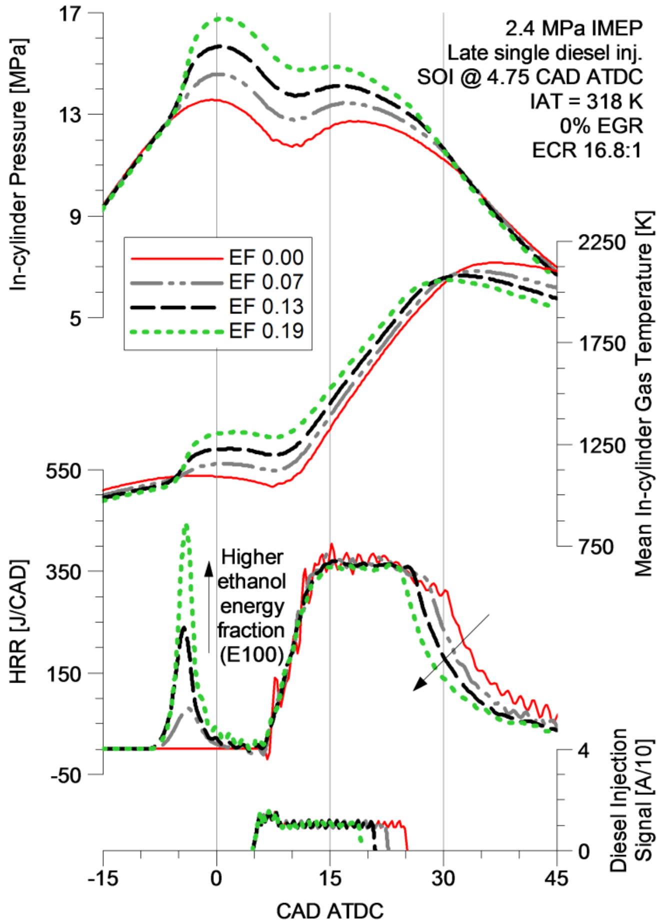

Figure 6.20 – The effect of ethanol energy fraction on anhydrous ethanol-diesel dual-fuel operation at an ECR of 16.8:1.

6.5.5 The effect of Miller cycle on full load dual-fuel operation

The subsequent dual-fuel combustion experiments were performed to explore the effect of Miller cycle via LIVC events. The baseline IVC timing was delayed by applying the same LIVC events used for the CDC operation in Subsection 6.5.3, resulting in ECRs of 15.7:1 and 14.4:1. Figure 6.21 reveals that the use of a lower ECR effectively retarded the autoignition of the ethanol fuel and slowed down the reaction rates when operating with an EF of ~0.19. This was primary a result of the lower mean in-cylinder gas temperatures attained during the compression stroke. However, the diesel injection duration became longer for the cases with lower ECRs, indicating a decrease in net indicated efficiency. This was likely caused by the richer dual-fuel combustion and higher heat transfer losses [97] obtained with a Miller cycle strategy at a constant boost pressure. The Φ was increased from 0.67 to 0.87 when reducing the ECR from 16.8:1 to 14.4:1 and holding the diesel SOI at 4.75 CAD ATDC.

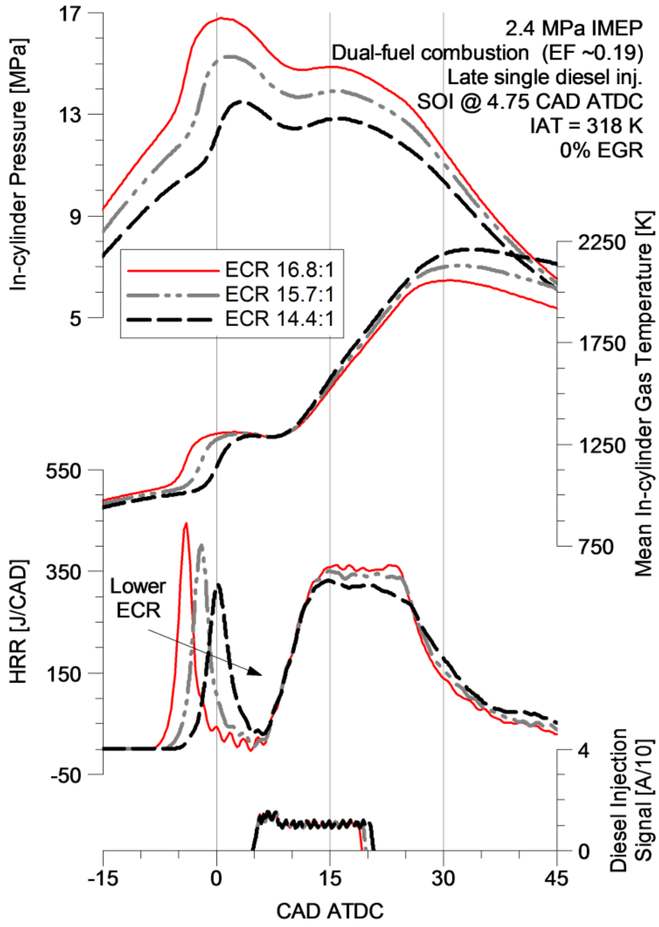

Figure 6.21 – The effect of Miller cycle on full load dual-fuel operation with an ethanol energy fraction of ~0.19.

6.5.6 The effect of anhydrous ethanol injection and Miller cycle on emission and net indicated efficiency of full load dual-fuel operation

The diesel SOI and the EF were swept to determine the actual potential of full load dual-fuel operation with anhydrous ethanol injection and lower ECRs to decrease NOx emissions and increase net indicated efficiency. The optimum SOIs were limited by the P_{max} of 18 MPa and PRRs of 3.0 MPa/CAD, as shown in Figure 6.22. Despite the lower compression pressures and temperatures achieved with a Miller cycle strategy, the maximum EF remained approximately 0.20.

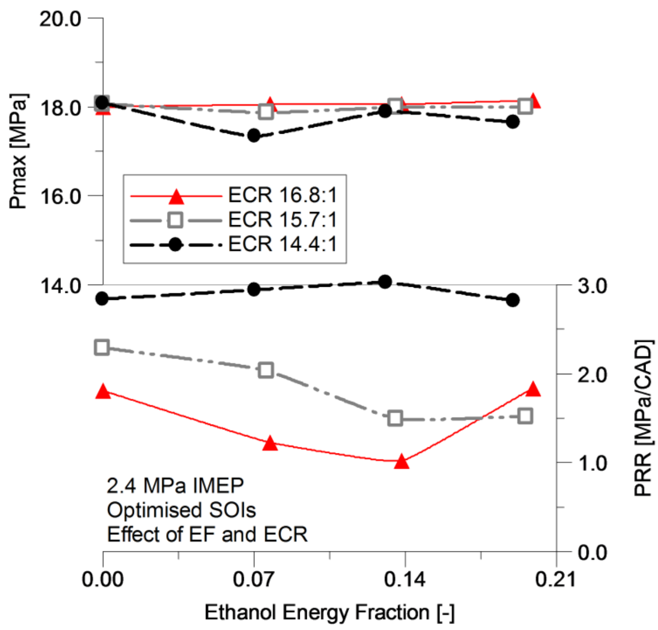

Figure 6.22 – Maximum in-cylinder pressure and pressure rise rate for anhydrous ethanol-diesel dual-fuel operation with different EFs and ECRs.

Figure 6.23 depicts the ISsoot, ISNOx, and variation in net indicated efficiency for full load dual-fuel operation with different EFs and ECRs. The plot shows that NOx emissions can be reduced and net indicated efficiency increased at higher ethanol energy fractions. The reduction in ISNOx achieved 12% at the ECR of 16.8:1, decreasing from 13.0 g/kWh in the CDC baseline to 11.4 g/kWh in the dual-fuel operating mode. This improvement was attained with an increase in net indicated efficiency of 1.8%.

The use of a lower ECR in the dual-fuel operation further decreased the levels of ISNOx. Dual-fuel combustion combined with Miller cycle allowed for up to 39% NOx reduction with a small decrease in net indicated efficiency of 0.4% compared to the CDC baseline. Soot emissions were consistently low at the ECRs of 16.8:1 and 15.7:1. The reduced combustion temperatures and lower oxygen availability increased the smoke numbers at an ECR of 14.4:1. Nevertheless, the use of a higher EF of ~0.20 helped maintain the ISsoot below 0.002 g/kWh, which is significantly lower than the measurements for the CDC operation with Miller cycle.

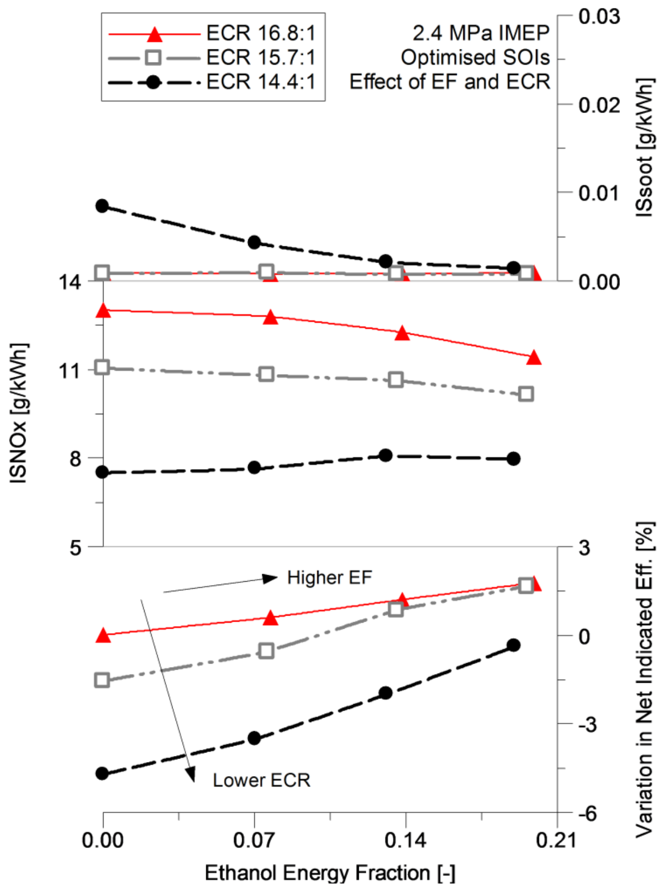

Figure 6.23 – ISsoot, ISNOx, and variation in net indicated efficiency for anhydrous ethanol-diesel dual-fuel operation with different EFs and ECRs.

6.5.7 The effect of wet ethanol injection on full load dual-fuel operation

The last parameter explored in this study was the water-in-ethanol content. This investigation was carried out at the baseline ECR of 16.8:1. Figure 6.24 shows the effect of wet ethanol injection on the dual-fuel combustion process with an ethanol energy fraction of ~0.19. The diesel SOI was set at 4.75 CAD ATDC.

The results revealed that wet ethanol with higher water content were effective in decreasing the compression temperatures, retarding the SOC, and slowing down the ethanol compression ignition combustion. The later and slower reaction rates reduced the first peak heat release. The trend was similar to that observed when decreasing the ECR in Figure 6.21. The diesel mixing-controlled combustion was practically unaffected as the water-in-ethanol content was increased. However, the use of E65W35 and E50W50 somewhat impaired the combustion process between 35 and 45 CAD ATDC. This was probably caused by lower end-of-combustion temperatures.

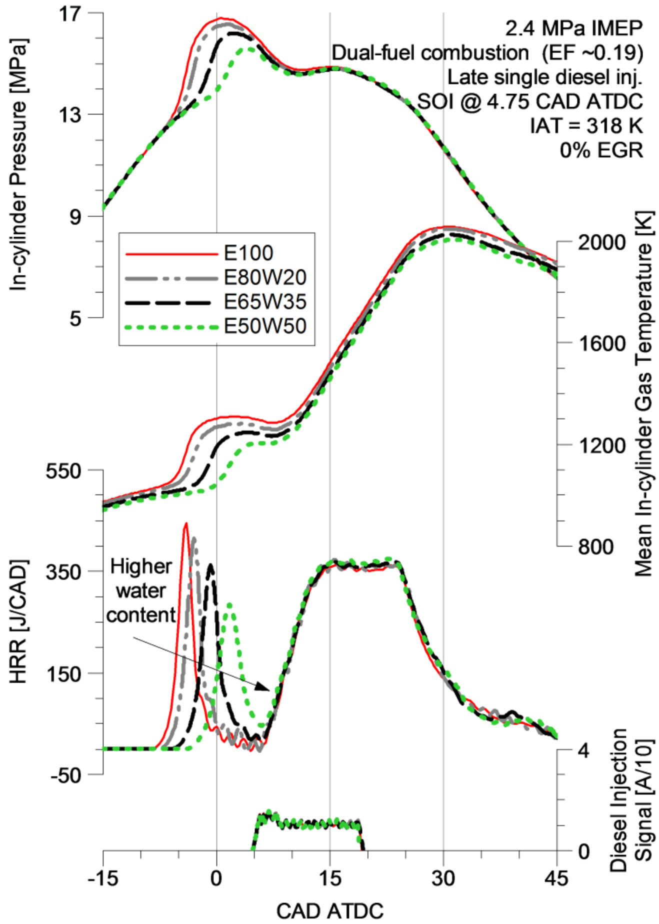

Figure 6.24 – The effect of water-in-ethanol content on full load dual-fuel operation with an ethanol energy fraction of ~0.19.

To demonstrate the thermal and dilution effects of water, a sweep of ethanol energy fraction with E50W50 is depicted in Figure 6.25. The E50W50-diesel dual-fuel operation led to different combustion behaviour than that attained with anhydrous ethanol injection in Figure 6.20. The autoignition timing and the position of first peak heat release were delayed as more E50W50 was injected. These findings can be attributed to the charge cooling and heat capacity effects as well as the intake air oxygen displacement introduced by a higher concentration of water.

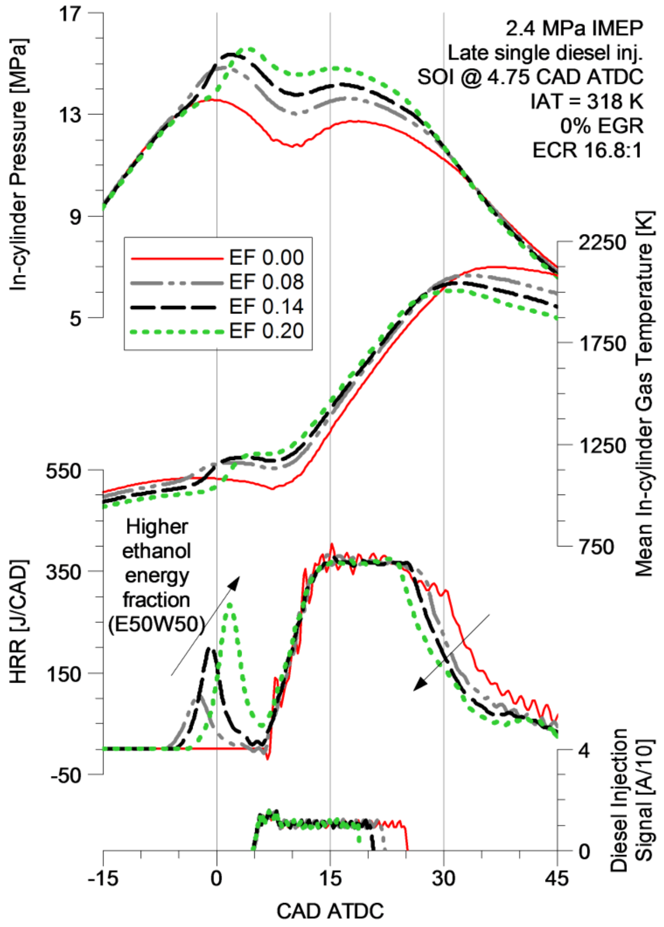

Figure 6.25 – The effect of ethanol energy fraction on full load E50W50-diesel dual-fuel operation at an ECR of 16.8:1.

6.5.8 The effect of anhydrous and wet ethanol injection on emission and net indicated efficiency of full load dual-fuel operation

To explore the potential of wet ethanol injection to curb NOx and increase net indicated efficiency, the diesel SOIs and the EFs were optimised up against the Pmax and/or PRR limit. Although the water-in-ethanol content introduced thermal and dilution effects, Figure 6.26 shows that the maximum ethanol energy fraction with E50W50 could not be increased by a large extent and was limited to 0.26. This was attributed to excessive PRRs produced by a simultaneous combustion of ethanol and diesel at higher ethanol energy fractions.

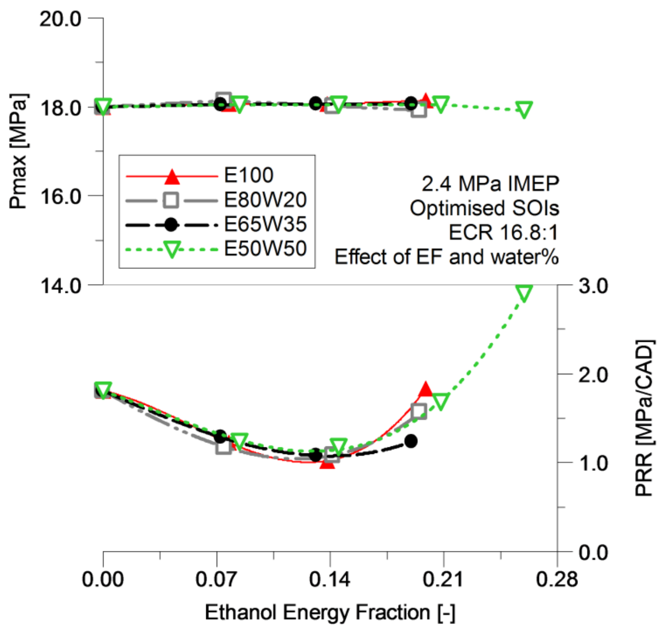

Figure 6.26 – Maximum in-cylinder pressure and pressure rise rate for full load dual-fuel operation with anhydrous and wet ethanol injection.

Figure 6.27 reveals how wet ethanol injection affected the exhaust gas temperature (EGT) and exhaust emissions. Increased water percentages helped reduce EGT and NOx emissions. This was probably a result of the higher specific heat capacity, charge cooling, and dilution effects introduced by the presence of water [157,162,181,196,200].

Compared to E100, the use of E50W50 decreased the ISNOx levels by 30% when operating the engine with an EF of 0.20-0.21. Soot emissions were effectively lower than the Euro VI emission limit of 0.010 g/kWh [26] and increased slightly at higher EFs. The later was linked to a decrease in combustion temperature, which is supported by the lower levels of NOx and a reduction of up to 63 K in the EGT compared to the CDC baseline.

The dual-fuel operation led to higher ISCO and ISHC as the EF was increased. This was likely caused by higher levels of premixed fuel found in the crevice volumes of the stock diesel combustion system and near the cylinder liner [57]. The water-in-ethanol content showed little influence on the CO and unburnt HC emissions at EFs below 0.14. However relatively higher levels of ISCO and ISCH were attained with wet ethanol as the EF was increased to ~0.20, which supports a dependence on in-cylinder gas temperature.

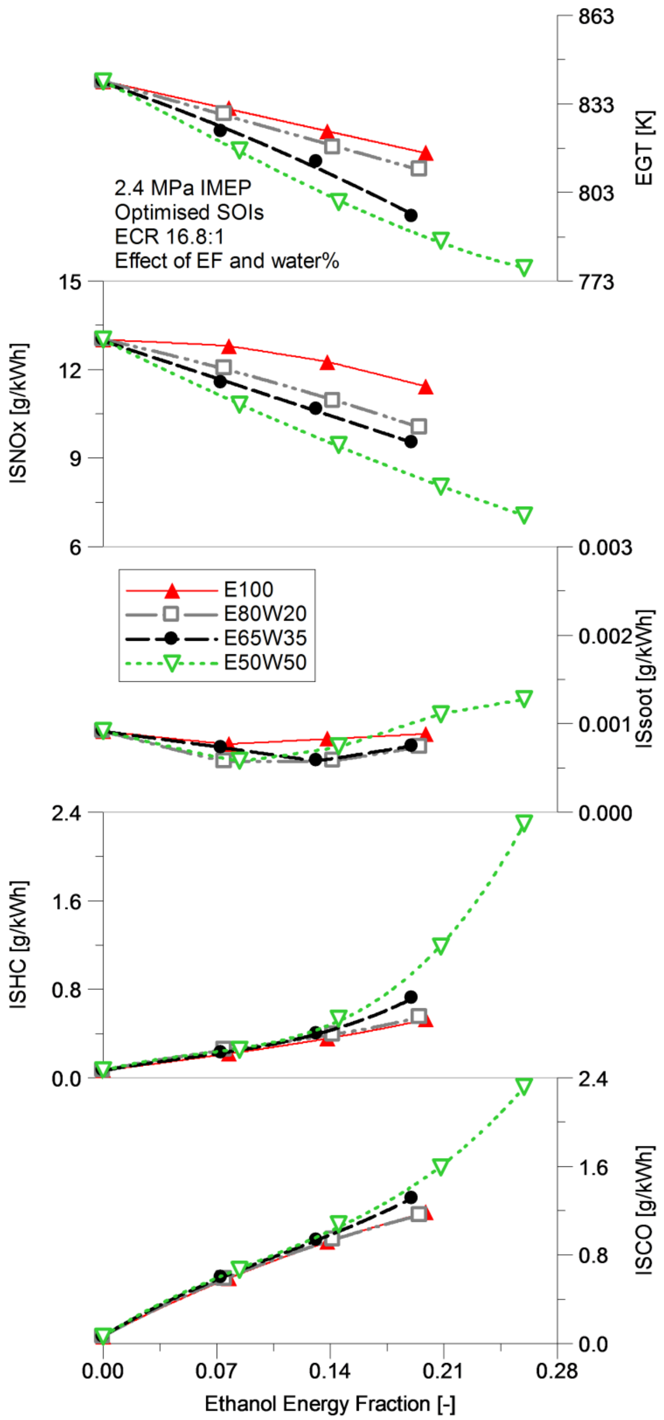

Figure 6.27 – EGT and exhaust emission for full load dual-fuel operation with anhydrous and wet ethanol injection.

Figure 6.28 depicts the exhaust emissions/net indicated efficiency trade-off for the dual-fuel operation with anhydrous and wet ethanol injection. The levels of ISsoot remained below 0.002 g/kWh for all cases. The most efficient engine operation was obtained by the E65W35-diesel dual-fuel combustion with an ethanol energy fraction of 0.19, which increased the net indicated efficiency by 2.6%. The injection of E50W50 reduced ISNOx by up to 46% to 7 g/kWh while increasing the net indicated efficiency in 1.4% over the diesel-only baseline highlighted by red circles.

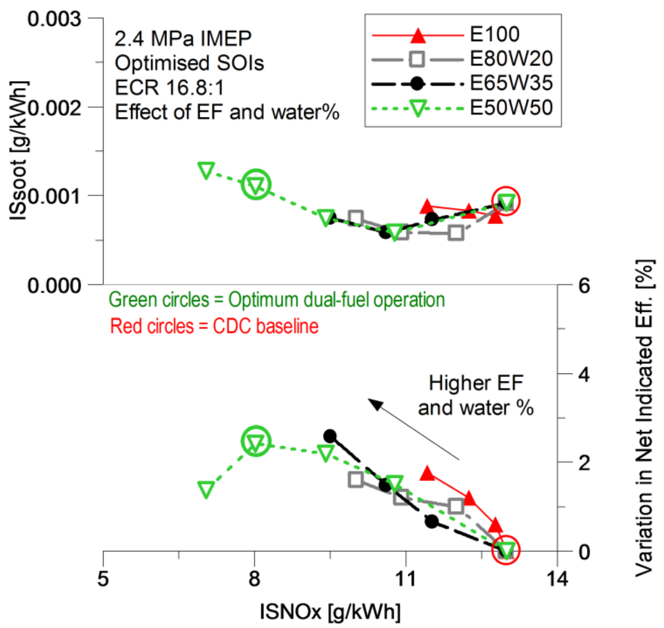

Figure 6.28 – Trade-off between ISNOx, ISsoot, and net indicated efficiency for full load dual-fuel operation with anhydrous and wet ethanol injection.

Figure 6.29 shows a comparison between the CDC baseline and the optimum dual-fuel case (see green circles in Figure 6.28). The dual-fuel operation with wet ethanol injection (E50W50) achieved 38% lower NOx emissions and 2.4% higher net indicated efficiency at an ethanol energy fraction of 0.21. These results indicate that the dual-fuel strategy can decrease the engine running costs of SCR equipped vehicles and machines, as supported by our previous study at mid-loads [3].

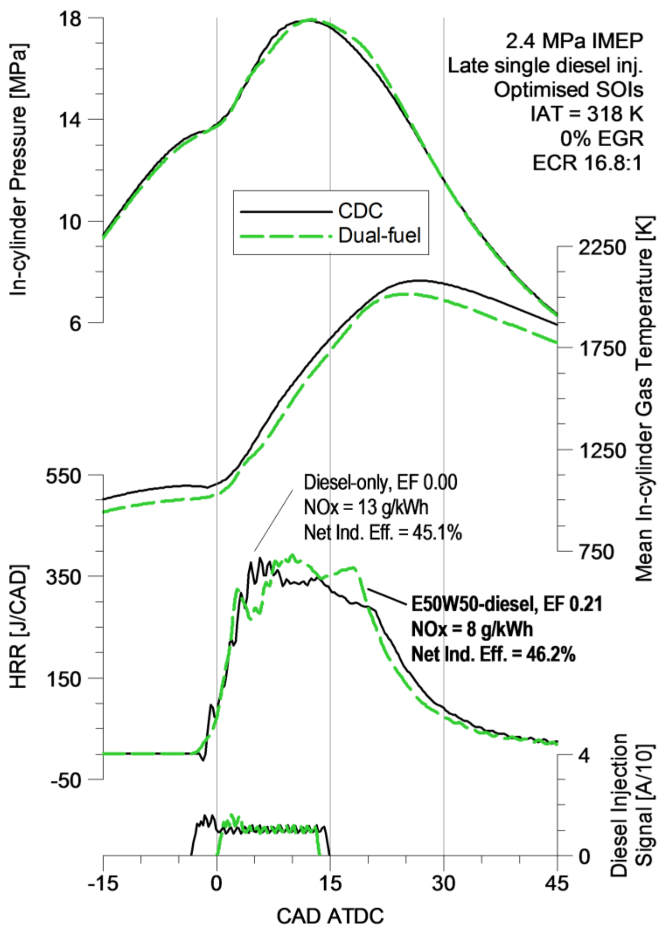

Figure 6.29 – Comparison between the CDC baseline and the optimum dual-fuel operation with wet ethanol injection (E50W50).

6.6 Summary

In this chapter, experiments were performed to characterise and optimise ethanol-diesel dual-fuel combustion at high engine loads of 1.8 and 2.4 MPa IMEP. Advanced combustion strategies were evaluated to maximise the use of ethanol and minimise the decrease in net indicated efficiency associated with the introduction of high EGR rates. The potential of Miller cycle via late intake valve closing (LIVC) events and charge air cooling via an air-to-water heat exchanger was explored to attain high efficiency and clean engine operation. The study also investigated the effect of ethanol energy fraction, EGR rate, intake manifold air pressure, and water-in-ethanol content on the dual-fuel combustion process. Combustion characteristics, exhaust emissions, and efficiencies were discussed and compared to diesel-only combustion baselines.

The primary findings of the ethanol-diesel dual-fuel operation at 1.8 MPa IMEP can be summarised as follows:

- Pressure rise rates (PRR) higher than 2.0 MPa/CAD were observed as the ethanol energy fraction (EF) was increased at the baseline intake valve lift profile and effective compression ratio (ECR) of 16.8:1. This was a result of an early autoignition process of the premixed charge, which took place prior to the diesel injection and limited the maximum EF to 0.26.
- The introduction of EGR rates of 15.7% and 21.2% had very little impact on the ethanol compression ignition timing. This was partially attributed to the increase in intake charge temperature when operating the engine with EGR.
- Changes to the global fuel/air equivalence ratio via different intake manifold pressures did not have a significant effect on the early ignition and combustion of the ethanol fuel.
- The utilisation of a Miller cycle strategy shortened the compression process and reduced the ECR from 16.8:1 in the baseline intake valve lift profile to 15.7:1 and 14.4:1 in the cases with LIVC events. This delayed the autoignition timing of the premixed charge and decreased the levels of PRR in dual-fuel mode.
- The combination of a small diesel pre-injection (of an estimated volume of 3 mm^3 and a constant dwell time of 7.2 CAD between pre- and main injection events), along with a Miller cycle strategy allowed for more advanced burn rates and the use of an EF of 0.79 at an ECR of 14.4:1.
- Optimised high load dual-fuel operation with Miller cycle attained higher net indicated efficiencies at an ECR of 14.4:1 (up to 46.85%) than the most efficient diesel-only case at the baseline ECR of 16.8:1 (46.1%). This improvement was achieved while reducing NOx emissions by up to 57% (from 17.3 g/kWh to 7.4 g/kWh).
- A reduction of 20 K in the intake manifold air temperature effectively decreased the compression temperatures and suppressed the early autoignition of ethanol, allowing for use of an EF of 0.65 at the baseline ECR of 16.8:1.
- Optimised high load dual-fuel operation with charge air cooling increased the net indicated efficiency by 4.1% to 48% and decreased NOx emissions by 44% to 9.7 g/kWh when compared against the most efficient conventional diesel combustion case at the baseline ECR of 16.8:1.

The primary findings of the ethanol-diesel dual-fuel operation at 2.4 MPa IMEP can be summarised as follows:

- Conventional diesel combustion presented an exhaust emissions/net indicated efficiency trade-off where lower NOx emissions led to higher levels of soot and lower net indicated efficiency. The use of late IVC timings in Miller cycle allowed for better results than retarded diesel injection timings.

- Full load dual-fuel operation yielded autoignition of the premixed anhydrous ethanol fuel prior to the diesel SOI at the baseline ECR of 16.8:1. Excessive PRRs and the maximum in-cylinder pressure of the engine limited the highest ethanol energy fraction to ~0.20.
- The introduction of a Miller cycle strategy via LIVC events decreased the ECR and thus the in-cylinder gas pressure and temperature prior to the start of combustion. This resulted in relatively longer ignition delays, effectively retarding the ethanol autoignition timing.
- E100-diesel dual-fuel combustion allowed for an increase in net indicated efficiency of 1.8% with 12% lower NOx emissions at a constant ECR of 16.8:1. Alternatively, the use of an ethanol energy fraction of 0.19 at an ECR of 14.4:1 reduced the levels of NOx by 39% with a decrease in net indicated efficiency of 0.4% over the CDC baseline.
- The port fuel injection of wet ethanol containing high water content (e.g. E50W50) helped delay the autoignition event and slow down the ethanol burn rate. Higher levels of wet ethanol injection also led to a similar trend, retarding the position of the first peak heat release when operating the engine with constant diesel injection timing. Nevertheless, PRR and P_{max} remained a challenge for a dual-fuel operation with wet ethanol injection, limiting the maximum EF to 0.26.
- NOx emissions were reduced when increasing the water-in-ethanol content. Up to 46% lower ISNOx levels than the diesel-only case were achieved with wet ethanol injection. In addition, the E65W35-diesel dual-fuel operation achieved 2.6% higher net indicated efficiency than the CDC baseline. The increase in net indicated efficiency and the NOx reduction were attained at the expense of higher CO and unburnt HC emissions.

Overall, this chapter has shown Miller cycle via LIVC events allowed for the use of substantially higher ethanol energy fractions without the need for EGR, enabling high efficiency and low NOx dual-fuel operation at high load conditions. Dual-fuel combustion with charge air cooling and wet ethanol injection also attained higher net indicated efficiency and lower NOx emissions than the diesel-only combustion. However, the analysis highlighted the sensitivity of ethanol autoignition to variations in intake manifold and in-cylinder gas temperatures.

Chapter 7

High efficiency and clean ethanol-diesel dual-fuel combustion from low to full engine load

7.1 Introduction

This chapter compares the ethanol-diesel dual-fuel operation against conventional diesel combustion (CDC) from low to full engine load. Experiments were performed using the same hardware setup and identical engine operating conditions. Boost pressure, exhaust manifold pressure, as well as valve timing and the resulting effective compression ratio were held constant for both the combustion modes at a given engine load. Moreover, all comparisons were carried out for the cases that attained the highest net indicated efficiencies after sweeps of diesel injection timings. Figure 7.1 shows where the test points are located over an estimated speed and load map of a HD diesel engine. Advanced dual-fuel combustion control strategies such as iEGR, Miller cycle, charge air cooling, and wet ethanol injection would require different test procedures and were not explored in this chapter.

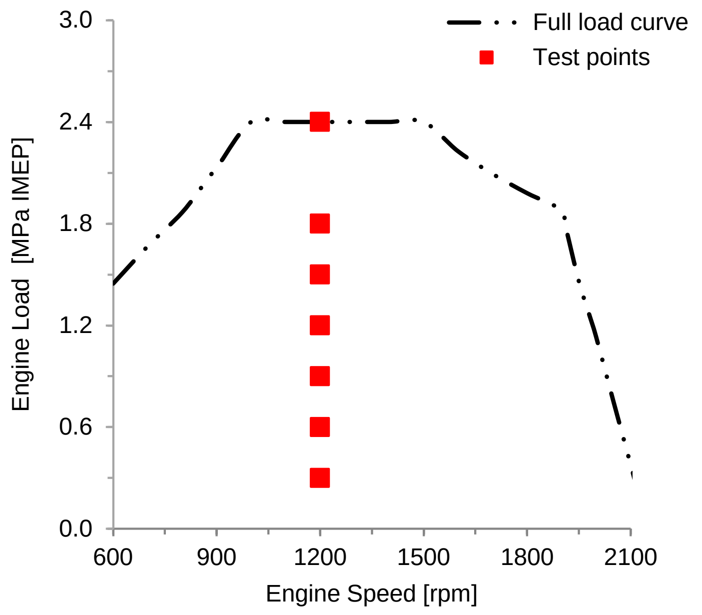

Figure 7.1 – Experimental test points over an estimated HD diesel engine speed-load map.

7.2 The effect of the engine load on CDC and dual-fuel operation

This section experimentally compares the controllability, emissions, efficiency, and potential engine operational cost for the dual-fuel operation and diesel-only combustion over a range of loads from 0.3 to 2.4 MPa IMEP at a medium engine speed of 1200 rpm.

7.2.1 Test procedure

Table 7.1 summarises the test conditions for the CDC and ethanol-diesel dual-fuel operating modes. Engine testing was carried out using an IVC at -155 ± 2 CAD ATDC and a pressure-based ECR of approximately 16.8:1. Stable engine operation was quantified by a COV_IMEP below 5%. The levels of PRR were limited to 2.0 MPa/CAD. The P_{max} limit was set to 18 MPa.

Table 7.1 – Operating conditions for the CDC and ethanol-diesel dual-fuel operation from low to full engine load at 1200 rpm.

Parameter	Unit	Engine load (MPa IMEP)						
		0.3	0.6	0.9	1.2	1.5	1.8	2.4
Intake pressure	kPa	115	125	155	190	230	260	300
Exhaust pressure	kPa	125	135	165	200	240	270	310
		Conventional diesel combustion (CDC)						
Diesel inj. pressure	MPa	105	125	140	155	170	190	220
EGR rate	%	25.1	25.3	25.2	24.9	25.2	19.6	10.9
Intake air temp.	K	307	309	314	318	324	322	322
		Ethanol-diesel dual-fuel combustion						
Diesel inj. pressure	MPa	50	90	110	125	140	160	190
EGR rate	%	25.0	25.1	25.1	24.8	24.9	20.2	11.4
Intake air temp.	K	306	310	315	319	324	325	323

The intake pressure set point was taken from a Euro V compliant multi-cylinder HD diesel engine in order to provide a sensible starting point, since an external boosting device was used in place of a turbocharger. The exhaust pressure was varied to maintain a constant pressure differential across the cylinder of 10 kPa. This allowed for exhaust gas recirculation, which was used to curb NOx formation.

The EGR rate was limited to ~25% between 0.3 and 1.5 MPa IMEP to avoid excessive smoke and a decrease in net indicated efficiency, as shown in Chapter 5, Subsection

5.3.4. At 1.8 and 2.4 MPa IMEP, the EGR rate was reduced to approximately 20% and 11%, respectively. This was required to achieve lean and efficient high load operation using the same levels of boost pressure as the multi-cylinder engine.

Diesel injection pressures were set to be 30 to 55 MPa higher in the CDC mode than those in the dual-fuel combustion due to the relatively higher diesel flow rates and longer injection durations at a given engine load. This was necessary to minimise soot emissions from the CDC operation via improved diesel atomisation and enhanced the fuel-air mixing process.

All comparisons were carried out for the cases that attained the highest net indicated efficiencies after sweeps of diesel injection timings. Additionally, the diesel injection strategy (i.e. number of diesel injections per cycle) was optimised and varied as the engine load was increased.

In the dual-fuel mode, the ethanol energy fraction was also optimised for minimum NOx and soot emissions [1,3,5–7]. Table 7.2 shows the optimum ethanol energy, mass, and volumetric fractions used at different loads. A maximum EF of 0.79 was achieved at 1.2 MPa IMEP. Advanced dual-fuel combustion control strategies such as Miller cycle [1] and internal exhaust gas recirculation (iEGR) [5] were not explored in this study as they would require different test procedures.

Table 7.2 – The effect of engine load on the optimum ethanol energy, mass, and volumetric fractions for the dual-fuel operation at 1200 rpm.

Parameter	Unit	Engine Load (MPa IMEP)						
		0.3	0.6	0.9	1.2	1.5	1.8	2.4
EF	-	0.56	0.65	0.77	0.79	0.76	0.25	0.19
MF	-	0.67	0.75	0.84	0.86	0.84	0.35	0.28
VF	-	0.68	0.76	0.84	0.86	0.84	0.36	0.29

7.2.2 Overview of the load sweep

Figure 7.2 depicts the effect of engine load on both the operating modes. CDC operation was characterised by longer mixing-controlled combustion phase as the load was increased. This was attributed to longer diesel injection periods and increased amount of fuel, which limited the fuel vapour-air mixing process [8,50]. The optimum CA50 in CDC mode varied as the engine load was increased, allowing for more advanced burn rates at mid-loads and delayed combustion events at high loads. The reasons behind this are described in the next subsection.

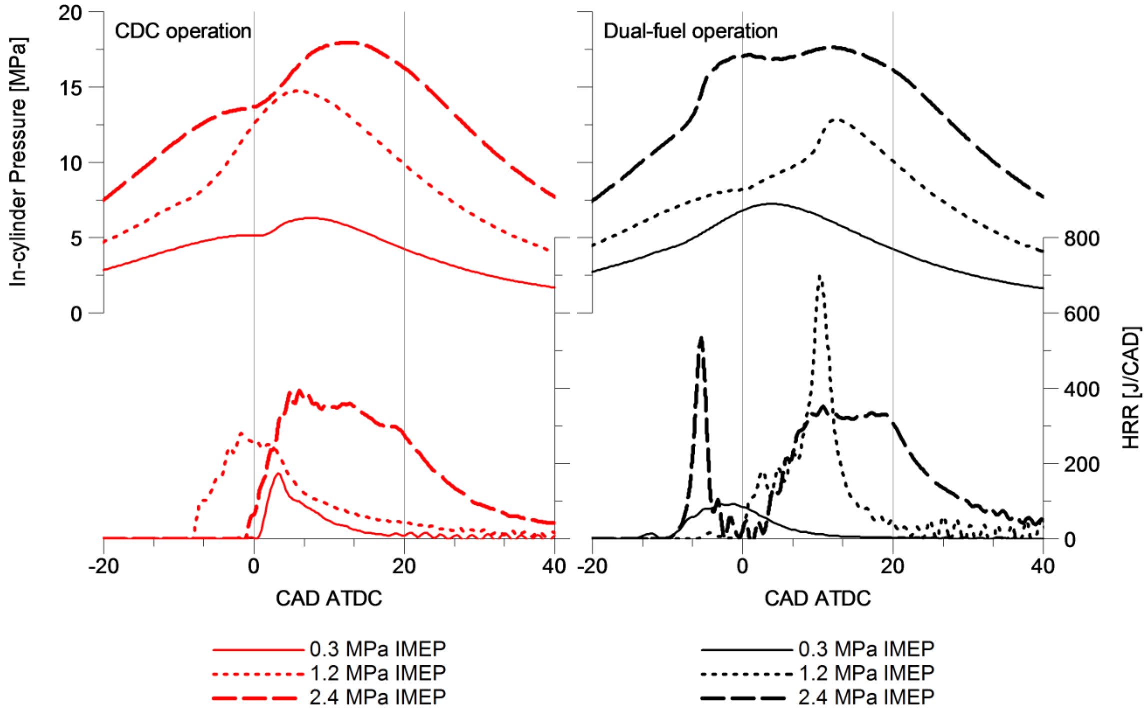

Figure 7.2 – The effect of engine load on CDC and ethanol-diesel dual-fuel operation at 1200 rpm.

The dual-fuel operation led to higher peak heat release than the CDC mode at all engine loads except 0.3 MPa IMEP. This required different diesel injection strategies and eventually later combustion process in order to control the PRRs as the engine load was increased. The combustion was triggered by and initiated after the start of diesel injection at low and medium load operations between 0.3 and 1.5 MPa IMEP. Higher compression pressures and temperatures accelerated the autoignition of the premixed ethanol fuel prior to the diesel injection at high engine loads of 1.8 and 2.4 MPa IMEP.

Figure 7.3 shows the optimum EF had to be rapidly reduced from 0.76 to 0.25 when increasing the engine load from 1.5 to 1.8 MPa IMEP. This was necessary in order to minimise the PRRs associated with the early autoignition of ethanol. It is important to bear in mind that modifications in the engine hardware (e.g. lower effective compression ratio via Miller cycle) and/or test procedure (e.g. lower intake manifold air temperature) can increase the maximum EF at higher loads, as revealed in Chapter 6.

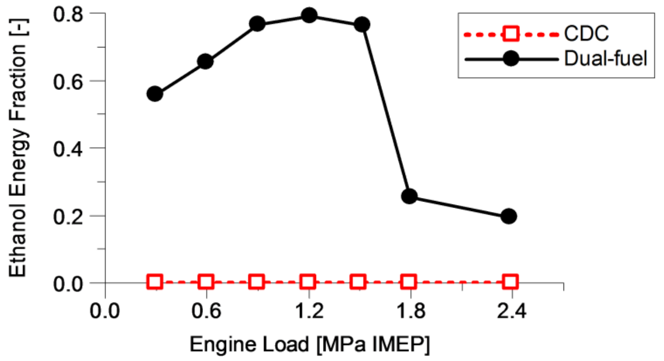

Figure 7.3 – Optimum ethanol energy fraction for varied engine loads at 1200 rpm.

7.2.3 Combustion characteristics

Figure 7.4 shows the diesel injection timings and in-cylinder pressure characteristics for optimised CDC and dual-fuel operation.

In the CDC mode, a 3 mm^3 diesel pre-injection with a constant dwell time of 1 ms was used to reduce the levels of PRR [3] between the engine loads of 0.3 MPa IMEP and 1.5 MPa IMEP. The lower PRRs were associated with the shorter ignition delay produced by the combustion of the diesel pre-injection and likely formation of a hot and reactive mixture prior to the main diesel injection [201].

At high engine loads of 1.8 and 2.4 MPa IMEP, relatively shorter ignition delays introduced by lower EGR rates and higher in-cylinder pressures and temperatures allowed for the use of a single diesel injection near firing top dead centre (TDC). The maximum SOI_2 advance was limited by the P_{max} while the PRRs were maintained within the limit of 2.0 MPa/CAD.

In the dual-fuel operation, the combination of an early single diesel injection at about -36 CAD after top dead centre (ATDC) and EFs of 0.56 and 0.65 allowed for long ignition delays (SOI_main–SOC) and better mixture preparation at 0.3 and 0.6 MPa IMEP. This enhanced the combustion process via a more progressive and probably sequential combustion from high to low reactivity regions [41]. This has also been identified in computational simulations performed by Desantes et al. [88] and is supported by the low levels of PRR. However, the P_{max} was increased when compared to that of the CDC operation due to earlier CA50 and shorter combustion for the dual-fuel mode at these particular loads (see Figure 7.5).

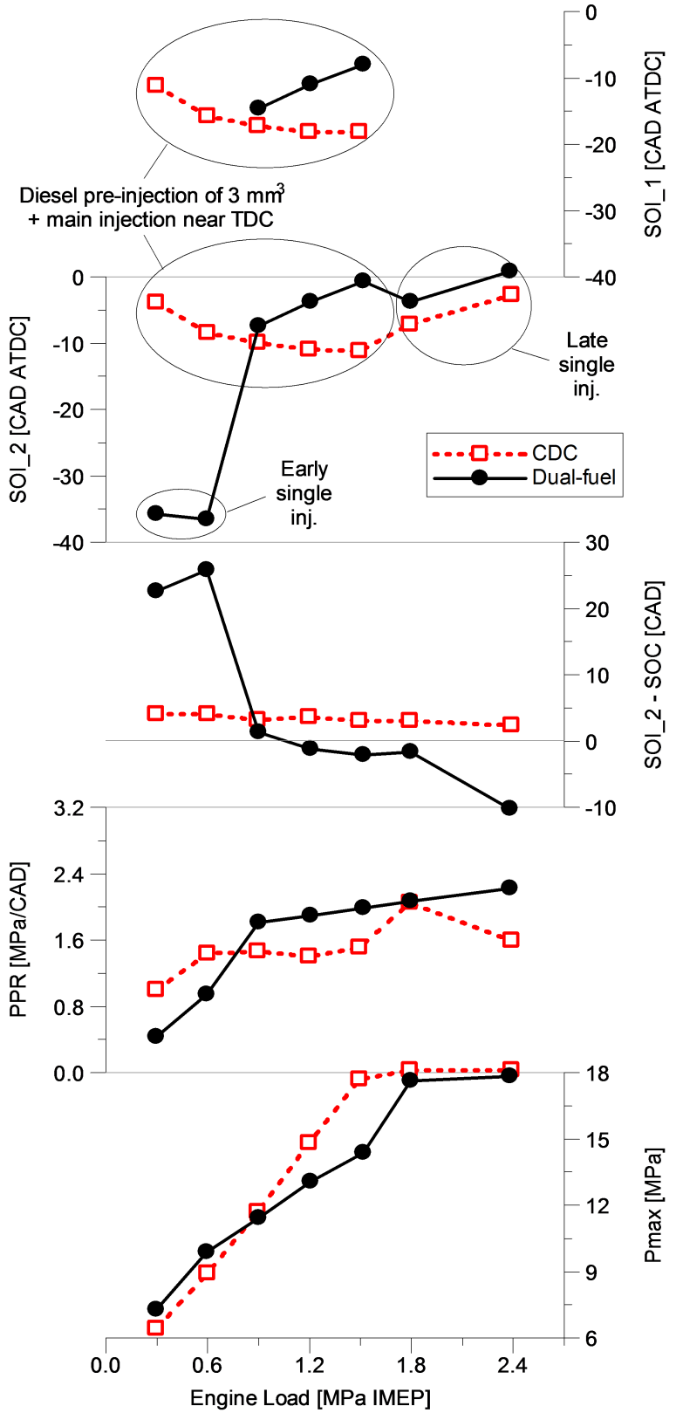

Figure 7.4 – Main diesel injection timings and combustion characteristics for optimised CDC and ethanol-diesel dual-fuel operation at 1200 rpm.

At mid-loads between 0.9 and 1.5 MPa IMEP, less partially premixed diesel fuel could be used in order to prevent an early ignition of the in-cylinder charge. Therefore, the mass of the diesel was divided into two direct injections using the same strategy employed in the CDC cases. The injection of a small amount of diesel prior to the SOI_2 was essential to mitigate excessive PRRs. This was a result of a shorter SOI_2–SOC period and elimination of the premixed combustion peak typically observed with a late single diesel injection strategy, as shown in Chapter 5, Subsection 5.2.4. Despite the controlled levels of PRR, the diesel injection timings were delayed by up to 10.5 CAD when compared against those of the CDC operation, helping lower the P_{max} levels.

At 1.8 and 2.4 MPa IMEP, the premixed ethanol fuel autoignited prior to the diesel injection. Low ethanol energy fractions and a single diesel injection near TDC were used to control the burn rate as well as the resulting PRR and P_{max}. The introduction of a diesel pre-injection would increase the PRR levels at these loads due to simultaneous and early combustion of the ethanol and pre-injected diesel fuel.

Figure 7.5 depicts the heat release characteristics for the CDC and dual-fuel operation. The optimum CA50 for the maximum net indicated efficiency was initially advanced and then retarded in the CDC mode. The advance in the CA50 when increasing the engine load from 0.3 to 0.6 MPa IMEP was likely linked to the longer CA10–CA90 period and relatively lower heat transfer losses obtained at 0.6 MPa IMEP. The CA50 delay at high load operations of 1.8 and 2.4 MPa IMEP was associated with the peak in-cylinder pressure limitation. Additionally, lower levels of EGR and higher combustion temperatures shortened the CA10–CA90 period and probably increased heat transfer losses of the CDC operation at these high load conditions.

In comparison, the dual-fuel operation often required later CA50 as the engine load was increased in order to avoid excessive PRRs. At high loads of 1.8 and 2.4 MPa IMEP, the CA50 and CA90 were similar for both the combustion modes due to the P_{max} limitation of 18 MPa and lower EFs used in the dual-fuel mode.

In general, an increase in engine load led to later CA90 and longer CA10–CA90 period as a result of the higher fuel flow rates. The higher degree of premixed combustion in the dual-fuel mode was likely the cause for the relatively earlier CA90 and faster CA10–CA90 period between 0.3 and 1.5 MPa IMEP. Nonetheless, the early ignition of the ethanol fuel produced longer burn rates than the CDC operation at 1.8 and 2.4 MPa IMEP.

In terms of combustion stability, the mixing-controlled combustion of the CDC operation decreased the coefficient of variation of IMEP (COV_IMEP) and P_{max} (COV_P_{max}) to 0.5% as the engine load was increased to 2.4 MPa IMEP. In the dual-fuel mode, later CA50s combined with the autoignition of ethanol increased the COV_IMEP between 0.9

and 2.4 MPa IMEP. This was associated with the lower mean in-cylinder gas temperatures and higher instability for a dual-fuel combustion taking place later in the expansion stroke. In addition, the dual-fuel operation resulted in higher COV_P_{max} at all engine loads except 0.3 MPa IMEP. Nevertheless, the COV_IMEP and COV_P_{max} for the optimised dual-fuel operation were held between 1.0% and 3.0%.

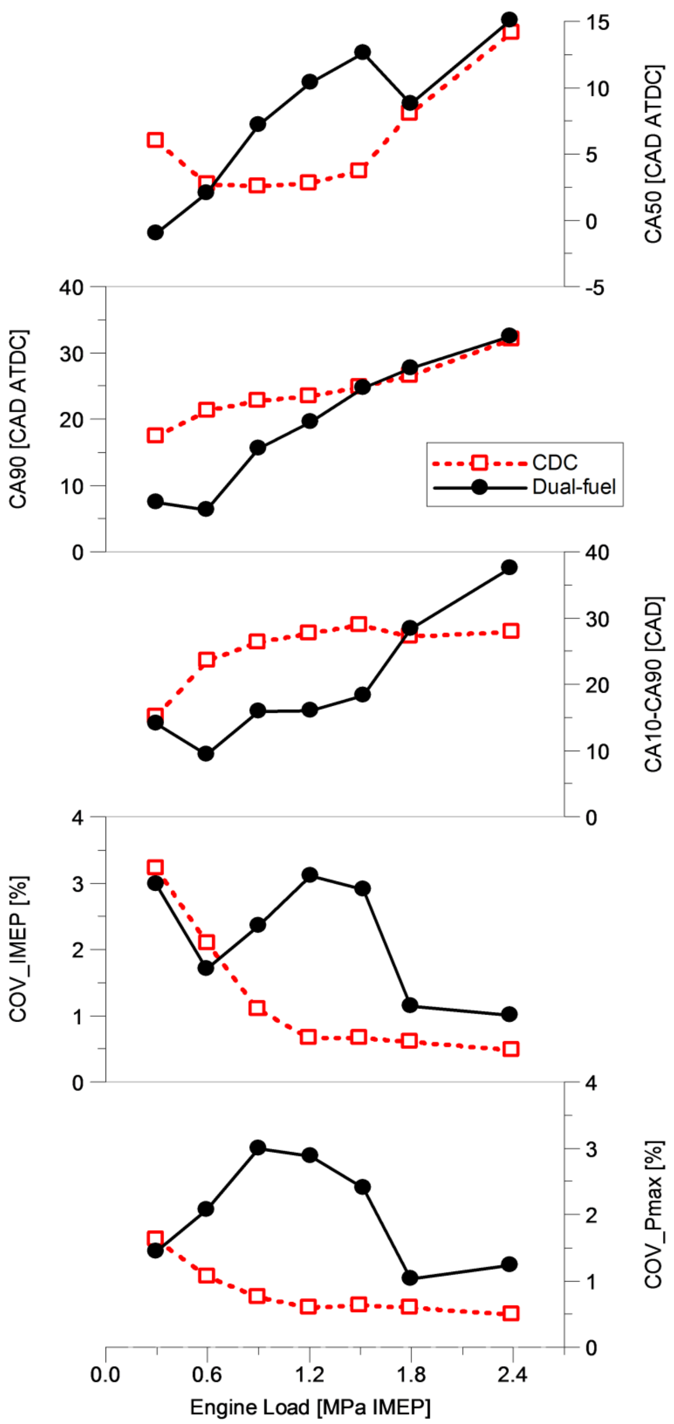

Figure 7.5 – Heat release characteristics for optimised CDC and ethanol-diesel dual-fuel operation at 1200 rpm.

7.2.4 Engine-out emissions and performance

Figure 7.6 shows the net indicated specific emissions for the optimum cases over a sweep of load. An EGR rate of ~25% was used to minimise NOx emissions at engine loads up to 1.5 MPa IMEP. This allowed for CDC operation with an average ISNOx of 3.9 g/kWh between 0.3 and 1.5 MPa IMEP. The use of lower EGR rates of 20% and 11% increased the combustion temperatures at 1.8 and 2.4 MPa IMEP, yielding higher ISNOx of 4.4 and 5.7 g/kWh, respectively.

Alternatively, the optimised dual-fuel operation achieved lower ISNOx than the CDC mode at all engine loads. This was linked to the premixed ethanol fuel, which likely decreased the amount of in-cylinder regions of high combustion temperature. Reductions in NOx emissions varied from 26% at 2.4 MPa IMEP up to 90% at 0.3 MPa IMEP for EFs of 0.19 and 0.56, respectively.

The lowest levels of ISNOx were attained at 0.3 and 0.6 MPa IMEP due to longer ignition delays and a relatively more homogenous combustion process when compared against the other dual-fuel cases with diesel injections closer to TDC. NOx emissions were decreased when increasing the engine load from 0.9 to 1.5 MPa IMEP due to later optimum CA50 and thus lower combustion temperatures. At high loads of 1.8 and 2.4 MPa IMEP, the ethanol autoignition process and shorter diesel mixing-controlled combustion helped reduce the peak in-cylinder gas temperatures [1], decreasing the ISNOx when compared to the CDC operation.

In the CDC mode, higher diesel injection pressures and in-cylinder gas temperatures helped curb soot emissions as the engine load was increased. In comparison, net indicated specific emissions of soot (ISsoot) were maintained consistently low in the dual-fuel operation because of reduced regions of fuel rich combustion, particularly at 0.3 and 0.6 MPa IMEP. This is a significant improvement over the CDC cases considering the dual-fuel combustion employed lower diesel injection pressures, as explained in Section 3.

At a mid-load of 1.5 MPa IMEP, the dual-fuel operation yielded an ISsoot of 0.011 g/kWh, which was significantly higher than the 0.003 g/kWh for the CDC case. This can be explained by the late CA50 and short ignition delay, which potentially reduced combustion temperatures and increased local fuel/air equivalence ratios.

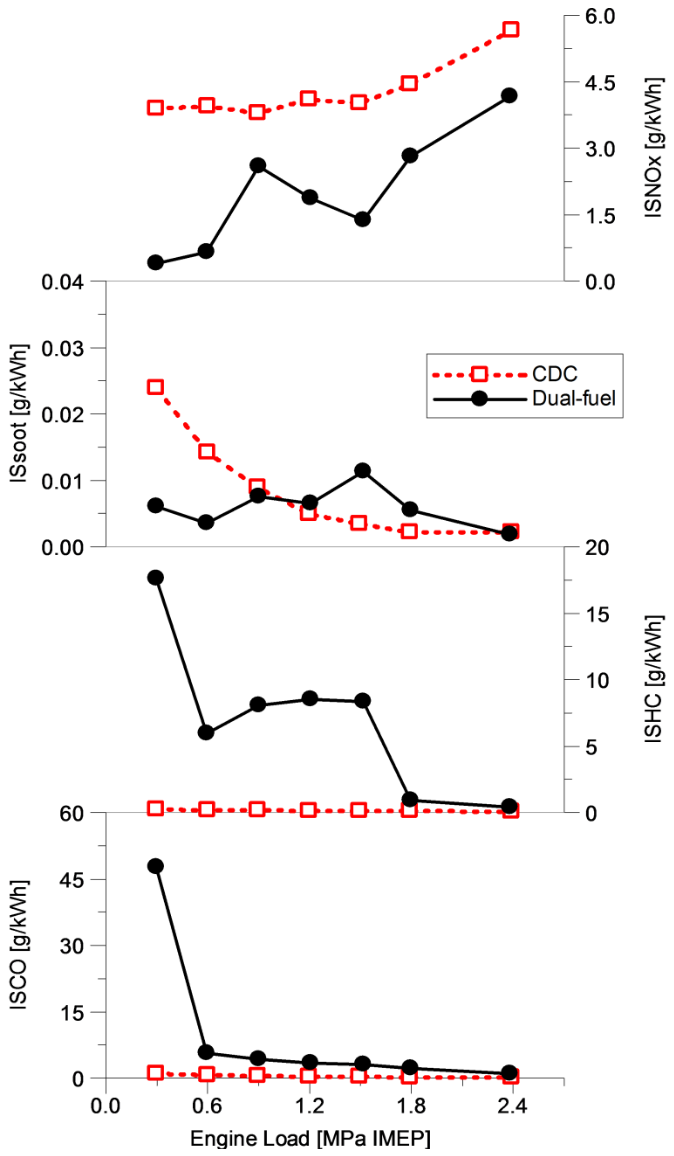

Figure 7.6 – Net indicated specific emissions for optimised CDC and ethanol-diesel dual-fuel operation at 1200 rpm.

Net indicated specific emissions of CO (ISCO) and unburnt HC (ISHC) increased significantly in the dual-fuel combustion when compared against the CDC operation. This was possibly a result of premixed fuel trapped in the crevice volumes of the stock diesel piston as well as lower local in-cylinder gas temperatures [57].

High levels of ISCO and ISHC were measured for the dual-fuel operation at 0.3 MPa IMEP. This can be attributed to excessively low combustion temperatures and overly lean regions that did not release enough heat in order to effectively oxidise the fuel [57]. These emissions can be significantly reduced by intake throttling and iEGR, as demonstrated in Chapter 4, Section 4.3. At 1.8 and 2.4 MPa IMEP, the use of lower EFs as well as lower EGR rates likely increased combustion temperatures, decreasing CO and unburnt HC emissions.

Figure 7.7 depicts the engine performance metrics for optimised CDC and ethanol-diesel dual-fuel operation. The global fuel/air equivalence ratio (Φ) of the dual-fuel combustion was either comparable or lower than that of the CDC mode at a given engine load. This was attributed to minor variations in the intake air flow rate (within 3% and not shown for the sake of brevity) and improvements in net indicated efficiency. Differences in LHV possibly balanced out changes in stoichiometric air/fuel ratio.

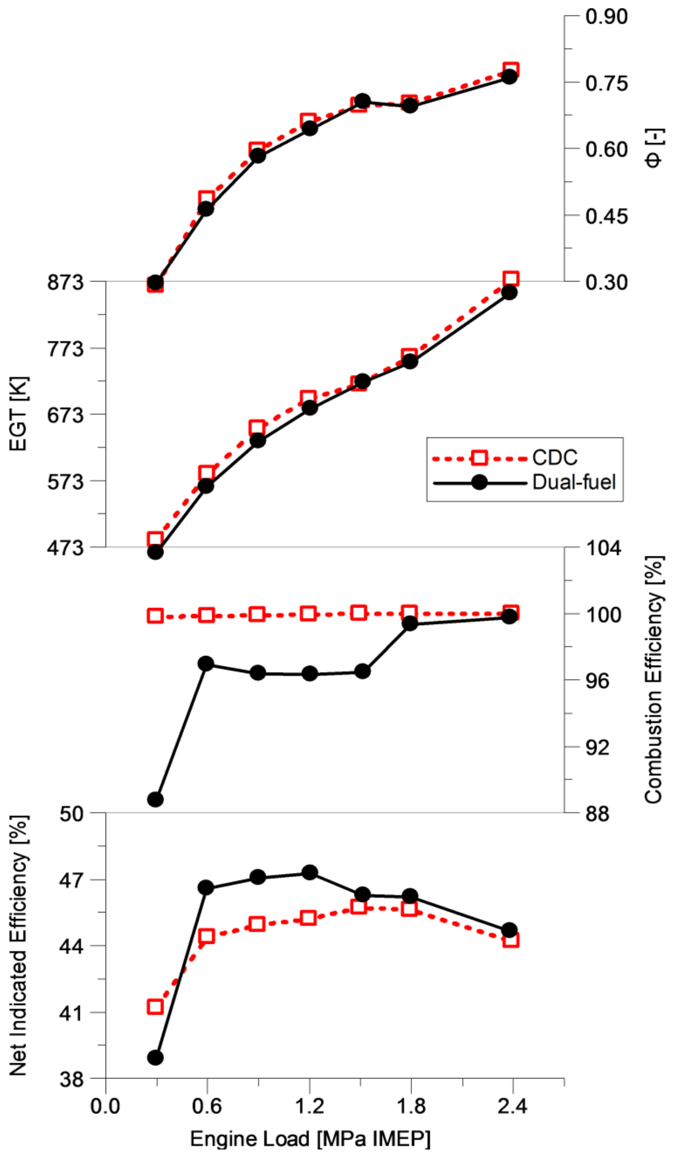

Figure 7.7 – Performance for optimised CDC and ethanol-diesel dual-fuel operation at 1200 rpm.

Higher exhaust gas temperatures (EGT) were measured as engine load was increased due to later CA90 and higher levels of fuel energy supplied. However, the dual-fuel operation produced EGTs up to 20 K lower than those of the corresponding CDC case. This was perhaps a result of a more homogenous and lower temperature combustion process for an engine operation with premixed ethanol fuel [1,5].

The dual-fuel mode also yielded lower combustion efficiencies than the CDC cases as supported by the ISCO and ISHC in Figure 7.6. At medium and high engine loads, combustion efficiency ranged between 96.3% and 99.7% despite the use of high EFs. This was attributed to relatively higher Φ and local in-cylinder gas temperatures.

At the lowest load of 0.3 MPa IMEP, the combination of a low combustion efficiency of 88.7% and an EGT of 463 K can represent a challenge for HD engine manufacturers. This is due to a reduction in the effectiveness of the oxidation catalyst in reducing CO and unburnt HC emissions [94,202]. In-cylinder control strategies such as intake throttling and iEGR can help increase the EGT while simultaneously minimising the levels of ISCO and ISHC [5]. Moreover, the low combustion efficiency adversely affected the performance of the dual-fuel operation at 0.3 MPa IMEP, limiting the net indicated efficiency to 38.9%.

Nonetheless, the ethanol-diesel dual-fuel combustion resulted in higher net indicated efficiencies than the CDC operation between 0.6 and 2.4 MPa IMEP. A peak net indicated efficiency of 47.2% was attained at 1.2 MPa IMEP and represented an increase of 4.4% over the 45.2% of the CDC mode. The maximum net indicated efficiency achieved by the CDC operation was 45.7% at 1.5 MPa IMEP.

The ethanol autoignition process likely helped decrease the combustion temperatures and thus the heat transfer losses [8], as supported by the NOx reduction in Figure 7.6. However, the use of a late CA50 at 1.5 MPa IMEP and low EFs at 1.8 and 2.4 MPa IMEP limited improvements in the net indicated efficiency of the dual-fuel operation. This was necessary in order to control the PRRs below 2.0 MPa/CAD.

7.2.5 Additional practical considerations

Additional practical aspects for ethanol-diesel dual-fuel operation were assessed in order to evaluate whether the combustion strategy can be successfully used in a Euro VI HD engine. The analysis focused on the total fuel flow rate, the estimated consumption of aqueous urea solution in the SCR system ($\dot{m}_{urea}$) to meet the Euro VI NOx limit of 0.4

g/kWh, and the SCR corrected net indicated efficiency ($Net\ Indicated\ Eff._{SCR\ corr.}$). The methodology for the calculation of these performance metrics has been described in our previous study [3].

Figure 7.8 shows the optimised ethanol-diesel dual-fuel combustion increased the total fuel consumption by up to 45.8% in comparison with the CDC mode (8.12 kg/h vs. 5.57 kg/h at 1.5 MPa IMEP). This is attributed to the relatively lower density ($\rho_{ethanol}$) and energy content ($LHV_{ethanol}$) of the ethanol fuel. Appropriate volumes of diesel and ethanol fuel tanks will have to be designed according to the application of the engine and duty cycle.

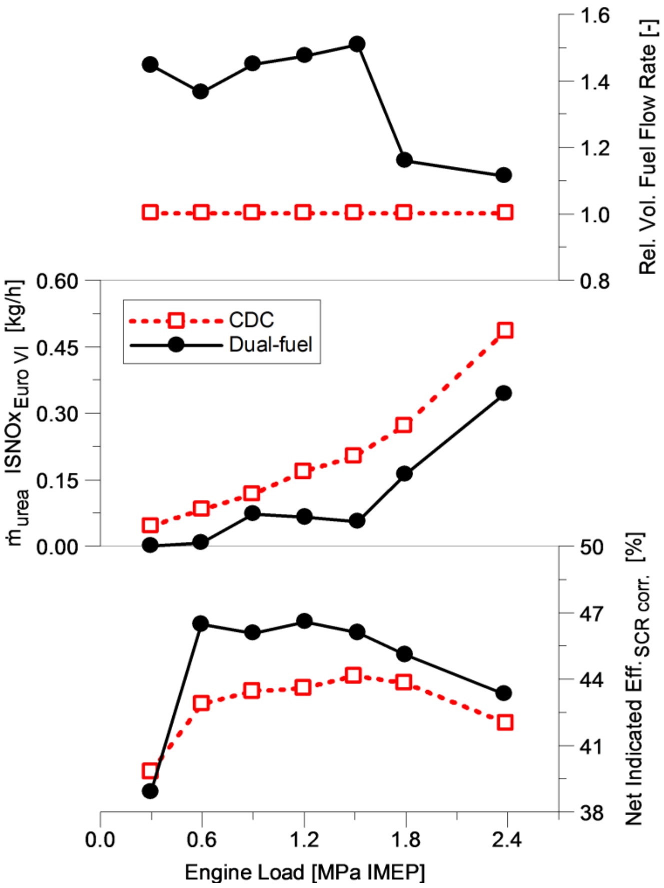

Figure 7.8 – Practical considerations for optimised CDC and ethanol-diesel dual-fuel operation on a Euro VI HD engine.

In terms of NOx aftertreatment, the ethanol-diesel dual-fuel combustion attained lower levels of ISNOx than the CDC operation, effectively decreasing the $\dot{m}_{urea}$ requirements. Higher $\dot{m}_{urea}$ were estimated for both the combustion modes as the engine load was increased. This was due to an increase in the production of NOx emissions (in g/h) as well as the reduction in the EGR rate at 1.8 and 2.4 MPa IMEP.

The lower urea consumption in the dual-fuel mode allowed for higher $Net\ Indicated\ Eff._{SCR\ corr.}$ between 0.6 and 2.4 MPa IMEP. The maximum $Net\ Indicated\ Eff._{SCR\ corr.}$ of 46.5% was achieved at 0.6 MPa IMEP and represented a relative increase of 8.4% over the CDC mode. Lowered combustion efficiency limited the $Net\ Indicated\ Eff._{SCR\ corr.}$.of the dual-fuel mode at 0.3 MPa IMEP, despite the low engine-out NOx of 0.4 g/kWh and $\dot{m}_{urea} = 0$.

These improvements can reduce the engine running costs depending on the volumetric price ratio between ethanol and diesel fuel as well as the cost of aqueous urea solution, as discussed in Chapter 5, Subsection 5.4.4. Nevertheless, the implementation of this dual-fuel combustion strategy on a HD engine would have to weigh the higher efficiency and lower NOx emissions against the additional complexity and upfront cost of a port fuel injection system and extra fuel tank.

7.2.6 Potential CO_2 reduction

The data in Table 7.3 reveal that the complete combustion of ethanol can reduce the emissions of CO_2 by ~4% when compared against the combustion of diesel at a given energy input. However, practical ethanol energy fractions in dual-fuel mode vary between 0.00 and ~0.80 while the actual fuel energy consumption changes with net indicated efficiency.

Table 7.3 – Theoretical CO_2 emissions for diesel and ethanol combustion.

Property	Diesel	Ethanol
Normalised molecular composition	$CH_{1.825}O_{0.0014}$	$CH_3O_{0.5}$
Lower heating value (LHV_{fuel})	42.9 MJ/kg	26.9 MJ/kg [8]
Normalised fuel's molar mass (M_{fuel})	13.87 g/mol	23.03 g/mol
Mass of CO_2 emissions per mole of fuel	44.01 gCO_2/mol	44.01 gCO_2/mol
Mass of CO_2 emissions per mass of fuel	3.17 gCO_2/g	1.91 gCO_2/g
Mass of CO_2 emissions per MJ of fuel	73.9 gCO_2/MJ	71 gCO_2/MJ
Specific CO_2 emissions reduction	n/a	~4%

The use of the engine-out CO_2 emissions in the calculation of net indicated specific emissions of CO_2 (ISCO_2) would result in incorrect trends for dual-fuel operation, with significant reductions at all engine loads. This is because of the partial oxidation of hydrocarbons and formation of CO. To remove the effect of incomplete combustion, the ISCO_2 (in g/kWh) was estimated using the Equation (7.1), which assumed a complete oxidation of the fuel injected to CO_2, either in-cylinder or in the aftertreatment system.

$$ISCO_2 = \left(\frac{\dot{m}_{diesel}}{M_{diesel}} + \frac{\dot{m}_{ethanol}}{M_{ethanol}}\right)\left(\frac{M_{CO_2}}{P_{ind}}\right) \times 10^3 \quad (7.1)$$

where M_{CO_2} is the molar mass of CO_2 of 44.01 g/mol [29].

Figure 7.9 shows the optimised dual-fuel operation can achieve lower $ISCO_2$ than the CDC mode from 0.6 to 2.4 MPa IMEP. The potential CO_2 reduction introduced by the ethanol-diesel dual-fuel strategy varied between 1.8% and 7.5%. This improvement was a result of the increase in net indicated efficiency combined with higher hydrogen to carbon ratio of the ethanol fuel [203,204]. The low net indicated efficiency at 0.3 MPa IMEP prevented any CO_2 reduction and actually increased the $ISCO_2$ by 3.7% when compared to the CDC mode.

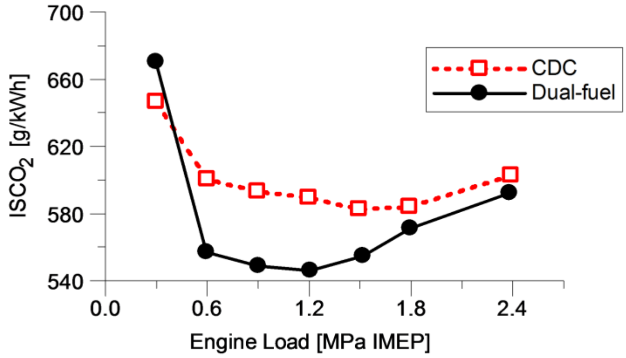

Figure 7.9 – Estimated $ISCO_2$ for optimised CDC and ethanol-diesel dual-fuel operation.

In order to provide additional insight into the CO_2 reduction, a TTW analysis was performed by calculating the ratio of the estimated mass of CO_2 emissions to the total fuel energy supplied to the engine (in MJ) as

$$TTW\ CO_2 = \frac{ISCO_2\ P_{ind}}{(\dot{m}_{diesel}LHV_{diesel} + \dot{m}_{ethanol}LHV_{ethanol})} \quad (7.2)$$

Figure 7.10 reveals the optimised ethanol-diesel dual-fuel combustion reduced the levels of TTW CO_2 emissions by up to 3.2% when compared against a constant 73.9 g/MJ produced by the CDC operation. This was attributed to the usage of the ethanol fuel, as the TTW CO_2 emissions are heavily dependent on the in-cylinder fuel characteristics (e.g. M_{fuel} and LHV_{fuel}).

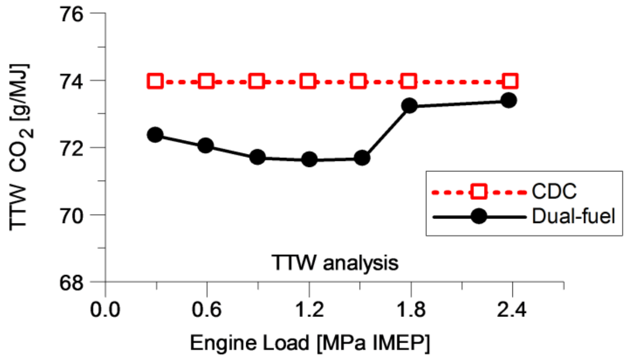

Figure 7.10 – Estimated TTW CO_2 emissions for optimised CDC and ethanol-diesel dual-fuel operation.

It is important bear in mind that the data plotted in Figure 7.9 and Figure 7.10 were obtained by assuming complete conversion of the fuel into CO_2. Additionally, the analysis neglected the CO_2 emissions produced by aqueous urea solution reactions in the SCR system [52], which were calculated [29] to be smaller than 0.4% of the estimated $ISCO_2$. For a more comprehensive analysis, the actual CO_2 emissions should be measured downstream of the aftertreatment system during the appropriate engine/vehicle test cycle.

7.2.7 Theoretical well-to-wheels analysis

A well-to-wheels (WTW) analysis can be used to assess the GHG emissions and energy expended over the production and use of a given fuel [141,205]. This holistic methodology now combines the TTW results with the well-to-tank (WTT). The WTT takes into consideration the GHGs emitted during the extraction or cultivation of raw materials, processing, transportation, and other processes necessary to physically get the fuel into the fuel tank.

The levels of GHGs were expressed as grams of CO_2 equivalent (CO_{2eq}) emissions per MJ of fuel injected. This was required because of the higher global warming potentials (GWPs) for methane (CH_4) and nitrous oxide (N_2O) compounds, which have GWPs equivalent to 25 and 298 times that of the CO_2 over a time span of 100 years [37].

If one considers that the CO_2 emissions produced from bioethanol combustion can be absorbed by plants during photosynthesis [141,205], the TTW CO_{2eq} emissions for a bioethanol-diesel dual-fuel engine will be determined by those emitted from diesel combustion only as

$$TTW\ CO_{2eq} = 73.9\ (1 - EF) \tag{7.3}$$

from which the WTW CO_{2eq} were calculated as

$$WTW\ CO_{2eq} = [WTT_{diesel}(1 - EF) + WTT_{ethanol}EF] + TTW\ CO_{2eq} \tag{7.4}$$

where WTT_{diesel} is the WTT CO_{2eq} emissions for fossil diesel fuel of 15.4 g/MJ [142], and $WTT_{ethanol}$ is the WTT CO_{2eq} emissions for sugarcane ethanol of 24.8 g/MJ [142]. The $WTT_{ethanol}$ excluded GHG emissions produced by indirect land use change (iLUC) due to the uncertainty over the predictions [146,206,207] and the potential bonus if biomass is obtained from restored degraded land [143].

Figure 7.11 shows the theoretical TTW CO_{2eq} and WTW CO_{2eq} emissions for CDC and bioethanol-diesel dual-fuel operation. The lowest TTW CO_{2eq} emissions were attained at mid-loads under the dual-fuel mode, where both the net indicated efficiency and EF were maximised. As a result, the bioethanol-diesel dual-fuel combustion decreased the levels of WTW CO_{2eq} by up to 57% when compared with the 89.3 g/MJ for a CDC operation. The reductions in TTW CO_{2eq} and WTW CO_{2eq} emissions can help combat climate change and achieve a more sustainable energy source for the transport sector.

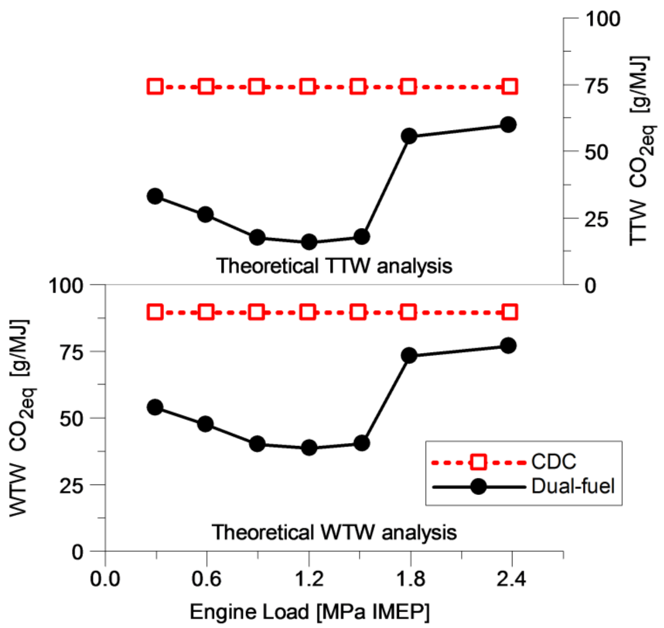

Figure 7.11 – Theoretical TTW CO_{2eq} and WTW CO_{2eq} emissions for optimised CDC and bioethanol-diesel dual-fuel operation.

7.3 Summary

In this chapter, experiments were performed to explore the ethanol-diesel dual-fuel combustion over different loads. The introduction of a premixed charge of ethanol was effective in reducing the well-to-wheels CO_2 equivalent emissions by up to 57% and the engine-out NOx emissions by up to 90% in comparison to a diesel-only operation. This can minimise the overall GHG emissions and the use of aqueous urea solution in the SCR system at the expense of higher volumetric fuel consumption. The adoption of optimised diesel injection strategies and EFs was a key enabler for controlling the PRRs while achieving high efficiency dual-fuel operation from low to full engine load.

Chapter 8

Conclusions and future work

After a review of experimental and modelling studies in the field of high efficiency compression ignition engines, experiments were performed on a single cylinder heavy-duty engine under diesel-only and ethanol-diesel dual-fuel combustion modes. Different fuel injection and engine control strategies were investigated to obtain high efficiency and low exhaust emissions dual-fuel operation. Alternative approaches were identified to overcome low, medium, and high load limitations and extend the dual-fuel operating range. The conclusions and the recommendations from this research are presented below.

8.1 Conclusions

A comparison with conventional diesel combustion (CDC) allowed for a better understanding of the overall requirements, potential, and limitations of the ethanol-diesel dual-fuel combustion, as mapped in Figure 8.1. Substantial reduction in engine-out NOx emissions was achieved with dual-fuel combustion when compared against a diesel-only operation. Moreover, tank-to-wheels and well-to-wheels analyses showed significant CO_2 reductions as ethanol was used as a partial substitute for diesel. In terms of performance, an optimised dual-fuel strategy attained higher net indicated efficiencies than the CDC mode between 0.6 and 2.4 MPa IMEP.

At light loads below 0.6 MPa IMEP, reduced in-cylinder temperatures and pressures allowed for the use of early diesel injections, resulting in long ignition delays and simultaneous low NOx and soot emissions. The lowest engine load of 0.3 MPa IMEP experienced a decrease in net indicated efficiency due to reduced combustion efficiency. This region of engine map also suffered from low exhaust gas temperatures caused by excessively lean and low temperature combustion. As a result, the effectiveness of the oxidation catalyst may be affected, possibly leading to no conversion of the CO and unburnt HC emissions [94]. Higher EGTs and combustion efficiencies were attained via intake throttling as well as when running the engine with higher internal or external exhaust gas recirculation [5]. However, these strategies can decrease the net indicated efficiency and lead to more challenge combustion control, especially during transient conditions.

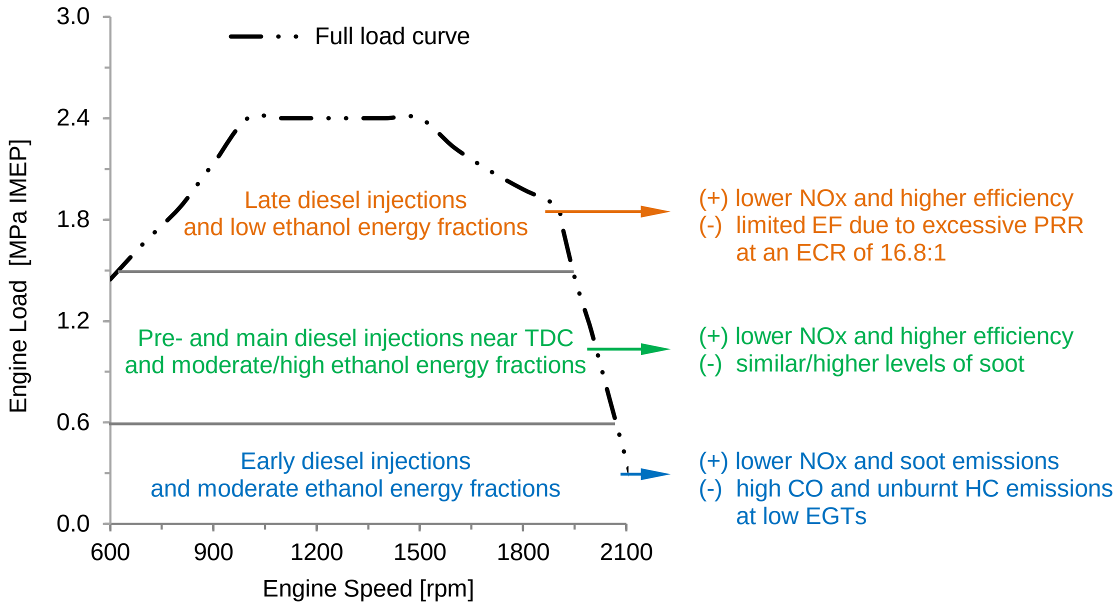

Figure 8.1 – Requirements and expected pros (+) and cons (-) of the ethanol-diesel dual-fuel operation compared to diesel-only combustion over an estimated HD engine speed-load map.

Higher ethanol energy fractions and a different diesel injection strategy were required to achieve an optimised dual-fuel operation as the engine load was increased to 1.5 MPa IMEP. A transition zone was observed between 0.6 MPa IMEP and approximately 1.0 MPa IMEP, where less diesel fuel could be partially premixed in order to avoid early ignition and excessive PRR. Therefore, the optimum mid-load dual-fuel combustion required a small diesel pre-injection prior to the main shot to minimise the levels of PRR and avoid pre-ignition/knock. A relatively higher degree of fuel stratification reduced the NOx and soot reduction benefit introduced by the dual-fuel operation at lighter loads. Nevertheless, the net indicated efficiencies were increased by up to 3% in comparison with diesel-only combustion.

The dual-fuel operation at high load conditions of 1.8 and 2.4 MPa IMEP was in-cylinder pressure limited. This required relatively lower ethanol percentages and later diesel injections when operating with the stock piston and compression ratio of 16.8:1. The use of high ethanol energy fractions led to unacceptable combustion noise as a result of early ethanol autoignition induced by the high in-cylinder gas temperatures and pressures at such conditions. Despite the limitations, fuel conversion efficiency was improved and NOx emissions were reduced. The utilisation of a Miller cycle strategy via LIVC events, lower intake air temperatures via an air-to-water charge air cooler, and wet ethanol effectively reduced the in-cylinder gas temperature during the compression stroke, extending the ethanol energy fraction limit.

Therefore, the dual-fuel combustion with a low carbon fuel such as ethanol is an effective means of decreasing petroleum dependence, reducing GHG emissions, and lowering the engine-out NOx emissions. The fuel flexibility combined with a high efficiency dual-fuel operation can also decrease the running costs of future compression ignition engines. Moreover, lower NOx emissions can improve the cost effectiveness of the dual-fuel technology via reduced consumption of aqueous urea solution in the exhaust aftertreatment system required to meet stringent emissions regulations.

Ultimately, the operational cost remains heavily dependent on the relative price ratio between diesel and ethanol fuels as well as on the cost of aqueous urea solution. In addition, the practical application on a heavy-duty engine would have to weigh the advantages of the dual-fuel combustion against the additional complexity and upfront cost of a port fuel injection system and extra fuel tank, the sensitivity to variations in intake air temperature, as well as the vehicle operator requiring additional ethanol fuel. These factors will decide whether ethanol-diesel dual-fuel combustion can be successfully introduced to the heavy-duty market.

8.2 Recommendations for future work

From the present study, it is concluded that there is scope for further improvements in the ethanol-diesel dual-fuel operation as follows:

- Experiments should be performed at other engine speeds and loads on a multi-cylinder turbocharged engine in order to explore the actual emissions and efficiency benefits introduced by the dual-fuel combustion mode.
- More research into a step-load transient operating condition as well as cycle-to-cycle control is necessary.
- The effects of lower exhaust gas temperatures and higher exhaust gas mass flow rates on the boosting and aftertreatment systems need to be investigated.
- The higher unburnt HC and CO emissions will likely require the development of high efficiency and low temperature oxidation catalysts [79,94,202].
- An optimised piston design with less surface area can potentially minimise heat transfer losses at risk of impairing combustion efficiency at certain engine loads [208,209].
- Investigate the particulate number and size distribution for ethanol-diesel dual-fuel operation and conventional diesel combustion.

- If implemented, the dual-fuel technology will require investigation into the startability and combustion stability in cold weather as well as design of appropriate volumes for the diesel and ethanol fuel tanks.
- A dual direct injection system [125] can possibly enhance the in-cylinder charge cooling effect introduced by the ethanol fuel. This might allow for the use of higher ethanol energy fractions at high engine loads.
- Intake valve re-opening and/or late intake valve closing strategies would likely require the installation of a variable valve actuation system. Alternatively, fixed intake camshaft timing could be designed. However, this approach can cause a decrease in net indicated efficiency at some speed and load conditions due to a greater demand on the boosting system (e.g. high pressure ratio) to maintain the desired fuel/air equivalence ratio.
- The effect of wet ethanol injection on dual-fuel engine efficiency and exhaust emissions should be explored at other engine loads.

Appendix A – Measurement device specification

Measured Variable	Device	Manufacturer	Dynamic Range	Linearity/ Accuracy	Repeatability
CO (low content)	AIA-721A	Horiba MEXA 7170 DEGR	0-2.5k ppm	≤ ± 1.0% FS or ± 2.0% of readings	Within ± 0.5% of full scale (FS)
CO (mid-high content)	AIA-722		0-12 vol%		
CO_2	AIA-722		0-20 vol%		
NOx	CLA-720MA		0-500 ppm or 0-10k ppm		
O_2	MPA-720		0-25 vol%		
Unburnt HC	FIA-725A		0-500 ppm or 0-50k ppm		
Diesel injector current signal	Current Probe PR30	LEM	0-20 A	± 1% of reading ± 2 mA	
Diesel flow rate (return)	PROline promass 83A DN01	Endress+ Hauser	0-100 kg/h	± 0.10% of reading	± 0.05% of reading
Diesel flow rate (supply)	PROline promass 83A DN02		0-20 kg/h	± 0.10% of reading	
Ethanol flow rate	PROline promass 80A DN02		0-100 kg/h	± 0.15% of reading	
Intake and exhaust pressures	Piezoresistive pressure sensor Type 4049A Amplifier Type 4622A	Kistler	0-1 MPa	≤ ± 0.50% of FS within 0-353 K	
In-cylinder pressure	Piezoelectric pressure sensor Type 6125C	Kistler	0-30 MPa	≤ ± 0.40% of FS	
	Amplifier FI Piezo	AVL		≤ ± 0.01% of FS	
Intake valve lift	S-DVRT-24 Displacement Sensor DEMOD-DVRT-TC conditioner	LORD MicroStrain	0-24 mm	± 1% of reading using straight line	± 1.0 µm
Intake air mass flow rate	Proline t-mass 65F	Endress+ Hauser	0-910 kg/h	± 1.5% of reading (10 to 100% of FS)	±0.5% of reading
Oil and ethanol pressure	Pressure transducer UNIK 5000	GE	0-1 MPa	< ±0.20% of FS	
Filter Smoke Number	415SE	AVL	0-10 FSN	-	Within ± 0.005 FSN + 3% of reading
Engine speed	AG150 Dynamometer	Froude Hofmann	0-8000 rpm	± 1 rpm	
Engine torque			0-500 Nm	± 0.25% of FS	
Temperature	Thermocouple K Type (Class 2)	RS	233-1473 K	≤ ± 2.5 K or ± 0.75% of readings	

Appendix B – Diesel fuel specification

PHILLIPS 66 LIMITED / JET :- UK MARKETING SPECIFICATION

SULPHUR FREE (MAXIMUM 10 PPM) GAS OIL TO BS 2869:2010-PART 1: CLASS A2

PROPERTY & UNITS	LIMIT		TEST METHOD Note (1)
Appearance		Free from visible water and sediment	Visual
Colour		Red	Visual
Odour		Merchantable	
Density @ 15C (kg/m3)	Typical Range	820.0 - 875.0	BS EN ISO 3675 / 12185
Cold Filter Plugging Point			BS EN 116
Winter C (Note 2)	Max	-12	
Summer C (Note 2)	Max	-4	
Cloud Point			ASTM D2500 / IP219
Winter C (Note 2)	Max	-2	
Summer C (Note 2)	Max	+3	
Flash Point (PMCC) C	Min	56	BS EN ISO 2719
Cetane Number / DCN	Min	45.0 (Note 5)	BS EN ISO 5165 / BS 2000-498
or Cetane Index	Min	45.0 (Note 5)	BS EN ISO 4264
Kinematic viscosity mm2/s @ 40C	Min - max	2.00 - 5.00	BS EN ISO 3104
Sulphur content (mg/kg)			
At point of manufacture	Max	10 (Note 8)	BS EN ISO 20846 / 20884
At point of distribution to end user	Max	20 (Note 8)	
Copper Corrosion (3 Hr @ 50C)	Class	1	BS EN ISO 2160
Carbon Residue (micro) :- Residue wt% on 10% Bottoms	Max	0.30	BS EN ISO 10370
Ash content % (m/m)	Max	0.01	BS EN ISO 6245
Particulate content (mg/kg)	Max	24	IP 415
Water content (mg/kg)	Max	200	BS EN ISO 12937
Distillation C			BS EN ISO 3405
% Vol Rec @ 350C	Min	85	
% Vol Rec @ 250C	Max	65	
50% Vol Recovered (Note 3)	Range	240 - 340	
Strong Acid Number (mgKOH/g)		Zero	BS ISO 6618
Lubricity (wear scar dia, micron)	Max	460	BS 2000 - 450
Oxidation stability			
0.0% - 7.0% FAME g/m3 (Note 6)	Max	25	BS 2000-388
2.0% - 7.0% FAME h	Min	20	BS EN 15751
FAME content (%v/v) (Note7)	Max	7.0	BS EN 14078

Notes.

1) Latest Test Methods or technical equivalent used

2) Unless otherwise advised the following seasonal dates apply ex refinery or import terminal:-
Summer : 16 March - 15 October inc
Winter : 16 October - 15 March inc
Winter : 01 November - 15 March inc for delivery from terminals

3) 50 % evaporated is an HMRC requirement.

4) Product will be marked with HMR&C statutory marker

5) May contain an ignition improver in which case
(i) the carbon residue test is not valid and
(ii) the cetane number minimum will apply.

6) This test applies to all fuels, additional Rancimat only applies to those fuels containing > 2.00% FAME

7) FAME must meet BS EN 14214

8) 10/20 ppm sulphur limits applicable from 1 January 2011

THIS SPECIFICATION IS ACCURATE AT THE DATE OF ISSUE, AND SUPERSEDES ALL PREVIOUS ISSUES.

PQ Issue 6 : July 2012

Appendix C – Diesel fuel analysis

Intertek Sunbury Technology Centre

ITS Testing Services (UK) Ltd
Sunbury Technology Centre
Unit 'A' Shears Way
Brooklands Close
Sunbury-on-Thames
Middlesex TW16 7EE
Tel : 01932 73 2100
Fax : 01932 73 2113

To:	John Williams BP Global Fuels Technology Castrol Technology Centre Whitchurch Hill Pangbourne Reading RG8 7QR	**Report No.** **Date:** Phoenix No. Order No. Quote No. Date Sample(s) Received Total Cost for Analysis	RT/FLS/5142 06/10/2014 UK760-0017458 4500083403 Email 08/09/2014 £394.00

Diesel Analysis Report

Lab Sample No: FST-264556
Sample Description: Brunel University Diesel sample

ANALYSIS	RESULTS	UNITS
D5291 (MT/ELE/13) Carbon Content	86.3	% wt/wt
D5291 (MT/ELE/13) Hydrogen Content	13.2	% wt/wt
D5622 (MT/ELE/21) Oxygen Content*	0.16	% wt/wt
IP12 Gross Calorific Value#	45.58	MJ/kg

* Test not UKAS accredited
# Test carried out an another Intertek Laboratory

Analysis has been carried out on samples as received, independent of sampling procedure, using the latest versions of all test methods. Samples will be disposed of after 1 month unless alternative arrangements have been made in agreement with the customer.

Reported By: A. Shadrake
Alison Shadrake
Fuels Analyst

Checked By: J.A. Amero
James Amero
Section Head, Fuels and Lubricants

Contact No.: +44(0)1932 732 157

Appendix D – Ethanol fuel specification

Haymankimia

Ethanol 100% BP/EP

This Product has been tested and conforms to the current BP 2017 / EP 9.0 monographs.

Definition	Content: NLT 99.5% V/V @ 20 °C	
Characteristics Appearance Solubility Boiling Point	Colourless, clear, volatile, flammable liquid, hygroscopic Miscible with water & methylene chloride It burns with a blue, smokeless flame About 78 °C	
Identification	Relative density: 0.790 – 0.793 Infrared Absorption	
Acidity or Alkalinity	The solution is pink (30 ppm, expressed as acetic acid)	
Absorbance (5cm Cell)	240 nm 250-260 nm 270-340 nm	NMT 0.40 NMT 0.30 NMT 0.10
	Spectrum shows steadily descending curve with no peaks or shoulders	
Volatile impurities (V/V)	Methanol Acetaldehyde and acetal Benzene Total of other impurities Disregard limit	NMT 200 ppm NMT 10 ppm, expressed as acetaldehyde NMT 2 ppm NMT 300 ppm NMT 9 ppm
Residue on evaporation	NMT 25 ppm m/V	

Haymankimia Ethanol 100% BP/EP is tested beyond these criteria as follows:

Strength	NLT 99.9% V/V @ 20 °C
Water Content	NMT 0.1%

List of references

[1] Pedrozo VB, Zhao H. Improvement in high load ethanol-diesel dual-fuel combustion by Miller cycle and charge air cooling. Applied Energy 2018;210:138–51. doi:10.1016/j.apenergy.2017.10.092.

[2] Pedrozo VB, Lanzanova TDM, Zhao H. The effects of wet ethanol injection and Miller cycle on a heavy-duty diesel engine operating at full load. Internal Combustion Engines Conference 2017 - IMechE 2017.

[3] Pedrozo VB, May I, Zhao H. Exploring the mid-load potential of ethanol-diesel dual-fuel combustion with and without EGR. Applied Energy 2017;193:263–75. doi:10.1016/j.apenergy.2017.02.043.

[4] Pedrozo VB, May I, Guan W, Zhao H. Efficient ethanol-diesel dual-fuel combustion: A comparison with conventional diesel combustion. 13th International Congress on Engine Combustion Processes (ENCOM 2017) 2017.

[5] Pedrozo VB, May I, Lanzanova TDM, Zhao H. Potential of internal EGR and throttled operation for low load extension of ethanol–diesel dual-fuel reactivity controlled compression ignition combustion on a heavy-duty engine. Fuel 2016;179:391–405. doi:10.1016/j.fuel.2016.03.090.

[6] Pedrozo VB, May I, Zhao H. Characterization of Low Load Ethanol Dual-Fuel Combustion using Single and Split Diesel Injections on a Heavy-Duty Engine. SAE Technical Paper 2016. doi:10.4271/2016-01-0778.

[7] Pedrozo VB, May I, Dalla Nora M, Cairns A, Zhao H. Experimental analysis of ethanol dual-fuel combustion in a heavy-duty diesel engine: An optimisation at low load. Applied Energy 2016;165:166–82. doi:10.1016/j.apenergy.2015.12.052.

[8] Heywood JB. Internal Combustion Engine Fundamentals. First Ed. McGraw-Hill, Inc.; 1988.

[9] Stone R. Introduction to Internal Combustion Engines. Fourth Ed. Palgrave; 2012.

[10] Delgado O, Lutsey N. The U.S. SuperTruck Program: Expediting the development of advanced heavy-duty vehicle efficiency technologies. The ICCT White Paper 2014.

[11] Inagaki K, Fuyuto T, Nishikawa K, Nakakita K, Sakata I. Dual-Fuel PCI Combustion Controlled by In-Cylinder Stratification of Ignitability. SAE Technical Paper 2006;01. doi:doi:10.4271/2006-01-0028.

[12] Exxon Mobil Corporation. 2017 Outlook for Energy: A View to 2040. Irving, Texas: 2017.

[13] U.S. Energy Information Agency. International Energy Outlook 2016. Washington, DC: 2016.

[14] Intergovernmental Panel on Climate Change (IPCC). Climate Change 2014 - Synthesis Report. IPCC Fifth Assessment Report 2015:1–112.

[15] United States Environmental Protection Agency. Climate Change Indicators: Atmospheric Concentrations of Greenhouse Gases. EPA's Climate Change Indicators 2016. https://www.epa.gov/climate-indicators/climate-change-indicators-atmospheric-concentrations-greenhouse-gases (accessed July 4, 2017).

[16] GISTEMP Team. GISS Surface Temperature Analysis (GISTEMP). NASA Goddard Institute for Space Studies 2017. https://data.giss.nasa.gov/gistemp/ (accessed July 4, 2017).

[17] United Nations Framework Convention on Climate Change. Paris Agreement - Status of Ratification. UNFCCC 2017. http://unfccc.int/paris_agreement/items/9444.php (accessed July 5, 2017).

[18] United Nations Framework Convention on Climate Change. Paris Agreement. UNFCCC 2015.

[19] Miller JD, Façanha C. The state of clean transport policy - A 2014 synthesis of vehicle and fuel policy developments. The ICCT Report 2014:73.

[20] Kodjak D. Policies to reduce fuel consumption, air pollution, and carbon emissions from vehicles in G20 nations. The ICCT Briefing Paper 2015:28.

[21] World Health Organization. WHO Air quality guidelines for particulate matter, ozone, nitrogen dioxide and sulfur dioxide. 2006.

[22] World Health Organization. Global health risks - Mortality and burden of disease attributable to selected major risks. Genova: 2009.

[23] European Environment Agency. Air quality in Europe — 2014 report. Copenhagen: 2015. doi:10.2800/92843.

[24] Williams M, Minjares R. A technical summary of Euro 6/VI vehicle emission standards. The ICCT Briefing Paper 2016.

[25] The European Parliament and the Council of the European Union. Regulation (EC) No 595/2009. Official Journal of the European Union 2009;188.

[26] The European Parliament and the Council of the European Union. Commission Regulation (EU) No 582/2011. Official Journal of the European Union 2011;167.

[27] The European Parliament and the Council of the European Union. Commission Regulation (EU) No 133/2014. Official Journal of the European Union 2014;47.

[28] EUR-Lex. Emissions from heavy duty vehicles (Euro VI): certification rules. Access to European Union Law n.d. http://eur-lex.europa.eu/legal-content/EN/TXT/?uri=URISERV:mi0029 (accessed July 6, 2017).

[29] Economic Commission for Europe of the United Nations (UN/ECE). Regulation No 49 - Uniform provisions concerning the measures to be taken against the emission of gaseous and particulate pollutants from compression-ignition engines

and positive ignition engines for use in vehicles. Official Journal of the European Union 2013;171.

[30] Posada F, Chambliss S, Blumberg K. Costs of emission reduction technologies for heavy-duty diesel vehicles. The ICCT White Paper 2016.

[31] Delgado O, Rodríguez F, Muncrief R. Fuel Efficiency Technology in European Heavy-Duty Vehicles: Baseline and Potential for the 2020-2030 Time Frame. The ICCT White Paper 2017.

[32] Miller J, Du L, Kodjak D. Impacts of World-Class Vehicle Efficiency and Emissions Regulations in Select G20 Countries. The ICCT Briefing Paper 2017.

[33] Environmental Protection Agency (EPA) - National Highway Traffic Safety Administration (NHTSA) - Department of Transportation (DOT). Greenhouse Gas Emissions and Fuel Efficiency Standards for Medium- and Heavy-Duty Engines and Vehicles - Phase 2. Federal Register - Rules and Regulations 2016;81.

[34] Environmental Protection Agency (EPA) - National Highway Traffic Safety Administration (NHTSA) - Department of Transportation (DOT). Greenhouse Gas Emissions and Fuel Efficiency Standards for Medium- and Heavy-Duty Engines and Vehicles. Federal Register - Rules and Regulations 2011;76.

[35] The European Parliament and the Council of the European Union. Regulation (EC) No 1999/96/EC. Official Journal of the European Union 1999;44.

[36] The International Council on Clean Transportation. United States Efficiency and Greenhouse Gas Emission Regulations for Model Year 2018-2027 Heavy-Duty Vehicles, Engines, and Trailers. The ICCT Policy Updates 2016.

[37] Intergovernmental Panel on Climate Change (IPCC). Climate Change 2007: The Physical Science Basis. Contribution of Working Group I to the Fourth Assessment Report of the Intergovernmental Panel on Climate Change 2007.

[38] Intergovernmental Panel on Climate Change (IPCC). Climate Change 2007 - Synthesis Report. IPCC Fourth Assessment Report 2007:104.

[39] Environmental Protection Agency (EPA). 40 CFR 86.007–11 - Emission standards and supplemental requirements for 2007 and later model year diesel heavy-duty engines and vehicles. Code of Federal Regulations 2003.

[40] Johnson T, Joshi A. Review of Vehicle Engine Efficiency and Emissions. SAE Technical Paper 2017. doi:10.4271/2017-01-0907.

[41] Reitz RD. Directions in internal combustion engine research. Combustion and Flame 2013;160:1–8. doi:10.1016/j.combustflame.2012.11.002.

[42] Görsmann C. Improving air quality while reducing the emission of greenhouse gases. Johnson Matthey Technology Review 2015;59:139–51. doi:10.1595/205651315X687524.

[43] O'Connor J, Borz M, Ruth D, Han J, Paul C, Imren A, et al. Optimization of an Advanced Combustion Strategy Towards 55% BTE for the Volvo SuperTruck

Program. SAE International Journal of Engines 2017;10:2017–01 – 0723. doi:10.4271/2017-01-0723.

[44] Stanton D, Charlton S, Vajapeyazula P. Diesel Engine Technologies Enabling Powertrain Optimization to Meet U.S. Greenhouse Gas Emissions. SAE International Journal of Engines 2013;6. doi:10.4271/2013-24-0094.

[45] Liu J, Wang H, Zheng Z, Zou Z, Yao M. Effects of Different Turbocharging Systems on Performance in a HD Diesel Engine with Different Emission Control Technical Routes. SAE Technical Paper 2016. doi:10.4271/2016-01-2185.

[46] Dallmann T, Menon A. Technology Pathways for Diesel Engines Used in Non-Road Vehicles and Equipment. The ICCT White Paper 2016.

[47] Chatterjee S, Naseri M, Li J. Heavy Duty Diesel Engine Emission Control to Meet BS VI Regulations. SAE Technical Paper 2017. doi:10.4271/2017-26-0125.

[48] Johnson T V. Diesel Emissions in Review. SAE International Journal of Engines 2011;4. doi:10.4271/2011-01-0304.

[49] Kamm S, Schraml S, MAN Truck & Bus AG. Future Requirements & Challenges on Aftertreatment of Heavy Duty Diesel Engines Future Requirements & Challenges. Presentation at SAE 2016 Heavy-Duty Diesel Emissions Control Symposium, Gothenburg: 2016.

[50] Zhao H. Advanced direct injection combustion engine technologies and development - Volume 2: Diesel engines. Cambridge: Woodhead Publishing Limited; 2010.

[51] Charlton S, Dollmeyer T, Grana T. Meeting the US Heavy-Duty EPA 2010 Standards and Providing Increased Value for the Customer. SAE International Journal of Commercial Vehicles 2010;3. doi:10.4271/2010-01-1934.

[52] Stanton DW. Systematic Development of Highly Efficient and Clean Engines to Meet Future Commercial Vehicle Greenhouse Gas Regulations. SAE International Journal of Engines 2013;6. doi:10.4271/2013-01-2421.

[53] López - De Jesús YM, Chigada PI, Watling TC, Arulraj K, Thorén A, Greenham N, et al. NOx and PM Reduction from Diesel Exhaust Using Vanadia SCRF®. SAE International Journal of Engines 2016;9:2016–01 – 0914. doi:10.4271/2016-01-0914.

[54] Walker A, Johnson Matthey. Catalyst-Based Emission Control Solutions for the Global HDD Market – What Does the Future Hold? Presentation at SAE 2016 Heavy-Duty Diesel Emissions Control Symposium, Gothenburg: 2016.

[55] Hanson R, Ickes A, Wallner T. Comparison of RCCI Operation with and without EGR over the Full Operating Map of a Heavy-Duty Diesel Engine. SAE Technical Paper 2016. doi:10.4271/2016-01-0794.

[56] Dec JE. A conceptual model of DI diesel combustion based on laser sheet imaging. SAE Technical Paper 1997. doi:10.4271/970873.

[57] Kokjohn SL, Hanson RM, Splitter D a, Reitz RD. Fuel reactivity controlled compression ignition (RCCI): a pathway to controlled high-efficiency clean combustion. International Journal of Engine Research 2011;12:209–26. doi:10.1177/1468087411401548.

[58] Musculus MPB, Miles PC, Pickett LM. Conceptual models for partially premixed low-temperature diesel combustion. Progress in Energy and Combustion Science 2013;39. doi:10.1016/j.pecs.2012.09.001.

[59] Iwabuchi Y, Kawai K, Shoji T, Takeda Y. Trial of New Concept Diesel Combustion System - Premixed Compression-Ignited Combustion -. SAE Technical Paper 1999. doi:10.4271/1999-01-0185.

[60] Imtenan S, Varman M, Masjuki HH, Kalam M a., Sajjad H, Arbab MI, et al. Impact of low temperature combustion attaining strategies on diesel engine emissions for diesel and biodiesels: A review. Energy Conversion and Management 2014;80. doi:10.1016/j.enconman.2014.01.020.

[61] Asad U, Zheng M, Ting DS-K, Tjong J. Implementation Challenges and Solutions for Homogeneous Charge Compression Ignition Combustion in Diesel Engines. Journal of Engineering for Gas Turbines and Power 2015;137. doi:10.1115/1.4030091.

[62] Bendu H, Murugan S. Homogeneous charge compression ignition (HCCI) combustion: Mixture preparation and control strategies in diesel engines. Renewable and Sustainable Energy Reviews 2014;38. doi:10.1016/j.rser.2014.07.019.

[63] Yao M, Zheng Z, Liu H. Progress and recent trends in homogeneous charge compression ignition (HCCI) engines. Progress in Energy and Combustion Science 2009;35:398–437. doi:10.1016/j.pecs.2009.05.001.

[64] Neely GD, Sasaki S, Huang Y, Leet J a, Stewart DW. New Diesel Emission Control Strategy to Meet US Tier 2 Emissions Regulations. SAE Technical Paper 2005. doi:10.4271/2005-01-1091.

[65] Kook S, Bae C. Combustion Control Using Two-Stage Diesel Fuel Injection in a Single-Cylinder PCCI Engine. SAE Technical Paper 2004. doi:10.4271/2004-01-0938.

[66] Kook S, Bae C, Miles PC, Choi D, Pickett LM. The Influence of Charge Dilution and Injection Timing on Low-Temperature Diesel Combustion and Emissions. SAE Technical Paper 2005. doi:10.4271/2005-01-3837.

[67] Opat R, Ra Y, Gonzalez D. MA, Krieger R, Reitz RD, Foster DE, et al. Investigation of Mixing and Temperature Effects on HC/CO Emissions for Highly Dilute Low Temperature Combustion in a Light Duty Diesel Engine. SAE Technical Paper 2007. doi:10.4271/2007-01-0193.

[68] Kimura S, Aoki O, Ogawa H, Muranaka S, Enomoto Y. New Combustion Concept for Ultra-Clean and High-Efficiency Small DI Diesel Engines. SAE Technical Paper 1999. doi:10.4271/1999-01-3681.

[69] Hasegawa R, Yanagihara H. HCCI Combustion in DI Diesel Engine. SAE Technical Paper 2003. doi:10.4271/2003-01-0745.

[70] Sellnau M, Foster M, Hoyer K, Moore W, Sinnamon J, Husted H. Development of a Gasoline Direct Injection Compression Ignition (GDCI) Engine. SAE International Journal of Engines 2014;7:835–51. doi:10.4271/2014-01-1300.

[71] Sellnau M, Moore W, Sinnamon J, Hoyer K, Foster M, Husted H. GDCI Multi-Cylinder Engine for High Fuel Efficiency and Low Emissions. SAE International Journal of Engines 2015;8. doi:10.4271/2015-01-0834.

[72] Kalghatgi GT, Risberg P, Ångström H-E. Partially Pre-Mixed Auto-Ignition of Gasoline to Attain Low Smoke and Low NOx at High Load in a Compression Ignition Engine and Comparison with a Diesel Fuel. SAE Technical Paper 2007. doi:10.4271/2007-01-0006.

[73] Manente V, Zander C, Johansson B, Tunestal P, Cannella W. An Advanced Internal Combustion Engine Concept for Low Emissions and High Efficiency from Idle to Max Load Using Gasoline Partially Premixed Combustion. SAE Technical Paper 2010. doi:10.4271/2010-01-2198.

[74] Manente V, Johansson B, Cannella W. Gasoline partially premixed combustion, the future of internal combustion engines? International Journal of Engine Research 2011;12:194–208. doi:10.1177/1468087411402441.

[75] Manente V, Johansson B, Tunestal P. Characterization of Partially Premixed Combustion With Ethanol: EGR Sweeps, Low and Maximum Loads. Journal of Engineering for Gas Turbines and Power 2010;132. doi:10.1115/1.4000291.

[76] Shen M, Tuner M, Johansson B, Cannella W. Effects of EGR and Intake Pressure on PPC of Conventional Diesel, Gasoline and Ethanol in a Heavy Duty Diesel Engine. SAE Technical Paper 2013;01. doi:10.4271/2013-01-2702.

[77] Shen M, Tuner M, Johansson B. Close to Stoichiometric Partially Premixed Combustion - The Benefit of Ethanol in Comparison to Conventional Fuels. SAE Technical Paper 2013. doi:10.4271/2013-01-0277.

[78] Kaiadi M, Johansson B, Lundgren M, Gaynor J a. Experimental Investigation on different Injection Strategies for Ethanol Partially Premixed Combustion. SAE Technical Paper 2013. doi:10.4271/2013-01-0281.

[79] Reitz RD, Duraisamy G. Review of high efficiency and clean reactivity controlled compression ignition (RCCI) combustion in internal combustion engines. Progress in Energy and Combustion Science 2015;46:12–71. doi:10.1016/j.pecs.2014.05.003.

[80] Benajes J, Molina S, García A, Belarte E, Vanvolsem M. An investigation on RCCI combustion in a heavy duty diesel engine using in-cylinder blending of diesel and gasoline fuels. Applied Thermal Engineering 2014;63:66–76. doi:10.1016/j.applthermaleng.2013.10.052.

[81] Kokjohn SL, Hanson R, Splitter D, Kaddatz J, Reitz RD. Fuel Reactivity Controlled Compression Ignition (RCCI) Combustion in Light- and Heavy-Duty

Engines. SAE International Journal of Fuels and Lubricants 2011;4. doi:10.4271/2011-01-0357.

[82] Li J, Yang W, Zhou D. Review on the management of RCCI engines. Renewable and Sustainable Energy Reviews 2017;69:65–79. doi:10.1016/j.rser.2016.11.159.

[83] Han X, Zheng M, Tjong J. Clean combustion enabling with ethanol on a dual-fuel compression ignition engine. International Journal of Engine Research 2015:1–13. doi:10.1177/1468087415575646.

[84] Divekar P, Yang Z, Ting D, Chen X, Zheng M, Tjong J. Efficiency and Emission Trade-Off in Diesel-Ethanol Low Temperature Combustion Cycles. SAE Technical Paper 2015. doi:10.4271/2015-01-0845.

[85] Molina S, García a., Pastor JM, Belarte E, Balloul I. Operating range extension of RCCI combustion concept from low to full load in a heavy-duty engine. Applied Energy 2015;143:211–27. doi:10.1016/j.apenergy.2015.01.035.

[86] Benajes J, García A, Monsalve-Serrano J, Boronat V. Achieving clean and efficient engine operation up to full load by combining optimized RCCI and dual-fuel diesel-gasoline combustion strategies. Energy Conversion and Management 2017;136:142–51. doi:10.1016/j.enconman.2017.01.010.

[87] Kokjohn SL, Musculus MPB, Reitz RD. Evaluating temperature and fuel stratification for heat-release rate control in a reactivity-controlled compression-ignition engine using optical diagnostics and chemical kinetics modeling. Combustion and Flame 2015;162:2729–42. doi:10.1016/j.combustflame.2015.04.009.

[88] Desantes JM, Benajes J, García A, Monsalve-Serrano J. The role of the in-cylinder gas temperature and oxygen concentration over low load reactivity controlled compression ignition combustion efficiency. Energy 2014;78:854–68. doi:10.1016/j.energy.2014.10.080.

[89] Asad U, Kumar R, Zheng M, Tjong J. Ethanol-fueled low temperature combustion: A pathway to clean and efficient diesel engine cycles. Applied Energy 2015. doi:10.1016/j.apenergy.2015.01.057.

[90] Divekar PS, Asad U, Tjong J, Chen X, Zheng M. An engine cycle analysis of diesel-ignited ethanol low-temperature combustion. Proceedings of the Institution of Mechanical Engineers, Part D: Journal of Automobile Engineering 2015. doi:10.1177/0954407015598244.

[91] Júnior RFB, Martins CA. Emissions analysis of a diesel engine operating in Diesel-Ethanol Dual-Fuel mode. Fuel 2014;148:191–201. doi:10.1016/j.fuel.2014.05.010.

[92] Ogawa H, Shibata G, Kato T, Zhao P. Dual Fuel Diesel Combustion with Premixed Ethanol as the Main Fuel. SAE Technical Paper 2014:2014–01 – 2687. doi:10.4271/2014-01-2687.

[93] Wang Y, Yao M, Li T, Zhang W, Zheng Z. A parametric study for enabling reactivity controlled compression ignition (RCCI) operation in diesel engines at

various engine loads. Applied Energy 2016;175:389–402. doi:10.1016/j.apenergy.2016.04.095.

[94] Prikhodko VY, Curran SJ, Parks JE, Wagner RM. Effectiveness of Diesel Oxidation Catalyst in Reducing HC and CO Emissions from Reactivity Controlled Compression Ignition. SAE International Journal of Fuels and Lubricants 2013;6. doi:10.4271/2013-01-0515.

[95] Sarjovaara T, Larmi M, Vuorinen V. Effect of charge air temperature on E85 dual-fuel diesel combustion. Fuel 2015;153:6–12. doi:10.1016/j.fuel.2015.02.096.

[96] Mayer A, Lutz T, Lämmle C, Wyser M, Legerer F. Engine Intake Throttling for Active Regeneration of Diesel particle. SAE Technical Paper 2003. doi:10.4271/2003-01-0381.

[97] Splitter DA, Reitz RD. Fuel reactivity effects on the efficiency and operational window of dual-fuel compression ignition engines. Fuel 2014;118. doi:10.1016/j.fuel.2013.10.045.

[98] Jung D, Iida N. Closed-loop control of HCCI combustion for DME using external EGR and rebreathed EGR to reduce pressure-rise rate with combustion-phasing retard. Applied Energy 2015;138:315–30. doi:10.1016/j.apenergy.2014.10.085.

[99] Sellnau MC, Sinnamon J, Hoyer K, Husted H. Full-Time Gasoline Direct-Injection Compression Ignition (GDCI) for High Efficiency and Low NOx and PM. SAE International Journal of Engines 2012;5:300–14. doi:10.4271/2012-01-0384.

[100] Balaji J, V GPM, Rao LN, Bandaru B. Modelling and Experimental Study of Internal EGR System for NOx Control on an Off-Road Diesel Engine. SAE Technical Paper 2014. doi:10.4271/2014-01-2645.

[101] Cairns A, Blaxill H. The Effects of Combined Internal and External Exhaust Gas Recirculation on Gasoline Controlled Auto-Ignition. SAE Technical Paper 2005. doi:10.4271/2005-01-0133.

[102] Fessler H, Genova M. An Electro-Hydraulic “Lost Motion” VVA System for a 3.0 Liter Diesel Engine. SAE Technical Paper 2004. doi:10.4271/2004-01-3018.

[103] Schwoerer J, Dodi S, Fox M, Huang S, Yang Z. Internal EGR Systems for NOx Emission Reduction in Heavy-Duty Diesel Engines. SAE Technical Paper 2004. doi:10.4271/2004-01-1315.

[104] Gehrke S, Weiskirch C, Eilts P. Development and Implementation of a Variable Valve Actuation System to a HD Diesel Engine. SAE Technical Paper 2008. doi:10.4271/2008-01-1359.

[105] Schwoerer J, Kumar K, Ruggiero B, Swanbon B. Lost-Motion VVA Systems for Enabling Next Generation Diesel Engine Efficiency and After-Treatment Optimization. SAE Technical Paper 2010. doi:10.4271/2010-01-1189.

[106] Kawasaki K, Hirota K, Nagata S, Yamane K, Ohtsubo H, Nakazono T. Improvement of Natural-gas HCCI Combustion by Internal EGR by Means of Exhaust Valve Re-opening. SAE International Journal of Engines 2009;2. doi:10.4271/2009-32-0079.

[107] Dalla Nora M, Zhao H. High load performance and combustion analysis of a four-valve direct injection gasoline engine running in the two-stroke cycle. Applied Energy 2015;159:117–31. doi:10.1016/j.apenergy.2015.08.122.

[108] Borgqvist P, Tunestal P, Johansson B. Comparison of Negative Valve Overlap (NVO) and Rebreathing Valve Strategies on a Gasoline PPC Engine at Low Load and Idle Operating Conditions. SAE Technical Paper 2013. doi:10.4271/2013-01-0902.

[109] Gehrke S, Kovács D, Eilts P, Rempel A, Eckert P. Investigation of VVA-Based Exhaust Management Strategies by Means of a HD Single Cylinder Research Engine and Rapid Prototyping Systems. SAE Technical Paper 2013. doi:10.4271/2013-01-0587.

[110] Bharath AN, Kalva N, Reitz RD, Rutland CJ. Use of early exhaust valve opening to improve combustion efficiency and catalyst effectiveness in a multi-cylinder RCCI engine system – A simulation study. Internal Combustion Engine Division Fall Technical Conference 2014;5534:1–10. doi:doi:10.1115/ICEF2014-5534.

[111] Roberts L, Magee M, Shaver G, Garg a., McCarthy J, Koeberlein E, et al. Modeling the impact of early exhaust valve opening on exhaust aftertreatment thermal management and efficiency for compression ignition engines. International Journal of Engine Research 2014;16:773–94. doi:10.1177/1468087414551616.

[112] Benajes J, Reyes E, Lujan JM. Intake Valve Pre-lift Effect on the Performance of a Turbocharged Diesel Engine. SAE Technical Paper 1996. doi:10.4271/960950.

[113] Zhang X, Wang H, Zheng Z, Reitz RD, Yao M. Effects of late intake valve closing (LIVC) and rebreathing valve strategies on diesel engine performance and emissions at low loads. Applied Thermal Engineering 2016;98:310–9. doi:10.1016/j.applthermaleng.2015.12.045.

[114] Edwards SP, Frankle GR, Wirbeleit F, Raab A. The Potential of a Combined Miller Cycle and Internal EGR Engine for Future Heavy Duty Truck Applications. SAE Technical Paper 1998. doi:10.4271/980180.

[115] Heuser B, Kremer F, Pischinger S, Rohs H, Holderbaum B, Körfer T. An Experimental Investigation of Dual-Fuel Combustion in a Light Duty Diesel Engine by In-Cylinder Blending of Ethanol and Diesel. SAE International Journal of Engines 2015;9:2015–01 – 1801. doi:10.4271/2015-01-1801.

[116] Chen Z, Liu J, Wu Z, Lee C. Effects of port fuel injection (PFI) of n-butanol and EGR on combustion and emissions of a direct injection diesel engine. Energy Conversion and Management 2013;76:725–31. doi:10.1016/j.enconman.2013.08.030.

[117] Tutak W. Bioethanol E85 as a fuel for dual fuel diesel engine. Energy Conversion and Management 2014;86:39–48. doi:10.1016/j.enconman.2014.05.016.

[118] Sarjovaara T, Larmi M. Dual fuel diesel combustion with an E85 ethanol/gasoline blend. Fuel 2015;139:704–14. doi:10.1016/j.fuel.2014.09.049.

[119] Asad U, Zheng M. Exhaust gas recirculation for advanced diesel combustion cycles. Applied Energy 2014;123:242–52. doi:10.1016/j.apenergy.2014.02.073.

[120] Asad U, Zheng M, Tjong J. Experimental Investigation of Diesel-Ethanol Premixed Pilot-Assisted Combustion (PPAC) in a High Compression Ratio Engine. SAE International Journal of Engines 2016;9. doi:10.4271/2016-01-0781.

[121] May I, Pedrozo V, Zhao H, Cairns A, Whelan S, Wong H, et al. Characterization and Potential of Premixed Dual-Fuel Combustion in a Heavy Duty Natural Gas/Diesel Engine. SAE Technical Paper 2016. doi:10.4271/2016-01-0790.

[122] Goldsworthy L. Fumigation of a heavy duty common rail marine diesel engine with ethanol-water mixtures. Experimental Thermal and Fluid Science 2013;47:48–59. doi:10.1016/j.expthermflusci.2012.12.018.

[123] Benajes J, García A, Monsalve-Serrano J, Balloul I, Pradel G. An assessment of the dual-mode reactivity controlled compression ignition/conventional diesel combustion capabilities in a EURO VI medium-duty diesel engine fueled with an intermediate ethanol-gasoline blend and biodiesel. Energy Conversion and Management 2016;123:381–91. doi:10.1016/j.enconman.2016.06.059.

[124] Lim JH, Reitz RD. High Load (21 Bar IMEP) Dual Fuel RCCI Combustion Using Dual Direct Injection. Journal of Engineering for Gas Turbines and Power 2014;136. doi:10.1115/1.4027361.

[125] Wissink M, Reitz RD. Direct Dual Fuel Stratification, a Path to Combine the Benefits of RCCI and PPC. SAE International Journal of Engines 2015;8:878–89. doi:10.4271/2015-01-0856.

[126] Wissink M, Reitz R. Exploring the Role of Reactivity Gradients in Direct Dual Fuel Stratification. SAE International Journal of Engines 2016;9:2016–01 – 0774. doi:10.4271/2016-01-0774.

[127] Wu Y, Reitz RD. Effects of Exhaust Gas Recirculation and Boost Pressure on Reactivity Controlled Compression Ignition Engine at High Load Operating Conditions. Journal of Energy Resources Technology 2015;137. doi:10.1115/1.4029866.

[128] Kavuri C, Kokjohn S. Investigating Air Handling Requirements of High Load Low Speed Reactivity Controlled Compression Ignition (RCCI) Combustion. SAE Technical Paper 2016. doi:10.4271/2016-01-0782.

[129] Han X, Divekar P, Reader G, Zheng M, Tjong J. Active Injection Control for Enabling Clean Combustion in Ethanol-Diesel Dual-Fuel Mode. SAE International Journal of Engines 2015;8:890–902. doi:10.4271/2015-01-0858.

[130] Benajes J, Pastor J V., García A, Monsalve-Serrano J. The potential of RCCI concept to meet EURO VI NOx limitation and ultra-low soot emissions in a heavy-duty engine over the whole engine map. Fuel 2015;159:952–61. doi:10.1016/j.fuel.2015.07.064.

[131] Benajes J, Pastor J V., García A, Boronat V. A RCCI operational limits assessment in a medium duty compression ignition engine using an adapted

compression ratio. Energy Conversion and Management 2016;126:497–508. doi:10.1016/j.enconman.2016.08.023.

[132] Kavuri C, Paz J, Kokjohn SL. A comparison of Reactivity Controlled Compression Ignition (RCCI) and Gasoline Compression Ignition (GCI) strategies at high load, low speed conditions. Energy Conversion and Management 2016;127:324–41. doi:10.1016/j.enconman.2016.09.026.

[133] Martins MES, Lanzanova TDM. Full-load Miller cycle with ethanol and EGR: Potential benefits and challenges. Applied Thermal Engineering 2015;90:274–85. doi:10.1016/j.applthermaleng.2015.06.086.

[134] Zhao J. Research and application of over-expansion cycle (Atkinson and Miller) engines – A review. Applied Energy 2017;185:300–19. doi:10.1016/j.apenergy.2016.10.063.

[135] Ickes A, Hanson R, Wallner T. Impact of Effective Compression Ratio on Gasoline-Diesel Dual-Fuel Combustion in a Heavy-Duty Engine Using Variable Valve Actuation. SAE Technical Paper 2015. doi:10.4271/2015-01-1796.

[136] Zhang Y, Sagalovich I, De Ojeda W, Ickes A, Wallner T, Wickman DD. Development of Dual-Fuel Low Temperature Combustion Strategy in a Multi-Cylinder Heavy-Duty Compression Ignition Engine Using Conventional and Alternative Fuels. SAE International Journal of Engines 2013;01:1481–9. doi:10.4271/2013-01-2422.

[137] Hanson R, Ickes A, Wallner T. Use of Adaptive Injection Strategies to Increase the Full Load Limit of RCCI Operation. Journal of Engineering for Gas Turbines and Power 2016;138:102802. doi:10.1115/1.4032847.

[138] U.S. Energy Information Administration. International Energy Outlook 2014. Washington: 2014.

[139] United Nations Environment Programme. Towards sustainable production and use of resources: assessing biofuels. 2009.

[140] The European Parliament and the Council of the European Union. Directive 2003/30/EC. Official Journal of the European Union 2003;123.

[141] Edwards R, Larivé J-F, Rickeard D, Weindorf W. Well-to-Wheels analysis of future automotive fuels and powertrains in the European context: Well-to-Tank Report - Version 4.a. Joint Research Centre of the European Commission, EUCAR, and CONCAWE 2014;4.a. doi:10.2790/95629.

[142] Edwards R, Larivé J-F, Rickeard D, Weindorf W. Well-to-Wheels analysis of future automotive fuels and powertrains in the European context: Well-to-Tank Appendix 2 - Version 4a. Joint Research Centre of the European Commission, EUCAR, and CONCAWE 2014:1–133. doi:10.2790/95629.

[143] The European Parliament and the Council of the European Union. Directive 2009/28/EC. Official Journal of the European Union 2009;140.

[144] The European Parliament and the Council of the European Union. Directive 2015/652. Official Journal of the European Union 2015;107.

[145] The European Parliament and the Council of the European Union. Directive 2015/1513. Official Journal of the European Union 2015;239.

[146] Laborde D. Assessing the Land Use Change Consequences of European Biofuel Policies. International Food Policy Institute (IFPRI), 2011.

[147] European Commission. State of the Art on Alternative Fuels Transport Systems in the European Union. 2015.

[148] PBL Netherlands Environmental Assessment Agency. Trends in global CO2 emissions: 2013 Report. The Hague: 2013.

[149] The European Parliament and the Council of the European Union. Directive 2009/30/EC. Official Journal of the European Union 2009;140.

[150] U.S. Energy Information Administration. Biofuels Issues and Trends. Washington: 2012.

[151] Kolbeck A, Shell International. Challenges and Fuels Options for Future HD Transportation. Presentation at SAE 2016 Heavy-Duty Diesel Emissions Control Symposium, Gothenburg: 2016.

[152] Renewable Fuels Association. World Fuel Ethanol Production 2017. http://www.ethanolrfa.org/resources/industry/statistics/ (accessed July 14, 2017).

[153] Associação Nacional dos Fabricantes de Veículos Automotores (ANFAVEA). Statistics 2017. http://www.anfavea.com.br/estatisticas.html (accessed July 14, 2017).

[154] ANP. Administrative Act ANP No. 19. 2015.

[155] Ministry of Agriculture and Supply. Ordinance No. 75. 2015.

[156] He B, Wang J, Shuai S, Yan X. Homogeneous Charge Combustion and Emissions of Ethanol Ignited by Pilot Diesel on Diesel Engines. SAE Technical Paper 2004. doi:10.4271/2004-01-0094.

[157] Brewster S, Railton D, Maisey M, Frew R. The Effect of E100 Water Content on High Load Performance of a Spray Guide Direct Injection Boosted Engine. SAE Technical Paper 2007. doi:10.4271/2007-01-2648.

[158] Munsin R, Laoonual Y, Jugjai S, Imai Y. An experimental study on performance and emissions of a small SI engine generator set fuelled by hydrous ethanol with high water contents up to 40%. Fuel 2013;106:586–92. doi:10.1016/j.fuel.2012.12.079.

[159] Lanzanova TDM, Dalla Nora M, Zhao H. Performance and economic analysis of a direct injection spark ignition engine fueled with wet ethanol. Applied Energy 2016;169:230–9. doi:10.1016/j.apenergy.2016.02.016.

[160] Martins M, Fischer I, Gusberti F, Sari R, Nora MD. HCCI of Wet Ethanol on a Dedicated Cylinder of a Diesel Engine. SAE Technical Paper 2017. doi:10.4271/2017-01-0733.

[161] Mack JH, Aceves SM, Dibble RW. Demonstrating direct use of wet ethanol in a homogeneous charge compression ignition (HCCI) engine. Energy 2009;34:782–7. doi:10.1016/j.energy.2009.02.010.

[162] Dempsey AB, Das Adhikary B, Viswanathan S, Reitz RD. Reactivity Controlled Compression Ignition Using Premixed Hydrated Ethanol and Direct Injection Diesel. Journal of Engineering for Gas Turbines and Power 2012;134:082806–082806 – 11. doi:10.1115/1.4006703.

[163] Fang W, Fang J, Kittelson DB, Northrop WF. An Experimental Investigation of Reactivity-Controlled Compression Ignition Combustion in a Single-Cylinder Diesel Engine Using Hydrous Ethanol. Journal of Energy Resources Technology 2015;137:031101–031101 – 7. doi:10.1115/1.4028771.

[164] Saffy H a, Northrop WF, Kittelson DB, Boies AM. Energy, carbon dioxide and water use implications of hydrous ethanol production. Energy Conversion and Management 2015;105:900–7. doi:10.1016/j.enconman.2015.08.039.

[165] López-Plaza EL, Hernández S, Barroso-Muñoz FO, Segovia-Hernández JG, Aceves SM, Martínez-Frías J, et al. Experimental and Theoretical Study of the Energy Savings from Wet Ethanol Production and Utilization. Energy Technology 2014;2:440–5. doi:10.1002/ente.201300180.

[166] Jacobs Vehicle Systems. Variable Valve Actuation n.d. http://www.jacobsvehiclesystems.com/products/variable-valve-actuation/ (accessed June 6, 2017).

[167] International Organisation of Legal Metrology (IOLM). International Recommendation No22 - Alcoholometry. First Ed. Paris: 1973.

[168] Zhao H, Ladammatos N. Engine Combustion Instrumentation and Diagnostics. Warrendale, Pa. USA: 2001.

[169] Takeda K, Koike H. Motor Exhaust Gas Analyzer MEXA-7000 Series 2. Downsizing and Modular Configuration of Analyzers. Horiba 1995.

[170] Kar K, Cheng WK. Speciated Engine-Out Organic Gas Emissions from a PFI-SI Engine Operating on Ethanol/Gasoline Mixtures. SAE International Journal of Fuels and Lubricants 2009;2. doi:10.4271/2009-01-2673.

[171] Wallner T. Correlation Between Speciated Hydrocarbon Emissions and Flame Ionization Detector Response for Gasoline/Alcohol Blends. Journal of Engineering for Gas Turbines and Power 2011;133. doi:10.1115/1.4002893.

[172] May IA. An experimental investigation of lean-burn dual-fuel combustion in a heavy duty diesel engine. Brunel University London, 2017.

[173] Wexler A. Vapor pressure formulation for water in range 0 to 100 C. A revision. Journal of Research of the National Bureau of Standards Section A: Physics and Chemistry 1976;80A:775. doi:10.6028/jres.080A.071.

[174] AVL. AVL 415SE Smoke Meter - Product Guide. Graz, Austria: 2013.

[175] Watson N, Pilley A, Marzouk M. A Combustion Correlation for Diesel Engine Simulation. SAE Technical Paper 1980. doi:10.4271/800029.

[176] Woschni G. A Universally Applicable Equation for the Instantaneous Heat Transfer Coefficient in the Internal Combustion Engine. SAE Technical Paper 1967. doi:10.4271/670931.

[177] Klos D, Janecek D, Kokjohn S. Investigation of the Combustion Instability-NOx Tradeoff in a Dual Fuel Reactivity Controlled Compression Ignition (RCCI) Engine. SAE International Journal of Engines 2015;8:821–30. doi:10.4271/2015-01-0841.

[178] Eichmeier J, Wagner U, Spicher U. Controlling Gasoline Low Temperature Combustion by Diesel Micro Pilot Injection. Journal of Engineering for Gas Turbines and Power 2012;134. doi:10.1115/1.4005997.

[179] Ortiz-Soto E a., Lavoie G a., Martz JB, Wooldridge MS, Assanis DN. Enhanced heat release analysis for advanced multi-mode combustion engine experiments. Applied Energy 2014;136:465–79. doi:10.1016/j.apenergy.2014.09.038.

[180] Caton JA. Combustion phasing for maximum efficiency for conventional and high efficiency engines. Energy Conversion and Management 2014;77:564–76. doi:10.1016/j.enconman.2013.09.060.

[181] Zhao H. HCCI and CAI engines for automotive industry. Cambridge: Woodhead Publishing Limited; 2007.

[182] Dec JE, Yang Y. Boosted HCCI for High Power without Engine Knock and with Ultra-Low NOx Emissions - using Conventional Gasoline. SAE Technical Paper 2010. doi:10.4271/2010-01-1086.

[183] Kokjohn S, Reitz RD, Splitter D, Musculus M. Investigation of Fuel Reactivity Stratification for Controlling PCI Heat-Release Rates Using High-Speed Chemiluminescence Imaging and Fuel Tracer Fluorescence. SAE International Journal of Engines 2012;5. doi:10.4271/2012-01-0375.

[184] Caton J a. Maximum efficiencies for internal combustion engines: Thermodynamic limitations. International Journal of Engine Research 2017:146808741773770. doi:10.1177/1468087417737700.

[185] Caton JA. An Introduction to Thermodynamic Cycle Simulations for Internal Combustion Engines. First. John Wiley & Sons Ltd; 2016.

[186] Han X, Xie K, Tjong J, Zheng M. Empirical Study of Simultaneously Low NOx and Soot Combustion With Diesel and Ethanol Fuels in Diesel Engine. Journal of Engineering for Gas Turbines and Power 2012;134. doi:10.1115/1.4007163.

[187] Padala S, Woo C, Kook S, Hawkes ER. Ethanol utilisation in a diesel engine using dual-fuelling technology. Fuel 2013;109:597–607. doi:10.1016/j.fuel.2013.03.049.

[188] Splitter D, Kokjohn S, Rein K, Hanson R, Sanders S, Reitz R. An Optical Investigation of Ignition Processes in Fuel Reactivity Controlled PCCI

Combustion. SAE International Journal of Engines 2010;3. doi:10.4271/2010-01-0345.

[189] Kokjohn SL, Hanson RM, Splitter DA, Reitz RD. Experiments and Modeling of Dual-Fuel HCCI and PCCI Combustion Using In-Cylinder Fuel Blending. SAE International Journal of Engines 2009;2. doi:10.4271/2009-01-2647.

[190] Westbrook CK. Chemical kinetics of hydrocarbon ignition in practical combustion systems. Proceedings of the Combustion Institute 2000;28:1563–77. doi:10.1016/S0082-0784(00)80554-8.

[191] Baumgarten C. Mixture formation in internal combustion engines. Springer-Verlag Berlin Heidelberg; 2006.

[192] Schaefer M, Hofmann L, Girot P, Rohe R. Investigation of NOx- and PM-reduction by a Combination of SCR-catalyst and Diesel Particulate Filter for Heavy-duty Diesel Engine. SAE International Journal of Fuels and Lubricants 2009;2. doi:10.4271/2009-01-0912.

[193] Johansen K, Widd A, Truck M a N, Ag B. Passive NO2 Regeneration and NOx Conversion for DPF with an Integrated Vanadium SCR Catalyst. SAE Technical Paper 2016. doi:10.4271/2016-01-0915.

[194] He X, Durrett RP, Sun Z. Late Intake Valve Closing as an Emissions Control Strategy at Tier 2 Bin 5 Engine-Out NOx Level. SAE International Journal of Engines 2008;1:2008–01 – 0637. doi:10.4271/2008-01-0637.

[195] Westbrook CK, Pitz WJ, Leppard WR. The Autoignition Chemistry of Paraffinic Fuels and Pro-Knock and Anti-Knock Additives: A Detailed Chemical Kinetic Study. SAE Technical Paper 1991. doi:10.4271/912314.

[196] Sjöberg M, Dec JE. Effects of EGR and its constituents on HCCI autoignition of ethanol. Proceedings of the Combustion Institute 2011;33:3031–8. doi:10.1016/j.proci.2010.06.043.

[197] Aceves SM, Flowers DL, Martinez-Frias J, Smith JR, Dibble R, Au M, et al. HCCI Combustion: Analysis and Experiments. SAE Technical Paper 2001. doi:10.4271/2001-01-2077.

[198] Benajes J, Molina S, Martín J, Novella R. Effect of advancing the closing angle of the intake valves on diffusion-controlled combustion in a HD diesel engine. Applied Thermal Engineering 2009;29:1947–54. doi:10.1016/j.applthermaleng.2008.09.014.

[199] Thermal-Fluids Central. Thermophysical Properties n.d. https://www.thermalfluidscentral.org/ (accessed May 17, 2017).

[200] Christensen M, Johansson B. Homogeneous Charge Compression Ignition with Water Injection. SAE Technical Paper 1999. doi:10.4271/1999-01-0182.

[201] Park C, Busch S. The influence of pilot injection on high-temperature ignition processes and early flame structure in a high-speed direct injection diesel engine. International Journal of Engine Research 2017. doi:10.1177/1468087417728630.

[202] Tsang KS, Zhang ZH, Cheung CS, Chan TL. Reducing Emissions of a Diesel Engine Using Fumigation Ethanol and a Diesel Oxidation Catalyst. Energy & Fuels 2010;24. doi:10.1021/ef100899z.

[203] Di Blasio G, Beatrice C, Molina S. Effect of Port Injected Ethanol on Combustion Characteristics in a Dual-Fuel Light Duty Diesel Engine. SAE Technical Paper 2013;01. doi:10.4271/2013-01-1692.

[204] Han X, Yang Z, Wang M, Tjong J, Zheng M. Clean combustion of n-butanol as a next generation biofuel for diesel engines. Applied Energy 2016. doi:10.1016/j.apenergy.2016.12.059.

[205] Ramachandran S, Stimming U. Well to wheel analysis of low carbon alternatives for road traffic. Energy Environ Sci 2015;8:3313–24. doi:10.1039/C5EE01512J.

[206] Wang M, Han J, Dunn JB, Cai H, Elgowainy A. Well-to-wheels energy use and greenhouse gas emissions of ethanol from corn, sugarcane and cellulosic biomass for US use. Environmental Research Letters 2012;7:045905. doi:10.1088/1748-9326/7/4/045905.

[207] Yan X, Boies AM. Quantifying the uncertainties in life cycle greenhouse gas emissions for UK wheat ethanol. Environmental Research Letters 2013;8:015024. doi:10.1088/1748-9326/8/1/015024.

[208] Benajes J, Pastor J V., García A, Monsalve-Serrano J. An experimental investigation on the influence of piston bowl geometry on RCCI performance and emissions in a heavy-duty engine. Energy Conversion and Management 2015;103:1019–30. doi:10.1016/j.enconman.2015.07.047.

[209] Benajes J, García A, Pastor JM, Monsalve-Serrano J. Effects of piston bowl geometry on Reactivity Controlled Compression Ignition heat transfer and combustion losses at different engine loads. Energy 2016;98:64–77. doi:10.1016/j.energy.2016.01.014.